

UNCLASSIFIED

AD NUMBER
ADB182832
NEW LIMITATION CHANGE
TO Approved for public release, distribution unlimited
FROM Distribution authorized to U.S. Gov't. agencies and their contractors; Administrative/Operational Use; MAY 1954. Other requests shall be referred to National Aeronautics and Space Administration, Washington, DC.
AUTHORITY
NASA TR Server website

THIS PAGE IS UNCLASSIFIED



CLASSIFIED

~~SECRET~~

(L)

NATIONAL ADVISORY COMMITTEE  
FOR AERONAUTICS

(u)

NACA CONFERENCE  
ON HELICOPTERS

DTIC  
ELECTE  
APR 14 1994  
S F D

A COMPILATION OF THE PAPERS PRESENTED

Langley Aeronautical Laboratory  
Langley Field, Virginia

"DTIC USERS ONLY"

MAY 12-13, 1954

94-11180

CLASSIFICATION CHANGED TO SECRET  
BY AUTHORITY OF SECDEF DATE 8-1-83



DTIC QUALITY ASSURANCE

CLASSIFIED DOCUMENT

This material contains information affecting the National Defense of the United States within the meaning of the espionage laws, Title 18, U.S.C., Secs. 793 and 794, the transmission or revelation of which in any manner to an unauthorized person is prohibited by law.

Proprietary

UNCLASSIFIED



94 4 12 082



UNCLASSIFIED

NACA CONFERENCE ON HELICOPTERS

A Compilation of the Papers Presented

Langley Aeronautical Laboratory  
Langley Field, Va.

May 12 and 13, 1954

Accession For	
NTIS GRA&I DTIC TAB Unannounced Justification	
By Distribution /	
Availability Codes	
Dist	Avail and/or Special
12	

"DTIC USERS ONLY"

UNCLASSIFIED

DTIC USERS ONLY



UNCLASSIFIED

TABLE OF CONTENTS

	Page
INTRODUCTION . . . . .	vii
LIST OF CONFEREES . . . . .	ix

TECHNICAL PAPERS PRESENTED

SESSION CHAIRMAN: Floyd L. Thompson

ROTOR AERODYNAMICS . . . . .	1
A. Airfoil Section Characteristics	
1. Airfoil Section Characteristics at High Angles of Attack . . . Laurence K. Loftin, Jr. . . . .	3
2. Airfoil Section Characteristics at Transonic Speeds (Confidential) . . . W. F. Lindsey . . . . .	13
B. Rotor Induced Flow	
3. Review of Information on Induced Flow of a Lifting Rotor . . . Alfred Gessow . . . . .	31
4. Flow-Field Measurements Around Single and Tandem Rotors in the Langley Full-Scale Tunnel . . . Harry H. Heyson . . .	47
C. Hovering	
5. Rotor Efficiency in Hovering . . . Alfred Gessow . . . . .	59
6. Hovering Performance of a Helicopter Rotor Using NACA 8-H-12 Airfoil Sections . . . Robert D. Powell, Jr. . . .	69
D. Forward Flight	
7. Some Recent Developments in Rotor Theory . . . Alfred Gessow and Almer D. Crim . . . . .	81
8. A Discussion of Forward-Speed Limitations Introduced by Stall and Mach Number Effects . . . F. B. Gustafson and Robert D. Harrington . . . . .	89
9. An Exploratory Investigation of Unloaded Rotors (Confidential) . . . John W. McKee and Robert J. Tapscott . . .	99

UNCLASSIFIED

UNCLASSIFIED

Page

E. Multirotor Configurations

10. Wind-Tunnel Studies of the Performance of Multirotor Configurations . . . Richard C. Dingeldein . . . . . 113

PROPULSION AND PARASITE DRAG . . . . . 123

A. Blade Tip Propulsion

11. An Investigation of Ram Jets for Helicopters (Confidential) . . . Paul J. Carpenter and Edward J. Radin . . . 125

12. An Investigation of a Pulse-Jet Engine for Helicopters (Confidential) . . . Edward J. Radin and Paul J. Carpenter . . . . . 133

13. An Analytical Study of a Large Pressure-Jet Helicopter . . William S. Miller and Richard P. Krebs . . . . . 141

B. Internal Flow

14. Aspects of Internal-Flow-System Design for Helicopter Propulsive Units (Confidential) . . . John R. Henry . . 149

C. Parasite Drag

15. Reduction of Helicopter Parasite Drag . . . Robert D. Harrington . . . . . 173

D. Noise

16. Some Aspects of the Helicopter Noise Problem . . . Harvey H. Hubbard and Leslie W. Lassiter . . . . . 181

17. Exhaust Mufflers As Applied to the Helicopter . . . George M. Stokes and Don D. Davis, Jr. . . . . 195

UNCLASSIFIED

UNCLASSIFIED

Page

SESSION CHAIRMAN: Hartley A. Soulé

STABILITY AND CONTROL . . . . . 203

A. Flying-Qualities Criteria

18. Flying-Qualities Criteria for General-Purpose Helicopters  
(Confidential) . . . John P. Reeder and F. B. Gustafson 205

19. An Investigation of the Effect of Damping on Precision  
Maneuvers and Instrument Flight (Confidential) . . .  
Almer D. Crim, James B. Whitten, and John P. Reeder . . 215

B. Design Methods and Data

20. Methods of Predicting Helicopter Stability (Confiden-  
tial) . . . Robert J. Tapscott and F. B. Gustafson . . . 221

21. Methods for Obtaining Desired Helicopter Stability Charac-  
teristics (Confidential) . . . F. B. Gustafson and  
Robert J. Tapscott . . . . . 237

22. Wind-Tunnel Studies of the Directional Stability Charac-  
teristics of Two Tandem Helicopter Fuselages . . . John  
D. Bird and James L. Williams . . . . . 249

23. Flight Tests of a Man Standing on a Rotor-Supported Plat-  
form (Confidential) . . . P. R. Hill . . . . . 257

LOADS, STRESSES, VIBRATION, AND FLUTTER . . . . . 263

24. A Study of Normal Accelerations and Operating Conditions  
Experienced by Helicopters in Service Usage . . . Marlin  
E. Hazen and Almer D. Crim . . . . . 265

25. Normal Accelerations Due to Maneuvers and Gusts as Studied  
in Flight . . . Almer D. Crim and F. B. Gustafson . . . 275

26. Preliminary Experiments on the Effects of Gusts on Heli-  
copter Blade Bending Moments . . . Domenic J. Maglieri  
and Joseph W. Jewel . . . . . 283

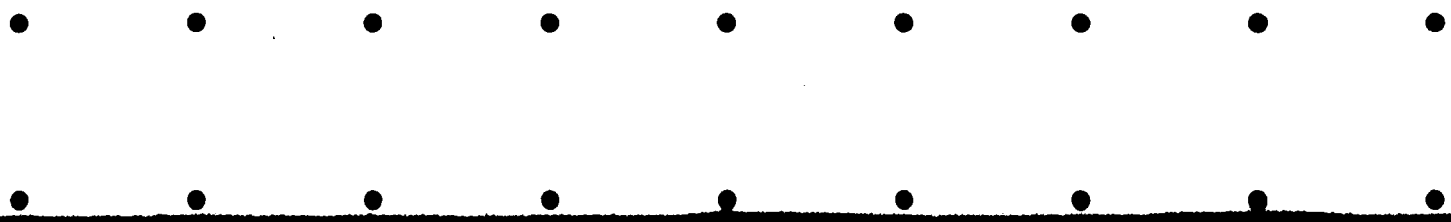
27. Helicopter Rotor-Blade Flutter Research (Confidential) . .  
Maurice A. Sylvester, A. Gerald Rainey, and George W.  
Brooks . . . . . 289

[REDACTED]

UNCLASSIFIED



	Page
28. A Dynamic-Model Study of the Effect of Concentrated Weights on the Vibratory Stresses in Helicopter Blades (Confidential) . . . John Locke McCarty . . . . .	303
29. Coupled Bending and Torsional Deformations of Rotating Beams Under Arbitrary Loading . . . George W. Brooks and John C. Houbolt . . . . .	311
30. Rapid Estimation of Bending Frequencies of Rotating Beams . . . Robert T. Yntema . . . . .	321
31. Dynamic-Model Design Techniques . . . George W. Brooks .	333
32. Methods of Predicting the Fatigue Characteristics of Structural Parts Containing Stress Concentrations . . . Herbert F. Hardrath . . . . .	347





## INTRODUCTION

This document contains reproductions of technical papers presented at the NACA Conference on Helicopters held at the Langley Aeronautical Laboratory May 12 and 13, 1954. The primary purpose of this conference was to convey to the military services, their contractors, and others concerned with the design of helicopters the results of NACA research on helicopters and to provide those attending an opportunity to discuss the results.

The papers in this document are in the same form in which they were presented at the conference in order to facilitate their prompt distribution. The original presentation and this record are considered as complementary to, rather than as substitutes for, the Committee's more complete and formal reports.

A list of the conferees is included.



[REDACTED]

LIST OF CONFEREES

The following were registered at the NACA Conference on Helicopters, Langley Aeronautical Laboratory, Langley Field, Va., May 12 and 13, 1954:

ABBOTT, Ira H.	NACA Headquarters
ADAMS, Hon. Joseph P.	Member, NACA
AMES, Milton B., Jr.	NACA Headquarters
ANDERSON, Arnold W.	David Taylor Model Basin
ASHER, Norman J.	Subcommittee on Helicopters
AULD, Charles D.	Bureau of Aeronautics
BAILEY, Frederick J., Jr.	NACA - Langley Laboratory
BALLAUER, Alb. C.	Parsons Corporation
BALLENTINE, Donald C.	David Taylor Model Basin
BANKER, Capt. Walter F.	XVIII Airborne Corps - Fort Bragg
BARE, Col. Walter E., Jr.	Army Field Forces - Fort Monroe
BARNES, Lt. Robert O., USN	NATC - Patuxent River
BATES, George P.	NACA Headquarters
BEARD, Myron G.	Committee on Operating Problems
BEHNFELDT, 1/Lt. M. J.	Wright Air Development Center
BERCHTOLD, Max	I-T-E Circuit Breaker Company
BERNHARDT, David E.	General Motors Corporation
BIRD, John D.	NACA - Langley Laboratory
BLADES, Lt. Jehu L., USN	NATC - Patuxent River
BLAKE, Charles L.	Office of Asst. Secretary of Defense
BOLLAY, Dr. William	Aerophysics Development Corporation
BOOTH, Robert A.	Bureau of Aeronautics
BOWLBY, Lt. Col. Lawrence	Army Field Forces - Fort Monroe
BRATT, Robert W.	Douglas Aircraft Company
BRENNING, Orin Z.	Wright Air Development Center
BREWER, Gerald W.	NACA - Langley Laboratory
BROOKS, George W.	NACA - Langley Laboratory
BROWN, Lt. Col. G. F., USAF	Office of Asst. Secretary of Defense
BROWN, Harvey H.	NACA Headquarters
BROWN, Wilbert R.	Reaction Motors
BRYE, James M.	Ryan Aeronautical Company
BUCKLEY, Edmond C.	NACA - Langley Laboratory
CAMPBELL, Lawrence F.	Naval Research Laboratory
CARPENTER, Paul J.	NACA - Langley Laboratory
CESARO, Richard S.	NACA Headquarters
COBEY, William E.	Transcendental Aircraft Corporation
COCKLIN, Henry S.	Aeronautical Engineering Div., USCG
COLLINS, Cdr. T. W., Jr., USN	Office of Asst. Secretary of Defense
COOPER, Kenneth S.	Civil Aeronautics Administration

[REDACTED]

CORNER, Arthur N.	Melpar
CRIM, Almer D.	NACA - Langley Laboratory
CROWLEY, John W.	NACA Headquarters
DAVIS, James N.	Office of Under Secretary of the Army
DE LOS SANTOS, Dr. S. T.	David Taylor Model Basin
DESMOND, Gerald L.	Bureau of Aeronautics
DINGELDEIN, Richard C.	NACA - Langley Laboratory
DONELY, Philip	NACA - Langley Laboratory
DONLAN, Charles J.	NACA - Langley Laboratory
DRALEY, Eugene C.	NACA - Langley Laboratory
DRYDEN, Dr. Hugh L.	NACA Headquarters
DUBERG, Dr. John E.	NACA - Langley Laboratory
DUTTON, Donnell W.	Georgia Institute of Technology
EMMERSON, John O.	The Kaman Aircraft Corporation
EPLEY, Cdr. Thomas F.	Aeronautical Engineering Div., USCG
ERICKSON, Capt. Frank A., USCG	Subcommittee on Helicopters
FANNON, Marcy B.	Trans World Airlines
FEDZIUK, Henry A.	NACA - Langley Laboratory
GARRICK, Isadore E.	NACA - Langley Laboratory
GESSOW, Alfred	NACA - Langley Laboratory
GILRUTH, Robert R.	NACA - Langley Laboratory
GILSTAD, Douglas A.	Bureau of Aeronautics
GOLAND, Leonard	Forrestal Research Center
GOPPERT, Maj. Jean G., USAF	Air Force Development Field
	Representative - Langley Field
GORANSON, R. Fabian	NACA Headquarters
GORDON, Samuel A.	Battelle Memorial Institute
GOUGH, Melvin N.	NACA - Langley Laboratory
GRISWOLD, Capt. Truman L.	Wright Air Development Center
GROVER, Horace J.	Battelle Memorial Institute
GUSTAFSON, F. B.	NACA - Langley Laboratory
HALABY, Najeeb E.	Office of the Messrs. Rockefeller,
	Rockefeller Plaza, New York
HALL, James B.	United Aircraft Corporation
HARDRATH, Herbert F.	NACA - Langley Laboratory
HARDY, Cyrus W.	Wright Air Development Center
HARPER, Charles W.	NACA - Ames Laboratory
HARRINGTON, Robert D.	NACA - Langley Laboratory
HARRIS, T. Aubrey	NACA - Langley Laboratory
HARRISON, Daniel E.	Goodyear Aircraft Corporation
HAYES, Miles Van Valzah	United Aircraft Corporation
HAZEN, Marlin E.	NACA - Langley Laboratory
HECK, Alan N.	McDonnell Aircraft Corporation

x

[REDACTED]

[REDACTED]

HEGLUND, Floyd W.	General Electric Company
HENRY, John R.	NACA - Langley Laboratory
HENSLEY, R. V.	Fairchild Engine & Airplane Corporation
HERZMARK, Ralph H.	McDonnell Aircraft Corporation
HEYSON, Harry H.	NACA - Langley Laboratory
HILL, P. R.	NACA - Langley Laboratory
HINSHAW, William D.	NATC - Patuxent River
HINTON, Sanford H.	Cessna Aircraft Company
HIRSCH, Harold	Hughes Tool Company
HODGE, Maj. James R.	8th Transp. Helicopter Bn. - Fort Bragg
HOUBOLT, John C.	NACA - Langley Laboratory
HOVGARD, Paul E.	Subcommittee on Helicopters
HUBBARD, Harvey H.	NACA - Langley Laboratory
HUBER, J. Richard	Eastern Rotorcraft Corporation
HUNTER, Hugh F.	Bureau of Aeronautics
JACKSON, Capt. Calvin W.	Tactical Air Command, Langley Field
JACOBSON, John W.	General Electric Company
JAQUIS, Robert E.	Bureau of Aeronautics
JEWEL, Joseph W., Jr.	NACA - Langley Laboratory
JUSTICE, Donald Alonzo	Marquardt Aircraft Company
KATZENBERGER, E. F.	Subcommittee on Helicopters
KATZOFF, Dr. Samuel	NACA - Langley Laboratory
KAUFMAN, Harold	NADC - Johnsville, Pennsylvania
KAUFMAN, Lawrence	Sperry Gyroscope Company
KAYTEN, Gerald G.	Bureau of Aeronautics
KIDDER, Robert C.	Cornell Aeronautical Laboratory
KLEIN, Harold	Douglas Aircraft Company
KLEINHANS, Schuyler	Douglas Aircraft Company
KNECHT, Robert S.	Bureau of Aeronautics
KOSCIUSKO, Cdr. Henry M.	Office of Naval Operations
KREBS, Richard P.	NACA - Lewis Laboratory
KUHN, Paul	NACA - Langley Laboratory
KURTZ, Guy O.	Melpar
LANDIS, Raymond B.	Prewitt Aircraft Company
LASSITER, Leslie W.	NACA - Langley Laboratory
LEE, John G.	Subcommittee on High-Speed Aerodynamics
LIGHTFOOT, Ralph B.	United Aircraft Corporation
LINDENBAUM, Bernard	Subcommittee on Helicopters
LINDSEY, W. F.	NACA - Langley Laboratory
LOESCH, Franklin C.	American Helicopter Company
LOEWY, Robert G.	Cornell Aeronautical Laboratory
LOFTIN, Laurence K., Jr.	NACA - Langley Laboratory
LONG, Lt. Col. Richard L., USA	Subcommittee on Helicopters

[REDACTED]

LUMSDEN, Lt. David, USN  
LUNDE, Otto H.  
LUNDQUIST, Dr. Eugene E.

NATC - Patuxent River  
Bureau of Aeronautics  
NACA - Langley Laboratory

MAGLIERI, Domenic J.  
MALOY, Raymond B.  
MANN, Kenneth  
MAUSER, Lt. Col. R. N., USA  
MAY, Ralph W., Jr.  
MAZUR, John W.  
McCARTY, John L.  
McGRAW, Harold

NACA - Langley Laboratory  
Subcommittee on Helicopters  
Hughes Tool Company  
Office of Asst. Secretary of Defense  
NACA Headquarters  
Doman Helicopters  
NACA - Langley Laboratory  
Minneapolis-Honeywell Regulator  
Company

McKEE, John W.  
McQUEEN, Kenneth  
MEALEY, Martin J., Jr.  
MICHEL, Philip L.  
MILLER, René H.  
MILLER, William S., Jr.  
MORRIS, Francis C.  
MOYER, Robert M.

NACA - Langley Laboratory  
NADC - Johnsville, Pennsylvania  
Transcendental Aircraft Corporation  
United Aircraft Corporation  
Subcommittee on Helicopters  
NACA - Lewis Laboratory  
Curtiss-Wright Corporation  
Curtiss-Wright Corporation

NIKOLSKY, Alexander A.

Forrestal Research Center

OGLESBY, Lt. Cdr. Earl V., USN  
OLEKSAK, William

NATC - Patuxent River  
Wright Air Development Center

PARKINSON, John B.  
PATCH, Lt. Cdr. Arthur E.  
PERRY, Julian P.  
PETERSON, Ivar C.

NACA - Langley Laboratory  
Office of Naval Research  
Eastern Rotorcraft Corporation  
Aircraft Industries Association of  
America

PHILLIPS, Franklyn W.  
PIERCE, Erol R.

NACA Headquarters  
Subcommittee on Engine Performance  
and Operation

PORTER, Carol D.  
POWELL, Robert D., Jr.  
PREWITT, Richard H.  
PUTNAM, Victor K.

Naval Research Laboratory  
NACA - Langley Laboratory  
Prewitt Aircraft Company  
Air Force Flight Test Center,  
Edwards AFB

RADIN, Edward J.  
RAINEY, A. Gerald  
RAPP, George C.  
REDDING, Arnold H.

NACA - Langley Laboratory  
NACA - Langley Laboratory  
General Electric Company  
Subcommittee on Engine Performance  
and Operation

REEDER, John P.  
REGIER, Arthur A.

NACA - Langley Laboratory  
NACA - Langley Laboratory

REID, Dr. H. J. E.  
RHODE, Richard V.  
RITCHEY, Wallace M., Jr.  
ROE, Robert B.  
ROGALLO, Vernon L.  
ROLLE, Stephen H.  
ROSCHE, Melvin G.  
ROSENBAUM, Robert  
RUMMEL, Robert W.  
RUSK, Stanley

SAYEN, Clarence M.  
SECKEL, Edward  
SEIBEL, Charles M.  
SHORT, Frederick R.  
SHORTAL, Joseph A.  
SHUNK, Cdr. Robert F., USCG  
SIMMONS, Paul A., Jr.  
SISSINGH, Dr. Gerhard J.  
SMETHERS, Rollo G.  
SMULL, Thomas L. K.  
SOULÉ, Hartley A.  
STACK, John  
STANGE, Robert A.  
STEFANO, Nicholas M.  
STEWART, William  
STOKES, George M.  
STOLLER, Morton J.  
STULEN, Frank L.  
STULTZ, Lt. Jack T., USNR-R  
SYLVESTER, Maurice A.

TALMAGE, Donald B.  
TAPSCOTT, Robert J.  
TAYLOR, Elwood B.

THOMPSON, Floyd L.  
THORSON, Morris H.  
TINSLEY, William F.

TURNER, Lt. Col. Henry E., Jr.  
TURNER, Lindsey I., Jr.

VALZ, Fred M.  
VAUGHEN, Jack F.  
VELASQUEZ, Joseph  
VERMONT, Paul V.  
VOGLEWEDE, Thomas J.

NACA - Langley Laboratory  
NACA Headquarters  
Wright Air Development Center  
Subcommittee on Helicopters  
NACA - Ames Laboratory  
Committee on Power Plants for Aircraft  
NACA Headquarters  
Civil Aeronautics Administration  
Trans World Airlines  
NADC - Johnsville, Pennsylvania

Committee on Operating Problems  
Forrestal Research Center  
Cessna Aircraft Company  
General Motors Corporation  
NACA - Langley Laboratory  
Office of Naval Operations  
Subcommittee on Helicopters  
Kellett Aircraft Corporation  
Bureau of Aeronautics  
NACA Headquarters  
NACA - Langley Laboratory  
NACA - Langley Laboratory  
NATC - Patuxent River  
Subcommittee on Helicopters  
British Joint Services Mission  
NACA - Langley Laboratory  
NACA - Langley Laboratory  
Parsons Corporation  
NATC - Patuxent River  
NACA - Langley Laboratory

Air Transport Association of America  
NACA - Langley Laboratory  
Subcommittee on Engine Performance  
and Operation  
NACA - Langley Laboratory  
General Electric Company  
Transportation Training Command,  
Fort Eustis  
XVIII Airborne Corps - Fort Bragg  
NACA - Langley Laboratory

Bureau of Aeronautics  
Bell Aircraft Corporation  
Weber Aircraft Corporation  
Melpar  
NACA - Langley Laboratory

[REDACTED]

VON DOENHOFF, Albert E.

NACA - Langley Laboratory

WALKER, Chapman J.  
WALKER, Maj. William A.  
WARSETT, Paul

General Electric Company  
Air Research & Development Command  
Minneapolis-Honeywell Regulator  
Company

WARSKOW, Martin A.  
WATSON, Cdr. Joseph T., USN  
WEEKS, William H.  
WEILER, Robert E.  
WEINIG, Friedrich S.  
WELIMAN, Maj. Roy J.  
WERNECKE, Thomas L.  
WHITTEN, James B.  
WILLIAMS, James L.  
WILLIAMS, Robert M.  
WILSON, Thomas L.

The Port of New York Authority  
NATC - Patuxent River  
Civil Aeronautics Administration  
Westinghouse Electric Corporation  
General Electric Company  
Development Headquarters, USAF  
NATC - Patuxent River  
NACA - Langley Laboratory  
NACA - Langley Laboratory  
Bureau of Aeronautics  
Air Transport Service Div.,  
Department of the Army  
Office of Asst. Secretary of Defense  
NACA Headquarters  
University of Colorado  
Wright Air Development Center

WITBECK, Norman C.  
WOOD, Clotaire  
WOOD, Karl D. (Prof.)  
WORTH, Weldon

YNTEMA, Robert T.  
YOUNG, Raymond A.  
YOUNG, William Morris

NACA - Langley Laboratory  
Douglas Aircraft Company  
Office of the Chief Signal Officer,  
Department of the Army  
Polytechnic Institute of Brooklyn

YUAN, Shao Wen

**ROTOR  
AERODYNAMICS**

## AIRFOIL SECTION CHARACTERISTICS AT HIGH ANGLES OF ATTACK

By Laurence K. Loftin, Jr.

Langley Aeronautical Laboratory

## SUMMARY

Information from the literature and from recent investigations is used herein to summarize briefly the effects of airfoil section parameters and flow variables on the aerodynamic characteristics of two-dimensional symmetrical airfoils at high angles of attack. The results presented indicate that airfoil thickness ratio, Reynolds number, Mach number, and surface roughness can all have an important effect on the maximum lift coefficient. The effect of surface roughness seems to be particularly important. Not only can surface roughness cause large decreases in maximum lift coefficient, but also the magnitudes of the effects of Reynolds number, Mach number, and airfoil thickness ratio are much reduced by surface roughness. Beyond the stall, changes in section thickness ratio appear to have little effect on the aerodynamic characteristics of airfoil sections. An investigation of one section through an angle-of-attack range of from  $0^\circ$  to  $360^\circ$  shows that the drag coefficient reaches a value of 2 at an angle of attack of  $90^\circ$ .

## INTRODUCTION

The present paper is concerned with certain aspects of the behavior of airfoil sections at high angles of attack with particular emphasis on the needs of the helicopter designer. The state of our knowledge of the effects of several airfoil design parameters and flow variables on the maximum lift coefficient will be summarized first. This summary will be limited to symmetrical airfoils operating in the range of Mach number below 0.4 and is based on information which has been in the literature for a number of years (refs. 1 to 4). Some of the trends shown by recent investigations of the lift, drag, and pitching-moment characteristics of airfoil sections in the angle-of-attack range well beyond the stall will then be presented. The investigations leading to these results were made in response to a need of the designer for airfoil characteristics corresponding to conditions on the retreating blade of a high-speed helicopter and are only partially reported at the present time (ref. 5).



## SYMBOLS

$c$	airfoil chord
$c_d$	section drag coefficient
$c_l$	section lift coefficient
$c_{l_{MAX}}$	maximum section lift coefficient
$M$	Mach number
$R$	Reynolds number
$t$	maximum thickness of airfoil section
$x_{CP}$	center-of-pressure position, percent $c$
$\alpha$	angle of attack, deg

## RESULTS AND DISCUSSION

The nature of the effects of airfoil thickness, leading-edge surface condition, and Reynolds number on the maximum lift coefficient is shown in figure 1 for a Mach number of about 0.15. The maximum lift coefficient is plotted on the ordinate and the airfoil thickness is on the abscissa. The curves shown are based on results contained in references 1 to 3 for NACA 63-series and 64-series thickness forms. These particular thickness forms were chosen for discussion because their characteristics are thought to represent a good compromise between various desirable qualities at both high and low speeds. The trends in figure 1, however, may be considered typical of other symmetrical thickness forms having reasonably large leading-edge radii, such as, for example, thickness forms of the NACA 4-digit-series family. The solid lines are for airfoils with smooth surfaces and the dotted lines are for airfoils with roughened leading edges. The smooth condition referred to here is one in which the contour of the model is held very close to the specified ordinates and the surface is kept completely free of all dust, dirt, lint, paint blisters, and other disturbances which can be felt or seen. The rough surface condition is one in which the leading edge of the 24-inch-chord model is covered with 0.011-inch-diameter carborundum grains. The two surface conditions are thought to represent about the best and the worst that could be obtained in practice.

The trend of maximum lift with thickness shown in figure 1 for smooth sections at a Reynolds number of  $6.0 \times 10^6$  is characterized by a large increase in maximum lift coefficient with airfoil thickness in the range of thickness between 6 and 12 percent. A gradual decrease in maximum lift is noted as the thickness is increased to 18 percent. Somewhat the same trend is evidenced by the results at a Reynolds number of  $20 \times 10^6$  except for the continued increase in maximum lift as the thickness is increased to 18 percent. A very large reduction in the maximum lift of most of the airfoils is noted as the Reynolds number is reduced from  $6.0 \times 10^6$  to  $1.0 \times 10^6$ , with the result that increases in airfoil thickness have a very much reduced effect on the maximum lift coefficient at a Reynolds number of  $1.0 \times 10^6$  in comparison with  $6.0 \times 10^6$ . The trends shown for Reynolds numbers of  $1.0 \times 10^6$  and  $20.0 \times 10^6$  may be thought of as limits, in that variations in Reynolds number outside of this range would be expected to have only a small effect on the maximum lift coefficient. The results for a Reynolds number of  $6.0 \times 10^6$  indicate that, for airfoils in the thickness range between 9 and 15 percent, the major portion of the scale effect takes place between Reynolds numbers of  $1.0 \times 10^6$  and  $6.0 \times 10^6$ ; whereas, for airfoils outside this range of thickness, variations in Reynolds number above  $6.0 \times 10^6$  cause increases in maximum lift which may be significant. In any case, the exact shape of the curve of maximum lift coefficient against Reynolds number varies with airfoil section design. Fortunately, however, sufficient airfoil section data are available so that, by proper interpolation and comparison, a reasonable estimate can be made of the maximum lift coefficient corresponding to some particular Reynolds number.

A comparison of the data at a Reynolds number of  $6.0 \times 10^6$  for the airfoils with rough and smooth surfaces indicates that leading-edge roughness can cause a very large reduction in maximum lift. The magnitude of the effect is greatest for thickness ratios of the order of 12 percent of the chord, is somewhat reduced for the larger thickness ratios, and is negligible for a thickness ratio of 6 percent of the chord. As a result, increasing thickness is relatively much less powerful as a means of increasing the maximum lift of airfoils in the rough surface condition than in the smooth surface condition. Leading-edge roughness is seen to have only a small effect on maximum lift for a Reynolds number of  $1.0 \times 10^6$ . This small effect would be expected since the values of the maximum lift coefficient for the smooth condition at this Reynolds number are approaching the flat-plate value. Comparison of the results for Reynolds numbers of  $1.0 \times 10^6$  and  $6.0 \times 10^6$  indicates that the scale effect is relatively small for airfoils in the rough surface condition. This is also the case for Reynolds numbers higher than  $6.0 \times 10^6$  as is shown by results in reference 3 for a 9-percent-thick section for which

increasing the Reynolds number from  $6.0 \times 10^6$  to  $25.0 \times 10^6$  caused no change in the maximum lift coefficient for the rough surface condition.

Some indication of the effect of small increases in Mach number on the maximum lift coefficient can be obtained from data in reference 4 presented here in figure 2. The maximum lift coefficient is plotted against Mach number for Mach numbers from 0.1 to 0.4 and for a constant Reynolds number of  $6.0 \times 10^6$ . The airfoils are of 6-, 10-, and 15-percent thickness. The 10- and 15-percent-thick sections have approximately 1 percent camber whereas the 6-percent-thick section is symmetrical. Direct comparisons of the maximum lift coefficients of the 6-percent-thick section with those of the 10- and 15-percent-thick sections should not, therefore, be made. The results shown in this figure indicate rather large reductions in the maximum lift of smooth sections to accompany increases in Mach number from 0.1 to 0.4, at least for the 10- and 15-percent-thick sections. The Mach number has no effect on the maximum lift of the 6-percent-thick section except for the small rise at Mach number 0.2. In the rough surface condition, the Mach number has been found to have little effect on the maximum lift coefficient.

The trends shown in figures 1 and 2 indicate that airfoil thickness, Reynolds number, Mach number, and surface roughness can all have an important effect on the maximum lift coefficient. The effect of surface roughness seems to be particularly important. Not only can surface roughness cause large decreases in maximum lift coefficient, but also the magnitudes of the effects of Reynolds number, Mach number, and airfoil thickness ratio are much reduced by surface roughness. Thus, in a sense, severe surface roughness may tend to simplify airfoil selection problems. In view of the magnitude of the effect of surface condition, a means for estimating the nature of the surface condition of a rotor blade in relation to the smooth and rough leading-edge conditions employed in wind-tunnel investigations seems particularly important. Since this problem involves not only methods of blade construction and fabrication, but also the extent to which bugs and dirt have accumulated on the leading edge, general rules are difficult to formulate. It seems significant, however, that investigations of several rotors on the Langley helicopter test tower have yielded results which could be reproduced by calculations employing airfoil section maximum lift coefficients corresponding to the rough leading-edge condition.

With this brief summary of the maximum-lift problem, some of the trends shown by the more recent results obtained on airfoils at high angles of attack will be discussed. Six symmetrical airfoils of the NACA 64-series family were investigated through an angle-of-attack range extending from  $0^\circ$  to  $30^\circ$ . The airfoil thickness varied from 6 to 18 percent of the chord. In addition, an NACA 0012 section was tested. Although measurements were made at several subsonic Mach numbers, the trends to be

shown are for a Mach number of 0.5 and may be considered typical of all the results obtained.

The lift characteristics of the seven airfoils are shown in figure 3 in which the lift coefficient is plotted against angle of attack. The data are for a Reynolds number of  $1.3 \times 10^6$  and a smooth surface condition. After the first peak in the lift coefficient, which is usually defined as the maximum lift coefficient, all the airfoils are characterized by a drop in lift after which the lift again increases with angle of attack. The important trend indicated by these results is that, after an angle of attack of about  $14^\circ$  to  $16^\circ$ , the lift characteristics of all the airfoils tend to look very much alike. Although some differences are seen in the curves for the various airfoils, these differences are not thought to be particularly important because of the relatively small values of the dynamic pressure which exist in the vicinity of the retreating blade on a helicopter. As would be expected on the basis of the results shown in figures 1 and 2, the maximum amount of the difference in maximum lift shown by all of the airfoils is only about 0.2. At higher Reynolds numbers and lower Mach numbers, the differences in the maximum lift coefficients of the airfoils would, of course, become larger. Beyond the stall, however, it is thought that the curves shown here can be interpreted in terms of lift results at higher Reynolds numbers. For example, if the maximum lift coefficient were 1.4 and this lift coefficient occurred at an angle of attack of  $15^\circ$ , the data shown in figure 3 would be expected to correspond to those at the higher Reynolds number for angles of attack above  $18^\circ$  or  $19^\circ$ . The addition of leading-edge roughness was found to have little effect on the lift characteristics of the airfoils beyond the stall.

The chordwise position of the center of pressure is shown plotted against angle of attack for the seven airfoils in figure 4. The center of pressure is seen to shift from about the 25-percent-chord station to about the 43-percent-chord station as the airfoil passes from the unstalled to the stalled condition. The angle of attack at which this transition begins varies with the airfoil section and corresponds to the angle at which the lift curve starts to bend preceding the attainment of maximum lift. Beyond the stall, however, there appears to be little effect of airfoil section thickness on the position of the center of pressure, nor does the center of pressure shift very much with angle of attack.

The section drag coefficient is plotted against angle of attack in figure 5 for the seven airfoil sections. Again the obvious conclusion is that variations in airfoil thickness have little effect on the drag beyond the stall.

Relatively large portions of the retreating blade on a high-speed helicopter may be operating at angles of attack in the range between  $0^\circ$

and  $180^\circ$ . In order to provide some indication of the characteristics of an airfoil section through such an angle-of-attack range, the NACA 0012 section has been tested through an angle-of-attack range extending from  $0^\circ$  to  $360^\circ$ . The Reynolds number of these tests was about  $2.0 \times 10^6$  and the Mach number was no greater than 0.15. The lift and drag characteristics obtained are plotted against angle of attack in figure 6. The high value of the drag at an angle of attack of  $90^\circ$  is to be noted. This value of 2.0 checks the value of 2.0 given by Wieselsberger in reference 6 for a two-dimensional flat plate perpendicular to the wind. These same German results show a marked effect of aspect ratio on the drag at an angle of attack of  $90^\circ$ . For example, the drag coefficient of an aspect-ratio-20 flat plate is shown to be about 1.48 in comparison with the two-dimensional value of 2.0. This result emphasized a basic question as to how two-dimensional data should be applied to a rotating wing for those cases in which the flow over one surface is characterized by extensive regions of separation. Unfortunately, little information dealing with this problem is available at present.

#### CONCLUDING REMARKS

The results presented indicate that airfoil thickness ratio, Reynolds number, Mach number, and surface roughness can all have an important effect on the maximum lift coefficient. The effect of surface roughness seems to be particularly important. Not only can surface roughness cause large decreases in maximum lift coefficient, but also the magnitudes of the effects of Reynolds number, Mach number, and airfoil thickness ratio are much reduced by surface roughness. Beyond the stall, changes in section thickness ratio appear to have little effect on the aerodynamic characteristics of the airfoil sections. The high value of the drag coefficient obtained with an airfoil section at an angle of attack of  $90^\circ$  is in agreement with the value of 2 given in the literature for an infinite flat plate inclined normal to the flow; the marked effect of aspect ratio on the drag at an angle of attack of  $90^\circ$  emphasizes the question as to how two-dimensional data should be applied to a rotating wing on which extensive regions of separation are present.

## REFERENCES

1. Abbott, Ira H., Von Doenhoff, Albert E., and Stivers, Louis S., Jr.: Summary of Airfoil Data. NACA Rep. 824, 1945. (Supersedes NACA WR L-560.)
2. Loftin, Laurence K., Jr., and Smith, Hamilton, A.: Aerodynamic Characteristics of 15 NACA Airfoil Sections at Seven Reynolds Numbers From  $0.7 \times 10^6$  to  $9.0 \times 10^6$ . NACA TN 1945, 1949.
3. Loftin, Laurence K., Jr., and Bursnall, William J.: The Effects of Variations in Reynolds Number Between  $3.0 \times 10^6$  and  $25.0 \times 10^6$  Upon the Aerodynamic Characteristics of a Number of NACA 6-Series Airfoil Sections. NACA Rep. 964, 1950. (Supersedes NACA TN 1773.)
4. Racisz, Stanley F.: Effects of Independent Variations of Mach Number and Reynolds Number on the Maximum Lift Coefficients of Four NACA 6-Series Airfoil Sections. NACA TN 2824, 1952.
5. Wilson, Homer B., Jr., and Horton, Elmer A.: Aerodynamic Characteristics at High and Low Subsonic Mach Numbers of Four NACA 6-Series Airfoil Sections at Angles of Attack From  $-2^\circ$  to  $31^\circ$ . NACA RM L53C20, 1953.
6. Wieselsberger, C.: Airplane Body (Non Lifting System) Drag and Influence on Lifting System. Vol. IV of Aerodynamic Theory, div. K, ch. II, sec. 1, W. F. Durand, ed., Julius Springer (Berlin), 1935, pp. 141-146.

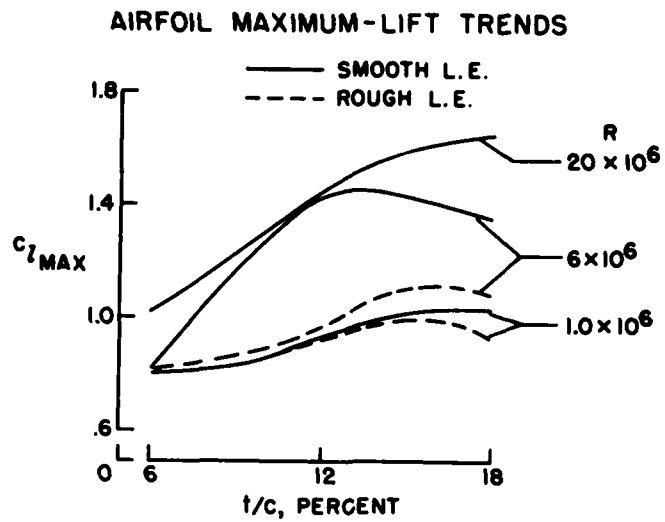


Figure 1

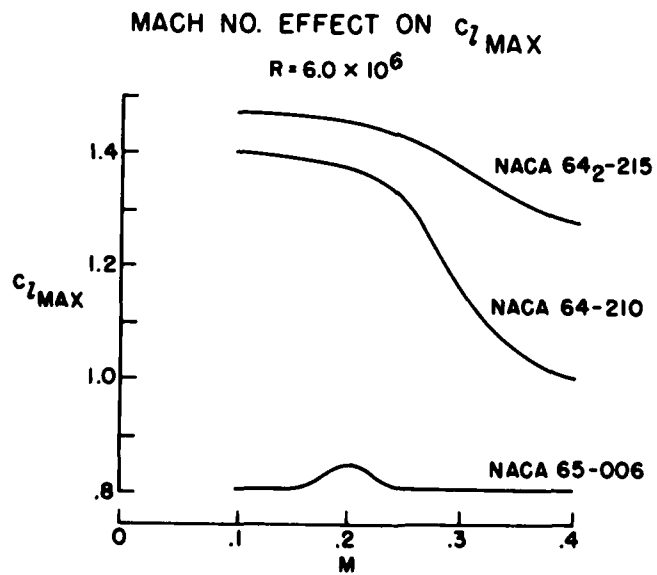


Figure 2

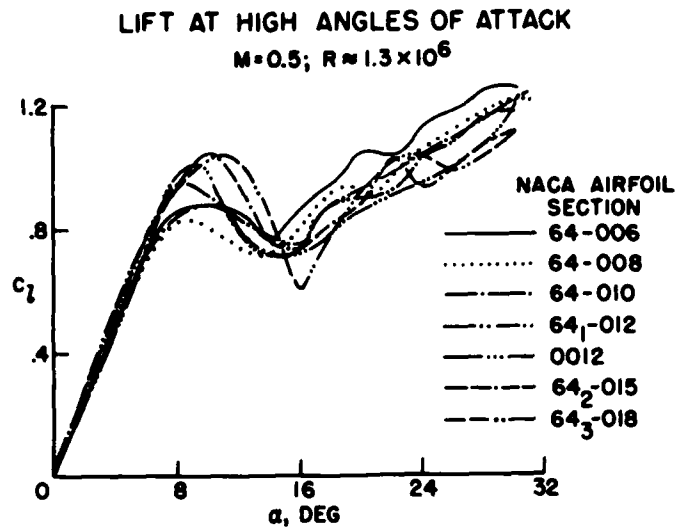


Figure 3

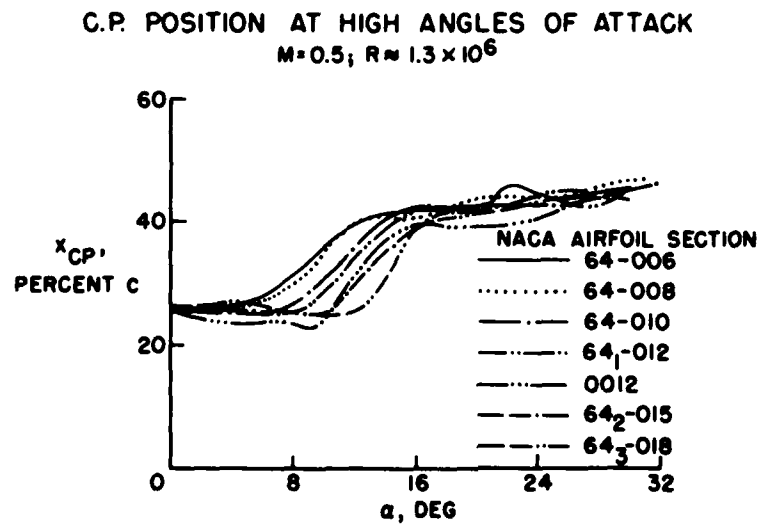


Figure 4



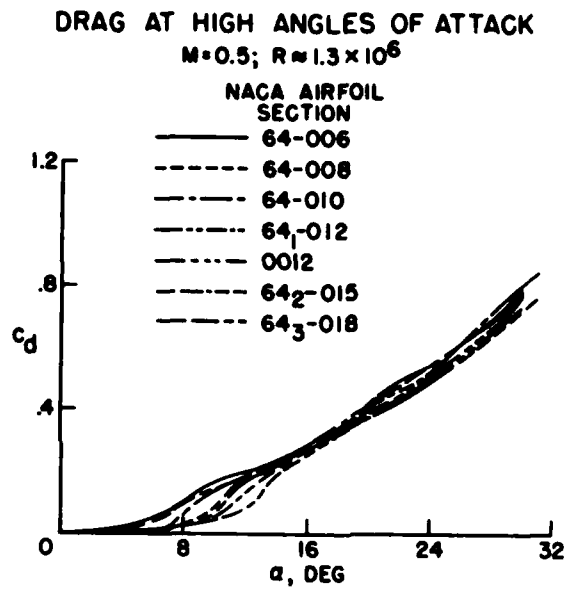


Figure 5

**LIFT AND DRAG FOR ANGLES OF ATTACK TO 360°**  
 NACA 0012 AIRFOIL SECTION

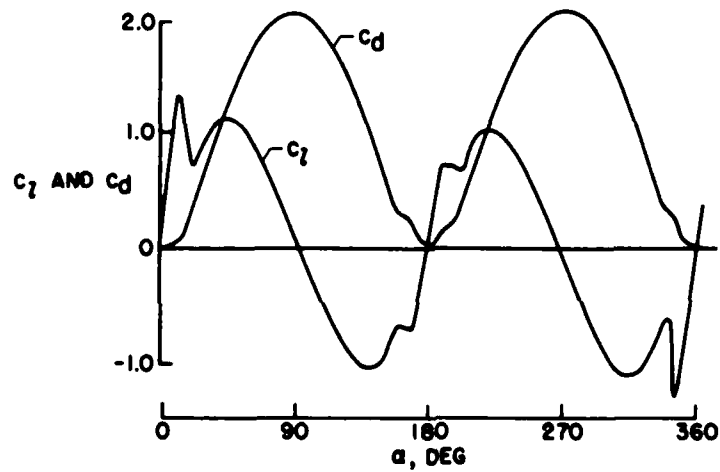


Figure 6

## AIRFOIL SECTION CHARACTERISTICS AT TRANSONIC SPEEDS

By W. F. Lindsey

Langley Aeronautical Laboratory

The tip Mach numbers for the rotor blades of high-performance helicopters now being considered extend into the lower supersonic range. The designer is thus concerned with the effects of blade-profile shape parameters on the aerodynamic characteristics and the variation of those characteristics throughout the speed range, from low speed through sonic and into the supersonic range. The purpose of this paper is to summarize present information on the variation of aerodynamic characteristics of two-dimensional profiles in the transonic Mach number range from about 0.7 to 1.5.

Before the data are summarized, however, the existence of numerical discrepancies between available data from different facilities is discussed. One factor is the difference in minimum drag coefficient, which is dependent upon Reynolds number, extent of laminar flow on the profile, model-surface condition, and the turbulence level in the tunnel. These differences can be reduced, however, by examining the data on the basis of pressure-drag coefficients, that is, the drag coefficient minus the skin-friction drag, which will be done in this paper. The factor however that contributes most to the discrepancies between facilities, particularly in the transonic or mixed-flow region, is usually the jet-boundary effects. One of the greatest difficulties in correctly assessing the true values of coefficients in the transonic speed range is the lack of an established standard of comparison. The only methods available at present are interpolation, extrapolation, and careful comparison with other results. A careful comparison of a multitude of available two-dimensional-airfoil data from various sources (refs. 1 to 18) has shown that, while differences exist in the numerical values of coefficients from the different facilities, all sources show the same trends in lift, drag, and pitching-moment characteristics as affected by changes in thickness, camber, and shape or thickness distribution.

Pressure-drag coefficients at zero lift on two 12-percent-thick profiles tested under different conditions are presented in figure 1. Tests on both profiles were made in a closed-throat tunnel on models of different sizes and corresponding changes in model-chord to tunnel-height ratio  $c/h$  are shown. The closed-throat tunnel has been the source of by far the largest part of two-dimensional-airfoil data. The data in this figure have been corrected, using the accepted methods of correcting for jet-boundary conditions (ref. 19). It is obvious that these test results are inadequately corrected at the higher test Mach numbers. If the model-chord to tunnel-height ratio had been smaller, requiring the

corrections for jet-boundary effects to be smaller, the corrected values would approach more closely a true value.

In order to avoid the choking restriction of a closed-throat tunnel, the open-throat tunnel was developed which permitted data to be obtained at indicated Mach numbers up to 1. The results of an investigation from an open-throat tunnel showing the effects of thickness, camber, and shape are available from an investigation by Daley and Dick (ref. 13). It is apparent from tests on the NACA 64<sub>1</sub>A012 airfoil that these uncorrected data are subject to jet-boundary effects, and in the opposite direction from the closed-throat-tunnel results. Whereas the corrections are adequately defined for the purely subsonic flow regime (refs. 20 and 21), they are inadequately substantiated for the high subsonic Mach numbers, especially those near 1 where the theoretical corrections approached infinity.

In order to avoid the Mach number limitations of the closed- and open-throat tunnels, and to minimize the jet-boundary effects (refs. 22 and 23), transonic tunnels have been developed recently to permit investigations to be conducted at Mach numbers continuously through 1 and into the supersonic range. Unfortunately, conditions have not permitted thorough investigations to be conducted on two-dimensional airfoils in these modern tunnels, although a facility is under construction specifically designed for two-dimensional-airfoil investigations through the transonic speed range. There is, however, some information from a very recent test on an NACA 0012 airfoil in a transonic or slotted-throat tunnel. The drag results from that investigation are shown in figure 1. A comparison of the data with the closed- and open-throat-tunnel data indicates that the values are probably of the correct order. Since the only source of information on the effects of profile variables on the aerodynamic characteristics of airfoils at Mach numbers in the range from 0.9 to 1.0 is from the open-throat-tunnel data (ref. 13), the subsonic part of the present paper will be based upon that data. As previously stated, while numerical discrepancies between data from various facilities are known to exist and have been pointed out, it is also known that the trends of all the data from the various sources are in agreement; therefore, the effects of profile variables that will be discussed can be considered as the general effects of many investigations.

In order to provide some background on the changes in the aerodynamic characteristics in the transonic speed range, schlieren photographs of the flow have been selected for a 9-percent-thick airfoil which is representative of thick airfoils (ref. 13). Figure 2 shows the flow pictures with superimposed pressure-distribution diagrams. At a Mach number of 0.79, the upper-surface shock is near the 50-percent-chord station. This location of the shock produces a large region of low pressures on the forward part of the profile. At a Mach number of 0.87, where the shock is more rearwardly located, separation is occurring

on the profile. At this Mach number the lower-surface shock is also starting to make its appearance and, simultaneously, the pressures on the lower surface are rapidly decreasing, which produces an opposing load. An increase in Mach number to 0.94 produces an increase in the suction pressures on the lower surface and, with the lower-surface shock located downstream of the upper-surface shock, a reverse load occurs on the rear of the airfoil. An examination of these pressure distributions at Mach numbers up to 0.94 shows that there has been a continuous decrease in load near the leading edge, a result of a decrease in upwash and circulation produced by the limitation imposed on the forward propagation of pressures by the supersonic-flow regions. At a Mach number of 1, shocks from both surfaces are near the trailing edge. The load distribution has approached a rectangular form, as opposed to the triangular loading at low speeds, and relatively stable conditions exist. Further increase in speed will produce only small changes in the character of the flow, as evidenced by figure 3, which shows similar data at a Mach number of 1.25. The pressure distribution for this figure was determined from the loading due to lift from reference 24 and the zero-lift pressure distribution computed by the method of reference 25. At this Mach number the bow wave is detached from the model and a mixed-flow region still exists. Further increase in speed would cause the bow wave to approach the leading edge.

The primary profile shape factors of airfoils are thickness, thickness distribution, and camber. Of these factors, tests at high subsonic speeds have shown that thickness is the most important variable, insofar as its effects on aerodynamic characteristics are concerned (refs. 1 to 18). Thickness distribution, or shape changes of a given thickness within reasonable limits, is a second-order effect in that shape changes can produce an improvement in the characteristics in some operating ranges although losses might occur in other ranges (refs. 2, 3, 9 to 13, 16, and 18). Differences between profiles of different thickness distribution in comparison with thickness effects are quite small. Camber (refs. 1, 3, 4, 5, 7, 8, 11, 13, 15, and 17) and thickness are similar insofar as their effects on maximum  $l/d$  are concerned. The effects of camber on lift-curve slopes are small. However, the changes in angle of zero lift that occur for cambered sections at low transonic speeds would require significant changes in angle of attack to maintain a given lift and thus are comparable to the effect of increasing thickness on decreasing lift-curve slope. The effects of camber on changes in pitching-moment characteristics are in large measure dependent on the shape of the camber line (refs. 5 and 18). Since thickness is a primary factor affecting the characteristics through the Mach number range from 0.7 to 1.5, this discussion will be confined principally to the effects of thickness.

The variation in pressure drag-coefficient at zero lift for profiles of various thicknesses is presented in figure 4. For the speed range

covered, and extending downward toward zero Mach number, the pressure-drag coefficient can be expressed as  $c_{dp} = k\left(\frac{t}{c}\right)^n$ . At very low speeds,  $c_{dp}$  is approximately zero and  $n$  can be taken as approximately zero.

At transonic speeds, particularly speeds near Mach number 1, the exponent  $n$  is, from the transonic similarity law (refs. 26 and 27), five-thirds. In the supersonic speed range the exponent becomes 2 (ref. 28). This exponential relation, however, holds only if the profile has a reasonable shape.

The variation of drag with thickness at Mach number 1 and also at a Mach number of 1.44 will be examined to determine what constitutes a reasonable shape. Figure 5 shows pressure-drag variation with thickness at Mach number 1. It is noted that the NACA 64A-series profiles in figure 4 form a curve that can be represented by  $c_{dp} = 3.7\left(\frac{t}{c}\right)^{5/3}$ . A correlation of the characteristics of 22 rectangular wings of symmetrical profile and various aspect ratios by McDevitt (ref. 29) indicated, by the use of the transonic similarity laws for the minimum pressure-drag coefficient, that the extrapolated values for two-dimensional flow would be  $3.55\left(\frac{t}{c}\right)^{5/3}$ , which is in very close agreement with the NACA 64A-series result. Some small variation in  $k$  with change in family might be expected (see ref. 24). The work of Guderley and Yoshihara (ref. 30) indicated that the drag of a wedge profile varies in accordance with  $4.1\left(\frac{t}{c}\right)^{5/3}$ , thus producing a higher drag than the round-nose profile. Figure 5 also shows that larger shape changes, for example, the slab profile having cylindrical leading and trailing edges extrapolated from an investigation at the University of Michigan (ref. 31), have a drag variation that is directly proportional to thickness. Unpublished data from the Langley 4- by 19-inch semiopen tunnel of a 2-percent-thick profile having the same section are in agreement with the tests at the University of Michigan. The tests in the Langley 4- by 19-inch semiopen tunnel show that a reduction in bluntness from a cylinder to a 10:1 ellipse produces a large reduction in drag. It is of interest to note that the drag of a cylindrical-leading-edge profile varies in accordance with an assumption that stagnation pressure exists forward of the thickness and stream static exists on the after part. This variation is of necessity a linear variation of drag with thickness ratio.

Similar data for Mach number 1.44 are presented in figure 6. At this speed the wedge profile has the least drag and it is approximately three-fourths of that for the circular-arc. Experimental data from an investigation by Czarnecki and Mueller (ref. 32) extrapolated to somewhat lower Mach numbers are shown in agreement with the theoretical drag. Contrary to the trends at Mach number 1, where the round-nose profiles provided less drag than the wedge, the results of an investigation by

[REDACTED]

Rainey (ref. 25) on a round-nose 9-percent-thick profile at supersonic speeds show higher drags than those for either circular-arc or wedge. The increase in drag was shown in reference 25 to be a direct result of the large region of high pressure encountered on the leading edge of the profile. Similar effects of bluntness are exhibited by the investigation of reference 31 for circular-arc profiles having somewhat blunt leading and trailing edges. The radii were equal to one-tenth of the thickness-chord ratio. Further blunting of the profile, or divergence from a reasonable shape (to  $20^\circ$  included angle, to  $40^\circ$  included angle, to cylindrical), caused large increases in drag and the drag variation with thickness approached a linear variation. ( $H_2$  is stagnation pressure behind a normal shock.) Similar effects were noted in the investigation by Busemann and Walchner (ref. 33) and by Holder and Chinneck (ref. 34).

Figures 5 and 6 show that the exponential variation of drag with thickness holds for reasonably shaped profiles and that what constitutes a reasonable shape can change as the Mach number is increased from 1 into the purely supersonic range.

The effects of thickness on pressure drag of reasonably shaped profiles are presented in figure 5 which shows that the Mach number at which the drag starts rising increases as the thickness ratio is decreased. This variation is in accordance with an earlier formation of shock on the thick profiles than on the thin ones, and the rise in drag is directly attributable to the formation and growth of compression shocks. This figure also presents a comparison of the data from a semiopen tunnel (ref. 13) with the results from drop tests of an NACA 65-series wing having an aspect ratio of 7.6 and thicknesses of 6, 9, and 12 percent (ref. 35). The correspondence of the test results from the two sources indicates good agreement, especially since previous tests on effects of aspect ratio (refs. 36 to 39) have indicated that for finite-span wings the Mach number for drag rise would be delayed to higher Mach numbers and that the peak drag would be alleviated.

At supersonic speeds theoretical values are presented for both wedge and circular-arc profiles. As previously stated, the wedge profile has about three-fourths of the drag of a circular-arc of the same thickness. Furthermore, the included angle of the wedge is smaller and shock attachment occurs at a lower Mach number. The Mach numbers for shock attachment are indicated by the ticks on the curves. The extension of the drag curves to Mach numbers below the ticks is necessarily hypothetical.

The manner of transition from Mach number 1 into the supersonic range would be dependent principally upon the leading-edge shape. Presumably, the drag of a round-nose profile would exceed that theoretically predicted for either the wedge or circular-arc profile for the same thickness ratio and would only approach the theoretical value at high supersonic Mach numbers; whereas, the wedge profile would closely approach the theoretical drag at a Mach number near the Mach number for shock attachment.

[REDACTED]

[REDACTED]

These results are for a lift coefficient of zero. At a higher lift coefficient, if the drag followed the usually assumed parabolic variation with lift, that is, the increment in drag is proportional to the square of the lift coefficient, the low-transonic drag pattern would be shifted to higher drag coefficients. The transonic similarity law, on the other hand, indicates that the increment in drag due to lift is proportional to the product of the lift coefficient squared and the thickness to the  $1/3$  power. This would produce increases in drag that were larger for the thick profile than for the thin. Experiment, however, shows that both approaches are approximations only and that neither approach is correct. The experimentally determined differences due to thickness at an increased lift coefficient are shifted to somewhat lower Mach numbers and the spread from thick to thin airfoil is decreased. The effect of angle of attack or lift coefficient in increasing the velocities on a profile at low speeds is dependent upon thickness, the thinner the profile the larger the increment in velocity near the leading edge for a given change in angle of attack or lift coefficient. As a consequence, the differences in the Mach number for shock formation as affected by thickness are reduced and the differences in drag rise are correspondingly reduced. Thus, at higher lift coefficients the relative effects of thickness would be somewhat less than shown for zero lift.

The lift-curve slopes for airfoils of various thicknesses are shown in figure 7 as a function of Mach number. The solid curves in the subsonic Mach number range were obtained at a lift coefficient of 0.2. Where an examination of the data (ref. 13) at lift coefficients from 0 to 0.2 revealed no appreciable nonlinearities for the thin (4 and 6 percent) profiles, the thicker profiles did exhibit considerable nonlinearity at Mach numbers around 0.9. Since it was believed that this nonlinear variation would be of interest, the region is indicated by including a curve for lift-curve slope at zero lift. It is noted that the extent of nonlinearity diminishes with a reduction in thickness. As in the case of the minimum drag coefficients shown in figure 4, the Mach number at which the lift-curve slope starts decreasing increases as the thickness is decreased. This behavior is in accord with the manner and growth of shocks and the relative movements of the shocks on the two surfaces of the airfoils. The continued rearward movement of the shock on the thin profile with no appreciable changes in flow on the lower surface results in a continued increase in lift and lift-curve slope to some maximum value at a high Mach number. On the thick profiles, however, the rapid growth of the shock on the lower surface and its rapid rearward movement, combined with the stoppage of shock movement on the upper surface, which was assisted by the occurrence of separation, produced a reversal in load, contributing to a rapid drop-off in the lift and consequent drop-off in the lift-curve slope. The erratic behavior of the lift, particularly for the thicker profiles, precludes lift-curve-slope correlation with similarity laws. A similar limitation was observed by McDevitt in correlating a series of rectangular wings, using the transonic similarity laws (ref. 29).

[REDACTED]

At supersonic speeds, the theoretical lift-curve slope is independent of thickness. Some comparisons with preliminary results (refs. 40 to 42) have indicated fair agreement. At Mach numbers above 1.5, experimental results by Czarnecki and Mueller (ref. 32) and Rainey (ref. 25) on both round-nose and sharp-nose profiles are in reasonably good agreement with theory and indicate that lift-curve slope is much less sensitive to shock attachment than is drag.

The maximum lift-drag ratios are presented in figure 8. At low Mach numbers the maximum lift-drag ratio increases with thickness. With increase in Mach number, however, a change occurs which follows from the previously discussed lift and drag variations and demonstrated flow conditions. The change is a decrease in the maximum lift-drag ratio with increase in thickness. At Mach numbers near 1 the lift-drag ratio varies in accordance with the transonic similarity law, which states that the product of thickness and lift-drag ratio is a constant. At supersonic speeds, the same trends are retained, as indicated by theory. These theoretical values do include an estimated skin-friction drag and result in some small variation in lift-drag ratio with Mach number.

The center-of-pressure positions of these airfoils at a lift coefficient of approximately 0.2 are shown in figure 9. The previously observed large variations in characteristics on the thicker profiles are still evident in the center-of-pressure shifts for the 9- and 12-percent-thick airfoils at Mach numbers around 0.9 and above. The large forward shifts in center of pressure are due entirely to the rapid growth and rearward movement of shocks on the lower surface and are accentuated by the deceleration in the rearward movement of the upper-surface shock. The combination of effects produces the load reversals shown in figure 2 and the forward location of the center of pressure. At supersonic speeds second-order theory, which has been used throughout this discussion, shows a small consistent effect of thickness, that is, a decrease in thickness causes a rearward movement of the center of pressure. Linear theory, essentially for very small disturbances, estimates a center-of-pressure location at 50 percent chord.

Results have been presented to show the variation in aerodynamic characteristics of airfoils through the transonic and into the supersonic speed range. The data indicated that erratic variations occurred in the low transonic speed range and, where comparisons were available at transonic and supersonic speeds, theory and experiment were in good agreement. The results, however, were for two-dimensional flows; whereas, for helicopter applications a three-dimensional flow exists. The flow is further complicated by having Mach number gradients along the radius of the blade and at transonic speeds the independence of blade elements from adjacent elements cannot be assumed. Cross flows will occur and adjacent elements will exert mutual influences. These effects have been observed in propeller tests. In the simple case of a rectangular wing,



tests have shown (refs. 36 to 39) that the overall magnitude of the changes will be reduced as a result of the relieving effect of the flow around the wing tip; also, the Mach number at which changes occur will be delayed to somewhat higher Mach numbers. The overall general behavior, and the effects of thickness on this behavior, however, are retained, even for an aspect ratio as low as 4.

## REFERENCES

1. Stack, John: The N.A.C.A. High-Speed Wind Tunnel and Tests of Six Propeller Sections. NACA Rep. 463, 1933.
2. Stack, John, and Von Doenhoff, Albert E.: Tests of 16 Related Airfoils at High Speeds. NACA Rep. 492, 1934.
3. Graham, Donald J., Nitzberg, Gerald E., and Olson, Robert N.: A Systematic Investigation of Pressure Distributions at High Speeds Over Five Representative NACA Low-Drag and Conventional Airfoil Sections. NACA Rep. 832, 1945.
4. Mair, W. A.: German High Speed Wind Tunnel Tests on Four Aerofoils of Different Camber, With Comments. Tech. Note Aero. 1685, British R.A.E., Sept. 1945.
5. Graham, Donald J.: The Development of Cambered Airfoil Sections Having Favorable Lift Characteristics at Supercritical Mach Numbers. NACA TN 1771, 1948.
6. Göthert, B.: Airfoil Measurements in the DVL High-Speed Wind Tunnel (2.7-Meter Diameter). NACA TM 1240, 1949.
7. Lindsey, W. F., Stevenson, D. B., and Daley, Bernard N.: Aerodynamic Characteristics of 24 NACA 16-Series Airfoils at Mach Numbers Between 0.3 and 0.8. NACA TN 1546, 1948.
8. Summers, James L., and Treon, Stuart L.: The Effects of Amount and Type of Camber on the Variation With Mach Number of the Aerodynamic Characteristics of a 10-Percent-Thick NACA 64A-Series Airfoil Section. NACA TN 2096, 1950.
9. Humphreys, Milton D., and Robinson, Raymond A.: The Effect of Changes in the Leading-Edge Radius on the Aerodynamic Characteristics of a Symmetrical, 9-Percent-Thick Airfoil at High-Subsonic Mach Numbers. NACA RM L9L09, 1950.
10. Summers, James L., and Graham, Donald J.: Effects of Systematic Changes of Trailing-Edge Angle and Leading-Edge Radius on the Variation With Mach Number of the Aerodynamic Characteristics of a 10-Percent-Chord-Thick NACA Airfoil Section. NACA RM A9G18, 1949.
11. Van Dyke, Milton D.: High-Speed Subsonic Characteristics of 16 NACA 6-Series Airfoil Sections. NACA TN 2670, 1952.

12. Loftin, Laurence K., Jr., and Von Doenhoff, Albert E.: Exploratory Investigation at High and Low Subsonic Mach Numbers of Two Experimental 6-Percent-Thick Airfoil Sections Designed To Have High Maximum Lift Coefficients. NACA RM L51F06, 1951.
- ✓ 13. Daley, Bernard N., and Dick, Richard S.: Effect of Thickness, Camber, and Thickness Distribution on Airfoil Characteristics at Mach Numbers Up to 1.0. NACA RM L52G31a, 1952.
14. Wilson, Homer B., Jr., and Horton, Elmer A.: Aerodynamic Characteristics at High and Low Subsonic Mach Numbers of Four NACA 6-Series Airfoil Sections at Angles of Attack From  $-2^{\circ}$  to  $31^{\circ}$ . NACA RM L53C20, 1953.
15. Hemenover, Albert D.: The Effects of Camber on the Variation With Mach Number of the Aerodynamic Characteristics of a 10-Percent-Thick Modified NACA Four-Digit-Series Airfoil Section. NACA TN 2998, 1953.
16. Berggren, Robert E., and Graham, Donald J.: Effects of Leading-Edge Radius and Maximum Thickness-Chord Ratio on the Variation With Mach Number of the Aerodynamic Characteristics of Several Thin NACA Airfoil Sections. NACA TN 3172, 1954.
17. Humphreys, Milton D.: Transonic Aerodynamic Characteristics of an NACA 64A006 Airfoil Section With a 15-Percent-Chord Leading-Edge Flap. NACA RM L53G23, 1953.
18. Loftin, Laurence K., Jr.: Aerodynamic Characteristics of the NACA 64-010 and 0010-1.10 40/1.051 Airfoil Sections at High and Low Subsonic Speeds and Relatively High Reynolds Numbers. NACA RM L54C11, 1954. (Prospective NACA TN.)
19. Allen, H. Julian, and Vincenti, Walter G.: Wall Interference in a Two-Dimensional-Flow Wind Tunnel, With Consideration of the Effect of Compressibility. NACA Rep. 782, 1944. (Supersedes NACA WR A-63.)
20. Katzoff, S., Gardner, Clifford S., Diesendruck, Leo, and Eisenstadt, Bertram J.: Linear Theory of Boundary Effects in Open Wind Tunnels With Finite Jet Lengths. NACA Rep. 976, 1950. (Supersedes NACA TN 1826.)
21. Goldstein, S., and Young, A. D.: The Linear Perturbation Theory of Compressible Flow, With Applications to Wind-Tunnel Interference. R. & M. No. 1909, British A.R.C., 1943.

22. Davis, Don D., Jr., and Moore, Dewey: Analytical Study of Blockage- and Lift-Interference Corrections for Slotted Tunnels Obtained by the Substitution of an Equivalent Homogeneous Boundary for the Discrete Slots. NACA RM L53E07b, 1953.
23. Boswinkle, Robert W., Jr.: Comparison of Lift-Curve Slopes for a Model Tested in Two Slotted Tunnels of Different Sizes at High Subsonic Speeds. NACA RM L53E20a, 1953.
24. Lindsey, Walter F., and Dick, Richard S.: Two-Dimensional Chordwise Load Distributions at Transonic Speeds. NACA RM L51I07, 1952.
25. Rainey, Robert W.: Pressure Measurements at Supersonic Speeds on a Section of a Rectangular Wing Having an NACA 65-009 Profile. NACA RM L9L16, 1950.
26. Busemann, Adolf: Application of Transonic Similarity. NACA TN 2687, 1952.
27. Kaplan, Carl: On Similarity Rules for Transonic Flows. NACA Rep. 894, 1948. (Supersedes NACA TN 1527.)
28. The Staff of the Ames 1- by 3-Foot Supersonic Wind-Tunnel Section: Notes and Tables for Use in the Analysis of Supersonic Flow. NACA TN 1428, 1947.
29. McDevitt, John B.: A Correlation by Means of the Transonic Similarity Rules of the Experimentally Determined Characteristics of 22 Rectangular Wings of Symmetrical Profile. NACA RM A51L17b, 1952.
30. Guderley, G., and Yoshihara, H.: The Flow Over a Wedge Profile at Mach Number 1. Jour. Aero. Sci., vol. 17, no. 11, Nov. 1950, pp. 723-735.
31. Amick, J. L., Clark, E. T., Culbertson, P. E., McLeish, W. M., and Liepman, H. P.: Wind Tunnel Tests of Seventeen Airfoils at Supersonic Speeds. Rep. No. WTM-240 (Contract AF-33(038)-17737-Part I E.O. No. 587-145 BR-1), Eng. Res. Inst., Univ. Mich., Mar. 1953.
32. Czarnecki, K. R., and Mueller, James N.: Investigation at Supersonic Speeds of Some of the Factors Affecting the Flow Over a Rectangular Wing With Symmetrical Circular-Arc Section and 30-Percent-Chord Trailing-Edge Flap. NACA RM L50J18, 1951.
33. Busemann, A., and Walchner, O.: Profileigenschaften bei Überschallgeschwindigkeit. Forsch. auf dem Geb. des Ingenieurw. Ausg. A, Bd. 4, Heft 2, Mar.-Apr. 1933, pp. 87-92.

- [REDACTED]
34. Holder, D. W., and Chinneck, A.: Observations of the Flow Past Elliptic-Nosed Two-Dimensional Cylinders and Bodies of Revolution in Supersonic Airstreams. Rep. No. F.M. 1597, British N.P.L. (Rep. No. 14,216, A.R.C.), Aug. 24, 1951.
  35. Thompson, Jim Rogers, and Marschner, Bernard W.: Comparative Drag Measurements at Transonic Speeds of an NACA 65-006 Airfoil and a Symmetrical Circular-Arc Airfoil. NACA RM L6J30, 1947.
  36. Stack, John, and Lindsey, W. F.: Characteristics of Low-Aspect-Ratio Wings at Supercritical Mach Numbers. NACA Rep. 922, 1949. (Supersedes NACA TN 1665.)
  37. Lindsey, W. F., and Humphreys, Milton D.: Effects of Aspect Ratio on Air Flow at High Subsonic Mach Numbers. NACA TN 2720, 1952. (Supersedes NACA RM L8G23.)
  38. Thompson, Jim Rogers, and Mathews, Charles W.: Measurements of the Effects of Thickness Ratio and Aspect Ratio on the Drag of Rectangular-Plan-Form Airfoils at Transonic Speeds. NACA RM L7E08, 1947.
  39. Nelson, Warren H., and McDevitt, John B.: The Transonic Characteristics of 17 Rectangular, Symmetrical Wing Models of Varying Aspect Ratio and Thickness. NACA RM A51A12, 1951.
  40. Hilton, W. F.: Force Coefficients on Round Nosed Aerofoils at Supersonic Speeds. Rep. No. F.M. 953, British N.P.L. (Rep. 9756, A.R.C.), June 24, 1946.
  41. Hilton, W. F., and Pruden, F. W.: Subsonic and Supersonic High Speed Tunnel Tests of a Faired Double Wedge Aerofoil. R. & M. No. 2057, British A.R.C., 1943.
  42. Pruden, F. W.: Tests of a Double-Wedge Aerofoil With a 30 Per Cent. Control Flap Over a Range of Supersonic Speeds. R. & M. No. 2197, British A.R.C., Sept. 1945.
- [REDACTED]

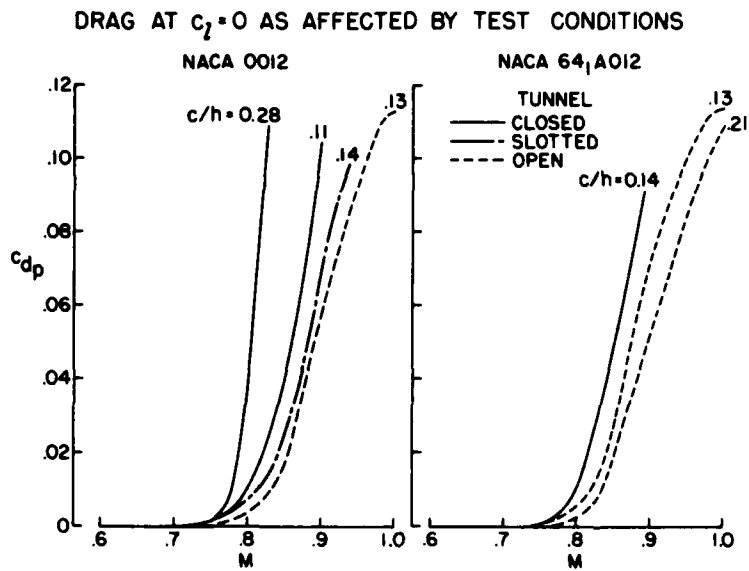


Figure 1

## FLOW AND LOADS FOR LIFTING AIRFOIL



Figure 2

FLOW AND LOAD ON LIFTING AIRFOIL  
M=1.25



Figure 3

PRESS-DRAG COEFF AT  $c_l = 0$

- EXP (NACA 64A-SERIES)
- - - DROP TESTS (NACA 65-SERIES, A-76)
- WEDGE THEORY
- - - CIRC ARC, THEORY

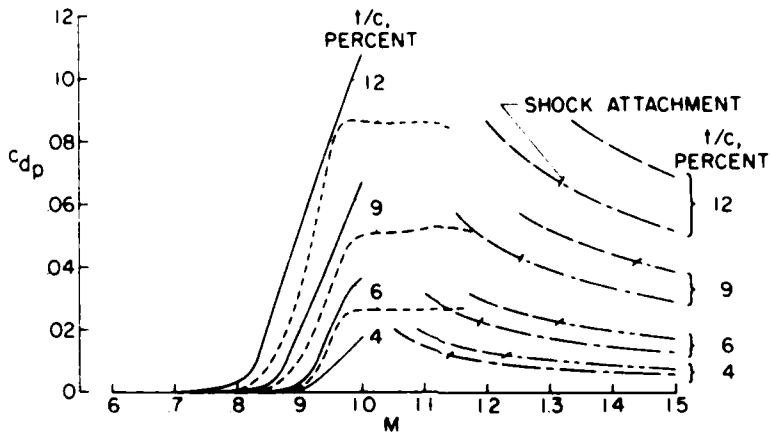


Figure 4

SHAPE EFFECTS ON PRESS.-DRAG COEFF. AT  $c_l=0$

M=1.0

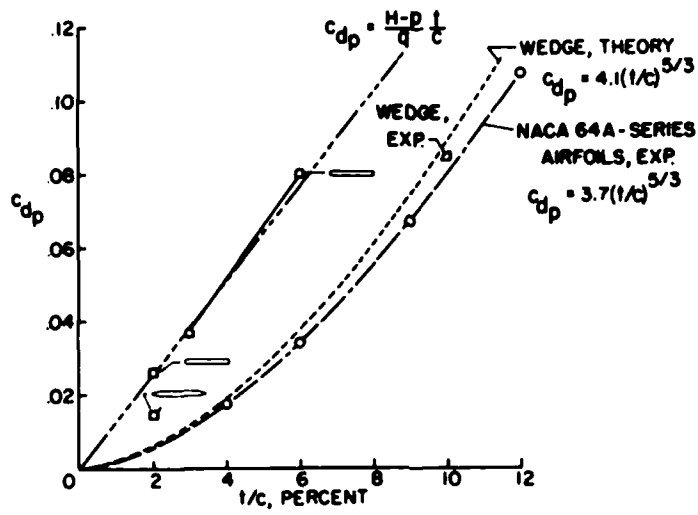


Figure 5

SHAPE EFFECTS ON PRESS.-DRAG COEFF. AT  $c_l=0$

M=1.44

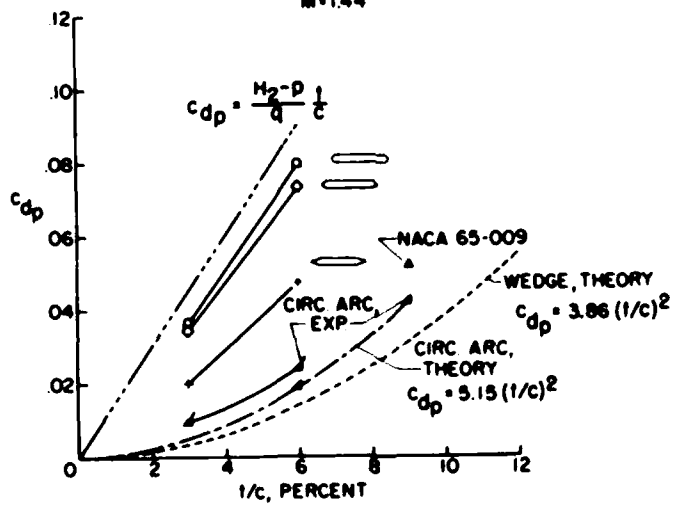


Figure 6





LIFT-CURVE SLOPE

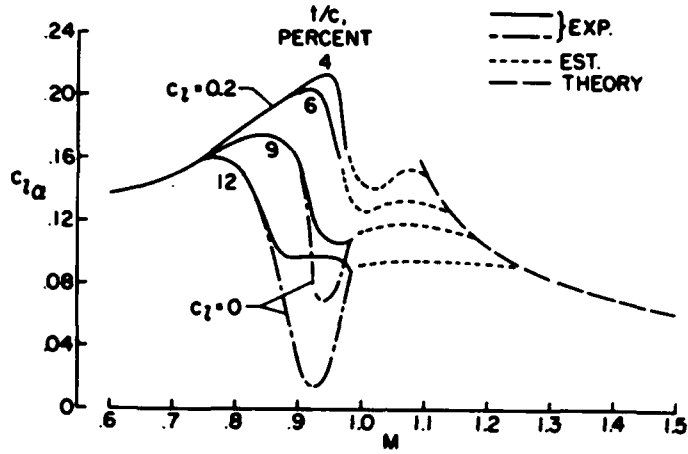


Figure 7

MAXIMUM LIFT-DRAG RATIOS

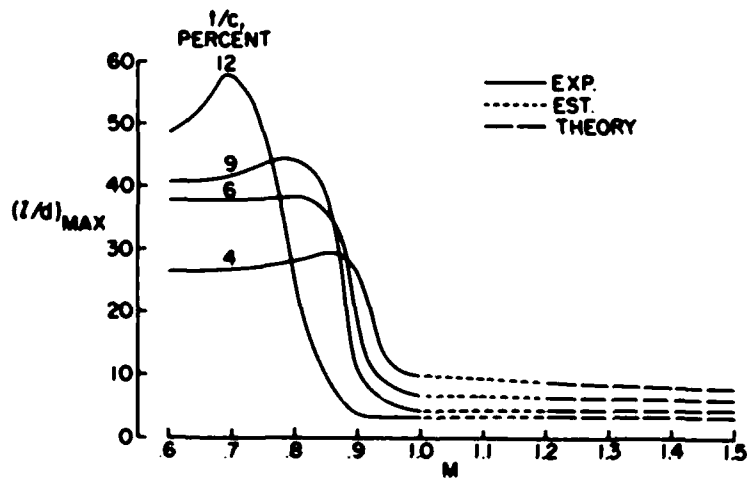


Figure 8



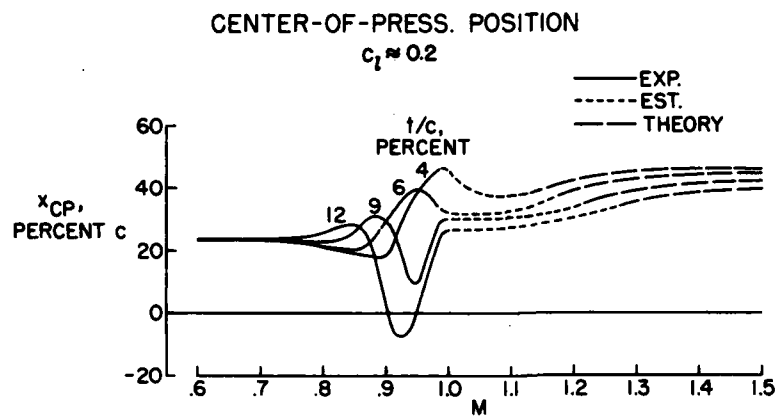


Figure 9

## REVIEW OF INFORMATION ON INDUCED FLOW OF A LIFTING ROTOR

By Alfred Gessow

Langley Aeronautical Laboratory

## SUMMARY

A brief review of the available information relating to induced flow of a lifting rotor is presented. The available material is summarized in a table as to flight condition, type of information, source, and the reference papers in which the data can be found. Some representative aspects of some of the reference material are discussed.

## INTRODUCTION

A knowledge of the inflow distribution through and about a lifting rotor is required in almost all fields of helicopter analysis. Precise, detailed information on the subject is meager, however, because of the rather formidable difficulties involved in measuring or calculating rotor downwash accurately. Fortunately, a superficial estimate of the inflow distribution has proven adequate for many types of helicopter analyses and a fair amount of general information, both theoretical and experimental, is available on the subject. In view of the stimulation of interest in rotor induced flow brought about by the current emphasis on loads, stability and control, and the expanded use of multirotor configurations, it is considered desirable to review such information.

## SYMBOLS

- $C_T$  thrust coefficient,  $\frac{T}{\pi R^2 \rho (\Omega R)^2}$
- $r$  radial distance to blade element, ft
- $R$  blade radius, ft
- $T$  rotor thrust, lb
- $v$  induced inflow velocity at rotor, always positive, fps
- $V$  true airspeed of helicopter along flight path, fps or mph

- Z vertical distance from plane perpendicular to rotor shaft, positive upward, ft
- $\alpha$  rotor angle of attack; angle between projection in plane of symmetry of axis of no feathering and line perpendicular to flight path, positive when axis is pointing rearward, radians
- $\epsilon$  downwash angle induced by rotor, radians
- $\mu$  tip-speed ratio,  $\frac{V \cos \alpha}{\Omega R}$
- $\rho$  mass density of air, slugs/cu ft
- $\Omega$  rotor angular velocity, radians/sec

Subscript:

HOV hovering

#### OUTLINE OF INFORMATION

The available material on rotor induced flow is summarized in table I as to flight condition, type of information, source, and the reference papers (see refs. 1 to 28) in which the data can be found. The flight conditions covered in the table are hovering, vertical ascent and descent, low-speed forward flight, and cruise and high-speed forward flight. A study of the information presented in the table shows that the inflow problem has been attacked theoretically, as well as by wind-tunnel tests on small- and large-scale models, by helicopter tower tests, and by flight tests on actual production helicopters. The experimental data consist of measurements of the magnitude and distribution of the rotor inflow, as well as flow-visualization data using smoke and balsa-dust techniques. It should be understood that both theory and experiment yield only time averages of the inflow at a particular spot in or about the rotor.

#### DISCUSSION

In this discussion, no attempt will be made to discuss in detail the available references listed in table I. Instead, some representative results of a few of the references will be touched upon in order to illustrate the state of knowledge of the rotor inflow field.

### Hovering

The hovering condition has been rather well explored, both experimentally and theoretically. Flow-visualization tests indicate that, above the rotor, the incoming air seems to be drawn into the rotor primarily in a horizontal direction and becomes part of a primarily vertical slipstream only after passing through the rotor. If the rotor is operating outside of the ground-effect region, the slipstream contracts and reaches its maximum velocity well within 1 radius below the rotor plane. In the outer few percent of the blade radius (or "tip loss" region), there is no well-defined slipstream above or below the rotor. Instead, there is a series of small vortices starting at the blade tip and continuing below the rotor that serve as a boundary between the slipstream beneath the rotor and the air outside of it.

In addition to flow-visualization studies, information exists as to the magnitude of the induced-velocity distribution across the rotor disk in hovering. The results of one such study (ref. 3) are shown in figure 1, which compares the induced velocity, as measured in flight, with that estimated by blade-element-momentum theory (ref. 1). Except for the tip-loss region, the agreement is seen to be quite good. Actually, the good agreement as to magnitude and distribution between theory and experiment should be regarded as a fortunate occurrence wherein very simple concepts give reasonable overall answers to a problem which in reality involves a complex flow state. Although similar data are lacking in vertical climb, it is expected that the theory should be as good as it is in hovering.

### Vertical Ascent and Descent

The available information regarding the vertical-flight region is summarized in figure 2, which shows the variation in rotor induced velocity with climb and descent velocity, all velocities being made nondimensional by dividing by the induced velocity in hovering. The plot is thus independent of disk loading and air density. The solid parts of the curve show the regions of climb and descent velocity wherein momentum theory (refs. 1 and 8) applies, which, as shown by the representative flow patterns sketched above the curve, are regions wherein a definite slipstream exists through the rotor. At intermediate rates of descent, simple momentum concepts become invalid in that a definite slipstream ceases to exist because of the "canceling" effect of the downward induced velocity by the upward-coming flight velocity. In this intermediate flight region, represented by the dashed curve, it is seen from the sketch that there is a recirculating flow through the rotor in the form of huge vortex rings; hence, the name "vortex ring" region. At large rates of descent, corresponding to power-off flight and beyond, the vortex rings are much smaller and are localized well above the disk.

The dashed curve shown for the vortex-ring state is a composite of flight and wind-tunnel measurements (refs. 6 and 9 to 14). The most important part of this region lies at the lower rates of descent between about 400 and 1,000 ft/min, where it can be seen that the slope of the curve is unstable; that is, the induced velocity increases at a faster rate than does the descent velocity. At fixed pitch, this results in a reduction in thrust with increased descent velocity. This type of instability is a contributing factor toward the well-known troubles that pilots experience when attempting to maintain steady flight in this region (refs. 1 and 15). Tests (ref. 16) have also shown that helicopter tail rotors may also run into this region of instability when the helicopter is experiencing certain rates of yaw.

#### Low-Speed Forward Flight

Another flight regime in which rotor inflow is the source of various troubles is the transition region in low-speed forward flight. In this region, which extends from about 15 to 30 mph, helicopters typically experience an increase in rotor-blade stress and vibration. The mechanism which gives rise to some of these troubles is not very well understood, but presumably the troubles are due to the fact that the flow changes from a vertical slipstream in hovering to an essentially horizontal flow pattern in forward flight. Certain general aspects of the wake behavior in this speed range are known, however. For example, as the forward speed increases from hovering, the skew angle of the wake increases, the mean value of the induced velocity decreases, and the longitudinal asymmetry of the inflow velocity increases.

The variation of skew angle of the wake with forward speed, as measured on the Langley helicopter test tower (unpublished) is shown in figure 3. As illustrated in the sketch, the skew angle is defined as the angular displacement of the wake from the vertical. It was measured in the region of maximum wake velocity. The data are compared with theory, represented by the solid line in the figure, and it can be seen that the agreement is fairly good.

The variation of the mean value of the induced velocity with forward speed, also obtained on the Langley helicopter test tower (ref. 22), is shown in figure 4. Here too, both the induced and forward-flight velocities are expressed nondimensionally. The calculated variation, shown by the solid line, serves as a pretty good fairing for the data, except at the upper end of the speed range, where the data themselves become questionable. This upper end of the curve corresponds to velocities of about 25 to 30 mph for normal disk loadings.

Some idea of the increase in the asymmetry of the distribution of wake velocity with forward speed is shown in figure 5. The curves represent unpublished test-tower measurements of wake velocity plotted against

nondimensional blade radius in both the forward and rearward parts of the disk, obtained in the vertical plane of symmetry of the rotor and several feet below the disk. The location of the horizontal survey plane of measurements is illustrated on the sketch. It can be seen from the curves that the inflow velocities over the front part of the disk are smaller than those over the rear of the disk, with the mean slope increasing with forward speed. This variation in inflow velocity from front to rear of the disk has been qualitatively known since the days of the early development of rotor theory by Glauert (ref. 18) who showed that its effect on rotor performance was nil. Years later, Seibel (ref. 23), using wind-tunnel gyroplane data, made a quantitative evaluation of the variation and showed how this variation, assumed to be linear, could cause the observed rise in the vibration level of a two-blade helicopter rotor in this region. Theories are available (refs. 18 to 21) that can predict the approximate location and magnitude of the maximum dissymmetry that occurs in the transition region, but the agreement is not precise.

#### Cruise and High-Speed Forward Flight

At higher speeds, corresponding to the speed for minimum power and beyond, the dissymmetry decreases, as does the magnitude and thus the importance of the induced velocity. Figure 6 (ref. 24) illustrates the variation of the mean inflow angles with forward speed in this higher speed range. The solid curves represent flow angles as measured in flight by a yaw vane located on the tail cone of a helicopter fuselage about  $5/8$  of a radius behind the center of rotation. As shown on the sketch, flow angles are referenced to the plane perpendicular to the rotor shaft. Measurements were taken at three power conditions and compared with simple momentum theory (assuming uniform inflow), represented by the dashed curve. It can be seen that the theory gives reasonable answers over most of the flight range and can be used, for example, in designing a horizontal tail surface for the helicopter so that it remains effective over a wide range of steady flight conditions.

An insight to the induced-velocity variation across the rotor disk at several speeds above minimum power is available from British flight tests (ref. 26) that used a smoke-visualization technique. A sample of the smoke-flow pictures obtained during the tests is shown in figure 7. The plane of the streamlines is approximately  $0.4R$  on the starboard side and the helicopter was flying at 53 mph. It can be seen that at this speed there is a slight upwash in front of the rotor and then an increasing downwash toward the rear of the disk. The swirls that show up so clearly are due to the main-rotor-blade tips cutting through the streamlines at successive intervals. Induced-velocity magnitudes obtained from photographs such as these can be regarded as only approximate, but the results are still of interest.

An example of the results thus obtained is shown in figure 8, in which the nondimensional induced velocity, measured at three lateral stations on the disk, is plotted against nondimensional radius. Within the scatter of the data, it is seen that the velocity increases toward the rear in an approximately linear fashion over most of the disk. The calculated variation (ref. 21) shown seems to represent fairly well the general idea as to what goes on in regard to the inflow.

In connection with the design and behavior of tandem helicopters, a knowledge of the vertical distribution of downwash some distance behind a rotor is very desirable. An example of such a distribution is available from wind-tunnel tests (ref. 28) and is shown in figure 9. The downwash angle  $\epsilon$ , expressed in nondimensional form by dividing by the downwash angle at the center line of the rotor  $C_T/2\mu^2$  (as calculated by simple momentum theory), is shown as a function of vertical height  $Z/R$  above and below the rotor hub for an intermediate tip-speed ratio. The data were obtained at  $1\frac{1}{2}$  radii behind the rotor center line at the three-quarter-radius position on the advancing and retreating sides of the disk. Calculated values (ref. 20) are represented by the dashed line and are seen to represent the shape of the measured distribution pretty well.

The interesting point made by these plots is that, as might be expected, the vertical distribution of downwash is nonuniform, with the maximum occurring approximately on a line drawn through the rotor hub and parallel to the flight velocity. The nonuniformity of velocity has explained certain stability and control phenomena that have been observed with a tandem helicopter. The variation in downwash angle experienced by the rear rotor of a tandem helicopter, for example, causes changes in angle-of-attack stability and speed stability with power changes, as well as contributing to a nonlinearity in angle-of-attack stability. Although the data must be considered approximate, it is interesting to note that, for the case shown, the maximum downwash angle reached is almost three times the value that would be calculated at the center of the rotor by simple momentum considerations. Unpublished information from a different series of wind-tunnel tests indicates that the maximum downwash angles measured in survey planes closer to the rotor disk (at the trailing edge of the disk, for example) are about twice the value calculated for the center of the rotor.

#### CONCLUDING REMARKS

From this brief review of rotor-inflow information, it is quite clear that much work remains to be done, both theoretically and experimentally, before our understanding of rotor inflow can be said to be



thorough. The problems are defined, but the answers are not quantitatively pinned down in all cases. Enough is known about the subject, however, to be extremely useful in calculating and explaining various aspects of rotor behavior.

#### REFERENCES

1. Gessow, Alfred, and Myers, Garry C., Jr.: Aerodynamics of the Helicopter. The Macmillan Co., c.1952.
2. Carpenter, Paul J., and Fridovich, Bernard: Effect of a Rapid Blade-Pitch Increase on the Thrust and Induced-Velocity Response of a Full-Scale Helicopter Rotor. NACA TN 3044, 1953.
3. Brotherhood, P.: An Investigation in Flight of the Induced Velocity Distribution Under a Helicopter Rotor When Hovering. Rep. No. Aero. 2212, British R.A.E., June 1947.
4. Carpenter, Paul J., and Paulnock, Russell S.: Hovering and Low-Speed Performance and Control Characteristics of an Aerodynamic-Servocontrolled Helicopter Rotor System As Determined on the Langley Helicopter Tower. NACA TN 2086, 1950.
5. Taylor, Marion K.: A Balsa-Dust Technique for Air-Flow Visualization and Its Application to Flow Through Model Helicopter Rotors in Static Thrust. NACA TN 2220, 1950.
6. Meijer Drees, J., and Hendal, W. P.: Airflow Patterns in the Neighbourhood of Helicopter Rotors. Aircraft Engineering, vol. XXIII, no. 266, Apr. 1951, pp. 107-111.
7. Harrington, Robert D.: Full-Scale-Tunnel Investigation of the Static-Thrust Performance of a Coaxial Helicopter Rotor. NACA TN 2318, 1951.
8. Glauert, H.: Notes on the Vortex Theory of Airscrews. R. & M. No. 869, British A.R.C., Dec. 1922.
9. Lock, C. N. H., Bateman, H., and Townend, H. C. H.: An Extension of the Vortex Theory of Airscrews With Applications to Airscrews of Small Pitch, Including Experimental Results. R. & M. No. 1014, British A.R.C., 1926.

10. Glauert, H.: The Analysis of Experimental Results in the Windmill Brake and Vortex Ring States of an Airscrew. R. & M. No. 1026, British A.R.C., Feb. 1926.
11. Castles, Walter, Jr., and Gray, Robin B.: Empirical Relation Between Induced Velocity, Thrust, and Rate of Descent of a Helicopter Rotor As Determined by Wind-Tunnel Tests on Four Model Rotors. NACA TN 2474, 1951.
12. Fail, R. A., and Eyre, C. W.: Wind Tunnel Tests of a 12 Ft Diameter Helicopter Rotor in the Vertical Flight Condition. TN No. Aero. 2010, British R.A.E., July 1949.
13. Lock, C. N. H.: Note on the Characteristic Curve for an Airscrew or Helicopter. R. & M. No. 2673, British A.R.C., June 1947.
14. Brotherhood, P.: Flow Through Helicopter Rotor in Vertical Descent. R. & M. No. 2735, British A.R.C., July 1949.
15. Stewart, Wm.: Helicopter Behaviour in the Vortex Ring Conditions. C. P. No. 99, British A.R.C., Nov. 1951.
16. Amer, Kenneth B., and Gessow, Alfred: Charts for Estimating Tail-Rotor Contribution to Helicopter Directional Stability and Control in Low-Speed Flight. NACA TN 3156, 1954.
17. Meijer Drees, J.: A Theory of Airflow Through Rotors and Its Application to Some Helicopter Problems. Jour. Helicopter Assoc. of Great Britain, vol. 3, no. 2, July-Aug.-Sept. 1949, pp. 79-104.
18. Glauert, H.: A General Theory of the Autogiro. R. & M. No. 1111, British A.R.C., 1926.
19. Coleman, Robert P., Feingold, Arnold M., and Stempin, Carl W.: Evaluation of the Induced-Velocity Field of an Idealized Helicopter Rotor. NACA WR L-126, 1945. (Formerly NACA ARR L5E10.)
20. Mangler, K. W.: Calculation of the Induced Velocity Field of a Rotor. Rep. No. Aero. 2247, British R.A.E., Feb. 1948.
21. Castles, Walter, Jr., and De Leeuw, Jacob Henri: The Normal Component of the Induced Velocity in the Vicinity of a Lifting Rotor and Some Examples of Its Application. NACA TN 2912, 1953.
22. Carpenter, Paul J.: Effect of Wind Velocity on Performance of Helicopter Rotors As Investigated With the Langley Helicopter Apparatus. NACA TN 1698, 1948.

23. Seibel, Charles: Periodic Aerodynamic Forces on Rotors in Forward Flight. Jour. Aero. Sci., vol. 11, no. 4, Oct. 1944, pp. 339-342.
24. Gustafson, F. B.: Desirable Longitudinal Flying Qualities for Helicopters and Means To Achieve Them. Aero. Eng. Rev., vol. 10, no. 6, June 1951, pp. 27-33.
25. Oliver, A. L.: The Low Speed Performance of a Helicopter. C. P. No. 122, British A.R.C., May 1952.
26. Brotherhood, P., and Stewart, W.: An Experimental Investigation of the Flow Through a Helicopter Rotor in Forward Flight. R. & M. No. 2734, British A.R.C., Sept. 1949.
27. Wheatley, John B., and Hood, Manley J.: Full-Scale Wind-Tunnel Tests of a PCA-2 Autogiro Rotor. NACA Rep. 515, 1935.
28. Fail, R. A., and Eyre, R. C. W.: Downwash Measurements Behind a 12 Ft Diameter Helicopter Rotor in the 24 Ft Wind Tunnel. TN No. Aero. 2018, British R.A.E., Sept. 1949.

TABLE I  
SUMMARY OF ROTOR-INDUCED-FLOW INFORMATION

Type of information	Source	Reference	Remarks
Hovering			
Theory	Blade-element--momentum	1, 2	Magnitude and distribution
Measurements and smoke flow	Flight tests	3	Magnitude and distribution
Measurements	Test tower	2, 4, unpublished	Magnitude and distribution
Balsa dust and smoke flow	Small scale (single and coaxial)	5, 6	Distribution
Applications	Performance calculations	1, 7	Single and coaxial
Vertical ascent and descent			
Theory	Momentum	1, 8	Mean value
Measurements and smoke flow	Small and large scale	6, 9, 10, 11, 12, 13	Magnitude and distribution
Smoke flow	Flight tests	14	Distribution
Applications	Performance	1	
	Stability and control	15, 16, 17	
Low-speed forward flight			
Theory	Vortex	18, 19, 20, 21	
Measurements	Test tower	4, 22, unpublished	Magnitude and distribution and flow angles
	Indirect	23	
Applications	Stability and control	17, 24	
	Vibrations	17, 23	
	Performance	17, 22, 25	
Cruise and high-speed forward flight			
Theory	Momentum and vortex	17, 18, 19, 20, 21	
Smoke flow	Small-scale and flight tests	6, 26	Flow angles and distribution
Measurements	Large-scale wind tunnel	27, 28	Magnitude and distribution
	Flight tests	24	Flow angles
Applications	Stability and control	24	
	Performance	1	

## INDUCED-VELOCITY DISTRIBUTION IN HOVERING

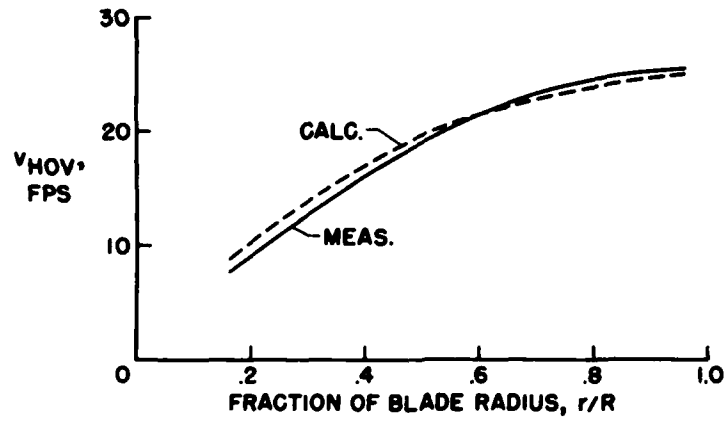


Figure 1

## INDUCED-VELOCITY RELATIONS IN VERTICAL FLIGHT

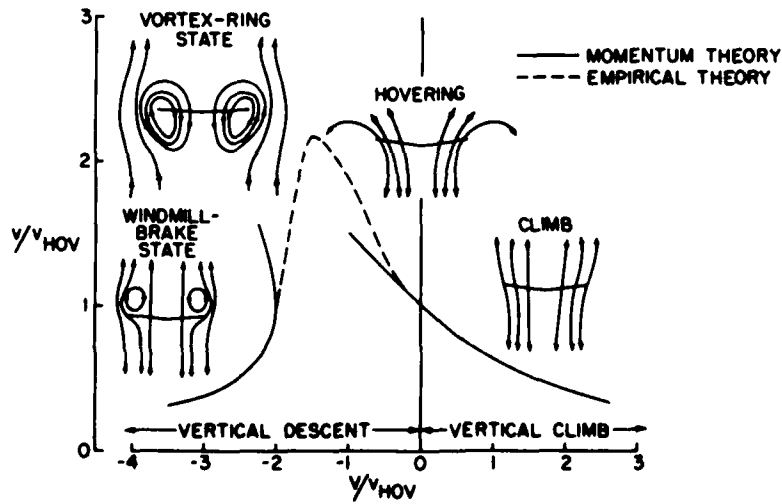


Figure 2

SKEW-ANGLE MEASUREMENTS AT LOW FORWARD SPEEDS

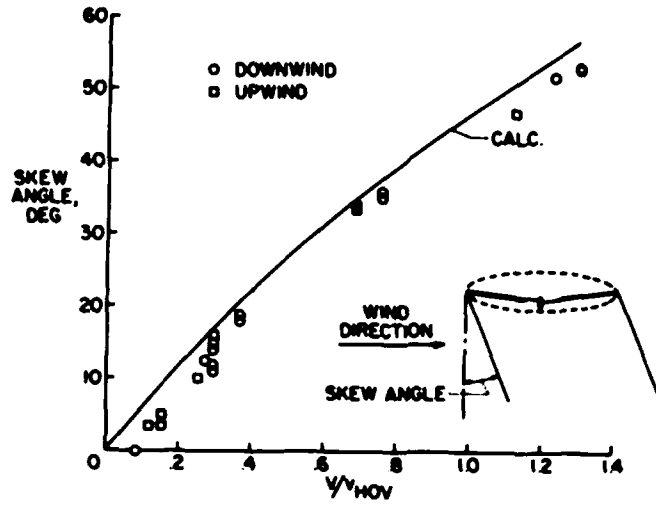


Figure 3

INDUCED-VELOCITY MEASUREMENTS AT LOW FORWARD SPEEDS

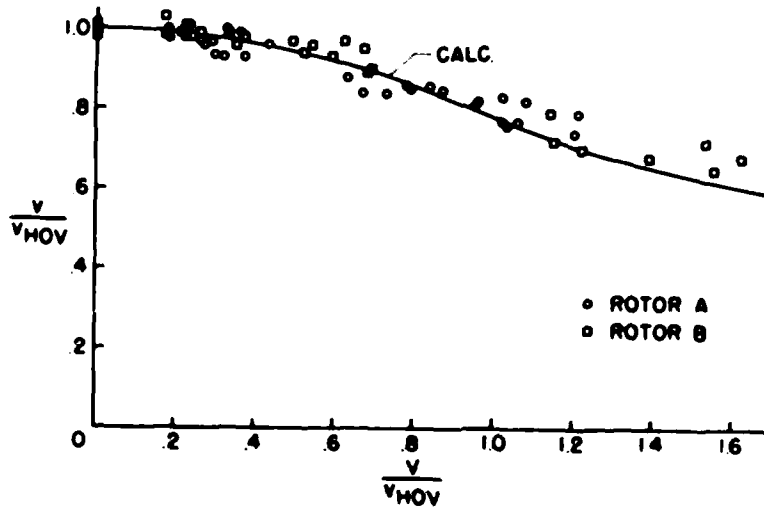


Figure 4

TEST-TOWER WAKE-VELOCITY SURVEY

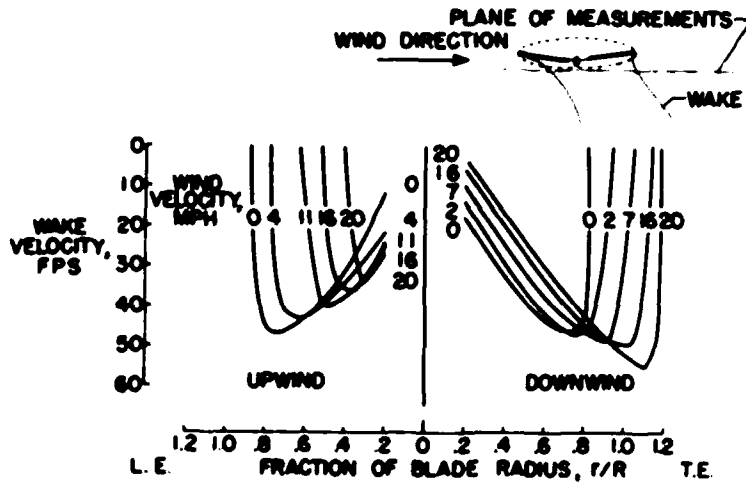


Figure 5

VARIATION OF FLOW ANGLE WITH SPEED AND POWER  
MEASURED AT  $\frac{3}{8}R$

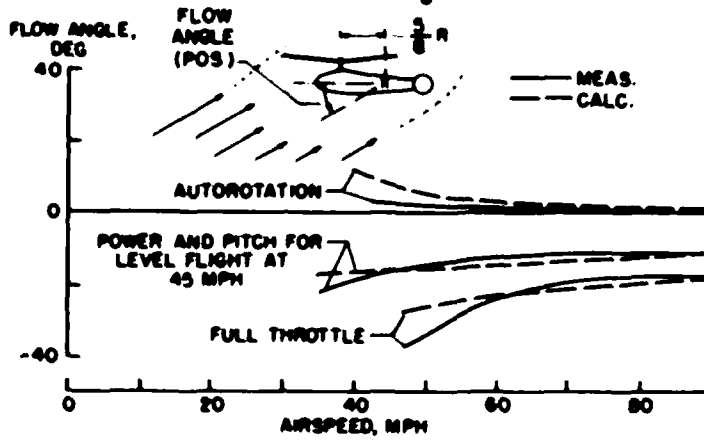


Figure 6

SMOKE FLOW TESTS IN FORWARD FLIGHT  
V = 53 MPH



Figure 7

INDUCED VELOCITY APPROXIMATED FROM  
SMOKE-FLOW PICTURES  
V = 53 MPH

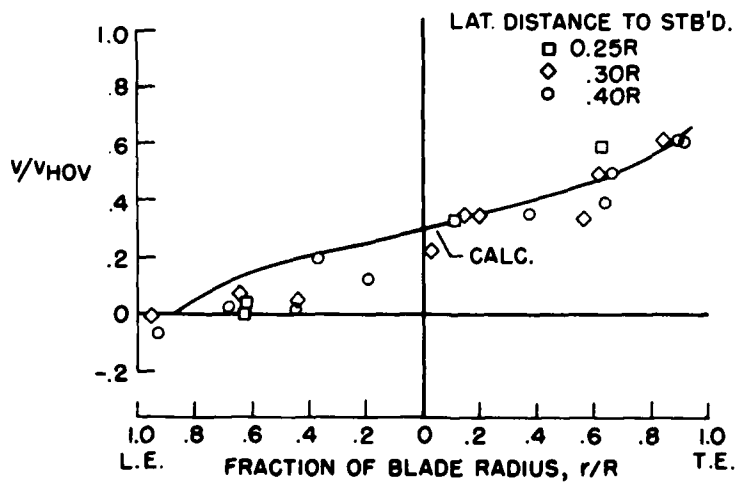


Figure 8



VERTICAL SURVEY OF DOWNWASH ANGLE AT 1.5R BEHIND  
ROTOR CENTER LINE

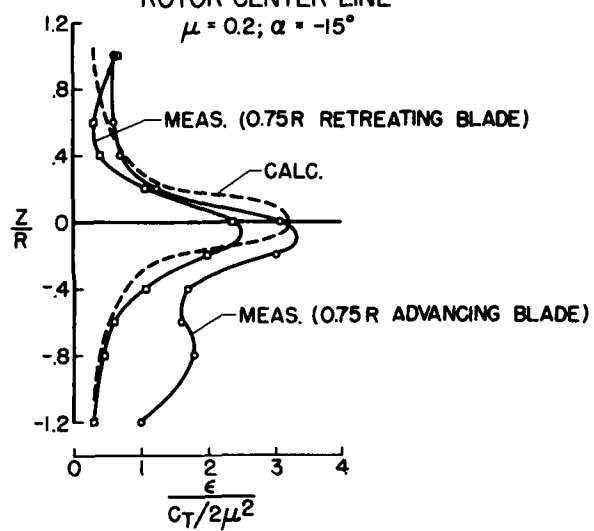


Figure 9

FLOW-FIELD MEASUREMENTS AROUND SINGLE AND TANDEM  
ROTORS IN THE LANGLEY FULL-SCALE TUNNEL

By Harry H. Heyson

Langley Aeronautical Laboratory

The preceding paper by Alfred Gessow has reviewed most of the experimental and theoretical knowledge of rotary-wing flow fields that has been generally available up to the present time. It is immediately evident that the greatest area of weakness in that knowledge is in the forward flight regimes of operation.

Approximately a year ago, the staff of the Langley full-scale tunnel undertook a small exploratory program on the flow around single and tandem rotors. By using the experience gained in this series of tests, a fairly complete test program on the single-rotor configuration, with a wide range of variables, was planned and was finally completed about April 1954. Only a portion of the data obtained in the more recent surveys has been reduced at the present time and the portion which is presented here should be considered preliminary. Only one tip-speed ratio is discussed, but the data should be applicable to most present-day helicopters at speeds near cruising.

The lines in figure 1 show the extent of the survey planes in the single-rotor tests. All the survey planes are perpendicular to the longitudinal center line of the tunnel. They are located at the leading edge of the rotor disk, one-fourth of the way back, at the center, three-fourths of the way back, and slightly behind the trailing edge of the rotor disk. Two additional planes farther rearward were also surveyed, but the results are not yet available.

The rotor was of the teetering or seesaw type and had rectangular, untwisted blades of NACA 0012 airfoil section. The rotor radius was  $7\frac{1}{2}$  feet and the rotor solidity was 0.0543.

In order to correct for the flow about this supporting mechanism, data were taken twice at each point in space - once with and once without the rotor blades installed. The difference is considered to be characteristic of the isolated rotor.

A five-tube pitch-yaw-pitot rake was used throughout the tests. It should be emphasized that this rake is incapable of measuring instantaneous variations of flow angles and velocities such as might be desired for a complete vibration analysis. Therefore, all data are time-averaged values.

Figure 2 maps the flow near the trailing edge. Figure 2(a) shows the angular variations in the flow. The vectors represent the deviation of the flow, in degrees, from a path parallel to the tunnel center line. The vertical component of the vector is the downwash angle; the lateral component is the sidewash angle. The general effect given by the figure is much like that given by a tuft-grid photograph. Notice the striking similarity to the flow behind a lifting wing. The sharp change in sidewash angle just below the level of the rotor indicates that the trailing vortex sheet is passing along about there. The strength of vorticity in the sheet increases from the center to the tips of the rotor. The beginning of the rolling up of the sheet into the large tip vortices which are almost directly behind the outboard edges of the rotor disk may be seen. Because of the different blade loading on each side of the disk, there is a slight asymmetry in the flow in this survey plane. The stronger tip vortex (behind the advancing side) has moved a little more toward the center of the rotor than has the weaker vortex (behind the retreating side).

Figure 2(b) shows the variation of local dynamic pressure in the same survey plane. It is evident that large velocity changes are confined to a relatively small area behind the rotor. The dynamic pressure in this area is greater than that of the free stream since the rotor, in helicopter operation, is adding energy to the airstream. The unusual humped shape of the pressure curves in the center of the chart is due to the forward tilt of the rotor. The center part, which is high, has just come off the raised trailing edge of the disk; the outer region, which is lower, comes from the lower outboard edges of the disk. Although it is not seen in figure 2(b), the velocities well below the rotor are slightly less than free stream, whereas those above the rotor are slightly greater. This effect is very much like that created by the circulation around a lifting wing.

Figure 3 shows the induced vertical velocity in the five survey planes. The ordinate is the vertical height, in terms of the radius, above the rotor. The tip path plane of the rotor is represented by  $Z/R = 0$ . The abscissa is the vertical induced velocity  $v$  divided by the theoretical downwash velocity at the center of the rotor  $v_0$ . The experimental points (circles) represent the average induced velocity across the disk. The theoretical values for the longitudinal center line, as calculated by Castles and De Leeuw (ref. 1), are shown as a solid line.

By comparing the two sets of values on this basis, it may be seen that the theory underestimates the induced velocity above the rotor. The agreement below the rotor is good in the three middle survey planes. At the leading edge of the rotor, the vertical extent of the upwash region is smaller than is predicted by theory. Near the trailing edge of the rotor, where the theory indicates a constant downwash of  $v/v_0$  equal to slightly more than 2, the experimental points indicate that

the downwash continues to build up across the wake and reaches a maximum value of about 3.

A knowledge of the induced velocity in the plane of the rotor itself is very useful in accurate performance and stability calculations. In order to get this information, lines were faired through the experimental points of figure 3 and the values at the rotor disk were picked off. These values were compared with the theoretical values for the disk. The comparison is shown in figure 4. It may be seen that the theory predicts the general shape of the curve well and that the accuracy in the rear portion of the rotor is very good. However, the accuracy in the forward portion of the rotor is somewhat poorer.

The results of the short exploratory investigation of the tandem-rotor system will now be discussed. These surveys covered the planes shown in figure 5. The survey planes were at the center line of the front rotor, the leading edge of the rear rotor, the center line of the rear rotor, and just behind the trailing edge of the rear rotor. The two rotors were at equal heights above the center line of the test machine; that is, there was no vertical offset. The gap between the rotors was very small - about 7 percent of a radius. Each rotor was equipped with exactly the same type of blades and hubs as in the single-rotor surveys previously discussed.

Before examining the data of the Langley full-scale tunnel, first look at a tuft-grid photograph taken in the Langley stability tunnel behind a tandem-rotor model (fig. 6). Despite the addition of a second rotor, there is still only one set of trailing vortices. Although distorted (note the vertical elongation of the retreating side vortex), the flow is still essentially the same as that behind a single rotor. Similar photographs, taken under a wide variety of operating conditions, indicate that this observation remains valid until either very high fuselage attitudes or very high lift coefficients are reached. For the surveys of the Langley full-scale tunnel that are shown in the following figures, the fuselage attitude and lift coefficient are both much lower than for this case. It would, therefore, be expected that the data would show the effect of a single pair of tip vortices.

Figure 7 shows the downwash angles, averaged across the span, as measured in the surveys. It should be noted, before examining the figures in detail, that the points indicate only the downwash angle - not downwash velocity. The points have been divided by the theoretical downwash angle at the center of the rotor. Also, in these charts  $Z/R = 0$  represents the tip path plane of the front rotor. For this condition, however, the rotors were trimmed in such a manner that both tip path planes are nearly coincident, and  $Z/R = 0$  may, therefore, be considered to represent the tip path plane of either rotor. The solid line represents the theoretical variation of downwash angle for a single rotor.

In the initial portion of these tests, the rear-rotor blades were removed and the front rotor was set to a given flight condition. This configuration was then surveyed as a single rotor. The results are shown in figure 7 as circles. It is evident from these points that, if the theory is used to predict only the downwash angles rather than the total induced velocity, it is considerably more accurate. The error is largest in the more rearward planes.

The rear rotor was then placed on the helicopter, and the overall tandem configuration was then set to operate at the same values of lift coefficient and useful drag-lift ratio as in the single-rotor portion of the test. In setting this condition, only the rear-rotor controls were used. The tandem rotor was then surveyed at the same points in space as the single rotor. The resultant values are plotted as squares in figure 7.

It is evident that the addition of the rear rotor affects the front rotor by adding a small, but significant, upwash component to the flow in the forward survey planes. Since the front-rotor control setting remained unchanged, this upwash must increase the blade angles of attack of the front rotor and, consequently, the portion of the total lift and drag that it carries. Thus, the tandem-rotor model is equivalent to a flight article having its center of gravity somewhat forward of the mid-point between the rotors.

It is also evident that, in the vicinity of the rear rotor, the additional downward impulse imparted to the air flow by adding a second rotor resulted in very large increases in the downwash angles. In each location, however, the general shape of the downwash curves, except for magnitude, is still the same. This effect is to be expected from the general flow pattern.

Figure 8 compares the downwash at the plane of each rotor as faired from the previous figures. In this particular flight condition, the rear rotor is seen to operate in a total downwash field approximately three times as great as that of the front rotor. Therefore, it might be expected that the rear rotor would require about three times as much induced power as the front rotor. Power measurements indicate that this condition is actually true. This subject will be covered in more detail later in a paper presented by Richard C. Dingeldein.

The results of these surveys indicate the following conclusions at cruising speeds:

1. The time-averaged flow field caused by a rotor in normal helicopter attitudes is very much like that of a wing.

2. The time-averaged downstream flow field generated by a lightly loaded, clean, tandem helicopter is much like that generated by a single-rotor helicopter.

3. These surveys indicate that the induced losses in tandem-rotor helicopter configurations may be explained and their approximate magnitude estimated if a sufficient knowledge of their flow field is available.

4. The theoretical flow fields about a rotor, as calculated by Castles and De Leeuw, may, with certain reservations, be used to calculate the induced flow or the downwash angles to a sufficient degree of accuracy to be adequate for initial design considerations.

#### REFERENCE

1. Castles, Walter, Jr., and De Leeuw, Jacob Henri: The Normal Component of the Induced Velocity in the Vicinity of a Lifting Rotor and Some Examples of Its Application. NACA TN 2912, 1953.

## SURVEY PLANES USED IN SINGLE-ROTOR TESTS

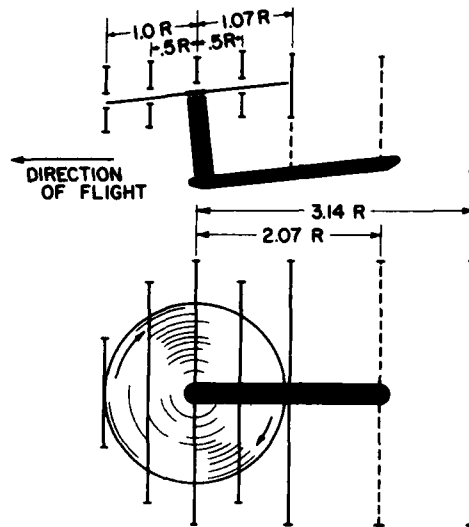


Figure 1

## STREAM ANGLES 7%R BEHIND TRAILING EDGE OF A SINGLE ROTOR

$$\mu = 0.15; C_L = 0.331$$

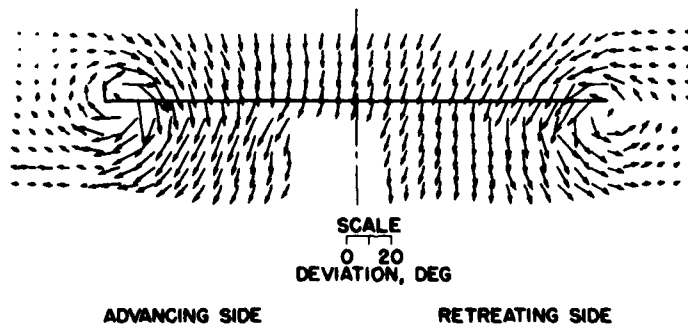


Figure 2(a)

VARIATION OF LOCAL DYNAMIC PRESSURE ( $q/q_0$ ) AT 7%R BEHIND TRAILING EDGE OF A SINGLE ROTOR

$\mu = 0.15; C_L = 0.331$

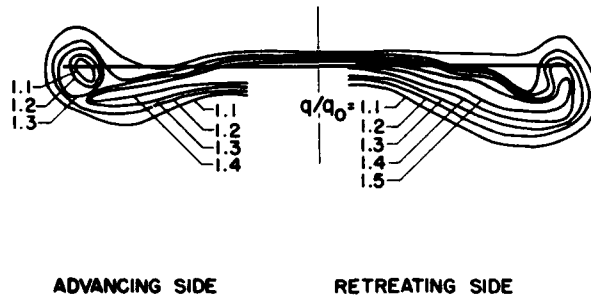


Figure 2(b)

VARIATION OF INDUCED VELOCITY NEAR A SINGLE ROTOR

$\mu = 0.15; C_L = 0.331; \chi = 79.5^\circ$

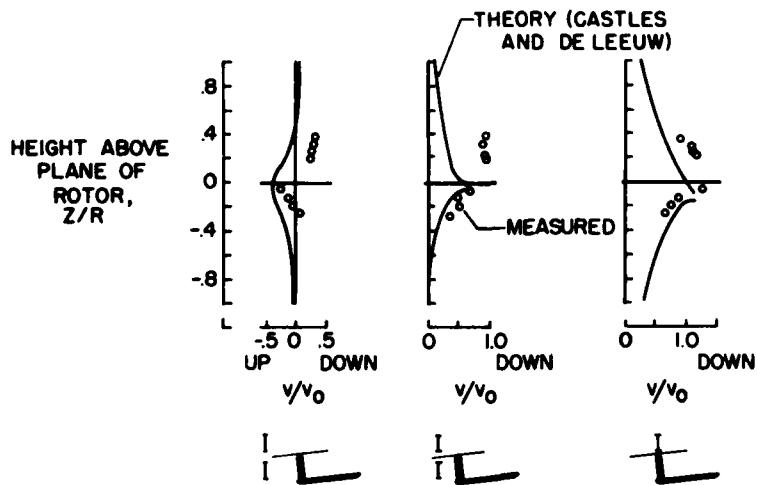


Figure 3(a)



VARIATION OF INDUCED VELOCITY NEAR A SINGLE ROTOR  
 $\mu=0.15$ ;  $C_L=0.331$ ;  $\chi=79.5^\circ$

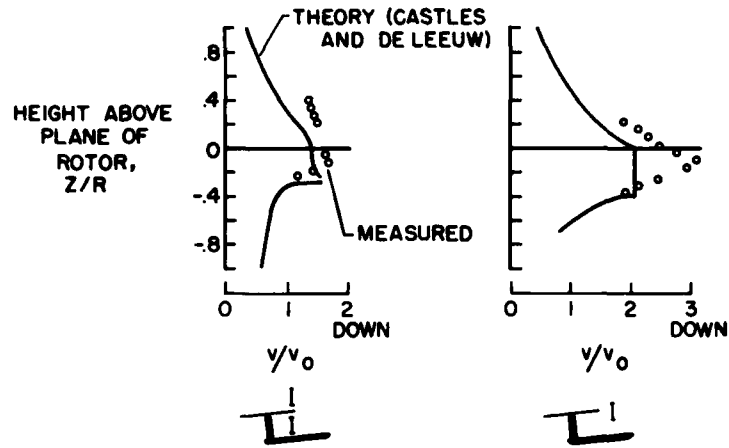


Figure 3(b)

VARIATION OF INDUCED VELOCITY IN PLANE OF ROTOR

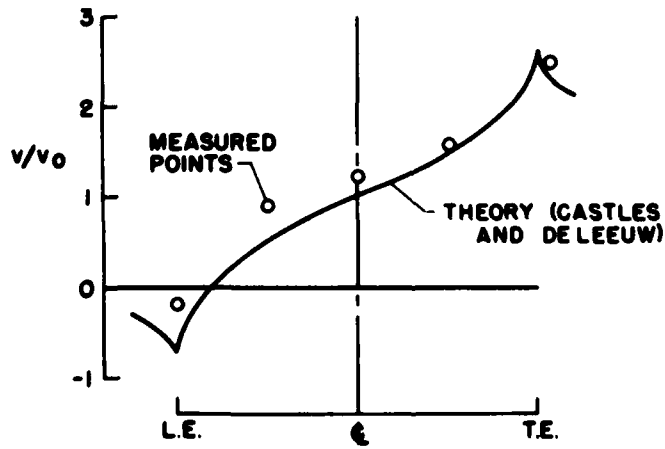


Figure 4

## SURVEY PLANES USED IN TANDEM-ROTOR TESTS

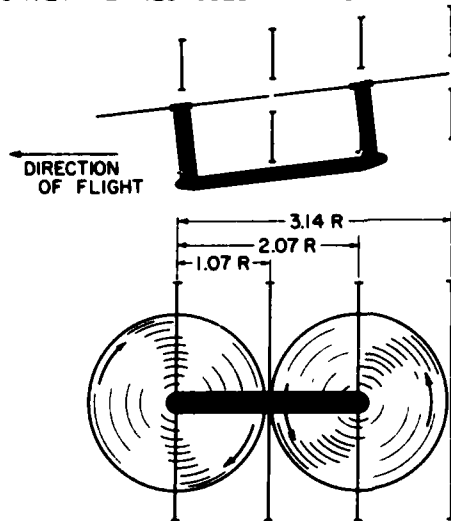


Figure 5

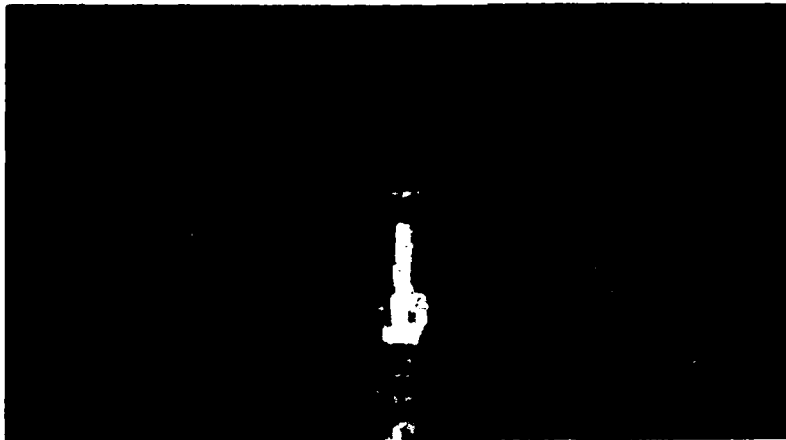
STABILITY-TUNNEL TUFT-GRID PHOTOGRAPH OF FLOW BEHIND  
A TANDEM HELICOPTER

Figure 6

VARIATION OF DOWNWASH NEAR SINGLE AND TANDEM ROTORS  
 $\mu = 0.15$ ;  $C_L = 0.302$ ;  $\chi = 83.4^\circ$

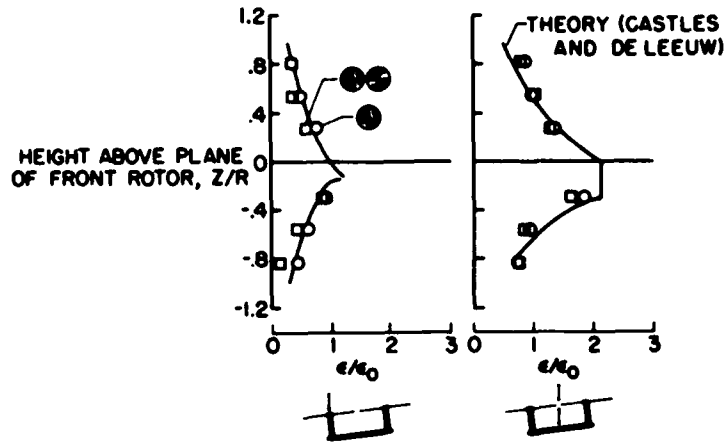


Figure 7(a)

VARIATION OF DOWNWASH NEAR SINGLE AND TANDEM ROTORS  
 $\mu = 0.15$ ;  $C_L = 0.302$ ;  $\chi = 83.4^\circ$

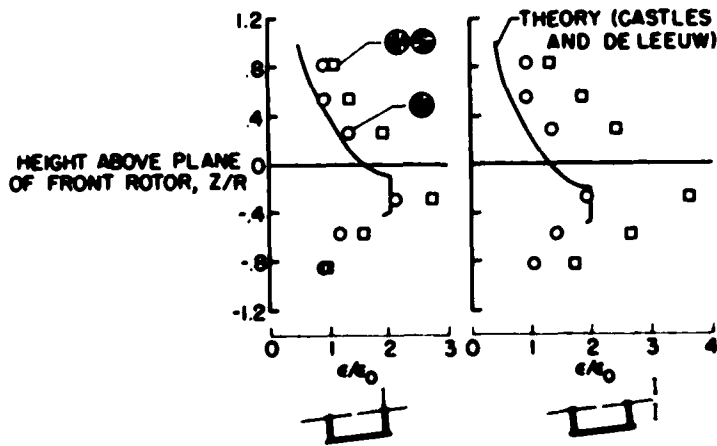


Figure 7(b)

COMPARISON OF DOWNWASH IN PLANE OF FRONT  
AND REAR ROTORS OF TANDEM HELICOPTER

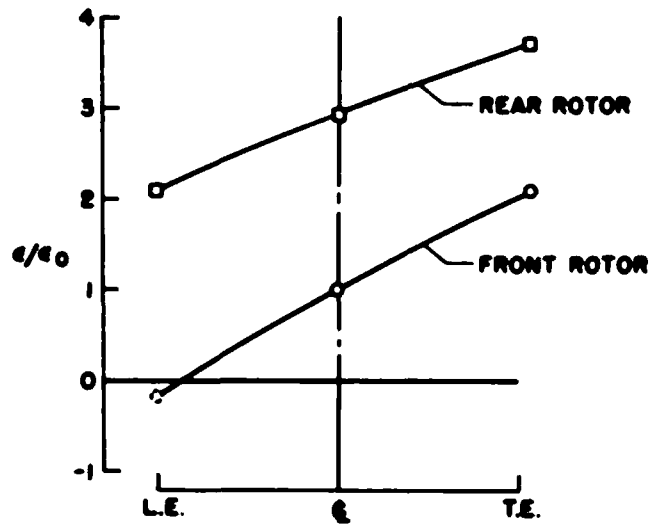


Figure 8

## ROTOR EFFICIENCY IN HOVERING

By Alfred Gessow

Langley Aeronautical Laboratory

### INTRODUCTION

The flight characteristic that distinguishes the helicopter from fixed-wing aircraft and from its sister ship the autogiro is its ability to hover and climb vertically. Although the time spent in hovering and vertical climb is normally small for most helicopter operations, it is this characteristic that justifies the additional complexity of using a powered rotating rotor rather than a fixed-wing or an autorotating rotor. Fortunately, most of the aerodynamic problems involved in the design of a rotor that will lift a given load and slowly carry it from one place to another are much more readily solved than the problems arising at the higher end of the helicopter speed range. From the analytical standpoint, the relative simplicity of hovering or vertical flight as opposed to forward flight arises, of course, from the fact that, in hovering, the angle of attack and resultant velocity of a blade element operating at a given radial distance are independent of its azimuth position. In addition, experimental hovering data can be obtained to supplement and check the theory without the use of complicated wind-tunnel or flight programs.

In hovering theory, the helicopter designer has a very useful tool that enables him to design and adequately predict the performance of an efficient load-lifter helicopter, to investigate the characteristics of various powerplant-rotor combinations, or to determine the extent to which hovering and vertical flight performance is compromised by a design that favors the higher end of the helicopter speed range. It is the purpose of this paper to illustrate the application of the theory by quantitatively examining the effect of variations in design parameters on rotor efficiency in hovering.

### SYMBOLS

b number of blades per rotor

$c_e$  equivalent blade chord (on thrust basis),

$$\frac{\int_0^R cr^2 dr}{\int_0^R r^2 dr}, \text{ ft}$$

$\bar{c}_l$	rotor mean lift coefficient (in hovering, equal to $6 C_T/\sigma$ )
$c_0/c_1$	ratio of extended chord at blade root to chord at blade tip
$C_Q$	rotor-shaft torque coefficient, $\frac{Q}{\pi R^2 \rho (\Omega R)^2 R}$
$C_T$	thrust coefficient, $\frac{T}{\pi R^2 \rho (\Omega R)^2}$
$Q$	rotor-shaft torque, lb-ft
$R$	blade radius, ft
$r$	radial distance to blade element, ft
$T$	rotor thrust, lb
$\theta_1$	difference between hub and tip pitch angles (positive when tip angle is larger), radians
$\rho$	mass density of air, slugs/cu ft
$\sigma$	rotor solidity, $bc_e/\pi R$
$\Omega$	rotor angular velocity, radians/sec

#### DISCUSSION

The usefulness of the theory is based on its being able to calculate accurately the two sources of energy loss that are present in producing thrust. The first is represented by the increase in kinetic energy of the rotor slipstream (so-called induced loss) and the second arises from the profile drag of the blades. For the range of disk loadings common to the helicopter, it has been shown that simple-momentum—blade-element considerations, together with an assumed tip-loss factor of 0.97, can accurately predict induced losses for a wide range of rotor designs. Two-dimensional section data inserted into a combination of momentum and blade-element theory is similarly adequate for predicting profile-drag losses, provided, of course, that the actual profile-drag coefficients of the "as-built" blade sections are known or estimated from experience.

Two examples of the manner in which theory can estimate power losses in hovering are shown in figure 1. The upper plot in the figure shows

the thrust-power variation (expressed in nondimensional coefficients) of a full-scale rotor having untwisted blades of conventional plan-form taper. The data points represent measured data obtained over a range of subsonic tip speeds, whereas the solid line is the theoretical prediction using a measured minimum profile-drag coefficient. The lower plot shows a corresponding setup except that the test rotor had  $-8^\circ$  of twist. In both cases, the agreement is excellent. (An explanation of hovering theory can be found in ref. 1. The data shown in the figure were obtained from ref. 2.)

The aerodynamic factors that affect rotor losses in hovering are summarized as follows:

Loss	Primary factors	Secondary factors
Induced	Disk loading Blade twist Plan-form taper	
Profile drag	Airfoil-surface condition Airfoil section Solidity Tip speed	Blade twist Plan-form taper

The induced losses are primarily influenced by rotor disk loading, as well as by blade twist and plan-form taper. Profile-drag losses are primarily dependent on the type of airfoil section chosen and the degree to which true aerodynamic contour and surface condition is achieved with the as-built blades under actual operating conditions, as well as on rotor solidity and tip speed. Induced losses are typically two to three times as large as those due to profile drag for the normal range of disk loadings. Some of these effects will now be discussed in terms of actual numbers.

The effect of disk loading on the induced loss can be seen from figure 2 (obtained from ref. 1) which represents the number of pounds of thrust produced by 1 horsepower as a function of disk loading for a uniform-inflow rotor operating at a constant mean lift coefficient and solidity. It can be seen that the benefits of low disk loading are large, and the maximum benefit is obtained at values less than 2. The present trend is toward increasing the disk loading from the conventional 2 to 3 to something between 3 to 6, and it can be seen that in this upper range the effect of a decrease in disk loading, although not as marked as in the lower range, is still quite significant percentage-wise, particularly from the standpoint of the effect on payload. A reduction in disk loading from 6 to 3, for example, increases the thrust

by about 30 percent, and the payload by perhaps three or four times that amount. It is realized, of course, that these aerodynamic considerations would be modified by other factors, such as overall size, weight, type of powerplant, and cost, which would also influence the choice of disk loading for a particular design. From the aerodynamic standpoint, however, load lifters should be designed with as low a disk loading as possible.

Low disk loadings are also beneficial in reducing adverse compressibility effects on profile-drag power when operation at high tip speeds is involved, in that low disk loadings result in low mean lift coefficients and thus higher force divergent Mach numbers. In forward flight, low disk loadings result in the achievement of higher forward speeds because of a delay in rotor stall effects.

Rotor blade twist and plan-form taper also have a significant effect on rotor induced losses, and to a lesser extent, on profile-drag losses as well. The predicted effects of twist and taper are summarized in figure 3. This figure shows the thrust produced, at constant power, solidity, and tip speed, by a large-diameter rotor differing only in amount of blade twist and plan-form taper. As a basis for comparison, the thrust produced by an "ideal" rotor, that is, a rotor operating with uniform inflow and zero profile drag, is also shown as the top bar in figure 3. In each case, the thrust is shown as the sum of empty weight plus fuel (represented by the shaded part of the bars) and payload (represented by the unshaded part of the bars). The weight empty plus fuel is the same for all of the designs and was assumed to be one-quarter of the thrust of the untwisted and untapered rotor.

It can be seen that the benefits of twist and taper are considerable, amounting to an increase in payload of approximately 3,000 pounds (or 43 percent) for  $-12^\circ$  twist and 3:1 taper over the untwisted, untapered case. An additional 600 pounds (approximately 6 percent) could be achieved with a rotor having twist and taper such that it produces uniform inflow and operates at a constant angle of attack all along the blade. The difference in payload between such a rotor and an ideal rotor amounts to almost 6,700 pounds (or 64 percent) and represents the effect of profile drag. With typical production blades, part of this 64-percent extra payload represented by the elimination of profile drag could conceivably be achieved with extra production effort or the use of more nearly optimum airfoil sections. The following paper by Robert D. Powell, Jr., discusses this point more fully in that it deals with the use of special airfoil sections and the effects of surface tolerances and roughness on hovering efficiency. (A more complete discussion of twist and taper effects can be found in refs. 1 and 3.)

In addition to the benefits of twist already discussed, blade twist is also beneficial in delaying and alleviating compressibility effects



on rotors, particularly those that are required to hover at high tip speeds because of powerplant or high-speed flight considerations. From tests performed at high tip speeds on the helicopter test tower (ref. 2) with two sets of 15-percent-thick blades, it was shown that at tip speeds high enough to cause compressibility effects on one or more of the rotors, the blades with  $-8^{\circ}$  of twist required about 15 percent less power for a given thrust and tip speed than untwisted blades. Although about one-fifth of this decrease may be ascribed to more favorable induced considerations, as previously discussed, the benefits of twist in minimizing compressibility effects are substantial.

So far, the effects of disk loading and blade design on hovering performance for a fixed tip speed and solidity have been demonstrated. The combination of tip speed and solidity itself is a very potent factor, inasmuch as it has a marked effect on profile drag. Its effect is shown in figure 4 which represents the efficiency of a constant-inflow rotor as a function of both rotor mean lift coefficient and solidity. The efficiency is expressed by the ordinate as the inverse ratio of the power required by the actual rotor to produce a given thrust to that required by the same rotor operating without any profile-drag losses. Thus, an ideal rotor would have an efficiency of 1 (or 100 percent). Rotor mean lift coefficient, as shown on the horizontal scale, is proportional to the thrust-coefficient-solidity ratio, which in turn is proportional to both tip-speed squared and solidity at constant disk loading.

It is seen from the figure that maximum hovering efficiency is obtained by that combination of thrust-coefficient and solidity that results in both a high mean lift coefficient and a high solidity. The reason for this statement becomes apparent if operation of a rotor at constant mean lift coefficient is considered. If the rotor solidity is increased, the tip speed correspondingly must be decreased in order to keep the thrust constant. However, since the profile power varies as the tip-speed cubed, whereas the thrust varies as the tip-speed squared, operation at the lower tip speed results in less profile power for a given thrust and hence in greater efficiency. Alternately, if the solidity as well as the thrust is fixed and operation is at a lower tip speed, and thus an increased mean lift coefficient, the "square-cube" tip-speed considerations just discussed will again result in increased efficiency. (See ref. 1, ch. 3, for a more complete discussion.)

Because the mean lift coefficient involves both tip speed and solidity, the effect of independent variations of the two can be seen more easily with the dimensional illustrative case shown in figure 5, which shows the variation of rotor thrust with tip speed produced at constant power at various solidities. Each of the curves shown is terminated at a tip speed corresponding to a mean lift coefficient of 1.2, on the assumption that the rotor would be badly stalled above that value. In the practical case, a margin is allowed between design mean

lift coefficient and the stall. In this case, the design mean lift coefficient  $\bar{c}_l$  was arbitrarily assumed to be 0.8; operation above this value is represented by the dashed portion of the curves.

Figure 5 indicates that if the designer were free to choose a tip-speed—solidity combination that would result in maximum hovering efficiency, he would choose a high-solidity—low-tip-speed combination. Such might be the case in the design of a pulse-jet-powered load lifter. On the other hand, if other considerations fix the tip speed in the higher range of speeds, a low solidity would be indicated. At the particular disk loading being considered in this example, however, the requirement that operation be confined to values of  $\bar{c}_l$  less than 0.8 would prohibit the use of as low a solidity as 0.02 over the tip-speed range shown.

Normally the choice of a particular solidity—tip-speed combination is influenced by stall considerations on the retreating blade in forward flight. In a few cases studied, sample calculations have indicated that different combinations of solidity and tip speed that produce the same angle of attack at the tip of the retreating blade in forward flight, and thus the same limiting forward speed, also yield the same hovering performance. (See ref. 4.)

Thus, in the design stage, if the hovering condition was considered about as important as the high end of the speed range, it would appear that other than purely aerodynamic considerations would fix the choice of a particular combination of solidity and tip speed. On the other hand, if high forward speeds were considered paramount, both high tip speeds and solidity might be employed. In such a case, the figure indicates that the penalty in hovering efficiency could be considerable. Such a penalty would be avoided, of course, in designs wherein high power could be obtained at both high and low tip speeds, as might be the case if certain types of gas-turbine powerplants or a gear-shift transmission were employed.

## REFERENCES

1. Gessow, Alfred, and Myers, Garry C., Jr.: Aerodynamics of the Helicopter. The Macmillan Co., c.1952.
2. Carpenter, Paul J.: Effects of Compressibility on the Performance of Two Full-Scale Helicopter Rotors. NACA Rep. 1078, 1952. (Supersedes NACA TN 2277.)
3. Gessow, Alfred: Effect of Rotor-Blade Twist and Plan-Form Taper on Helicopter Hovering Performance. NACA TN 1542, 1948.
4. Gustafson, F. B., and Gessow, Alfred: Effect of Rotor-Tip Speed on Helicopter Hovering Performance and Maximum Forward Speed. NACA WR L-97, 1946. (Formerly NACA ARR L6A16.)

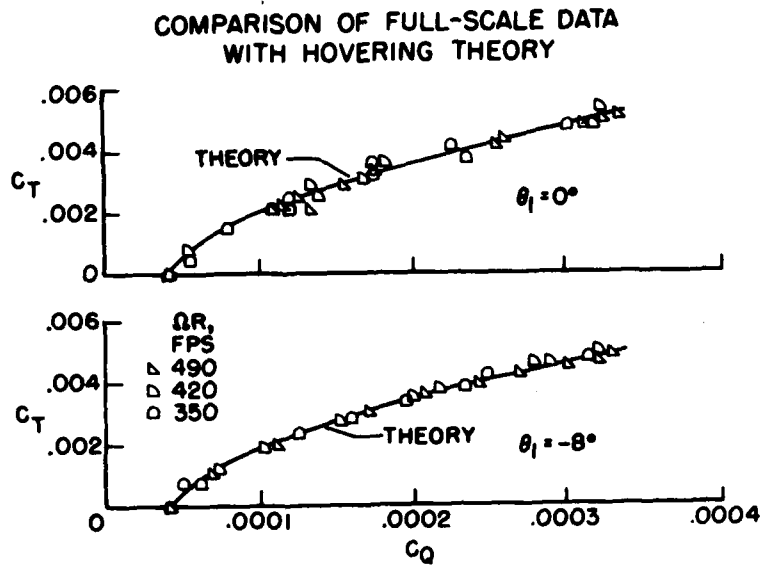


Figure 1

**EFFECT OF DISK LOADING ON THRUST-POWER RATIO IN HOVERING**  
 $\bar{c}_t$  AND  $\sigma$  CONSTANT

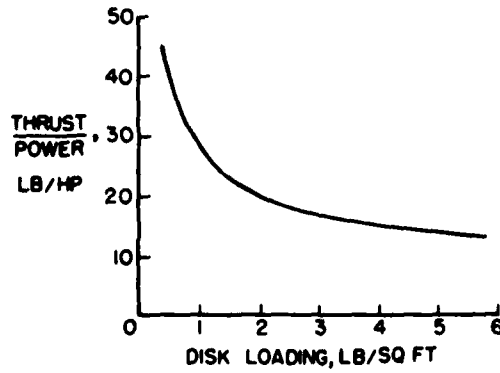


Figure 2

EFFECT OF BLADE DESIGN ON HOVERING PAYLOAD  
 2,000 HP; R = 60 FT;  $\Omega R = 550$  FPS;  $\sigma = 0.06$

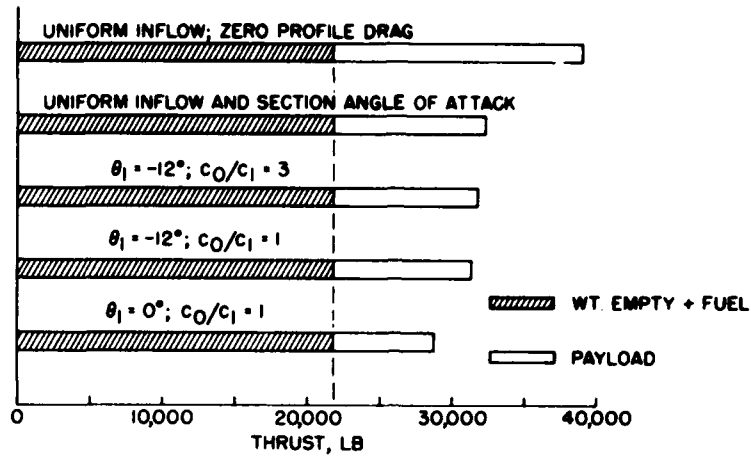


Figure 3

EFFECT OF  $\bar{c}_1$  AND  $\sigma$  ON ROTOR EFFICIENCY IN HOVERING

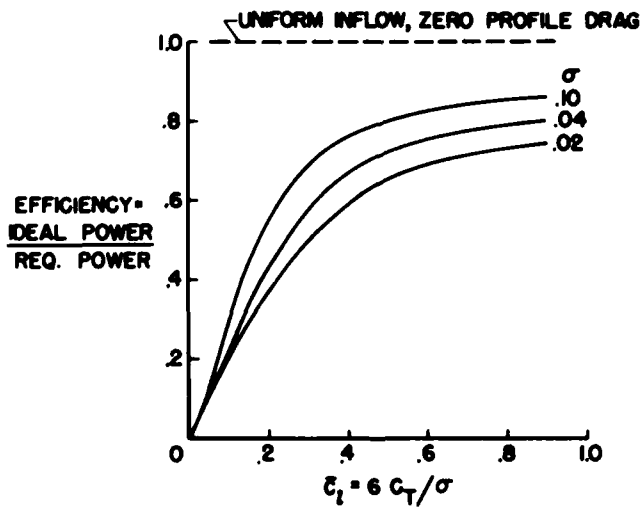


Figure 4

VARIATION OF THRUST WITH TIP SPEED AT CONSTANT  
POWER AND SOLIDITY  
2,700 HP, R=60 FT; DISK LOADING  $\approx 3\frac{1}{2}$  LB/SQ FT

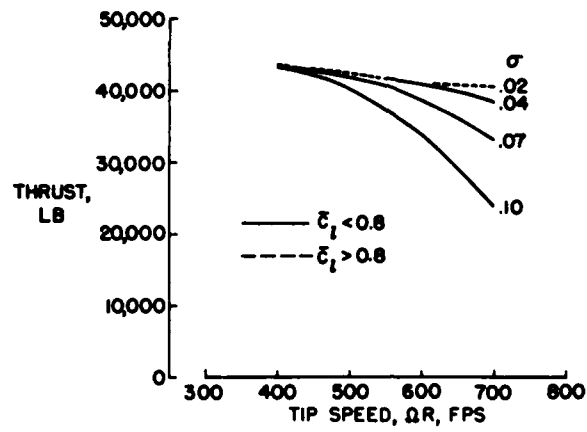


Figure 5

HOVERING PERFORMANCE OF A HELICOPTER ROTOR  
USING NACA 8-H-12 AIRFOIL SECTIONS

By Robert D. Powell, Jr.

Langley Aeronautical Laboratory

SUMMARY

A helicopter rotor employing an NACA 8-H-12 airfoil section has been tested on the Langley helicopter test tower. Two blade surface conditions were investigated, first with a filled blade which was within 0.002 inch of true airfoil shape obtained by use of plastic filler, and second with the filler removed resulting in a surface condition within 0.020 inch of true airfoil shape. Tests were conducted for the two surface conditions at a tip speed of 455 feet per second and over a tip-speed range from 455 to 650 feet per second for the blades with filler removed. The NACA 8-H-12 blades with the filled surface showed an average reduction of 6 to 7 percent in total torque coefficients.

INTRODUCTION

As previously reported in reference 1, the problem of designing a rotor for minimum induced power is fairly well understood and further increases in rotor performance must come from a decrease in the profile power losses. In this connection, the National Advisory Committee for Aeronautics has derived a group of airfoil sections having low profile-drag characteristics that have been developed specifically for use on helicopter rotor blades. From this group of airfoils the NACA 8-H-12 airfoil section, which appeared to be the most promising, was incorporated in a rotor blade for tests on the Langley helicopter test tower.

SYMBOLS

R        blade radius, ft  
b        number of blades  
c        blade section chord, ft

$\sigma$	rotor solidity, $bc/\pi R$
$\rho$	density of air, slugs/cu ft
$T$	rotor thrust, lb
$Q$	rotor-shaft torque, lb-ft
$M_b$	measured rotor-blade pitching moment, positive for moment tending to increase blade pitch, lb-ft
$\Omega$	rotor angular velocity, radians/sec
$c_{d_0}$	section profile-drag coefficient
$c_l$	section lift coefficient
$C_T$	rotor thrust coefficient, $\frac{T}{\pi R^2 \rho (\Omega R)^2}$
$C_Q$	rotor-shaft torque coefficient, $\frac{Q}{\pi R^2 \rho (\Omega R)^2 R}$
$C_{Q_0}$	rotor-shaft profile-drag torque coefficient
$C_{m_c}/4$	rotor-blade pitching-moment coefficient, $\frac{M_b}{\frac{1}{2} \rho (\Omega R)^2 c R}$
$\theta$	blade-section pitch angle measured from line of zero lift, radians

#### APPARATUS

The present investigation was conducted on the Langley helicopter test tower (fig. 1) described in reference 2. The only change in the instrumentation was the addition of individual blade pitching-moment indicators. This addition consisted of a ring strain gage mounted on the pitch control rod; the signal from the strain gage was transmitted through a silver slip ring to the oscillograph where it was recorded.

The two rotor blades were of fiber-glass construction and were covered with a 0.004- to 0.005-inch-thick stainless-steel skin. The



blades had a radius of 18.63 feet from the center line of rotation, a constant chord of 1.2 feet, zero twist, a rotor solidity of 0.041, a torsional stiffness of 600 in-lb/deg of twist, and an NACA 8-H-12 airfoil section. Plan-form views of one of the test blades are shown in figure 2. A cutaway view showing the details of the blade construction is shown in figure 3. The inner core of the blade was made of strips of foam plastic wrapped with one layer of 0.005-inch fiber glass. The trailing-edge core was made of birch veneer and was bonded to the fiber glass and plastic foam core. A birch veneer block was also bonded to the forward section of the plastic core. This assembly was then covered (except for the forward part of the birch veneer block) with several layers of fiber-glass cloth impregnated with Paraplex resin. Blade chordwise balance was obtained by bonding a steel leading edge to the birch veneer block. The entire assembly was then covered by bonding a stainless-steel skin to the core. The stainless-steel skin served to carry about 20 percent of the centrifugal loads and gave a uniform and corrosion-proof exterior surface.

### RESULTS AND DISCUSSION

Figure 4 shows some of the results of the tests of the two-dimensional airfoil (ref. 3) together with data from tests of the NACA 0012 airfoil section (ref. 4) which are presented for comparison purposes. Before describing the basic airfoil-section characteristics, it might be of interest to consider the reason for the shape of the NACA 8-H-12 airfoil. Since the interest is in the low drag, a low-drag thickness form was used. The airfoil was cambered so that the low drag would be realized at positive lift coefficients. This effect also means a high lift-drag ratio is achieved. In order to counteract the pitching moments introduced by camber, the trailing edge was reflexed. Figure 4 shows section drag coefficient plotted against section lift coefficient. These tests showed that the smooth NACA 8-H-12 airfoil had very good low profile-drag characteristics as compared with the NACA 0012 airfoil section, especially in the lift-coefficient range in which most of the rotor disk operates. Therefore, any decrease in drag in this range is very important. At the higher lift coefficients, the NACA 8-H-12 airfoil section does not look as attractive because of its higher drag; however, this high drag is out of the region of major power losses, at least until the stall limit in forward flight is approached.

It is of interest to know that, if these two airfoils are compared for the condition with leading-edge roughness, the profile polars are practically identical. The only difference is that for the NACA 8-H-12 airfoil, because of its camber, the minimum drag occurs at a positive lift coefficient rather than at zero lift coefficient.

It is important to know whether this low profile drag can be achieved on actual rotor blades. Therefore, a program was initiated to build a set of NACA 8-H-12 airfoil blades to as near perfect contour as possible and to test them on the Langley helicopter test tower (fig. 1). When the blades were completed, the departure from true airfoil contour was within 0 to  $-0.020$  inch. A filler was then applied to the blades over the top 40 percent and bottom 80 percent of the chord which represent the theoretical extent of laminar flow on this airfoil. After careful sanding and polishing, the blade contour was within 0 to  $-0.002$  inch of the true airfoil contour. The general smoothness and fairness was such that laminar flow could be reasonably expected on at least half the blade if it were tested as a two-dimensional airfoil.

The effect of the surface condition on the profile torque is shown in figure 5 where the thrust-coefficient—solidity ratio is plotted against profile torque coefficient for the NACA 8-H-12 blades. The data were obtained at a tip speed of 455 feet per second with a rotor solidity of 0.041. The profile torque coefficient was obtained by subtracting the calculated induced torque coefficient from the total measured torque coefficient. The calculated curve to the left indicates the profile torque that would have been obtained if the smooth drag curve shown in the two-dimensional-airfoil results had been realized. The middle curve represents the experimentally determined profile torque for the blades with the filled surface. The curve to the right represents the experimental data for the blades with their original surface (filler removed).

Over a representative range of hovering mean lift coefficient, from about 0.3 to 0.6, the profile power would have been reduced from 45 to 60 percent if the smooth-two-dimensional-airfoil results had been obtained from the rotor. Actually, only about half this reduction was obtained with the filled blades, which amounted to a reduction in the total power being absorbed by the rotor of the order of 6 to 7 percent.

Figure 6 shows a comparison between the results obtained for the blades with their original surface and a calculated curve based on the empirical drag polars (ref. 5) that has been found from experience to be representative of well-built rotor blades having conventional airfoil sections. Most of the published NACA rotor-performance charts are based on this polar.

The curves show that there is very little difference in rotor performance except at the very high thrust coefficients above a thrust-coefficient—solidity ratio of 0.10. This increase in profile torque was indicated by the two-dimensional-airfoil results and may not be of great importance because helicopters very seldom hover in this range. In the range from 0.06 to 0.09 where they do operate, some small benefits may be derived.

In the course of the investigation, data were obtained at various tip speeds. Figure 7 shows a plot of thrust coefficient against total torque coefficient for the NACA 8-H-12 blades with their original finish at tip speeds of 455 and 650 feet per second. These two curves show very little difference in rotor performance. At the lower rotor thrust coefficients there was a slight scale effect and at the higher thrust coefficients there was an increase in power required as a result of compressibility losses. In general, there are no gross effects for the two tip speeds shown.

The blade pitching moments were also measured during the tests; figure 8 shows the variations of the pitching-moment coefficient about the quarter-chord point as a function of blade pitch angle in degrees for a tip speed of 455 feet per second. The NACA 8-H-12 blade pitching moments tend to remain zero from about  $3^{\circ}$  to  $9^{\circ}$ . Slight positive pitching moments are indicated at zero blade pitch and increasingly negative pitching moments are indicated at the higher blade pitch angles. In general, the pitching moments were similar to those that have been measured on rotor blades having conventional airfoil sections. The variation shown is typical of all the measured pitching moments on the NACA 8-H-12 blades with their original surface at the various tip speeds.

#### CONCLUDING REMARKS

From an investigation of the hovering performance of a helicopter rotor using NACA 8-H-12 airfoil sections it appears that the performance of the NACA 8-H-12 blades in the condition in which they arrive from the shop, that is, smooth and fair and within 0.020 inch of the true airfoil contour, was comparable to what might be expected from good practical-construction rotor blades. Improving the surface-contour accuracy to within 0.002 inch of the true airfoil contour resulted in getting about half the theoretical reductions in profile drag that would be expected on the basis of tests of the smooth two-dimensional airfoil. This effect amounted to an average reduction in total torque coefficients of 6 to 7 percent.

## REFERENCES

1. Gessow, Alfred, and Myers, Garry C., Jr.: Aerodynamics of the Helicopter. The Macmillan Co., c.1952.
2. Carpenter, Paul J.: Effect of Wind Velocity on Performance of Helicopter Rotors As Investigated With the Langley Helicopter Apparatus. NACA TN 1698, 1948.
3. Schaefer, Raymond F., and Smith, Hamilton A.: Aerodynamic Characteristics of the NACA 8-H-12 Airfoil Section at Six Reynold Numbers From  $1.8 \times 10^6$  to  $11.0 \times 10^6$ . NACA TN 1998, 1949.
4. Smith, Hamilton A., and Schaefer, Raymond F.: Aerodynamic Characteristics at Reynolds Numbers of  $3.0 \times 10^6$  and  $6.0 \times 10^6$  of Three Airfoil Sections Formed by Cutting Off Various Amounts From the Rear Portion of the NACA 0012 Airfoil Section. NACA TN 2074, 1950.
5. Bailey, F. J., Jr., and Gustafson, F. B.: Charts for Estimation of the Characteristics of a Helicopter Rotor in Forward Flight. I - Profile Drag-Lift Ratio for Untwisted Rectangular Blades. NACA WR L-110, 1944. (Formerly NACA ACR L4HO7.)

THE LANGLEY HELICOPTER TEST TOWER



Figure 1

PLAN-FORM VIEW OF NACA 8-H-12 ROTOR BLADE  
SHOWING 80% OF CHORD SURFACE FILLED

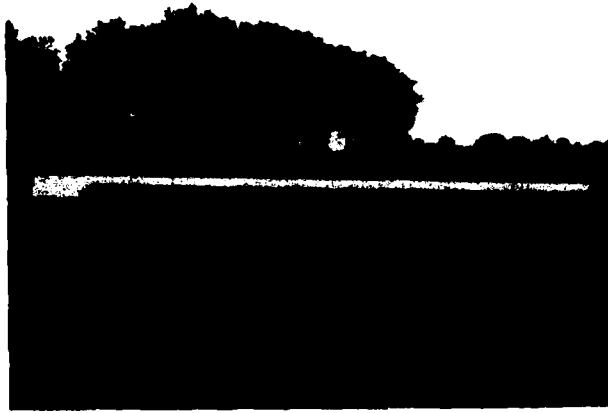


Figure 2(a)

PLAN-FORM VIEW OF NACA 8-H-12 ROTOR BLADE  
SHOWING 40% OF CHORD SURFACE FILLED



Figure 2(b)

CUTAWAY VIEW OF NACA 8-H-12 BLADE SECTION  
SHOWING CONSTRUCTION DETAIL

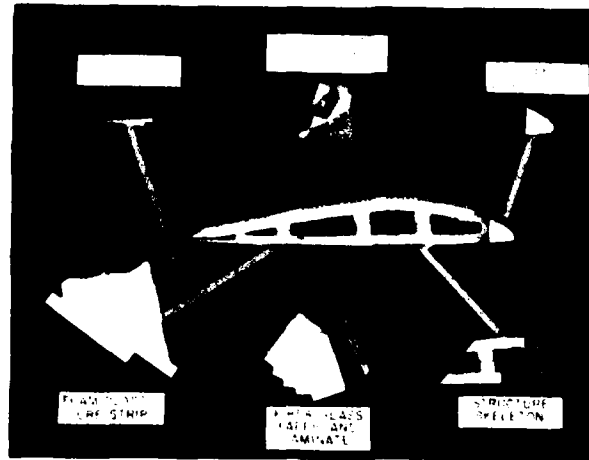


Figure 3

AERODYNAMIC CHARACTERISTICS OF NACA 8-H-12  
AIRFOIL SECTION AS COMPARED TO AN NACA 0012  
AIRFOIL SECTION

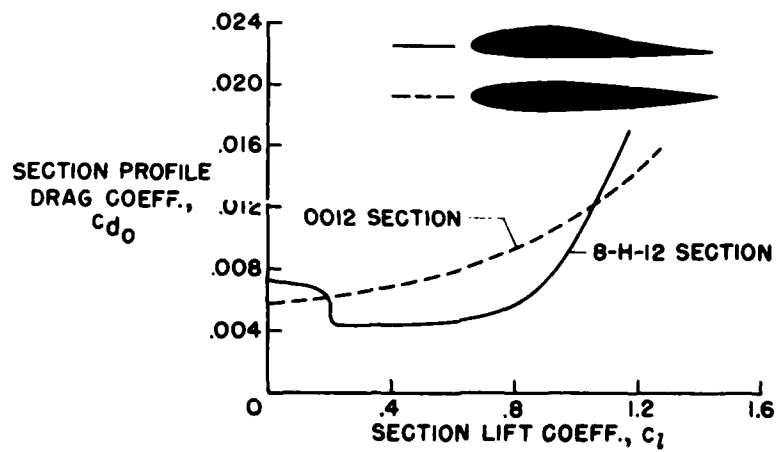


Figure 4

PROFILE TORQUE CURVES OF NACA 8-H-12 ROTOR BLADES  
 $\Omega R = 455 \text{ FPS}$ ;  $\sigma = 0.041$

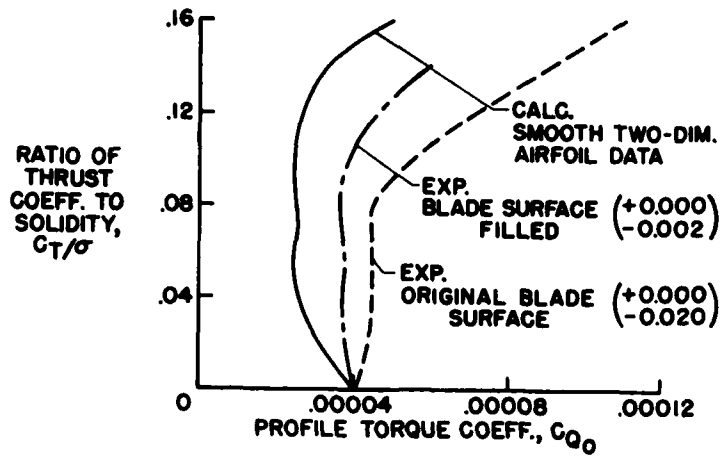


Figure 5

COMPARISON OF NACA 8-H-12 ROTOR (ORIGINAL SURFACE) WITH CALC. USING EMPIRICAL DRAG POLAR

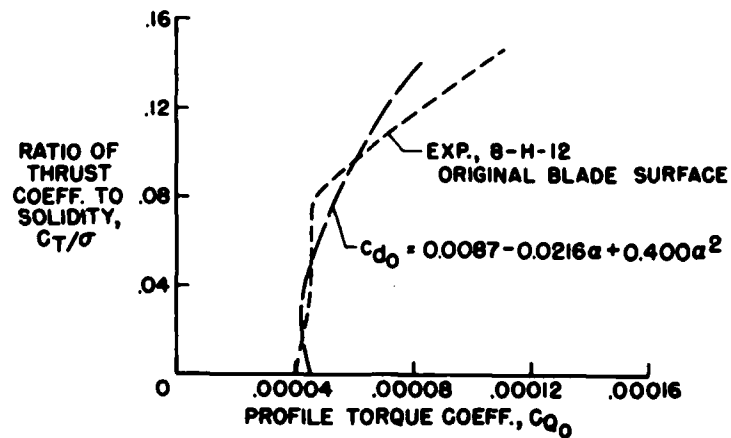


Figure 6



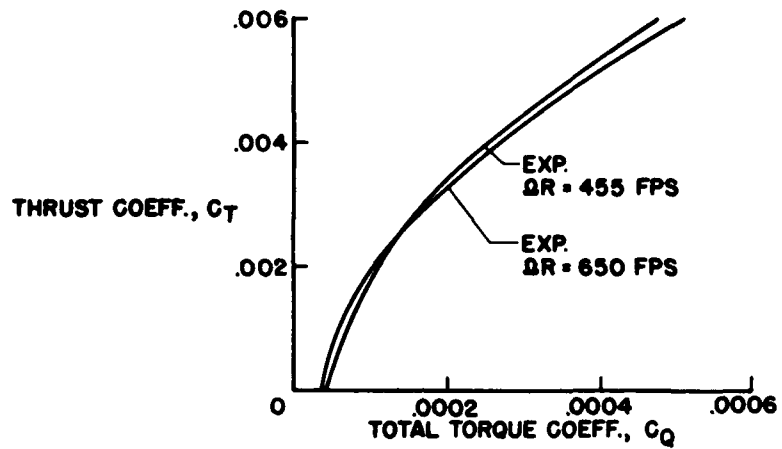
HOVERING PERFORMANCE OF NACA 8-H-12 BLADES AT  
TWO TIP SPEEDS

Figure 7

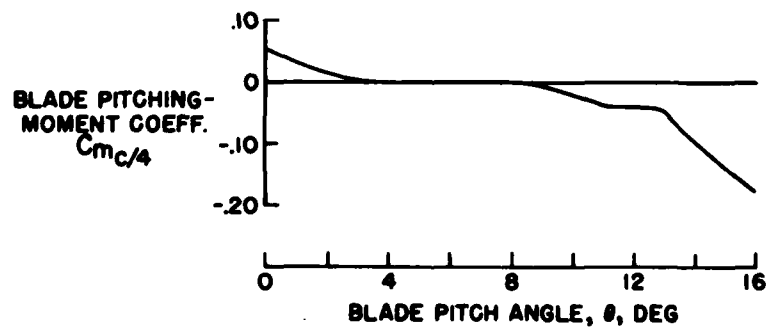
MEASURED NACA 8-H-12 ROTOR BLADE PITCHING-  
MOMENT COEFF. ABOUT QUARTER CHORD

Figure 8

## SOME RECENT DEVELOPMENTS IN ROTOR THEORY

By Alfred Gessow and Almer D. Crim

Langley Aeronautical Laboratory

## INTRODUCTION

The problem of determining the aerodynamic characteristics of a lifting rotor basically consists of calculating the forces and moments on a rotating three-dimensional wing from statically measured two-dimensional airfoil-section data. Because of the large number of degrees of freedom involved, and the complications introduced by the variation in section angles of attack and velocities over the rotor disk, an analytical approach to the problem necessarily contains various assumptions and simplifications. The largest number of such simplifying assumptions is found in the original efforts of Glauert and Locke, published almost thirty years ago. Since that time, the theory has been progressively improved in accuracy and in convenience of application by a number of investigators. The purpose of this discussion is to summarize some of the more recent developments made by the NACA in helicopter rotor theory.

## SYMBOLS

a	slope of section lift curve
$C_p$	shaft power coefficient
$C_{p_0}$	profile-drag power coefficient
$C_T$	rotor thrust coefficient
dD	blade-section drag
dL	blade-section lift
M	Mach number
R	rotor-blade tip radius
V	forward velocity
$\alpha_r$	blade-element angle of attack measured from line of zero lift

$\theta$	blade-section pitch angle
$\theta_0$	blade pitch angle at hub
$\theta_1$	difference between hub and tip pitch angles
$\mu$	tip-speed ratio
$\sigma$	rotor solidity
$\phi$	inflow angle
$\psi$	blade azimuth angle
$\Omega$	rotor angular velocity

### DISCUSSION

The theory of reference 1, which was later used in the preparation of charts (refs. 2 and 3), has been extensively used by the NACA in performance calculations and as a basis for stability, vibration, and loads studies. This theory has given good correlation with flight test results and appears to be adequate for predicting the performance of present-day helicopters.

Because of certain restrictive assumptions contained in the theory, however, it was considered that it might not be applicable to helicopters capable of greatly increased performance and for certain types of convertible aircraft with rotors that operate through a large angle-of-attack range. Some of these assumptions may be illustrated with the aid of figure 1. The assumptions referred to include:

- (1) Inflow angles small enough that the sine may be replaced by the angle and the cosine by unity
- (2) Velocity at a blade element approximated by the tangential component
- (3) Section lift and drag curves that do not account for stall

Because the flight of high-performance helicopters and convertiplanes involves operation at high inflow angles, and because relatively large regions of reversed velocity are present at high tip-speed ratios, the theory was extended (ref. 4) to remove the inflow-angle assumptions, to consider the resultant velocity at a blade element, and to permit the use of more realistic lift and drag coefficients in the reversed-flow

region. Part of this extension was accomplished by utilizing a suggestion from reference 5 that, although the individual inflow and blade pitch angles might be large, the difference between the two, which is the angle of attack, would usually be small. Any small-angle assumptions necessary could therefore be more appropriately applied to the angle of attack. As in the theory of reference 1, the extended method did not account for stall outside of the reversed-velocity region, or for compressibility effects on the airfoil section characteristics.

In connection with stall effects, it should be pointed out that design charts based on either method contain limit lines that indicate not only the limiting flight conditions at which the theory becomes optimistic because stall is not taken into account, but also the most efficient conditions of operation.

A comparison of the two methods showed that little difference existed at inflows and tip-speed ratios common for current helicopters. However, under other conditions, significant differences can occur, as illustrated in figure 2. This figure shows the computed ratios of profile power to thrust for two inflow conditions over a range of tip-speed ratios. At the low-inflow condition, corresponding to a low power, the two methods give essentially the same answers over the range of tip-speed ratios shown. At the high-inflow condition, corresponding to a high rate of climb or to a large forward tilt of the rotor at high speed, the two theories agree only at low tip-speed ratios and diverge very rapidly at the higher ones. At  $\mu = 0.5$  the difference is about 2 to 1.

Since the extended theory still contains some resultant-velocity and small-angle assumptions, particularly in the reversed-velocity region, the validity of these simplifications was verified by a number of check calculations which eliminated the necessity for these particular assumptions. The results were in good agreement.

Because some of the equations of the extended theory are lengthy, the thrust, power, and torque relationships over a range of flight conditions, including tip-speed ratios up to 0.5, were evaluated and are being used to prepare design charts. A sample chart is shown in figure 3, which graphically expresses the relationship between nondimensional rotor profile-drag power, shaft power, thrust, and pitch angle, all for a given value of blade twist and tip-speed ratio. The power ratios  $C_{P0}/C_T$  and  $C_P/C_T$  correspond to the more familiar helicopter parameters  $(D/L)_0$  and  $P/L$ , respectively, but are based on tip speed rather than forward speed and thus avoid infinite values as the tip-speed ratio approaches zero. Inboard and outboard limit lines are also shown on the charts in order to aid in determining the onset of stall. It might be pointed out that, contrary to the previously published NACA helicopter performance

charts, the form of the charts shown does not involve a trial-and-error method of determining profile drag and shaft power.

As previously mentioned, the extended method and the charts based upon it do not take into account compressibility effects or stall outside of the reversed-velocity region. In order to account for these effects, as well as for changes in such design parameters as hinge offset, blade cutout, and blade mass factor, it would seem more practical to calculate such effects numerically (perhaps by automatic computing machines) for a relatively small number of conditions and to apply the results as correction factors to the charts, rather than further to complicate the already lengthy analytical expressions.

An example of the results that have been obtained thus far from numerical point-by-point calculations made at the Langley Laboratory is shown in figure 4, which illustrates rotor compressibility effects in forward flight. The figure shows a plan-form view of a rotor in forward flight at a speed of 200 miles per hour and a rotor tip speed of 750 feet per second. The solid lines represent contours of constant angle of attack; the dashed lines contours of constant Mach number; and the shaded area the region in which the drag-divergence Mach number has been exceeded for the particular airfoil section chosen.

The profile-drag power loss corresponding to this condition was computed by using airfoil-section data corresponding to the angle-of-attack and Mach number combinations shown. Then, in order to compare compressibility effects, the power loss was again computed, keeping the same tip-speed ratio but assuming a much lower tip speed (350 fps).

The profile-drag power losses thus obtained differed by a factor of about 2, the larger answer of course corresponding to the higher tip speed. Although the example shown was somewhat extreme, rotor thrust was not affected to a significant extent by Mach number. If a number of such cases were computed for the particular airfoil section considered, it is expected that the increase in profile-drag power could be used as a correction to the incompressible power values given on the previously described analytical charts.

Since the airfoil used in this study stalled at an angle of attack of about  $10^\circ$  or  $11^\circ$ , it may be seen from the angle-of-attack contour lines of figure 4 that a fairly large area of the rotor disk is stalled, and it might be of interest to see how the power losses are distributed between the advancing and retreating blades.

Figure 5 shows such a distribution. Profile-drag power coefficient is plotted against azimuth angle for both tip speeds. Values of blade azimuth  $\psi$  from  $0^\circ$  to  $180^\circ$  correspond to positions of the advancing blade and from  $180^\circ$  to  $360^\circ$  to positions of the retreating blade. The

area under each curve is proportional to the power loss, and for the lower tip speed (with little or no compressibility losses), it may be seen that the advancing blades (with low angles of attack but high velocity) and the retreating blades (stalled but with lower velocities) contribute about equally to the total loss. For the higher tip speed, however, there is some change on the retreating side but a very large increase on the advancing side. It is thus seen that, for this case, the effect of compressibility is greatest on the advancing side and is far greater than the increase in power due to stall already present on the retreating side.

#### CONCLUDING REMARKS

In summary, it might be said that, except perhaps for very specialized purposes, the extension of the general rotor theory by explicit analytical means has been carried about as far as is considered feasible. Effects of stall, compressibility, and other design variables on rotor power requirements, as well as stability and control and loads and vibration characteristics, may be numerically evaluated with high-speed computing machines, with the analytical theory serving as a base line for interpreting and extending the results of the numerical computations.

#### REFERENCES

1. Bailey, F. J., Jr.: A Simplified Theoretical Method of Determining the Characteristics of a Lifting Rotor in Forward Flight. Rep. 716, 1941.
2. Bailey, F. J., Jr., and Gustafson, F. B.: Charts for Estimation of the Characteristics of a Helicopter Rotor in Forward Flight. I - Profile Drag-Lift Ratio for Untwisted Rectangular Blades. NACA WR L-110, 1944. (Formerly NACA ACR L4H07.)
3. Gustafson, F. B.: Charts for Estimation of the Profile Drag-Lift Ratio of a Helicopter Rotor Having Rectangular Blades With  $-8^{\circ}$  Twist. NACA RM L53G20a, 1953.
4. Gessow, Alfred, and Crim, Almer D.: An Extension of Lifting Rotor Theory To Cover Operation at Large Angles of Attack and High Inflow Conditions. NACA TN 2665, 1952.
5. Castles, Walter, Jr., and New, Noah C.: A Blade-Element Analysis for Lifting Rotors That Is Applicable for Large Inflow and Blade Angles and Any Reasonable Blade Geometry. NACA TN 2656, 1952.

VELOCITIES, ANGLES, AND FORCES  
AT A BLADE ELEMENT

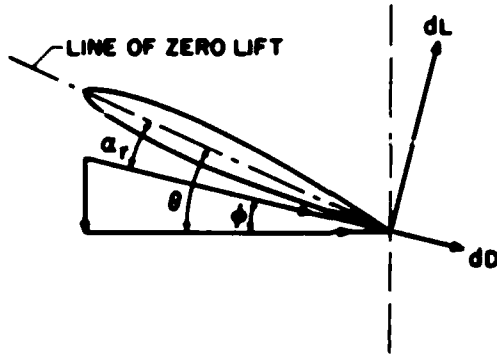


Figure 1

COMPARISON OF ROTOR PROFILE - DRAG POWER LOSS

$$\frac{2C_T}{\sigma a} = 0.01$$

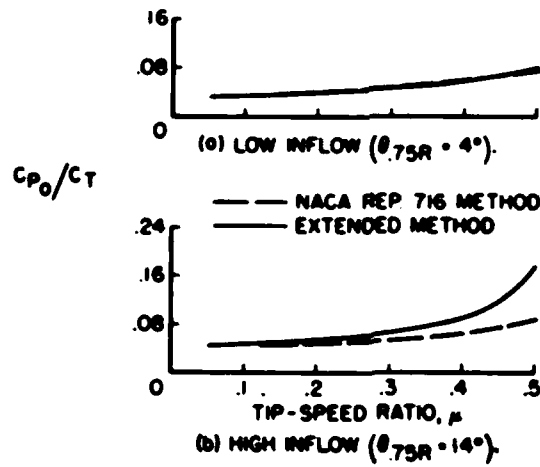


Figure 2

SAMPLE PERFORMANCE CHART FOR GIVEN BLADE TWIST  
AND TIP-SPEED RATIO

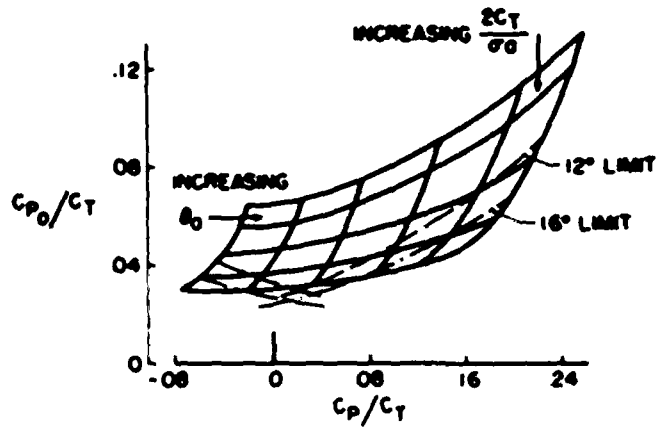


Figure 3

ANGLE-OF-ATTACK AND MACH NUMBER CONTOURS  
V = 200 MPH; BR = 750 FPS, β<sub>1</sub> = -8°

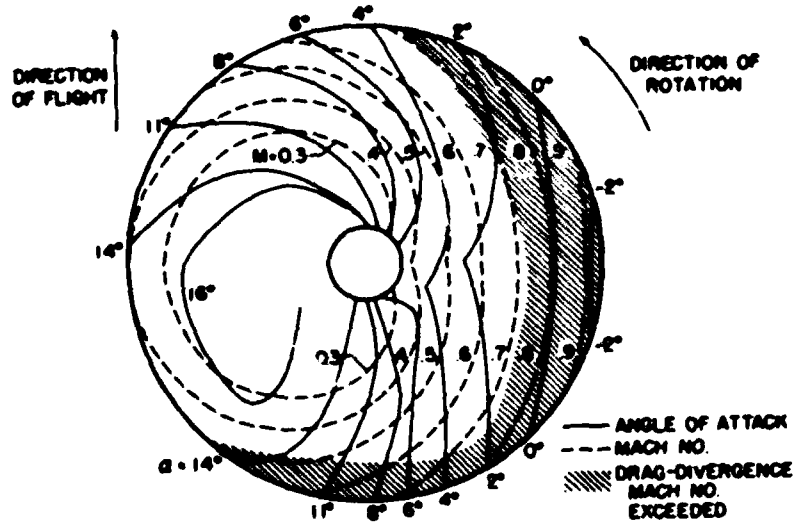


Figure 4



EFFECT OF COMPRESSIBILITY ON PROFILE-POWER  
VARIATION WITH AZIMUTH ANGLE

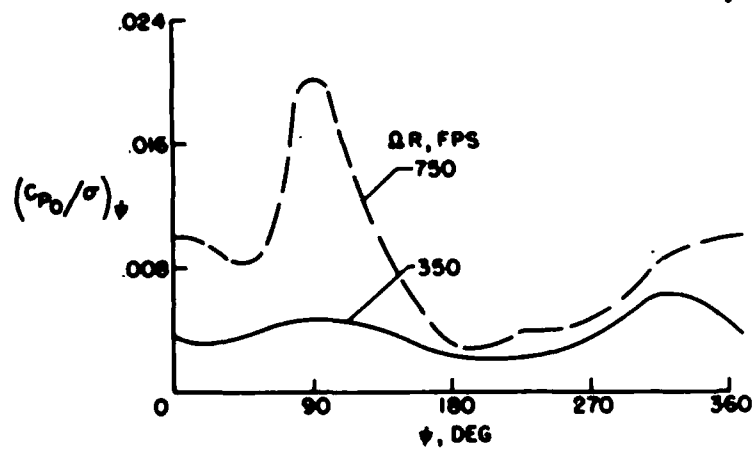


Figure 5

A DISCUSSION OF FORWARD-SPEED LIMITATIONS INTRODUCED  
BY STALL AND MACH NUMBER EFFECTS

By F. B. Gustafson and Robert D. Harrington

Langley Aeronautical Laboratory

The subject of forward-speed limitations is distinguished from ordinary power-required considerations where small percentages are treated in that "limits," so-called, involve extreme increases in power plus difficulties of stability and control, vibration, and blade stress.

There are classes of helicopter uses, including the ship-to-shore type of assault mission on the one hand and commercial feeder-line transportation on the other, where increased speed has great value. Also, even for limiting forward speeds of only 80 mph or so, design compromises with hovering are often involved. This paper therefore reviews the current knowledge on forward-speed limitations. Part of this material is well-known but it is included for completeness.

The first of these limitations to be discussed is blade stalling. It is well-known that the blade on the retreating side encounters stalling at high forward speeds. Since this blade goes backwards, it operates at lower air velocities with increased forward speed and, to maintain its lift, operates at higher and higher angles of attack.

This problem has already been explored experimentally for the autogiro (ref. 1), but since the problem is somewhat different for the helicopter, additional studies have been made. These studies have been summarized in figure 1.

As the first step, tuft studies of blade stalling were made in reference 2. It was found that existing theory could predict the condition at which stalling would begin. Note that on the lower sketch in figure 1 the predicted and measured stall areas are both small and are reasonably located. The figure shows that the approximate rate of growth of the stalled area was predictable, as indicated by the upper contour plot which corresponds to severe stalling.

For these predictions, available wind-tunnel section data on the stall angle of an actual rotor-blade specimen, as tested at the correct Reynolds and Mach numbers, were used.

The next characteristic studied was performance as affected by stalling (refs. 3 and 4). When the measured rotor profile drag-lift ratio was divided by a value deliberately calculated on the assumption

of no stalling and plotted against the calculated blade section angle of attack at the retreating tip, an abrupt rise occurred from about 1.0 at a tip angle of  $12^\circ$  to about 2.0 at a tip angle of  $16^\circ$ . By means of a different method of calculation, it was found that an increase of this order is predictable from wind-tunnel section data for stalled airfoils.

At the same time, it was found that the expected effects on vibration and difficulty of control showed up soon after initial stalling. With the test helicopter, the limit for maintaining steady flight corresponded to conditions such that the calculated tip angle of attack was  $4^\circ$  beyond the section stall angle or, in other words, at  $16^\circ$ . Beyond this condition, vibration and control difficulties were so severe as to make steady flight impossible. For this aircraft and for later designs for which similar flight test results are available, typical section stall angles have been around  $12^\circ$  or  $13^\circ$ ; thus, if the  $4^\circ$  increment is assumed to apply, the limit for steady operation is indicated to correspond thus far to  $16^\circ$  or  $17^\circ$  tip angle of attack.

So far it has been found practical to study all these results in terms of the predicted tip angle of attack on the retreating side. It is anticipated that, for cases where the angle-of-attack distribution over the rotor disk differs greatly from that for the test helicopters, deviations as to rate of increase of power required will occur; there is also some experimental indication of appreciably different rates of change for different blade contours, possibly due to variance in deformation under load. For more varied reasons, such as the degree of irreversibility in the control system, the limiting condition for steady flight would not always be that for a calculated tip angle just  $4^\circ$  beyond the section stall angle. As far as can be seen, however, the procedure of correlating these items with the calculated tip angle should remain a useful one for a wide variety of types and conditions.

The outstanding way to delay the limits imposed by stalling appears to be to increase the rotor tip speeds, since both the average angle of attack and the tip-speed ratio are then reduced. Sooner or later this procedure leads to compressibility-effect limitations.

Compressibility is most naturally thought of as an advancing-tip problem, where the forward speed adds to the rotational tip speed. Actually, the force-break Mach numbers are so much lower at high angles of attack that Mach number has thus far, for production designs, been a problem which could instead affect the amount of stall on the retreating side.

If, however, the probable rate of growth of losses is considered, and, particularly, operation at distinctly higher tip-speed ratios than current ones is anticipated, then the extent to which stall can be delayed by increased tip speed again appears likely to be determined

essentially by the conditions for which compressibility problems on the advancing side become excessive. The example presented in the previous paper by Alfred Gessow and Almer D. Crim is a good illustration.

A conservative limit for the advancing tip, which was formerly used for lack of better information, would be the condition where the blade tip reached the critical Mach number (speed of sound attained locally on blade surface) as derived from low-speed pressure-distribution data or from theoretical pressure-distribution values. There are at least the following reasons, however, for being more optimistic:

First, as is well-known, section data for drag-divergence (force-break) Mach number commonly show values higher than those just described; this is particularly true for sections having relatively low critical Mach numbers. Since force-break data for the advancing-side section angles of attack are now available for most airfoils of interest, this step is somewhat obsolete; that is, it is possible to forget the derived critical values and start with the measured force-break values.

Next, it appears likely that the rotor blade tip can reach a Mach number about 0.06 higher than the measured section force-break value before the force break occurs on the actual blade tip. In terms of helicopter limiting forward speed, an added 10 or 15 mph is thus indicated for fixed tip-speed ratios. It has been found in studies of propeller efficiencies that to obtain best agreement between theory and experiment, an increment of 0.06 at the tip, dropping linearly to zero at 0.6 propeller radius, should be used. The section data are in effect shifted bodily to higher Mach numbers in accordance with these increments.

The mechanism involved has not been completely investigated but may logically be viewed as relating to three-dimensional flow at the tip. Wind-tunnel tests of drag rise for the tip portion of a propeller blade showed a similar increment (see fig. 18 of ref. 5). Tower tests of a helicopter rotor, necessarily in the hovering condition, also lend plausibility to such an increment, particularly when consideration is given to the known surface defects of the blades tested (ref. 6).

Another item is the small initial disk area affected, just as was discussed with stalling. When initial power losses and, also, the blade bending stresses associated with lift-coefficient changes are considered tolerable, there remains the question of blade pitching-moment changes as they affect blade torsion and in turn stability and control. In this connection there are again some favorable circumstances.

Although beyond the drag rise the drag only goes up, the moment coefficients for some sections wobble first one way and then the other with the result that moments on adjacent blade portions, at different Mach numbers, will partially cancel. Also, for some blade profiles the Mach number at

which the large changes in pitching-moment coefficients begin is materially higher than the drag-rise Mach number. The tower tests already mentioned for a rotor in the hovering condition showed that, for rotor blades having NACA 23015 airfoil sections, the blade pitching-moment change as measured in the pitch-control mechanism is indeed postponed materially beyond the initial power increase.

In summarizing this phase of the problem, there are four separate favorable considerations as regards limiting Mach numbers for the advancing tip:

- (1) difference between section calculated critical values and measured section force-break values
- (2) "tip relief"
- (3) the initially small disk area affected
- (4) in some cases, difference between drag-rise Mach number and that for serious moment changes.

On the adverse side it must be remembered that some allowance must be made for practical-construction defects in surface contour and finish and, also, that some safety margin will often be required to allow for maneuvers.

Since compressibility problems can arise either with the high angles on the retreating side or the low angles on the advancing side of the rotor disk, a good question is, what about the intermediate angles which occur at the front and rear of the rotor disk? Figure 2 illustrates the possibility of almost simultaneous occurrence of compressibility effects at all azimuth values. In this figure the section angle of attack as the ordinate is plotted against the Mach number as the abscissa. The solid line represents the highest Mach number reached at any point on the sample rotor for each value of section angle of attack. It was obtained by reading values from contour plots similar in nature to the example given in the previous paper, but for a flight condition which was chosen to illustrate a different aspect of the problem.

The point marked (A) comes from the advancing tip and thus has the highest Mach number. The point marked (R) comes from the retreating tip. The line in between is made up of points from the front or the rear of the rotor disk. Angles of attack below about  $3^{\circ}$  are found only at inboard radii and hence the corresponding maximum Mach numbers are lower which accounts for the part of the curve below point (A).

The dashed line represents the force-break Mach number as obtained from wind-tunnel airfoil-section data. This line is fixed once the

airfoil section is chosen. The line for the rotor, however, will move to the right in a proportionate manner if a higher tip speed is assumed and will have a steeper slope if a higher tip-speed ratio is chosen. Thus, near this tip-speed ratio there could be a combination of conditions where the initial compressibility problems would not be confined to the advancing and retreating blade tips. (The flight condition for the angle-of-attack contour plot used corresponds to: inflow ratio,  $\lambda = -0.0695$ ; tip-speed ratio,  $\mu = 0.30$ ; and collective pitch,  $\theta = 11^\circ$ .)

Although most of the comments made previously for the advancing side apply here also, there would be far less chance, for this rather special case, of tolerating conditions far beyond initial force or moment breaks.

In spite of the eventual conflict between stalling and compressibility losses, if present production designs are considered as a base line, it appears from such studies as have been made (including those of ref. 7) that increased tip speeds first and tip-speed ratios later may well be the cheapest methods per mile per hour for obtaining moderate increases in helicopter limiting forward speeds. However, as may be inferred, the characteristics of rotors operating with high forward speeds and high tip speeds combined are not yet experimentally established. The basic question is whether the characteristics of such rotors can be predicted by using airfoil-section data, even when relatively exact analyses of the sort discussed in the previous paper are used. It is hoped that this question may be answered by means of a special wind-tunnel apparatus which is being constructed.

Some of the other methods, aside from increased tip speeds and tip-speed ratios, which help delay both stall and compressibility limits are listed in table I.

First, an increased number of blades can be used as one means to increase the total chord. The average angle of attack is thus reduced and stalling delayed. The added number of blades also serves to reduce the vibration transmitted to the fuselage - a problem which tends to be aggravated by the higher tip-speed ratios appropriate to high-speed designs.

A relatively high blade twist may be used. By reducing the tip angles of attack, both stall and compressibility effects are delayed. An angle of twist of  $12^\circ$ , for example, as compared with no twist might delay both stalling and compressibility limits by about 10 to 15 mph at fixed rotational tip speed. Discussion of effects of blade twist may be found in references 8 and 9. There appeared to be a possibility that unusually high twist values might lead to higher periodic blade stresses and, hence, increased vibration and reduced fatigue life; however, a theoretical check for one sample case showed no significant difference,

suggesting that increased twist can be used. It is believed that the net effect of blade twist on blade fatigue life may be either favorable or unfavorable depending on the individual design.

Another approach is drag reduction. The reduction of parasite drag acts as a substitute for blade twist in delaying tip stall, entirely aside from the direct effects on power required as discussed in a subsequent paper by Robert D. Harrington.

Provided that the design has some means other than the rotor controls for balancing moments, offset hinges can be used in such a way as to reduce the angle-of-attack variation around the disk and hence to delay stalling. The design compromises here are more difficult to judge than for the preceding methods. The point seems worth mentioning, however, since offset hinges will in any event serve to minimize a stability problem which, as described in reference 10, has been anticipated for high-speed designs.

The list of methods just discussed is not complete, especially regarding more complex approaches such as use of boundary-layer control to delay stall. To name two still more basic configuration changes, a propeller can be used to change the forward tilt required and thus even out the angle-of-attack distribution much like blade twist does, and a fixed wing can be used to unload the rotor and delay both stall and Mach number limitations.

The problems and possibilities of use of fixed wings to unload the rotor are very extensive and the next paper by John W. McKee and Robert J. Tapscott treats of some specific investigations now underway on this subject.

In summary, it appears feasible to obtain at least moderate increases in helicopter forward speeds even aside from major configuration changes. That such increases in speed can be obtained relative to speeds representative of helicopters actually in general use has been well-demonstrated by speed records made with new designs within the past year. As is well-known, these records are around 150 mph. Still further increases can be expected but, since the amounts are not clearly predictable, both theoretical and experimental studies are in progress in an attempt to clear up the more basic uncertainties in this field.

## REFERENCES

1. Bailey, F. J., Jr., and Gustafson, F. B.: Observations in Flight of the Region of Stalled Flow Over the Blades of an Autogiro Rotor. NACA TN 741, 1939.
2. Gustafson, F. B., and Myers, G. C., Jr.: Stalling of Helicopter Blades. NACA Rep. 840, 1946. (Supersedes NACA TN 1083.)
3. Gustafson, F. B., and Gessow, Alfred: Effect of Blade Stalling on the Efficiency of a Helicopter Rotor as Measured in Flight. NACA TN 1250, 1947.
4. Gustafson, F. B., and Gessow, Alfred: Analysis of Flight-Performance Measurements on a Twisted, Plywood-Covered Helicopter Rotor in Various Flight Conditions. NACA TN 1595, 1948.
5. Lindsey, W. F., Stevenson, D. B., and Daley, Bernard N.: Aerodynamic Characteristics of 24 NACA 16-Series Airfoils at Mach Numbers Between 0.3 and 0.8. NACA TN 1546, 1948.
6. Carpenter, Paul J.: Effects of Compressibility on the Performance of Two Full-Scale Helicopter Rotors. NACA Rep. 1078, 1952. (Supersedes NACA TN 2277.)
7. Gustafson, F. B., and Gessow, Alfred: Effect of Rotor-Tip Speed on Helicopter Hovering Performance and Maximum Forward Speed. NACA WR L-97, 1946. (Formerly NACA ARR L6A16.)
8. Gessow, Alfred: Flight Investigation of Effects of Rotor-Blade Twist on Helicopter Performance in the High-Speed and Vertical-Autorotative-Descent Conditions. NACA TN 1666, 1948.
9. Gustafson, F. B.: Charts for Estimation of the Profile Drag-Lift Ratio of a Helicopter Rotor Having Rectangular Blades With  $-8^\circ$  Twist. NACA RM L53G20a, 1953.
10. Amer, Kenneth B.: Theory of Helicopter Damping in Pitch or Roll and a Comparison With Flight Measurements. NACA TN 2136, 1950.



TABLE I  
METHODS FOR DELAY OF FORWARD-FLIGHT LIMITS

METHOD	PURPOSE
MORE BLADES	PROVIDES INCREASED SOLIDITY TO DELAY STALL; REDUCES VIBRATION TRANSMITTED TO FUSELAGE
HIGHER BLADE TWIST	DELAYS STALL AND COMPRESSIBILITY
REDUCED PARASITE DRAG	DELAYS STALL
OFFSET HINGES	DELAYS STALL IF SUFFICIENT MEANS PROVIDED FOR BALANCING MOMENTS; REDUCES DECAY IN PITCH AND ROLL DAMPING MOMENTS

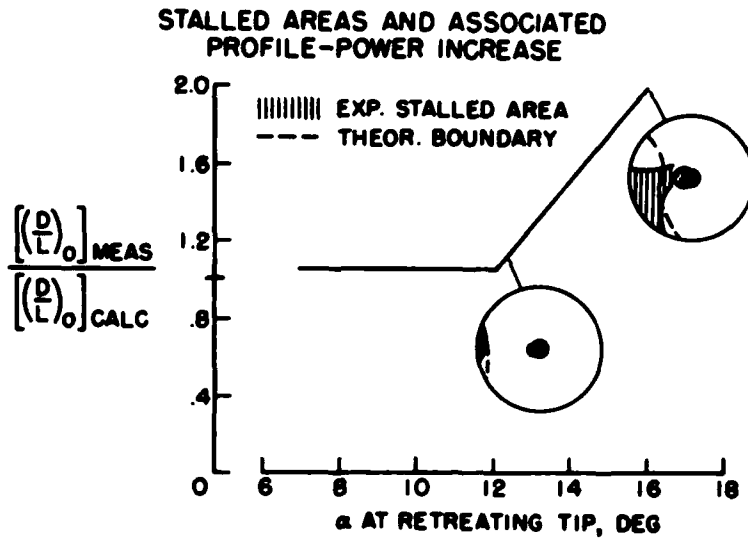


Figure 1

**SIGNIFICANT ANGLES OF ATTACK FOR SAMPLE CASE  
 $\mu = 0.3$**

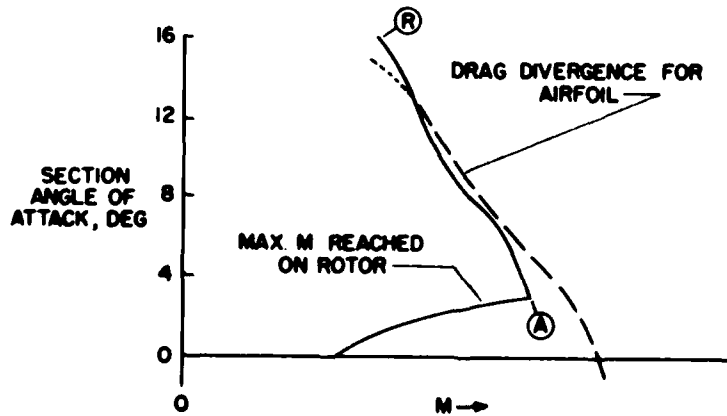


Figure 2

## AN EXPLORATORY INVESTIGATION OF UNLOADED ROTORS

By John W. McKee and Robert J. Tapscott

Langley Aeronautical Laboratory

## INTRODUCTION

In the previous paper by F. B. Gustafson and Robert D. Harrington, the limitations of forward speed brought about by stall of the retreating blades and Mach number effects were discussed. The possibility of delaying these limitations by unloading the rotor with a fixed wing and providing a propeller to take over the propulsive duties of the rotor was mentioned. The rotor would then be running under conditions quite different from those of normal helicopter operation. The tip-speed ratio would become abnormally high and the rotor would be absorbing little power, perhaps autorotating. The rotor would become an unnecessary appendage in high-speed flight, but the question that arises is: Will the unloaded rotor be a troublesome appendage? It is the purpose of this paper to discuss some of the characteristics that are known of rotors operating in this unloaded condition.

## DISCUSSION

Aircraft configurations combining rotary and fixed wings are not novel. Figure 1 shows the Pitcairn PCA-2 autogiro. It was similar to the suggested configuration, having a propeller and a fixed wing which partially unloaded the rotor. The PCA-2 autogiro was tested at Langley 20 years ago and considerable data were obtained and published which are of current interest from the point of view of an autorotating unloaded rotor. These data include flight tests of the complete autogiro and tunnel tests of the rotor alone (refs. 1 to 5).

The PCA-2 data show that the amplitude of the blade flapping motion increased with tip-speed ratio, and in the low angle-of-attack, high tip-speed-ratio range, where low rotor lift coefficients were obtained, the rotor speed was very sensitive to angle-of-attack change. The PCA-2 autogiro was extremely sensitive to control motions and gusts, in flight at high speeds, or perhaps more relevant, at high tip-speed ratios. The records of some abrupt turns, with approximately 4g accelerations, show that the portion of the lift carried by the wing rose as high as 65 percent and fell as low as 5 percent. In the flight tests, 145 miles per hour was the highest recorded flight speed, 45 percent of the load was the most carried by the wing in steady flight, and 0.77 was the highest tip-speed ratio.

Helicopter rotor data are generally limited to tip-speed ratios of about 0.4, with flight experience limited to about 0.3. In view of the current interest in increasing the high-speed potentialities of helicopters, tests have been made in the Langley 300 MPH 7- by 10-foot tunnel of some simple two-blade rotor configurations for the condition of autorotation. The tests were undertaken to study further some rotor operating characteristics, to explore the extreme upper limit of tip-speed ratio, and to determine the effect of change of some rotor geometric parameters. A simplified sketch of the rotor model is shown in figure 2. The blades had symmetrical 12-percent-thick sections and were mass balanced at the quarter-chord line. Several sets of blades were tested with a range of blade mass constant  $\gamma$  from 2.3 to 14.5. The rotor was tested free to cone (designated "coning" in figures) with a flapping hinge having zero hinge offset and also tested with the two blades fastened together to form a seesaw rotor. The axis of the flapping hinge was perpendicular to the blade span, and stops limited the flapping to approximately  $+28^\circ$  and  $-23^\circ$ . No drag hinges were provided.

Two types of data were obtained: (1) steady state and (2) the response of the rotor to a sudden change of angle of attack.

Some of these data for the steady-state conditions are shown in figure 3. Tip-speed ratio  $\mu$  and maximum up and down flapping angle  $\beta$  of the autorotating seesaw rotor with blades of mass constant  $\gamma$  of 14.5 and blade pitch angle  $\theta$  of  $0^\circ$  are presented for an angle-of-attack range of  $-6^\circ$  to  $12^\circ$ . The blade mass constant  $\gamma$  is a nondimensional term that expresses the ratio of air forces to mass forces. A typical helicopter value of  $\gamma$  is about 8 and these blades with  $\gamma$  of 14.5 are rather light blades. The seesaw rotor is shown to operate through the complete angle-of-attack range. The points of greatest interest are found in the region of  $\alpha$  equal to  $0^\circ$  where the lift would be low, the unloaded rotor condition. A tip-speed ratio of about 2.0 is present from  $\alpha = -3^\circ$  to  $\alpha = 2^\circ$  and the tip-speed ratio changes rapidly with angle of attack from  $2^\circ$  to  $4^\circ$ . The amplitude of maximum flapping is high where the tip-speed ratio is high. Shaded areas are shown in the angle-of-attack range where the higher tip-speed ratios are found. These areas indicate that variations in rotor rotational speed and maximum flapping amplitude were present.

The free-to-cone rotor, shown in figure 4, also having a value of blade mass constant of 14.5 and zero blade pitch angle, has a maximum tip-speed ratio of 1.3 at an angle of attack of  $1^\circ$ . The tests were run using  $1^\circ$  increments of angle of attack, but just slightly below  $\alpha = 1^\circ$  the positive flapping exceeded  $28^\circ$  and the forward blade was hitting the up-flapping stop. Attempts to run in the negative angle-of-attack range were unsuccessful as the down flapping of the forward blade wanted to exceed the stop setting of  $-23^\circ$ .

[REDACTED]

A tendency was noted, in these regions of variable operation, for the rotor characteristics to be unfavorably affected by reductions in the test airspeed. The data shown in these and subsequent figures were obtained at an airspeed that matches dynamically the condition of a 40-foot-diameter rotor at a forward speed of 260 miles per hour.

It was very difficult to achieve good blade tracking at the high tip-speed ratios. A small change of blade pitch angle or difference in blades due to construction tolerances had a big effect on the tracking behavior.

Figures 5 and 6 show the effect of blade pitch angle  $\theta$  for the seesaw and free-to-cone conditions, respectively. These curves present the extreme values of flapping angle  $\beta$  and tip-speed ratio  $\mu$  in the regions where variable behavior was experienced. For the seesaw rotor (fig. 5), there is no significant effect to be noted except a shift along the angle-of-attack scale. For the free-to-cone condition (fig. 6), blade pitch angle reduced the positive angle-of-attack operating range. It was possible to run in a limited negative angle-of-attack range, but extreme values of downward flapping are shown.

Figures 7 and 8 show the effect of blade mass constant  $\gamma$  on the operating characteristics. There is shown a trend, at a low angle of attack, for the rotational speed to be lower, or  $\mu$  to be higher, for the heavy blades; that is, those with low values of  $\gamma$ . The driving force here would be mainly attributable to drag differences between the retreating blade operating entirely in reversed flow and the advancing blade. The rib and silk covering construction of the light blades presumably caused greater drag differences than the solid construction of the heavy blades. Although the heavy blades reached higher values of  $\mu$ , the flapping of the heavy blades was considerably less than that of the light blades.

For the free-to-cone condition (fig. 8), the heavy blades had some negative angle-of-attack range of operation but the range was limited by excessive downward flapping. An even heavier blade,  $\gamma = 2.3$ , not shown in this figure, would operate through the angle-of-attack range, experiencing downward flapping of  $15^\circ$  from  $\alpha = 0^\circ$  to  $\alpha = -2^\circ$ .

It should be emphasized that where data are not shown the rotor blades were hitting the flapping stops although generally the rotor continued to rotate. The flapping limits, up  $28^\circ$  and down  $23^\circ$ , were rather generous in terms of angles normally encountered by helicopters, particularly the down limit. Where large flapping angles occur, they should be attributed to the effect of large tip-speed ratio, with the flapping of the advancing blade being either up or down as determined by the combined angle of attack and blade pitch angle.

[REDACTED]

It was found that, if the restriction of autorotation was removed from the test procedure and the rotor was driven by a motor to maintain a sufficiently high rotational speed, operation through the angle-of-attack range was possible with even the lightest blades for the free-to-cone condition. Figure 9 presents again the autorotation data of the rotor with  $\gamma = 5.6$  and  $14.5$ . Data obtained from powered operation, maintaining a tip-speed ratio not greater than  $1.0$ , have been added. The tendency to have large downward flapping angles at negative angle of attack is still present, especially for the light blades.

The effect of blade mass constant  $\gamma$  on the maximum up and down values of flapping angle  $\beta$  for the free-to-cone rotor with blade pitch angle equal to zero was also studied by means of some theoretical calculations. These calculations were made using an iterative procedure that consisted of starting with an estimated set of flapping coefficients, inserting these coefficients into the conventional blade flapping-moment equilibrium equation (for example, eq. (6-2) of ref. 3), and then solving the resulting equation to obtain a new set of coefficients. The process was repeated until the "input" and "output" flapping coefficients differed by a negligible amount. In order to take into account blade stall and the region of reversed velocity, as well as to avoid some limitations of conventional analytical theory such as assumptions regarding small angles and the dropping of high powers of tip-speed ratio, the blade flapping equation was integrated numerically by means of automatic computing machines.

Figure 10 shows a comparison of the theoretical maximum flapping angles and experimentally determined values as a function of  $\gamma$ . At a tip-speed ratio of  $1.0$ , both theory and experiment show increasing values of flapping, in the positive direction, as blade weight decreases and  $\gamma$  increases, with the experimental values being somewhat higher than the calculated angles. At a value of  $\mu$  of  $2.2$ , the calculated flapping angles show a very rapid increase as  $\gamma$  increases. Two test points at a value of  $\mu$  of  $2.0$  are shown at values of  $\gamma$  of  $2.3$  and  $3.2$  which are in general agreement with the calculated amplitude for a value of  $\mu$  of  $2.2$ . The other sets of rotor blades with values of  $\gamma$  of  $5.6$ ,  $11.4$ , and  $14.5$  would not run at a value of  $\mu$  as high as  $2.0$ .

After the steady-state operating range of the various rotor configurations had been established, tests were made to determine the response of the rotor to sudden angle-of-attack changes. In each test of this type, steady-state operation was first established and then the angle of attack was given a sudden incremental change, either plus or minus, of  $2^\circ$ .

Figure 11 presents some of the recorded data for the free-to-cone rotor with light blades subjected to a sudden change in angle of attack from  $3^\circ$  to  $5^\circ$ . Plotted as a function of time are  $\alpha$ ,  $\mu$ , and the envelopes of maximum up and down values of  $\beta$ . It can be seen that the rotor

rotational speed, as evidenced by the gradual reduction of  $\mu$  from the initial value of about 0.8, did not show an extreme sensitivity but that the positive flapping experienced an immediate and very large increase in amplitude. In the time of one rotor revolution, the maximum positive  $\beta$  increased from an initial value of  $16.5^\circ$  to  $27.5^\circ$ . This is equivalent to a tilt of the tip-path plane 2.5 times greater than the angle-of-attack change. At a time of 6 seconds after the step in angle of attack, the rotor had essentially stabilized at its new trim operating condition.

The maximum up and down values of flapping angles before and immediately after a  $2^\circ$  increase of angle of attack are shown in figures 12 and 13 for two values of  $\gamma$  and for the seesaw and free-to-cone conditions, respectively. It is quite evident that the increment of flapping tends to follow the same trend as the steady-state flapping; in particular the flapping is greater at the lower initial angles of attack where the tip-speed ratio is high. The results obtained from  $2^\circ$  decreases of angle of attack were less alarming in that if the initial angle of attack was positive, the flapping always tended to decrease.

#### CONCLUDING REMARKS

In order to overcome limitations of the high speed of helicopters, it has been suggested that the rotor could be unloaded by the use of fixed wings. As forward speed increased, the rotor would operate at tip-speed ratios higher than those normally encountered and it is logical to assume that new problems in rotor operation would appear. A review of some old autogiro data and tests of some rotor configurations for the condition of autorotation have been made. These tests were exploratory in nature and help to define and serve to illustrate the nature of rotor characteristics at high tip-speed ratios. The results of the tests, obtained with the use of a very simple type of rotor, leave unanswered many questions of the effect of parameters such as hinge offset and skew. It was found that flapping amplitude increased with tip-speed ratio and that erratic variations of tip-speed ratio and blade-flapping behavior were present at the higher tip-speed ratios. The seesaw rotor had more desirable characteristics than the free-to-cone rotor and heavy blades resulted in less flapping than light blades.

## REFERENCES

1. Wheatley, John B.: Lift and Drag Characteristics and Gliding Performance of an Autogiro As Determined in Flight. NACA Rep. 434, 1932.
2. Wheatley, John B.: Wing Pressure Distribution and Rotor-Blade Motion of an Autogiro As Determined in Flight. NACA Rep. 475, 1933.
3. Wheatley, John B.: An Aerodynamic Analysis of the Autogiro Rotor With a Comparison Between Calculated and Experimental Results. NACA Rep. 487, 1934.
4. Wheatley, John B., and Hood, Manley J.: Full-Scale Wind-Tunnel Tests of a PCA-2 Autogiro Rotor. NACA Rep. 515, 1935.
5. Wheatley, John B.: The Influence of Wing Setting on the Wing Load and Rotor Speed of a PCA-2 Autogiro As Determined in Flight. NACA Rep. 523, 1935.



MODEL OF PITCAIRN PCA-2 AUTOGIRO

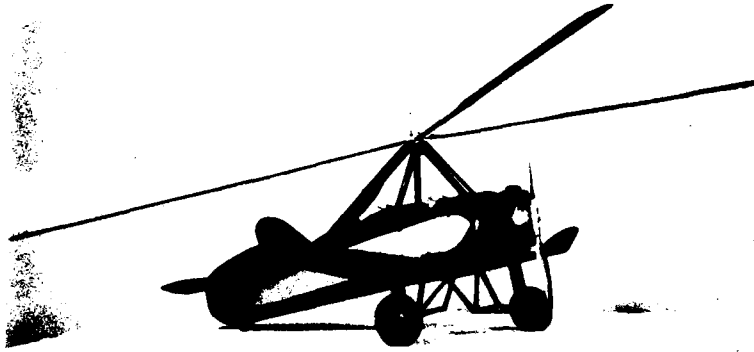


Figure 1

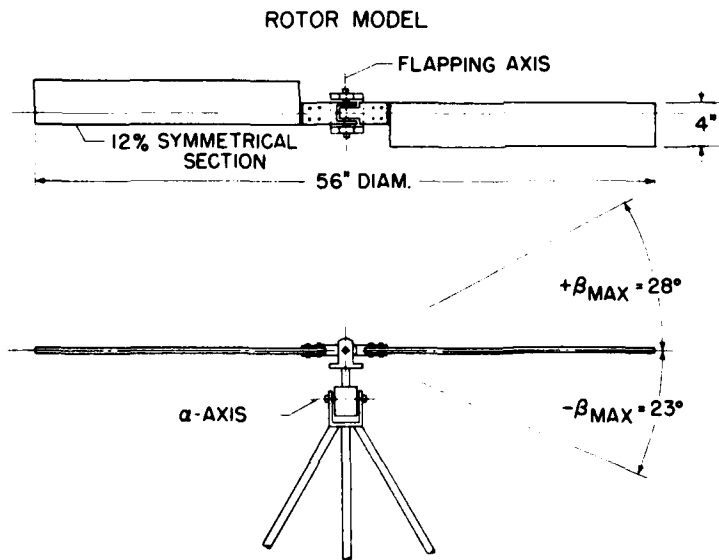


Figure 2

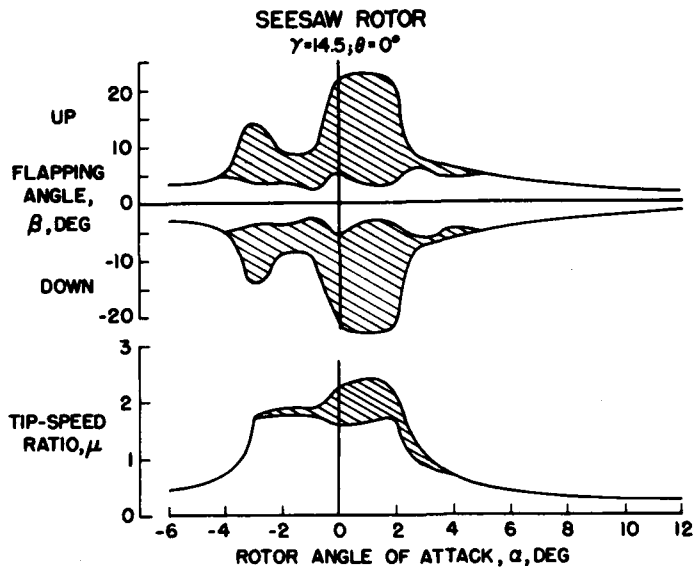


Figure 3

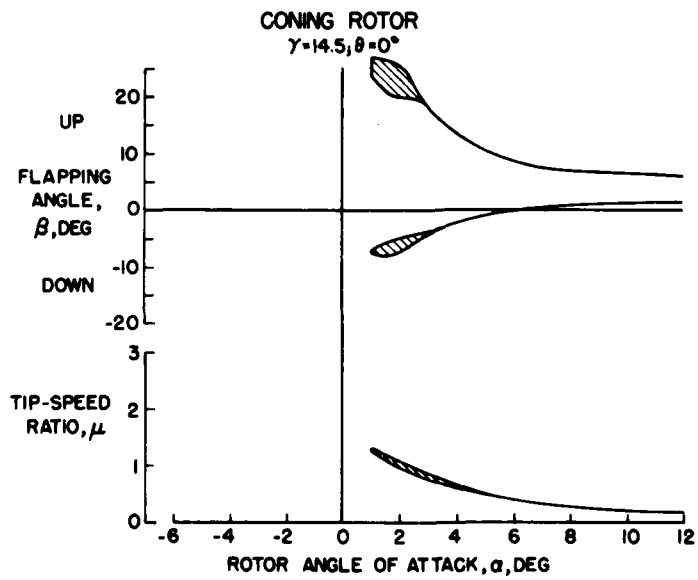


Figure 4

EFFECT OF BLADE PITCH ANGLE  
 $\gamma = 14.5$ ; SEESAW

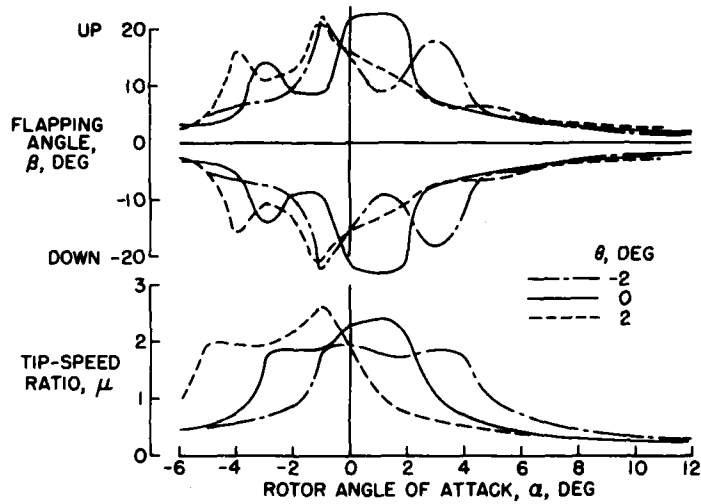


Figure 5

EFFECT OF BLADE PITCH ANGLE  
 $\gamma = 14.5$ ; CONING

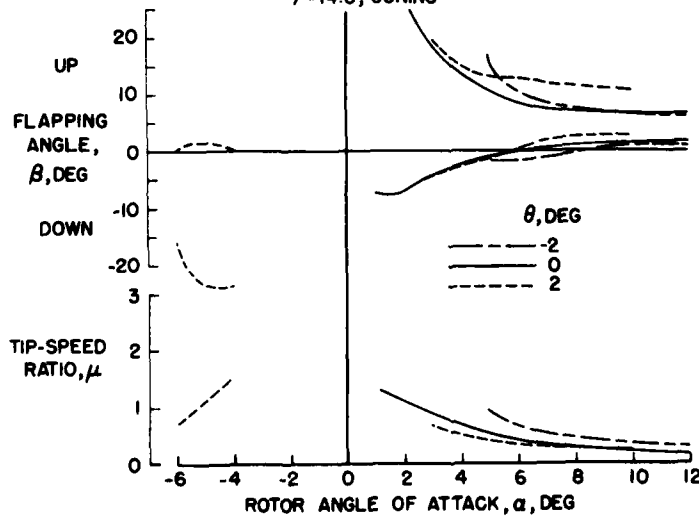


Figure 6

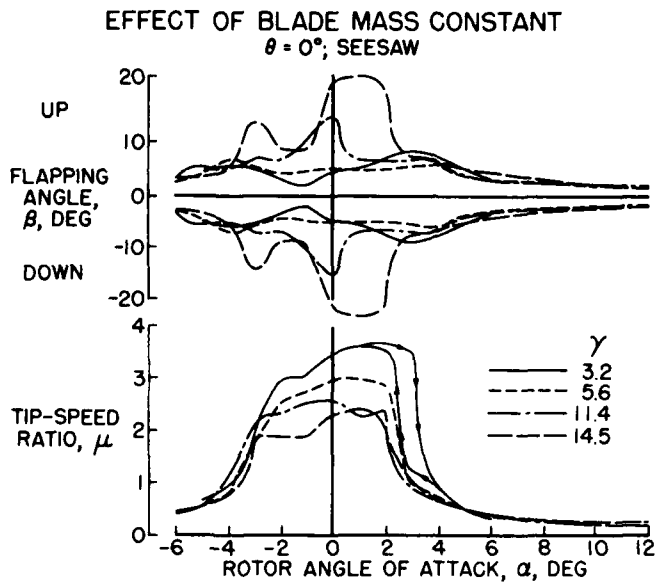


Figure 7

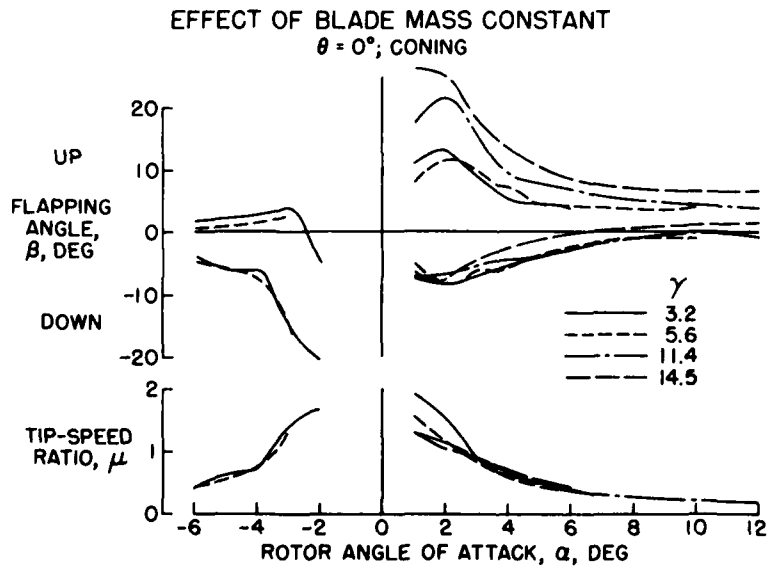


Figure 8

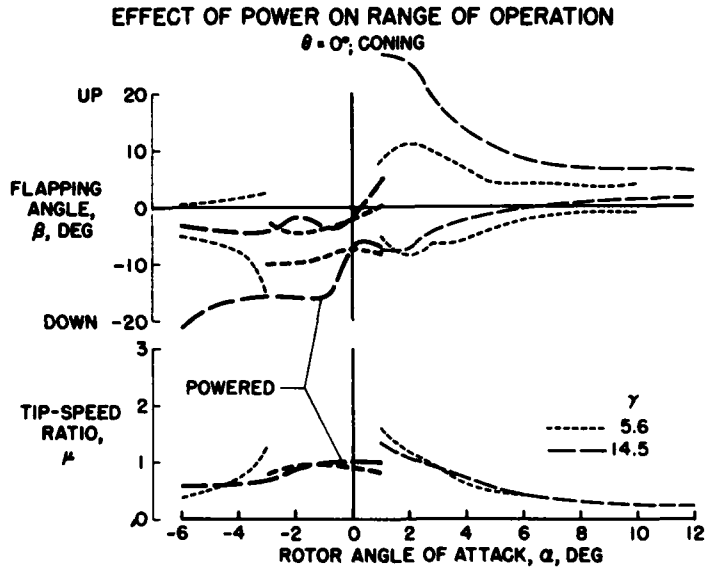


Figure 9

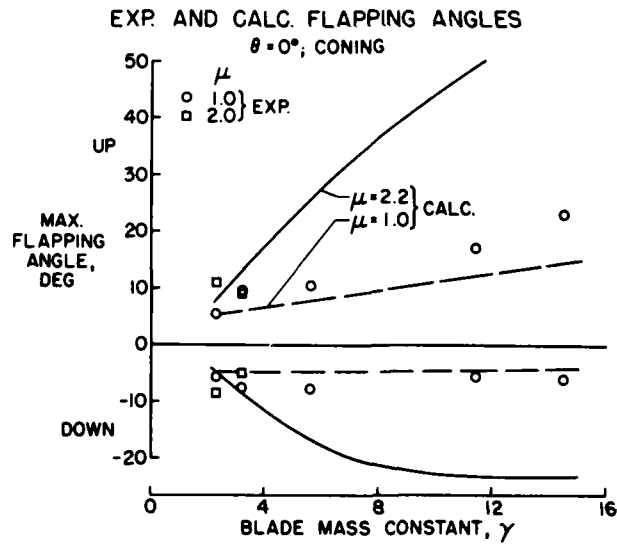


Figure 10

TIME HISTORY AFTER  $\alpha$ -CHANGE FROM 3° TO 5°  
 $\gamma = 14.5$ ; CONING

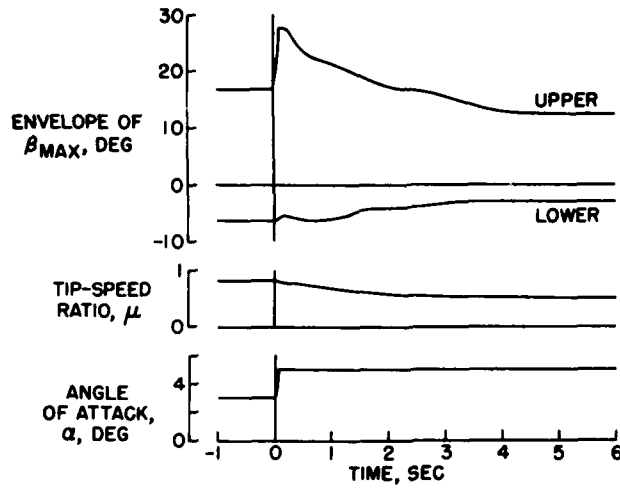


Figure 11

CHANGE IN FLAPPING ANGLE DUE TO  $\alpha$ -STEP  
 $\Delta\alpha = 2^\circ$ ; SEESAW

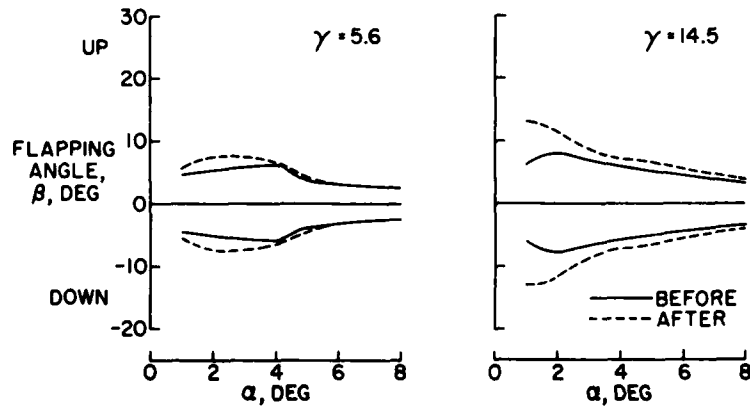


Figure 12

CHANGE IN FLAPPING ANGLE DUE TO  $\alpha$ -STEP  
 $\Delta\alpha = 2^\circ$ ; CONING

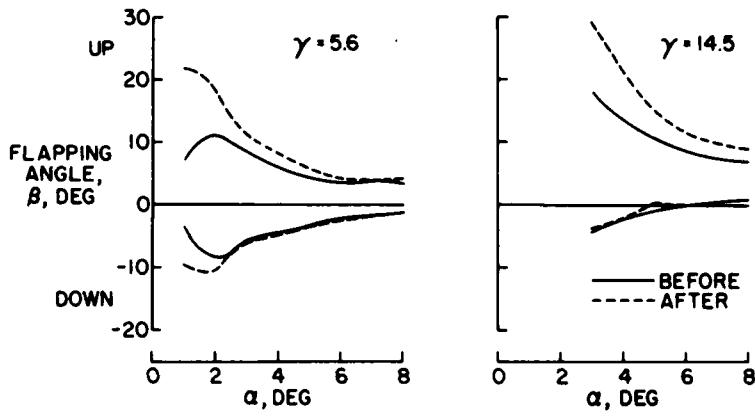


Figure 13

WIND-TUNNEL STUDIES OF THE PERFORMANCE OF  
MULTIROTOR CONFIGURATIONS

By Richard C. Dingeldein

Langley Aeronautical Laboratory


SUMMARY

The power requirements measured in static thrust and in level forward flight are presented for two helicopter rotor configurations. One is a coaxial rotor arrangement having the rotors spaced approximately 19 percent of the rotor radius; the other is a tandem configuration in which the rotor-shaft spacing is 3 percent greater than the rotor diameter and in which the rotors lie in the same plane. The experimental measurements are compared with the results of calculations based on existing NACA single-rotor theory.

INTRODUCTION

For several years a general research program on the subject of helicopter rotor configurations has been underway at the Langley full-scale tunnel. This program is set up to evaluate different rotor arrangements on the basis of relative aerodynamic efficiency and, in its broadest sense, may involve measuring for various flight conditions the power required, the blade motions, the flow angles in the rotor wake, and the rotor static stability. The advantages and disadvantages associated with different rotor configurations in regard to such things as overall dimensions, center-of-gravity travel, structural weight, and so forth, are generally known and are not repeated here. These are items the designer must evaluate for himself and consider along with the aerodynamic gains or losses. The purpose of the general research program is to provide this latter information.

This paper presents some of the results obtained so far on two rotor configurations - one a coaxial arrangement and the other a tandem system having no rotor overlap or vertical offset. The emphasis is on the power requirements in hovering and in level flight, and a comparison between the experimental results and what can be predicted from the available single-rotor theory is included.





## SYMBOLS

D	propeller diameter, ft
$\Omega$	angular velocity, radians/sec
R	rotor radius, ft
$C_T$	rotor thrust coefficient, $\frac{\text{Rotor thrust}}{\rho(\Omega R)^2 \pi R^2}$
$C_Q$	rotor torque coefficient, $\frac{\text{Rotor torque}}{\rho(\Omega R)^2 \pi R^3}$
$\mu$	rotor tip-speed ratio
$\rho$	air density, slugs/ft <sup>3</sup>

## TEST EQUIPMENT

The rotor configurations tested are shown in figure 1. The coaxial rotor system was part of an actual helicopter and had a diameter of 25 feet and a rotor spacing equal to 19 percent of its radius. Each rotor had two blades, and the total solidity of the coaxial configuration, based on the projected area, was 0.054. A complete description of this equipment is given in reference 1.

The tandem model had two two-blade rotors 15 feet in diameter. The rotor shafts were parallel. Each rotor had a solidity of 0.054. The blades were untwisted and untapered and had an NACA 0012 airfoil section. This is a general research model constructed to investigate side-by-side and tandem rotor arrangements. The rotors could be moved toward each other to mesh the blades up to 75 percent of the radius and could be offset vertically to cover a range of gap ratios of interest in tandem helicopters. The results discussed in this paper are confined to the tandem configuration shown in figure 1, for which the rotor-shaft spacing was 3 percent greater than the rotor diameter.

## RESULTS AND DISCUSSION

It is known from some early flow-visualization studies that the air flow through and around rotors operating near one another may be very

different from what occurs for an isolated single rotor or from what is considered in the general rotor theory. As an illustration, figure 2 shows the flow through a model coaxial rotor in a hovering condition. Balsa-wood dust introduced into the air above the rotor defines the flow lines associated with the blade-tip-vortex filaments and, in this case, indicates the strong downflow affecting the lower rotor inboard of the 0.8-radius station. Since this configuration is usually operated with equal power input to each rotor to provide trim in yaw, there would be a tendency for the tips of the lower rotor to stall at the higher thrust coefficients. Because of the unsymmetrical downflow over the lower rotor, some question would exist as to whether the single-rotor theory would apply in making a performance analysis of this configuration.

#### Static Thrust

Coaxial rotor.- The static-thrust performance measured on the full-scale coaxial rotor shown in figure 1 is given in figure 3, in which is plotted the variation of rotor thrust coefficient and rotor torque coefficient for the coaxial rotor configuration and for the upper and the lower rotors tested separately. There were some rather obvious contour defects on these blades which made it desirable to test the rotors separately in order to adjust the drag polar to be used in succeeding theoretical calculations. The polar was initially determined for the airfoil section at the 0.75-radius station considering smooth blades by using the method of reference 2.

The extent of the adjustment was to alter the value of the constant term of the polar to provide agreement with the measured data at zero thrust. The circles represent data points measured on the upper and lower rotors tested separately, and the curve shows the calculated performance based on the adjusted drag polar and using blade-element momentum theory (ref. 3). Data points measured on the coaxial system, trimmed in yaw, are plotted as squares. The curve passing through most of these data points represents the calculated hovering performance of a single rotor having the same solidity as the coaxial arrangement. It is seen that the performance of this equivalent single rotor closely approximates the measured coaxial results. The measurements show the coaxial rotor to be slightly more efficient as the thrust coefficient is increased, although this advantage disappears at the highest thrust coefficients shown, perhaps as a result of stalling on the outboard portions of the lower rotor. A similar comparison with theory has also been obtained on a different coaxial rotor system having about the same rotor spacing but approximately three times the solidity of this rotor (ref. 1). The general conclusion is that the available single-rotor theory can be used to predict the static-thrust power requirements of a coaxial rotor with fairly good accuracy.

Tandem rotor.- The static-thrust performance of the tandem configuration (which, in hovering, can also be considered as a side-by-side rotor arrangement) is shown in figure 4, with circles showing measured points obtained for one rotor, squares showing the points measured on the tandem configuration, and a single curve representing the calculated performance for both of these configurations (ref. 3). Again, the agreement is excellent for the single rotor. The measured performance of the tandem rotor is much better than that for the single rotor. At a typical thrust coefficient of 0.0035, the measured data show approximately 18 percent less power required than for the single rotor. This improved performance may be due to a reduction in induced power associated with a favorable interference effect. The two rotors in combination may influence a larger mass of air than the total of what they would influence if placed far apart. As a result, the induced velocity would be lower and the induced power would be reduced. Improved hovering performance of the order shown in this figure would occur if the effective disk area were increased by 15 or 20 percent. This amount is roughly equivalent to the cusp-shaped areas between the two rotor disks. From a practical standpoint, however, this improved hovering efficiency may not be so important after all, as is discussed later in this paper.

#### Level Flight

Coaxial rotor.- The horsepower required for a coaxial helicopter using the rotor system tested and operating in level flight over a range of tip-speed ratios at a constant rotor thrust coefficient and tip speed is shown in figure 5. For this small coaxial helicopter, an equivalent flat-plate parasite-drag area of 10 square feet was used. Measurements made with one rotor compared with a calculated performance curve based on references 2 and 4 and corrected empirically for the effect of blade stalling (ref. 5) show very good agreement. The test results obtained with the coaxial rotor, trimmed in yaw, are shown at the top of the figure. The hovering point is also given, together with the power estimated for a single-rotor helicopter of equivalent solidity.

The data measured by using the coaxial rotor arrangement show that up to 14 percent more horsepower is required for this configuration than would be required for a single rotor of equivalent solidity operating under the same conditions. This difference represents increases in profile and induced power associated with rotor interference effects, but so far analysis based on the available theory has not indicated how these losses arise. The indications remain, however, that the coaxial arrangement tested required more power in forward flight than an equivalent single rotor, although there are certain advantages to the configuration which may offset the larger power requirement in certain applications.

Tandem rotor.-- The level-flight performance curve obtained by using the tandem rotor configuration tested, as well as a breakdown of the power going into the front and rear rotors, is given in figure 6. The equivalent flat-plate parasite-drag area used in this test was 2 square feet, which is representative of a very clean tandem helicopter. This test was made with the total rotor thrust measured on the tunnel balance. The circles designate the points obtained with one of the rotors removed. There is quite a bit of scatter in the data; however, the calculated performance curve (refs. 2 and 4) is a good fairing of the test points and shows the accuracy of the theory in predicting the forward-flight power requirements for this particular set of rotor blades.

Next, the rear rotor was added to form the tandem configuration. The resultant rotor lift and useful drag forces that were set at each tip-speed ratio for the single rotor were doubled for the tandem arrangement by adjusting the controls of the rear rotor only. The reduced downwash field in the plane of the front rotor created by the rear rotor probably resulted in greater lift on the front rotor, which means that the measured performance data are representative of a tandem helicopter having its center of gravity located slightly forward of the midpoint between the two rotors. The power absorbed by the front and rear rotors was measured at each tip-speed ratio and is plotted separately in the figure. The single-rotor theory is seen to be applicable to the front rotor of this particular tandem arrangement. The power required by the rear rotor is considerably higher. Most of this difference represents greater induced losses, since flow surveys show that the rear rotor is operating in the fully developed downwash of the front rotor (see ref. 6). If this is taken into account in applying the rotor theory, a curve that is in fair agreement with the measured points is calculated. Adding the power required for the front and rear rotors gives the diamond-shaped points, which are compared with the equivalent calculated curve. Agreement with the theory tends to be good at low and at high tip-speed ratios. However, the measured power is higher than the calculated power at cruising conditions, much the same as noticed for the coaxial rotor, although the percentage difference is much less. An important thing to see here is the unusual shape of the measured tandem-helicopter power-required curve at the low-speed end. Instead of the customary flattened performance curve, the increased hovering efficiency that was measured on the tandem and discussed previously in this paper has reduced the hovering power required so that the curve has a different shape. The manner in which the measured data points should be faired at the extremely low values of tip-speed ratio has not been determined from these tests. This favorable interference effect is probably confined to a true hovering condition and probably disappears at extremely low forward speeds. It is therefore not expected to be of any practical importance.

## CONCLUDING REMARKS

As a result of these tests, it appears that the power requirements of a coaxial rotor in static thrust can be predicted with good accuracy from the available theory, although more power is required in level flight than for the equivalent single rotor. The tandem rotor configuration which has the rotor shafts spaced approximately a rotor diameter apart is indicated to have greatly improved hovering efficiency that is probably due to a reduction in induced power, but which is not expected to be of any practical importance. The power requirements for this tandem arrangement in level flight can be predicted fairly well from the available single-rotor theory by considering the rear rotor to be operating in the fully developed downwash of the front rotor.

## REFERENCES

1. Harrington, Robert D.: Full-Scale-Tunnel Investigation of the Static-Thrust Performance of a Coaxial Helicopter Rotor. NACA TN 2318, 1951.
2. Bailey, F. J., Jr.: A Simplified Theoretical Method of Determining the Characteristics of a Lifting Rotor in Forward Flight. NACA Rep. 716, 1941.
3. Gessow, Alfred: Effect of Rotor-Blade Twist and Plan-Form Taper on Helicopter Hovering Performance. NACA TN 1542, 1948.
4. Bailey, F. J., Jr., and Gustafson, F. B.: Charts for Estimation of the Characteristics of a Helicopter Rotor in Forward Flight. I - Profile Drag-Lift Ratio for Untwisted Rectangular Blades. NACA WR L-110, 1944. (Formerly NACA ACR L4HO7.)
5. Gustafson, F. B., and Gessow, Alfred: Effect of Blade Stalling on the Efficiency of a Helicopter Rotor as Measured in Flight. NACA TN 1250, 1947.
6. Heyson, Harry H.: Flow-Field Measurements Around Single and Tandem Rotors in the Langley Full-Scale Tunnel. (Prospective NACA paper.)

## ROTOR CONFIGURATIONS TESTED

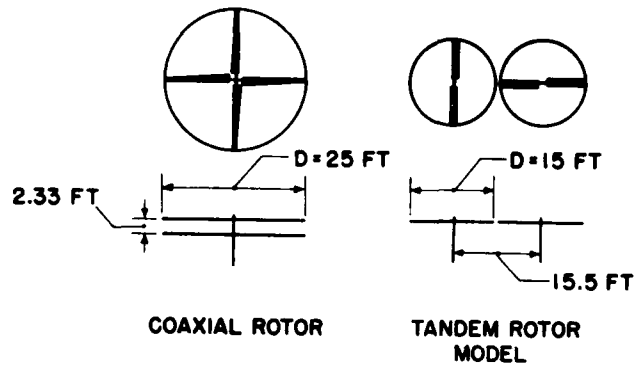


Figure 1

## AIR FLOW THROUGH A MODEL COAXIAL ROTOR IN STATIC THRUST

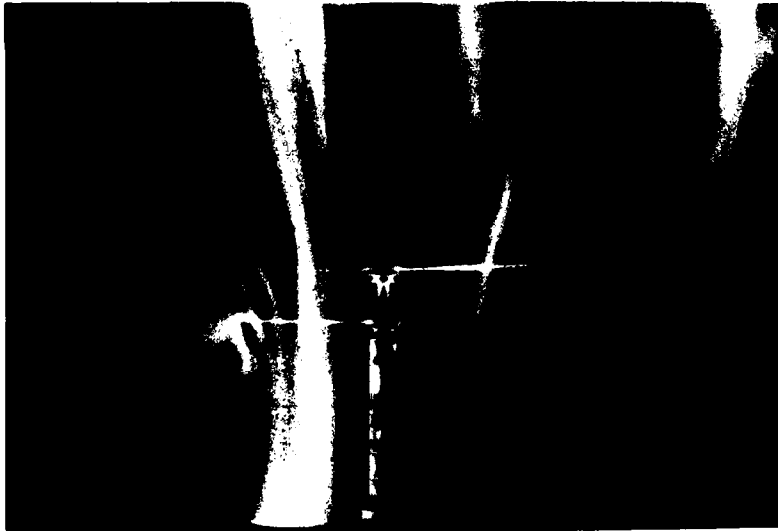


Figure 2

STATIC-THRUST PERFORMANCE OF A COAXIAL ROTOR  
 $\Omega R = 500$  FPS

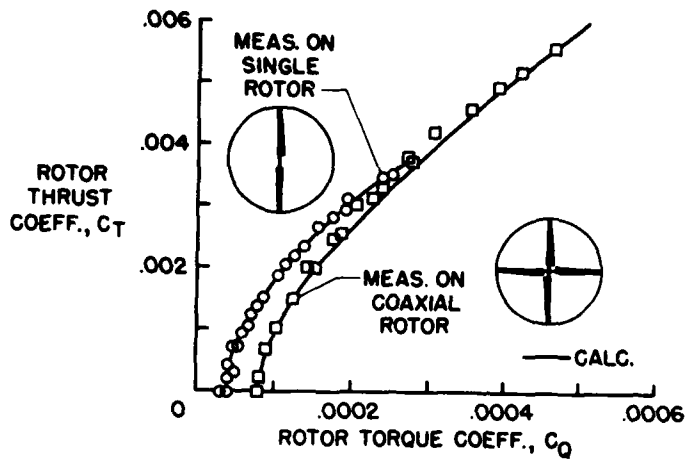


Figure 3

STATIC-THRUST PERFORMANCE OF A TANDEM ROTOR  
 $\Omega R = 500$  FPS

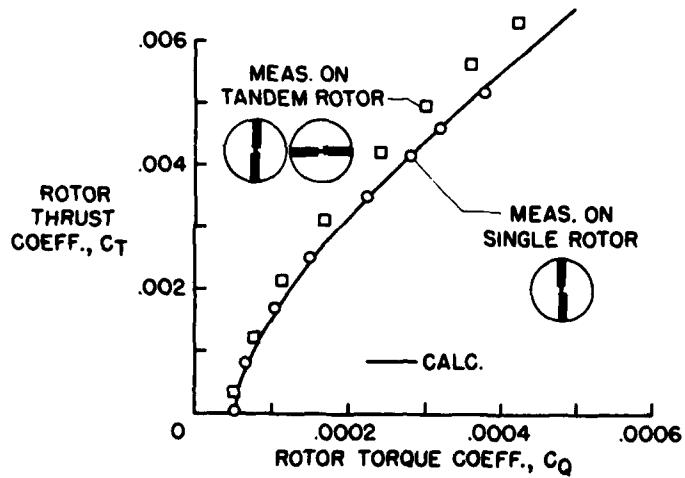


Figure 4

## LEVEL-FLIGHT PERFORMANCE WITH COAXIAL ROTOR

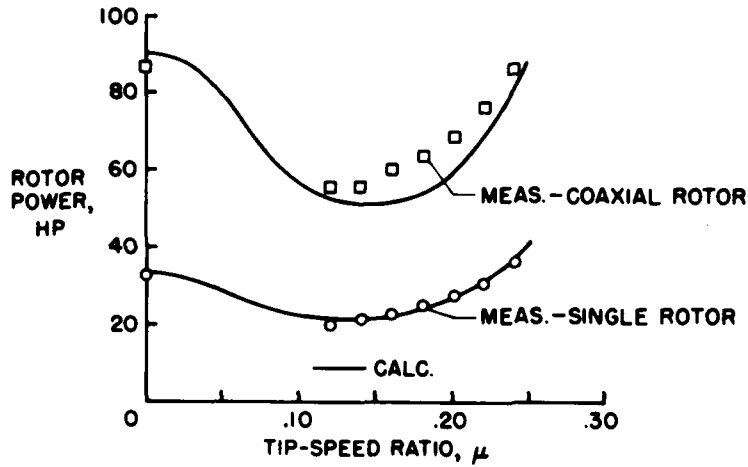
 $C_T = 0.0048$ ;  $\Omega R = 469$  FPS

Figure 5

## LEVEL-FLIGHT PERFORMANCE WITH TANDEM ROTOR

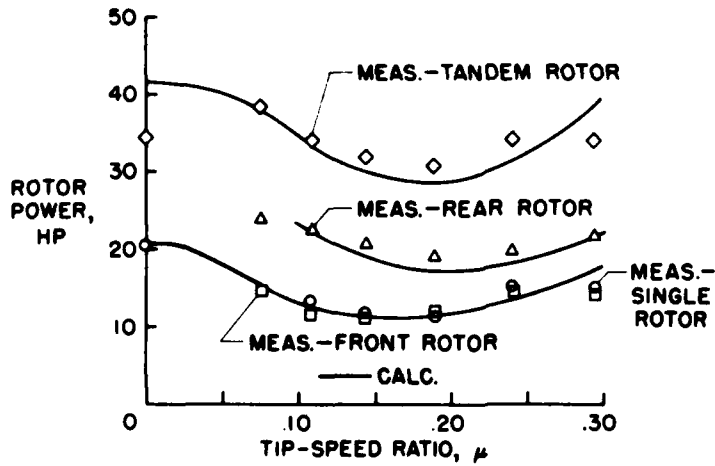
 $C_T = 0.0034$ ;  $\Omega R = 500$  FPS

Figure 6



**PROPULSION AND  
PARASITE DRAG**

## AN INVESTIGATION OF RAM JETS FOR HELICOPTERS

By Paul J. Carpenter and Edward J. Radin

Langley Aeronautical Laboratory

The use of blade-tip-mounted jet engines to drive helicopter rotors is being considered for applications where a high payload-to-gross-weight ratio for short durations is a primary consideration. A program, therefore, was initiated to determine the characteristics of ram-, pulse-, and pressure-jet-driven rotors. The objective of these tests was to provide an understanding of the problems peculiar to jet-driven rotors and to provide basic information on the thrust characteristics of jet engines operating in a high centrifugal acceleration field at the tip of the whirling blade.

The first tests were with a small ram-jet-powered rotor (refs. 1 and 2) and this paper deals primarily with a discussion of those tests. The installation of the rotor is shown in figure 1. The figure shows the tower, the rotor, the blades, and the engines. Fuel was supplied to the rotor by an overhead line, transferred to the blades through a rotating fuel seal, and thence out to the engines. A separate ignition coil was provided for each engine.

A sketch of the ram-jet engine used is shown in figure 2. The engine was developed for the U. S. Air Force to be used for a small one-man helicopter. It has an overall length of 18 inches, a maximum diameter of  $7\frac{1}{4}$  inches, and a weight of about  $9\frac{1}{4}$  pounds. The sketch shows the inlet, the diffuser, the radial flameholders, the spray nozzles, the combustion chamber, and the exit nozzle.

Because considerable testing and development work on ram-jet engines is done on static thrust stands by utilizing a free-air jet of about the same diameter or even smaller than the engine diameter, it is pertinent to describe the methods used in obtaining the engine thrust characteristics both in a free-air-jet thrust stand and on the whirling rotor blade. With a small-diameter air jet, the true external drag is not realized and unless care is taken to correct these results, the data so obtained are not indicative of the propulsive thrust that would be obtained with the unit completely immersed in the airstream.

The propulsive thrust  $F_p$  is the force which the engine exerts over and above its own drag at  $0^\circ$  angle of attack. The method of obtaining the propulsive thrust in a small free-air jet is as follows:

$$F_p = (\text{Net force change from power on to power off}) - (\text{True power-off drag})$$

In the free-air jet, the net force change from power on to power off is measured. From this force is subtracted the true power-off drag obtained either in a large wind tunnel or on the tip of a whirling blade.

The whirling thrust is determined similarly as shown by the following equation by measuring the net force change from power on to power off at a given rotor thrust and tip speed and by subtracting from this value the true engine power-off drag at  $0^\circ$  angle of attack:

$$F_p = (\text{Net force change from power on to power off at given tip speed and rotor lift}) - (\text{True engine power-off drag at zero angle of attack}) + (\text{Fuel-pumping term})$$

In addition, for the whirling case the engine must supply the thrust necessary to accelerate the fuel mass flow from zero at the rotor head to the speed of the engine. The fuel-pumping term is therefore added to the expression.

In the course of the test program it became apparent that the full thrust of the whirling engine as indicated by the free-air-jet test results could not be realized. A comparison of some of the whirling and free-air-jet results is shown in figure 3. In this figure the propulsive thrust in pounds is plotted against fuel consumption in pounds per hour. A large decrease in whirling maximum thrust as compared with the free-air-jet thrust is indicated. The ticks on the curves indicate the point of minimum specific fuel consumption. Free-air-jet tests with various fuel nozzles had indicated that the engine thrust was very sensitive to fuel spray wetting the walls which in turn indicated that the whirling thrust would also be decreased if fuel particles were thrown against the outer wall under the influence of high centrifugal accelerations. For these particular tests, the centrifugal accelerations were about 1,500g. Fuel stains inside the burner indicated that a considerable amount of fuel was actually being thrown against the outer wall.

As a result of these observations, the analysis section of the Langley Full-Scale Research Division undertook a theoretical study of the paths of various-size fuel particles in a helicopter-type ram jet. The results of that study have been reported previously (ref. 3). An illustration of the fuel-particle paths for a typical operating condition is shown in figure 4. The resultant paths of particles 0.006, 0.004, and 0.002 inch in diameter are shown for an engine speed of 700 ft/sec and a centrifugal acceleration of 1,500g. By first considering those particles with an initial straightforward injection path it can be

seen that the larger particles impinge on the wall toward the forward part of the engine. As the particle size is decreased, the resultant paths lie nearer the center of the ram jet. An actual fuel nozzle, of course, covers a wide spectrum of fuel-particle sizes, but this illustration is sufficient to show the general effect of high centrifugal acceleration ( $g$ ) forces. For comparison purposes, the path of a 0.004-inch-diameter particle injected at a  $45^\circ$  angle inboard is also plotted and its path lies nearer the center of the engine.

Since the centrifugal acceleration appears to exert a large influence on the engine propulsive characteristics, tests were made using the same engine at similar speeds and fuel flows but at one-half the former  $g$  loading. This was accomplished by doubling the rotor radius. Some of the results of these tests are shown in figure 5 as the effect of centrifugal force on the engine specific fuel consumption. The vertical scale is minimum specific fuel consumption in pounds of fuel per hour per horsepower and the horizontal scale is centrifugal acceleration in  $g$  units. Results from the free-air-jet tests, the 18-foot-radius rotor, and the original 9-foot-radius rotor are plotted for several engine speeds. The effect in all cases is an increase in specific fuel consumption as  $g$  loading is increased. The percentage increase in specific fuel consumption at a given  $g$  loading is larger at the lower tip speeds. This is primarily due to lower combustion-chamber velocities which allow more of the fuel particles to impinge farther forward on the engine shell instead of being swept back into the combustion chamber. It also appears that for this particular engine,  $g$  loads of about 400g or less did not have any appreciable detrimental effect. In other words, it appears that there is a cutoff point below which centrifugal effects are negligible. Larger diameter rotors with resultant low blade-tip centrifugal accelerations will likely not be adversely affected, but this is a real problem for the designer of small-diameter, high-tip-speed, one- and two-man machines.

Several methods of lessening the detrimental effects of centrifugal force have been proposed. Among these are vaporization of fuel to achieve smaller particle sizes, skewing of the combustion chamber to follow the fuel-particle paths, and radial elongation of the combustion chamber. Figure 6 shows the particular configurations which are being explored.

The first is the original ram jet with a perforated cone set in its combustion chamber. The cone acts as a hot surface to vaporize those fuel particles which impinge on it. The fuel nozzle is arranged so that the major portion of the fuel is injected from the inboard-pointing nozzle. This modification was tried on the free-air-jet thrust stand. The vaporization of the fuel plus the added turbulence caused by the perforated cone resulted in increased combustion efficiency. The net effect was about a 15-percent decrease in specific fuel consumption. Some preliminary whirling tests were attempted with this engine; however, the increased combustion efficiency ~~increased~~ increased the available

[REDACTED]

combustion-chamber temperature rise that the engine shell was weakened and collapsed before the engine was up to full operating speed. From a combustion viewpoint, this was an improvement and the problem now appears to be a purely mechanical one of fabricating an engine and cone to withstand the high g loads.

The second configuration embodies the skewed-combustion-chamber idea. The spray nozzles have been pointed farther inboard so that the fuel-particle paths will lie close to the center of the combustion chamber. To date only a plastic model of this engine has been built. This model was built to study the characteristics of the flow in the inlet and diffuser sections. Two small guide vanes were inserted in the inlet in order to obtain good flow at large skew angles. This inlet was designed to operate over a range of skew angles so that the angle of the engine with respect to the blade could be varied to determine the optimum setting. Further power-on tests, however, will be necessary to determine if any real overall gains can be realized by this method.

Figure 6 represents a flattened-out version of the original circular engine which is called a two-dimensional ram jet. This flattening out results in a radial elongation of the combustion chamber and it is hoped that good burning will be obtained even at the high g loads by proper fuel distribution through the spray nozzles. The shape of the unit also has an obvious advantage in that it can be faired into the blade contour thereby reducing its drag or act as an extension of the blade lifting surface. The figure also illustrates a frontal view of the engine attached to the blade to extend the lifting surface. This engine has been tested on the free-air-jet thrust stand and indicated performance comparable to that obtained with the circular engines. As yet no data have been obtained with these engines under whirling conditions. In general, there is now an understanding of the major ram-jet problems and ways are being explored to minimize them.

[REDACTED]

## REFERENCES

1. Carpenter, Paul J., and Radin, Edward J.: Investigation of a Ram-Jet-Powered Helicopter Rotor on the Langley Helicopter Test Tower. NACA RM L53D02, 1953.
2. Radin, Edward J., and Carpenter, Paul J.: Comparison of the Performance of a Helicopter-Type Ram-Jet Engine Under Various Centrifugal Loadings. NACA RM L53H18a, 1953.
3. Katzoff, Samuel, and Smith, Samuel L., III: A Theoretical Analysis of the Distortion of Fuel-Spray-Particle Paths in a Helicopter Ram-Jet Engine Due to Centrifugal Effects. NACA RM L53A02, 1953.

RAM-JET ROTOR  
RADIUS, 9 FT

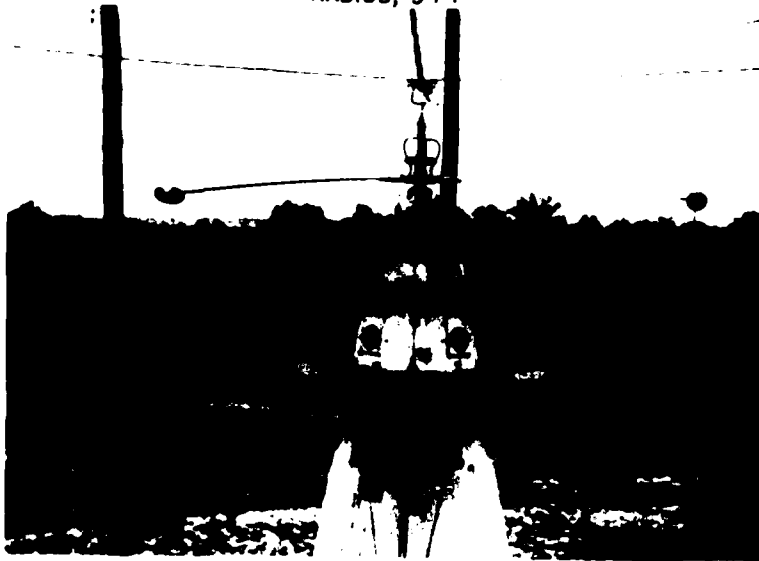


Figure 1

RAM-JET ENGINE

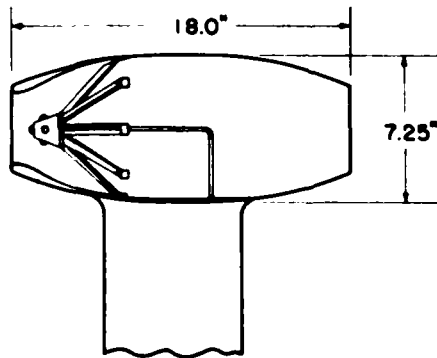


Figure 2

RAM-JET PROPULSIVE-THRUST CHARACTERISTICS

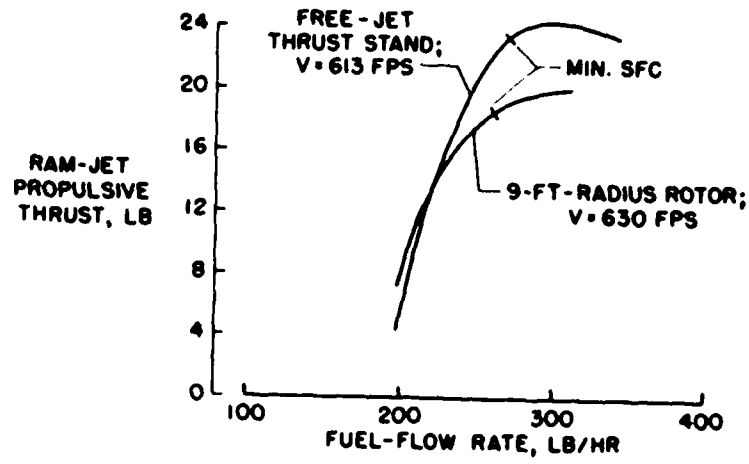


Figure 3

CALCULATED FUEL-PARTICLE PATHS

ENGINE SPEED 700 FT/SEC  
CENTRIFUGAL ACCELERATION OF 1,500g

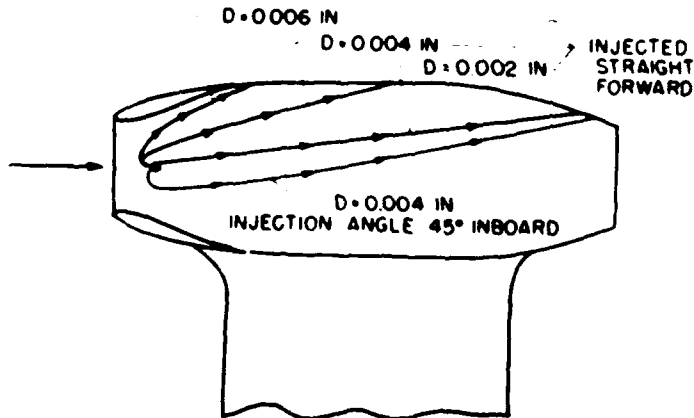


Figure 4



EFFECT OF CENTRIFUGAL FORCE  
ON SPECIFIC FUEL CONSUMPTION

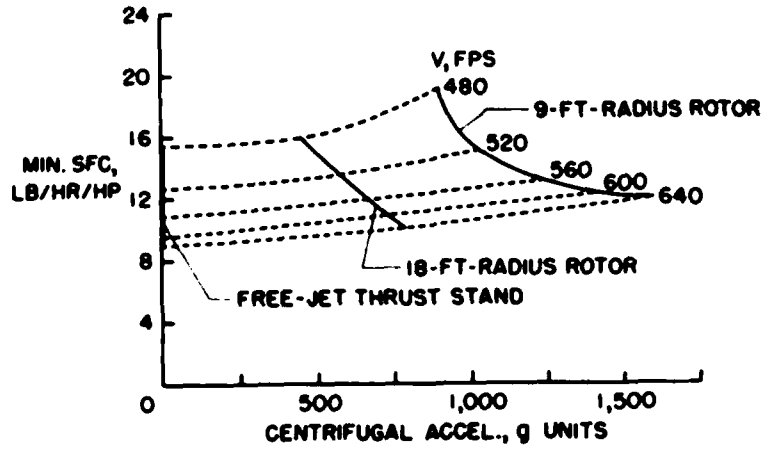


Figure 5

PROPOSED METHODS OF ALLEVIATING CENTRIFUGAL EFFECTS

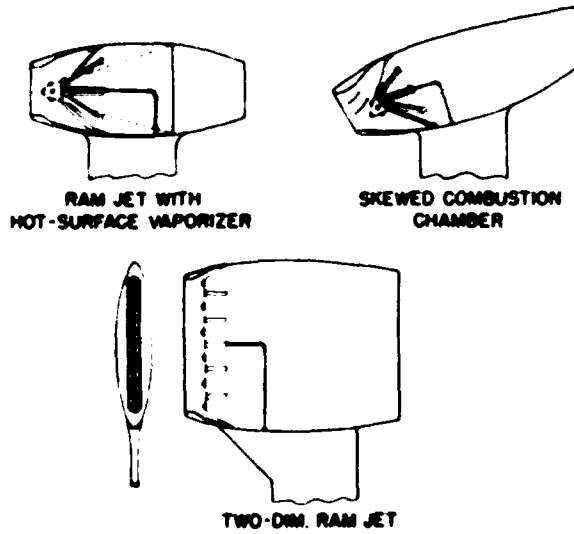


Figure 6

## AN INVESTIGATION OF A PULSE-JET ENGINE FOR HELICOPTERS

By Edward J. Radin and Paul J. Carpenter

Langley Aeronautical Laboratory

In addition to ram jets, the application of blade-tip-located pulse-jet engines to power helicopter rotors is of considerable interest. The engine is relatively simple, has a high ratio of thrust to power-off drag, has a lower specific fuel consumption than the ram-jet engine discussed in the previous paper by Paul J. Carpenter and Edward J. Radin, and has the characteristic of producing considerable power at the low speeds. Although these advantages have generally been understood, it was desired to gain operating experience with an actual installation to give an idea of the exact nature of the characteristics of the engine, its limitations, and its advantages. As of now, only that part of the study made on the Langley helicopter test tower is complete; however, preparations are underway to determine the nonrotating characteristics, that is, at zero centrifugal acceleration. The results of the tower tests are reported in detail in reference 1. The results of the work are now reviewed with special emphasis on the propulsive characteristics.

A sketch of the blade-engine combination that was used is shown in figure 1 and the general installation at the tower was about the same as described in the preceding paper on ram jets. The rotor had a radius of about 19 feet to the center line of the engine and had a solidity of 0.073. This rotor was tested in two configurations: First, the engine was rigidly attached to the blade spar and, second, the engine was free to pivot in pitch. In this second configuration, a tail fin was added to the jet engine so that the unit stayed at  $0^\circ$  angle of attack throughout the range of blade pitch angles. This pivoting may be desirable in the forward-flight condition to reduce the blade torsional inertia loads as the blade pitch varies during the cycle. Inasmuch as no difference in propulsive characteristics was noted between the two configurations even at blade pitch angles of  $10^\circ$  to  $12^\circ$ , only those results obtained with the engines rigidly attached to the blade are presented.

Figure 2 shows a sketch of the pulse-jet engine. This particular engine was developed for the U. S. Air Force. The engine had an operating frequency of about 100 cps, weighed 36 pounds, and was about 50 inches long with a maximum diameter of 9.4 inches. The fuel was injected into the pulse jet through nozzles located to the rear of the valve assembly.

Because of the importance of engine drag on autorotative characteristics, the first phase of the investigation at the Langley helicopter test tower was to determine ~~the power and~~ drag of the engine over a range

[REDACTED]

of speeds. The results of these power-off tests are shown in figure 3 in the form of drag coefficient as a function of engine velocity for both the basic engine and the same engine with the inlet completely blocked. One might ordinarily expect that the two curves would be similar since the valves would act to block the inlet in the power-off condition. This was not the case, however, because as the speed was increased, the valves opened more and more so that the internal losses were increased. This resulted in the type of increase in power-off drag coefficient shown by the basic-engine curve. With the inlet completely blocked, the drag coefficient is constant over the speed range. In autorotation it is desirable to store as much kinetic energy in the rotor as possible prior to the landing flareout. This is accomplished by operating at as high a tip speed as possible. At the higher tip speeds, these data indicate the desirability of blocking the inlet in the event of power failure to reduce the engine drag. Even without the inlet blocked, the pulse-jet rotor is somewhat less of a problem in autorotation than a ram-jet rotor because of the larger size ram jet for a given thrust and its higher speed.

The results with the pulse-jet engine operating appear in figure 4, in which the propulsive thrust in pounds is plotted as a function of fuel-flow rate in pounds per hour over a range of speeds from 0 to 422 fps. The curve for zero speed is the static case. The curves indicate the primary characteristic of the pulse-jet engine, which is decreased maximum propulsive thrust with increased speed. This decrease in propulsive thrust with increased speed is attributed to the failure of the inlet valves to close completely at the higher speeds, increased external drag, effect of increased speed on the engine resonating characteristics, and a decrease in tailpipe charging. This tailpipe charging is the phenomenon by which the engines obtain air through the tailpipe as well as the inlet. This reduced tailpipe charging and the previously mentioned factors tend to decrease the combustion-chamber pressure ratio and thereby cause a decrease in the propulsive thrust with increasing speed.

The points at which the engine failed to resonate because of an increase in fuel are called "rich blowout" and are indicated on the curves. For the whirling conditions these points are at maximum engine thrust and are characterized by a drastic loss of power accompanied by a long yellow flame out of the tailpipe. The maximum thrust values therefore cannot be utilized for design purposes inasmuch as some margin of safety must be provided to avoid a sudden loss of power while in flight. Of course, with sufficient altitude, this rich blowout may not be too dangerous - the flame is still there, and it was possible to start the engines resonating again by merely reducing the fuel rate before the tip speed dropped below 200 fps. Rich blowout was not reached at the highest speed because of inlet-cowling failure at fuel-flow rates greater than those shown.

[REDACTED]

Although no evaluation of the effects of centrifugal acceleration on the propulsive characteristics of the pulse-jet engine has been made, these effects would be expected to be small since the highest acceleration reached during the tests was about 300g.

Incidentally, at the maximum thrust condition and a tip speed of 319 fps, the noise level was very high. A raucous body-shaking noise that had a level of 132 decibels was measured at a station on the ground 40 feet below the rotor and 90 feet from the center of rotation. This noise intensity is 15 to 20 decibels louder than a value measured in the cockpit of a Sikorsky H-19 helicopter in powered flight. With a decrease in thrust to a value where the engine would probably be operating most of the time, the noise intensity decreases to a more bearable level.

The whirling data are replotted in figure 5 to indicate more closely the effect of velocity on the engine characteristics. The upper curve shows the propulsive thrust in pounds per square inch of frontal area as a function of engine velocity. Although the maximum-thrust point was not reached at 422 fps (fig. 4), based on the data that were obtained in the higher speed range, the curve is extrapolated to indicate the trends at this speed. The thrust is fairly constant at a value of about 1 pound per square inch of frontal area over the lower speed range but begins to drop off rapidly at speeds above 350 fps. This dropping off is obviously an undesirable characteristic and at the present time limits the maximum rotor tip speed. There are some limited data (ref. 2) which indicate that the thrust could be increased and the operating range could be extended to higher speeds.

The bottom curve shows the specific fuel consumption in pounds per hour per horsepower as a function of engine velocity. The data for this curve have also been extrapolated to 422 fps in a manner similar to that of the top curve. This curve indicates that the most economical tip-speed range for this engine is 320 to 360 fps. Here again reference 2 indicates that the specific fuel consumption could be lowered and the operating range extended to higher velocities.

Now in order to put the pulse-jet engine in the proper perspective, the helicopter-type ram-jet engine discussed in references 3 and 4 is compared with the pulse-jet engine. Figure 6 shows the propulsive-thrust and specific-fuel-consumption characteristics of these two engines over their respective speed ranges. It is seen that the thrust of the ram jet is about half that of the pulse jet. The ram-jet specific fuel consumption ranges from 20 to about 12 pounds per hour per horsepower as compared with  $7\frac{1}{2}$  to  $6\frac{1}{2}$  for the pulse jet. For some applications, the low speed at which the pulse-jet engine develops its power is an advantage, since the ratio of rotor lift to power required increases with decreased tip speed. This factor plus the lower specific fuel consumption of the

[REDACTED]

pulse jet indicates that a pulse-jet-powered rotor can develop two to three times the lift of a ram-jet rotor at the same fuel consumption.

## REFERENCES

1. Radin, Edward J., and Carpenter, Paul J.: Investigation of a Pulse-Jet-Powered Helicopter Rotor on the Langley Helicopter Test Tower. NACA RM L53L15, 1954.
  2. Brown, Harry W.: Summary Report - Development Tests of Pulse Jet Engines. Rep. No. P.P.-11 (Project 30-29, Phase 3, Contract No. NOa(s) 8520), Marquardt Aircraft Co., Nov. 26, 1947.
  3. Carpenter, Paul J., and Radin, Edward J.: Investigation of a Ram-Jet-Powered Helicopter Rotor on the Langley Helicopter Test Tower. NACA RM L53D02, 1953.
  4. Radin, Edward J., and Carpenter, Paul J.: Comparison of the Performance of a Helicopter-Type Ram-Jet Engine Under Various Centrifugal Loadings. NACA RM L53H18a, 1953.
- [REDACTED]

SKETCH OF PULSE-JET-ENGINE-BLADE COMBINATION  
ROTOR SOLIDITY, 0.073

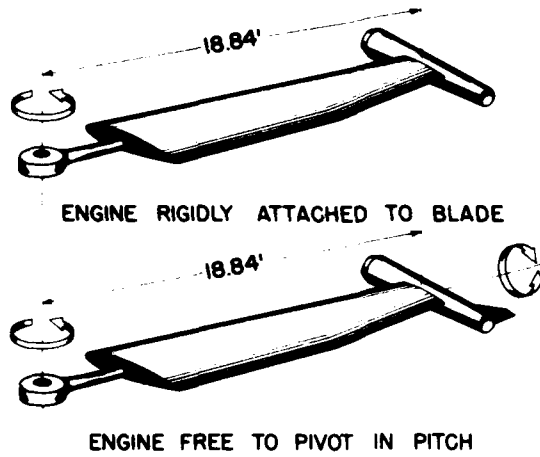


Figure 1

SKETCH OF PULSE-JET ENGINE

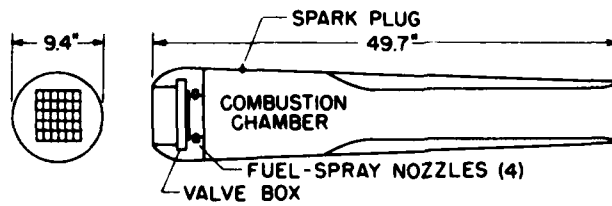


Figure 2

PULSE-JET POWER-OFF DRAG

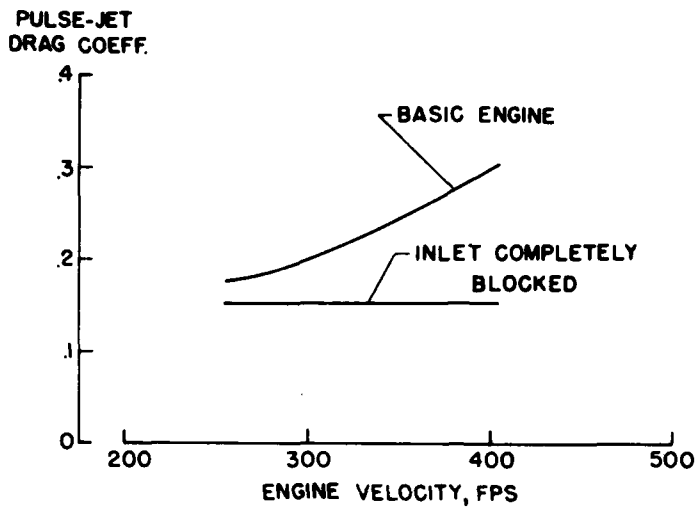


Figure 3

PULSE-JET PROPULSIVE THRUST

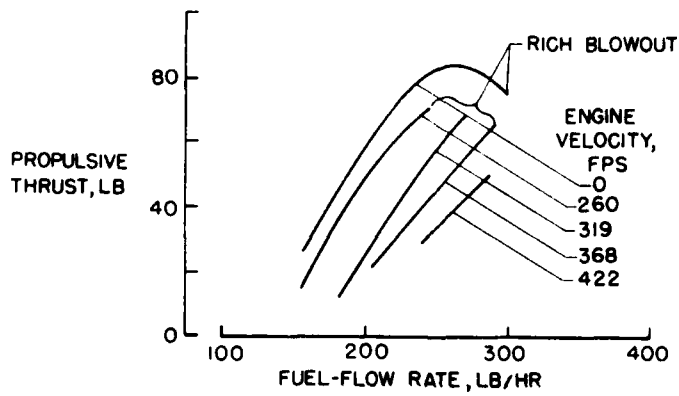


Figure 4

PULSE-JET-ENGINE SFC AND THRUST CHARACTERISTICS

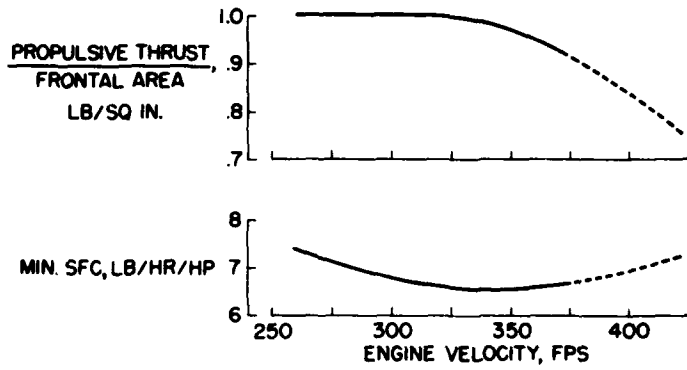


Figure 5

HELICOPTER RAM-JET AND PULSE-JET CHARACTERISTICS

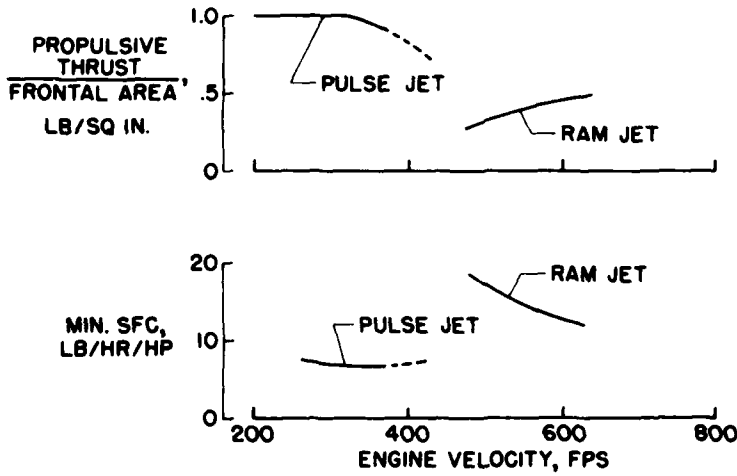


Figure 6



## AN ANALYTICAL STUDY OF A LARGE

## PRESSURE-JET HELICOPTER

By William S. Miller and Richard P. Krebs

Lewis Flight Propulsion Laboratory

Some of the characteristics of two members of the tip-drive family, the pulse jet and the ram jet, were outlined in the two preceding papers by Paul J. Carpenter and Edward J. Radin. In this brief presentation, the results of an analytical study of a third member of the family, the pressure jet, are given.

In the pressure-jet system there are three independent powerplant parameters: namely, jet pressure ratio, jet temperature, and tip speed. It was the purpose of this analysis to determine the effect of changes in these parameters on the hovering time and range of a helicopter. Furthermore, the best combination of these parameters as indicated by a study of the integrated performance of the pressure-jet system and the helicopter was sought. As a starting point, a 30,000-pound helicopter shown as an artist's concept in figure 1 was assumed. The figure shows that the pressure-jet system is completely conventional. A gas turbine engine is directly coupled to an auxiliary compressor that provides compressed air for the system. At compressor exit temperature and pressure, air is brought through a large duct to the rotor pylon and, from there, through smaller blade ducts to tip-mounted combustion chambers. Since the conventional tail rotor is not required in the pressure-jet helicopter, directional control in hovering can be provided by lateral deflection of the gas-turbine jet.

It was anticipated, before the numerical results were tabulated, that the optimum design for the pressure-jet system would represent a compromise. For example, a given thrust from the jets can be obtained with high air flows and low jet temperatures or, conversely, with low air flows and high jet temperatures. In the first case, high air flows require large gas turbines and compressors and high engine fuel flows. These disadvantages are partly offset by low tip-burner fuel rates and high propulsive efficiencies. On the other hand, if a small engine and compressor are selected, engine weight and engine fuel flow are reduced but high tip fuel rates and low propulsive efficiencies result. Regardless of the compromise that is made on air-flow rates, the auxiliary compressor pressure ratio must still be selected. Here again, a compromise choice based on engine weight, fuel rates, and propulsive efficiencies must be made.

The effects on helicopter performance of two design-point parameters, pressure ratio and jet temperature, are shown in figure 2. In this figure

hovering time is plotted against design jet temperature for three pressure ratios: 2.25, 3.0, and 5.0. The design jet temperature is the temperature required for hovering at maximum gross weight. The operation of the pressure-jet system at design-point and off-design-point conditions can be illustrated if an all-hovering flight represented by each point on these curves is considered.

As hovering flight begins, the helicopter weight is 30,000 pounds, the auxiliary compressor is at design pressure ratio, say 3.0, and jet temperatures are at design point, say 3000° R. As fuel is consumed and helicopter weight decreases, constant-altitude hovering requires that pressure-jet power be progressively reduced. In this analysis, two methods of obtaining this off-design power were investigated. In the first method, pressure-jet power was decreased by gradually reducing the fuel flow to the tip burners while air flow and pressure ratio were held constant. This requires a continuous adjustment of the tip nozzle area. In the second method, tip nozzle area was held fixed and power was reduced by simultaneously decreasing the speed of the gas turbine and the fuel flow to the tip burners.

The data for figure 2 were based on the variable-area configuration. As can be seen, except for the very low pressure ratios, hovering time is relatively insensitive to design jet temperatures. For a pressure ratio of 2.25, hovering at maximum gross weight is impossible for jet temperatures below 3100° R. However, for pressure ratios in the middle range, say from 2.5 to 5.0, there is only a 10-percent change in hovering time with a maximum of 5.5 hours at a pressure ratio of 3.0.

As hovering flight progresses, tip-burner temperatures are gradually reduced from the design value to match the decreasing power requirements of the helicopter. In contrast, increased pressure-jet power for climbing or high-altitude hovering is obtained by raising operational jet temperatures above the design value. In order to provide a 20-percent reserve over the hovering power, design temperatures have been restricted to values below 3000° R, as shown by the vertical dashed line.

Forward flight range at a speed of 83 knots was calculated for each set of design coordinates (that is, jet temperature and pressure ratio). As in the hovering condition, the best forward flight range was found in the low-middle range of auxiliary compressor ratios - 2.5 in forward flight as compared with 3.0 in hovering. For all pressure ratios that were investigated, the range increased slightly with design temperature. Because of this characteristic of the range plot and in order to fulfill the reserve-power requirements, a design jet temperature of 3000° R was selected for all the performance results that follow.

A composite chart showing helicopter performance in hovering and in forward flight while carrying different payloads is presented in

figure 3. In this figure pressure ratio has been fixed at 3.0, tip speed at 700 ft/sec, and design jet temperatures at 3000° R. The weights shown represent the payloads that can be carried for the all-hovering missions shown on the left or the all-forward-flight missions on the right. The figure shows that doubling the payload from 6000 to 12,000 pounds decreases the hovering time from 2 hours and 45 minutes to 50 minutes and decreases the range from 390 nautical miles to 130 nautical miles.

Rotor tip speed is the third primary design parameter that influences pressure-jet performance. The effect of changes in this parameter is shown in figure 4. Hovering time and range are plotted against tip speed. The flatness of the curves indicates that both hovering time and range are insensitive to changes in the tip speed between 500 and 700 ft/sec. In this range the increased propulsive efficiency has overcome the increased rotor drag at higher tip speeds. The choice of tip speed, in this range, might favor the 700-ft/sec value because of tip-stall considerations. Both hovering time and range are penalized when tip speed is increased to 900 ft/sec. The hovering-time and range values at this speed are optimistic since no allowances were made for drag divergence in the rotor computations.

Previously, it was pointed out that two methods of off-design operation of the pressure-jet system were considered in the analysis: namely, variable- and fixed-area operation. The performance values that have been presented so far were all based on the variable-area technique. Helicopter performance for the two methods of operation is compared in figure 5. In both hovering and forward flight, the variable-area nozzle gives appreciably better performance, 5 hours 25 minutes compared with 3 hours 30 minutes in hovering and 715 miles compared with 400 miles in forward-flight range.

The difference in performance that is obtained by the two methods of operation can be explained as follows: With variable-area operation, jet temperatures gradually decrease during a flight and propulsive efficiencies continually improve. With fixed-area operation, the matching of compressor and burners required that constant jet temperature be maintained as compressor pressure ratio and air flow were reduced. Consequently, the initially high jet temperatures remain high for the duration of the flight and propulsive efficiencies remain correspondingly low.

Aside from its dependence on the three primary variables, pressure ratio, jet temperature, and tip speed, pressure-jet-helicopter performance in hovering and forward flight is also a function of the area of the duct that brings the air to the tip burners. The effect of changes in duct area, assuming a constant rotor solidity and thickness-chord ratio, is shown in figure 6. Hovering time on the left and range on the right are plotted against the ratio of the duct area to blade-section area. This figure shows that there is a lower critical value

for the duct area and, for the present analysis, this area is 0.2 of the section area. Range and hovering time are not appreciably increased when duct areas exceed the critical value but fall off rapidly as duct areas are reduced below the critical value.

The performance penalties on the pressure-jet system are the same whether duct area is reduced by decreasing the duct-area—section-area ratio, by decreasing the rotor solidity, or by using thinner blade sections.

Figure 7 sums up the results of this investigation of the pressure-jet system. It has been shown that helicopter performance is relatively insensitive to changes in pressure ratio, jet temperature, and tip speed. However, there is a representative set of values which gives near-optimum performance for the assumed configuration.

The helicopter has an 80-foot-diameter rotor with a tip speed of 700 ft/sec. The gas turbine produces approximately 2100 horsepower, consumes 1565 pounds of fuel per hour, and weighs, with the auxiliary compressor, 1400 pounds. Because the engine is so light, pressure-jet-helicopter performance is insensitive to changes in engine specific weight. An increase in the assumed specific weight from 0.65 pound per horsepower to 1.0 pound per horsepower was found to reduce hovering time about 7 percent.

The auxiliary compressor has a pressure ratio of 3.0, provides 30 pounds of air per second at sea level, and has a frontal area of about 2 square feet.

Design jet temperatures should be about 3000° R and, for best performance, the jet nozzle should have a variable area. Fuel rates to the tip in hovering decrease from 4100 pounds per hour at maximum gross weight to 265 pounds per hour at a gross weight of 14,000 pounds.

**PRESSURE-JET HELICOPTER**  
**30,000 LBS GROSS WEIGHT**

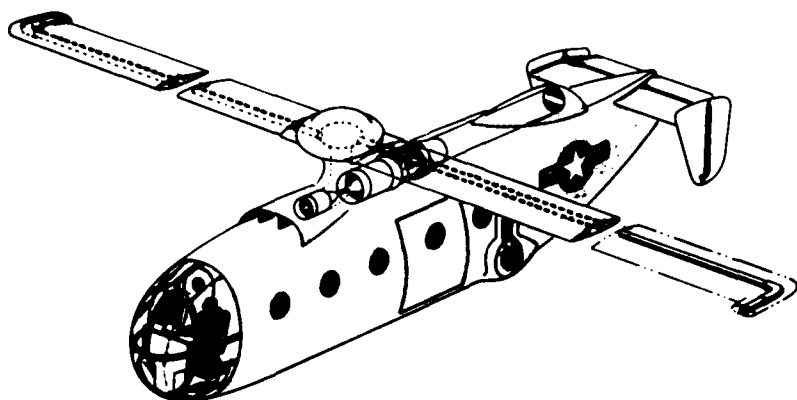


Figure 1

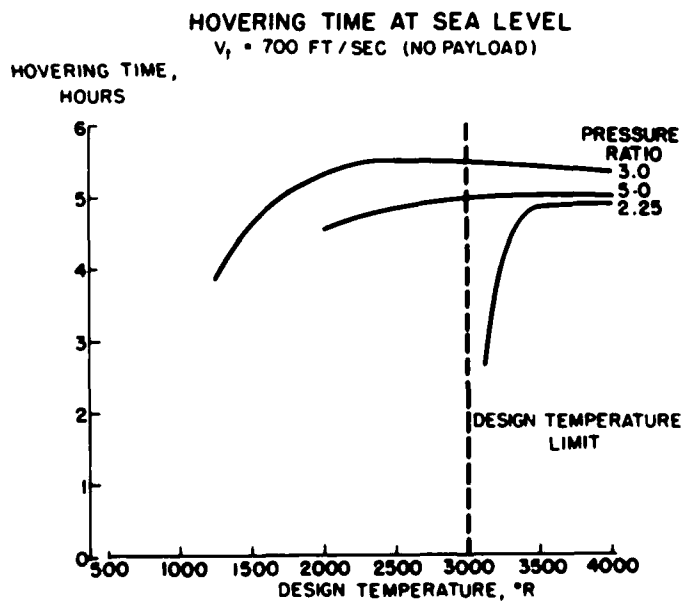


Figure 2

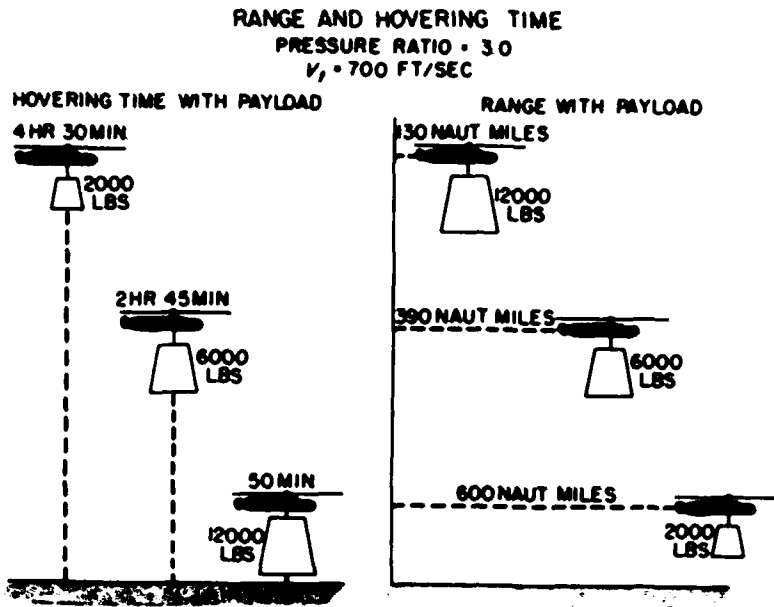


Figure 3

**EFFECT OF TIP SPEED ON HELICOPTER PERFORMANCE**  
 VARIABLE-AREA NOZZLE

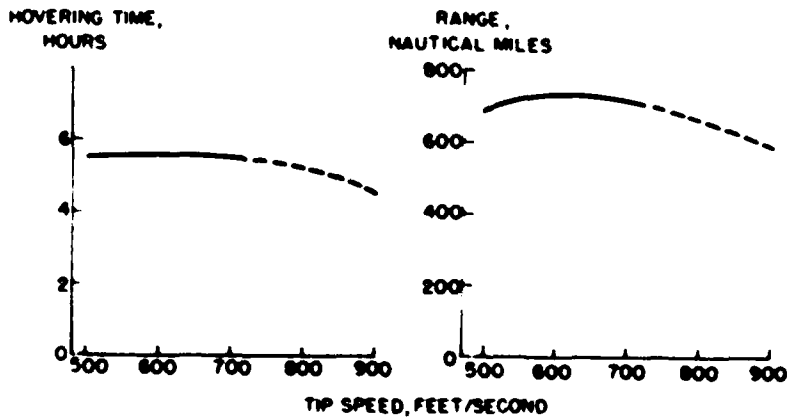


Figure 4

COMPARISON OF VARIABLE-AND FIXED-NOZZLE-AREA PERFORMANCE  
PRESSURE RATIO = 30  
 $V_1 = 700 \text{ FT/SEC}$   
 $T_{30} = 3000^\circ \text{ R}$

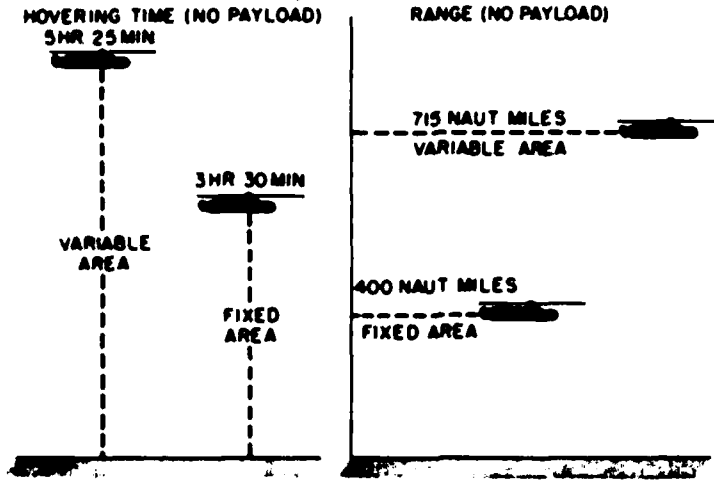


Figure 5

EFFECT OF DUCT AREA ON HELICOPTER PERFORMANCE  
VARIABLE-AREA NOZZLE

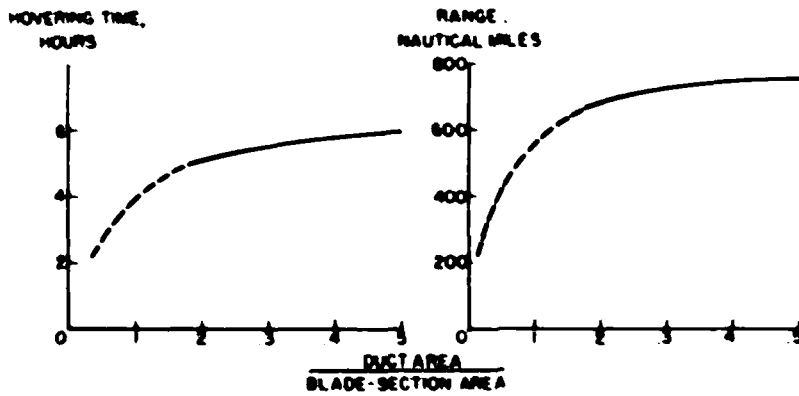


Figure 6

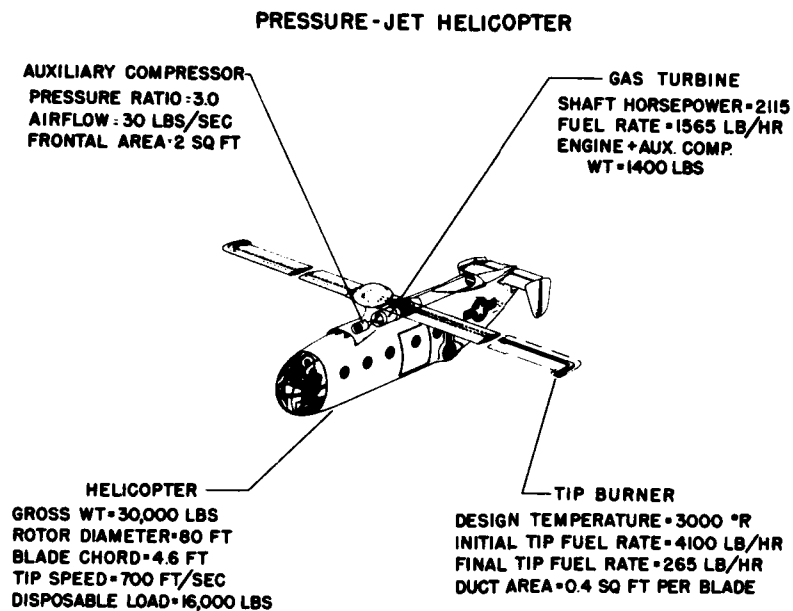


Figure 7



[REDACTED]

ASPECTS OF INTERNAL-FLOW-SYSTEM DESIGN FOR  
HELICOPTER PROPULSIVE UNITS

By John R. Henry

Langley Aeronautical Laboratory

SUMMARY

Pertinent items relating to the design of internal-flow systems for reciprocating engine, turbine engine, and pressure-jet installations in helicopters are discussed. The importance of the following items is emphasized: controllable exit and ram recovery for reciprocating-engine cooling; performance penalties possible in turbine-engine installations attributed to distortions in the flow distribution at the face of the axial compressor; the effects of high subsonic flow velocities on the performance of duct elements; and the effects of centrifugal forces on the flow in a ducted helicopter rotor. Data on the maximum flow capacities of bends are included.

INTRODUCTION

Helicopter performance requirements have pushed the flight speed range up from 100 mph to perhaps 150 to 200 mph. Such speed-range changes in the history of the conventional airplane influenced the design of ducting and air-cooling systems in certain respects. It is desirable to reexamine current and future helicopter designs and requirements to determine any design trends indicated by the increasing flight speeds. First, the reciprocating-engine cooling-system installations are examined and then the internal-flow problems related to other types of powerplant installations - for instance, the gas turbine - are discussed. The purpose of this paper is to touch on various pertinent items relating to internal flow, not to present a detailed set of design rules and data.

SYMBOLS

A     cross-sectional area, sq ft  
 $a_0$    speed of sound in free stream, ft/sec  
 $C_p$    pressure-rise coefficient

[REDACTED]

[REDACTED]

D diameter of fan rotor or circular duct, as indicated  
H total pressure, lb/sq ft, abs  
h height of rectangular duct, ft  
M Mach number  
n fan rotational speed, rps  
Q volume flow, cu ft/sec  
 $q_c$  dynamic pressure corrected for compressibility  
 $q_0$  flight dynamic pressure  
R rotor-blade radius to tip, ft  
r radius (various radii are defined where used)  
 $V_0$  flight velocity relative to free stream, ft/sec except as indicated otherwise  
 $V_x$  exit velocity relative to helicopter, ft/sec  
w width of rectangular duct, ft  
 $\Delta H$  total-pressure change, lb/sq ft  
 $\eta$  fan efficiency  
 $\rho$  mass density  
 $\Omega$  angular velocity of rotor blade, radians/sec

## Subscripts:

C cooler  
D duct  
F fan  
1 at diffuser inlet  
2 at diffuser exit

[REDACTED]

HUB at blade hub

TIP at blade tip

### RECIPROCATING-ENGINE INSTALLATION

The type of reciprocating-engine internal-flow system to be discussed is illustrated in figure 1. The air enters a plenum chamber through a screened inlet, proceeds through a fan and diffuser, and then splits into parallel streams. Each of the parallel ducts contains an air-using unit - such as the carburetor, the transmission-oil cooler, the engine-cylinder cooling ducts, and the engine-oil cooler. The air exhausted from these various units, with the exception of the carburetor, is then collected in a compartment containing an exit to atmosphere.

In typical existing systems of this type, the following characteristics generally apply: The inlets and exits are large and the intention is not to recover ram pressure at the inlet or thrust at the exit; the fan operates at engine speed and may or may not have contravanes; the engine cooling air flow requires 50 to 60 percent of the total internal air flow; and the rear compartment is not generally airtight.

The purpose of the following discussion is to determine whether there are particular methods of design and operation which will produce an appreciable saving in horsepower expenditure for the cooling system. An airtight system will be assumed, since it is impossible to determine drag quantities with indeterminate leakages. Before the effect of flight velocity is discussed, a review of the role of the cooling fan in the system is necessary.

The total power  $P$  in units of horsepower chargeable to the cooling system may be expressed as follows:

$$\sum P = \frac{Q \Delta H_F}{550\eta} + \frac{Q(\Delta H_C + \Delta H_D - \Delta H_F)}{550} + \frac{Q_0}{550 \times 2} (V_0 - V_X)^2$$

The preceding equation assumes no compressibility or heating effects but is sufficiently accurate for the application to be discussed. The first term on the right-hand side is the fan-shaft horsepower. The second term is, by definition, the "residual pumping" horsepower or the air-pumping power required to overcome total-pressure losses of the system in excess of the total-pressure rise supplied by the fan. The third term is the wake horsepower or power associated with kinetic energy left in the air after it is discharged to the atmosphere. The sum of the last two terms may be shown algebraically to correspond to the conventional equation for internal drag.



In order to illustrate the effect of the fan and duct losses on the total cooling horsepower, some simplified configurations are presented in figure 2, together with cooling-horsepower calculations for the case where the cooler total-pressure loss is equal to the fan total-pressure rise, which is equal to the flight dynamic pressure  $q_0$ . It is a familiar axiom that, for an efficient ducting system, if the cooling fan is designed just to overcome the system total-pressure losses, a minimum overall cooling-drag power results. This condition is represented by the configuration of figure 2(a), where the net total-pressure loss is zero and, thus, the only horsepower expenditure is the fan-shaft horsepower,  $q_0 Q / 550 \eta$ . The configuration of figure 2(b), which consists of an inefficient duct without cooler or fan and with a total-pressure loss equal to  $q_0$ , requires an infinite exit area since the exit total pressure is equal to free-stream static pressure. Under these conditions, the exit velocity is essentially zero, and the sum of the residual-pumping and wake horsepowers is approximately twice the total cooling horsepower of the efficient cooling design (fig. 2(a)). Adding the fan and cooler to the configuration of figure 2(b) produces an inefficient cooling system (configuration of fig. 2(c)), which also has a net total-pressure loss equal to  $q_0$ . Figure 2 indicates that the total cooling horsepower for this system is approximately three times that of the efficient cooling system. With inefficient fan designs and air leaks, this value may be much higher. The excessive horsepower of the configuration of figure 2(c) results from the fact that total-pressure losses not compensated for by the fan produce penalties in horsepower twice - once in residual-pumping power and once in wake power.

In order to examine the cooling-horsepower problem further, particularly with regard to the effect of flight velocity on magnitudes, some calculations were made for the helicopter model of reference 1. The helicopter has the following specifications:

Gross weight, lb . . . . .	10,000
Tip speed, fps . . . . .	500
Solidity . . . . .	0.07
Disk loading, lb/sq ft . . . . .	2.5
Flat-plate parasite drag, sq ft . . . . .	40
Rated engine power, hp . . . . .	1,000

The curve for helicopter power required, calculated for level equilibrium flight, and the assumed fuel-air-ratio variation are given in figure 3. The system cooling requirements, which were estimated by assuming an air temperature of 100° F and parallel air circuits similar to that shown in figure 1, are presented in figure 4. The cooling-fan performance characteristics assumed on the basis of data in reference 2 are presented in figure 5. In matching the fan characteristics to the cooling requirements, the hovering condition was assumed to correspond to a  $Q/nD^3$  of 0.3,



and the fan pressure rise for hovering was assumed to be 20 percent greater than the required cooling air pressure drop.

Some of the resulting cooling-horsepower calculations are shown in figure 6 as a function of flight speed  $V_0$ . The curves shown correspond to the condition where the correct amount of cooling air flow is obtained at each flight speed by controlling the exit area. The amount of horsepower has been referenced to the cooling horsepower required in hovering for the lowest curve. In current practice, this value of cooling horsepower (unity) may range between approximately 4 and 10 percent of the engine normal rated power. The curve shapes resemble the shape of the curve of engine horsepower required, as would be expected, except for the drop in cooling horsepower at the high-speed end. This effect is due to richer mixtures at high engine powers, since fuel cooling results and thus the air cooling requirements are reduced. In the two lower curves, an efficient duct system or 100-percent ram recovery was assumed. In the lowest curve, the fan efficiency was held constant at 75 percent, presumably by controlling some component of the fan geometry. In the middle curve, a typical variation of fan efficiency with volume flow was assumed; in other words, a fixed fan geometry. The advantage of variable fan geometry is indicated by figure 6 to be small (on the order of 5 to 10 percent). The top curve assumes an inefficient duct system or a complete loss of ram recovery. Complete loss of ram added 30 percent to the horsepower in the cruise range (90 mph) and doubled the power at about 120 mph, the rated horsepower condition. In addition, in the range of the dashed curve the exit areas required to obtain the necessary cooling air flows were over twice that which was considered a reasonable value. At the higher flight speeds now contemplated for helicopters, the increased cooling powers produced by loss of ram would be even larger.

Cooling-horsepower calculations for the condition of a fixed exit area equal to that required for the hovering condition are presented in figure 7. The curve of figure 6 for a fixed fan and controllable exit area is also given again for reference purposes. In the curve for 100-percent ram recovery, the fan just meets the cooling requirements in hovering. As the flight speed increases with a fixed exit area, the ram recovery forces more air through the system, so that the cooling requirements are exceeded and the horsepower is increased. This effect adds about 70 percent to the cooling horsepower in cruising and 50 percent at rated power. The effect would be larger for helicopters designed for higher flight speeds. Thus, it is seen that a controllable exit area is a powerful device for maintaining minimum cooling powers. To produce an effective exit-area control, however, leaks must be minimized.

The top curve of figure 7, because it corresponds to zero ram recovery and fixed exit area, is for a fixed air flow. Consequently, the curve indicates that, for a complete loss of ram, the wake and residual-pumping powers increase rapidly with increasing flight speed. The dashed portion of the curve corresponds to conditions where cooling is not quite adequate

because the required cooling air flow is slightly more for the rated-power condition than for the hovering condition. The fact that the two upper curves are almost coincident indicates that the cooling horsepower for a fixed exit-area design is not appreciably reduced by a high ram recovery.

In connection with the general problem of the design of cooling systems, a large amount of data is available in the literature and the more important references have been listed. References 3 to 17 contain diversified information including design procedures and fundamental concepts and have become basic references in this field. References 18 to 30, in general, contain data on specific configurations or aerodynamic effects in the low-speed or incompressible-flow range. References 31 to 41 are reports of investigations of diffusers and bends in which boundary-layer-control devices were evaluated. References 42 to 44 and reference 2 are useful in designing cooling fans.

### TURBINE-ENGINE INSTALLATION

The conventional turbine engine with an axial-flow compressor is a convenient package unit of favorable aerodynamic shape with apparently a minimum of ducting complications. Investigations reported in references 45 to 51 and other unpublished data have indicated, however, that some engines of this type are sensitive to distortions in the air flow and pressure distribution at the face of the compressor. Some of the engines tested have exhibited very serious reductions in performance due to this effect.

Figure 8 outlines some of the effects on the individual engine components for one of the most distorted distributions investigated (ref. 51). The air-flow maldistribution was set up by the installation of a screen in one of the twin intake ducts, which resulted in a 62 percent to 38 percent distribution of the air flow and a pressure distortion just upstream from the compressor face of  $\pm 19$  percent of the absolute pressure. The inlet pressure distortion was smoothed out by the compressor, and pressure distributions throughout the rest of the engine were approximately normal. A small distortion of  $\pm 5$  percent was measured at the turbine exit. As a result of the unequal pressure ratios across the two halves of the compressor, a temperature distortion of  $+15$  percent to  $-6$  percent of the absolute temperature was present at the compressor outlet. These conditions led to a  $\pm 54$ -percent temperature distortion at the turbine inlet and  $\pm 6$  percent at the turbine outlet. The compressor efficiency was lowered 17 percent; the combustion efficiency was unaffected; and an 8-percent reduction was obtained in the turbine efficiency. The net effect of these changes in the component performances was a loss in thrust of 26 percent and an increase in specific fuel consumption of 23 percent. Because of unfavorable effects on the compressor stall and surge characteristics, the engine operating range was curtailed. It should be emphasized

[REDACTED]

that the numbers given here are the maximum values observed over the operating range tested. An engine modified for helicopter application would be expected to produce similar results.

The seriousness of this problem in helicopter installations is difficult to predict. Helicopter air inlets are subject to operation over a very wide range of angle of attack and yaw and, therefore, may operate inefficiently. Siamese inlets, under some operating conditions, may set up large distortions due to the fact that one inlet may be recovering approximately full ram while the other is operating in the fuselage wake. It is difficult to imagine, however, that pressure distortions at the compressor face will approach the  $\pm 19$ -percent value shown in figure 8. Nevertheless, the penalties are so high that helicopter designers should attempt to minimize the effect.

One solution is to adapt the installation to the engine. This adaptation might be accomplished by feeding the compressor inlet from a plenum chamber similar to that used for conventional cooling installations of reciprocating engines. Another solution is to adapt the engine to the installation, which means employing engines insensitive to inlet irregularities - for instance, the centrifugal compressor-type engines.

#### HIGH-SPEED EFFECTS IN DUCTS

High subsonic flow velocities in duct elements, such as diffusers and bends, produce performances appreciably different from low subsonic velocities. These effects are probably due to increases in both Reynolds and Mach numbers; as yet, sufficient data are not available to isolate the two variables. Since high subsonic flow velocities are anticipated in some of the duct elements in turbine-engine installations and in pressure-jet-type powerplants, high-speed effects are of interest to helicopter designers.

Figure 9 presents some data for conical diffusers on the effect of speed on diffuser loss coefficient. The Mach number at station 1 has been selected as the index to speed. The diffuser area ratio is 2.0 and a moderate boundary-layer thickness was present at the inlet. The ratio of loss coefficient obtained at some inlet Mach number to the loss coefficient obtained at an inlet Mach number of 0.2 is given as a function of diffuser expansion angle,  $2\theta$ , for curves of constant inlet Mach number. The curves show that for short diffusers, expansion angle in the range of  $20^\circ$  to  $24^\circ$ , the loss coefficient at high subsonic Mach numbers may reach values approaching twice that corresponding to a Mach number

[REDACTED]

[REDACTED]

of 0.2. The increased total-pressure loss is, of course, accompanied by more distorted exit-velocity distributions. Additional data on these effects are given in references 52 to 63. Similar performance trends have been observed for flow around bends and are discussed in reference 64.

#### CHOKING MACH NUMBER FOR BENDS

In the design of pressure-jet systems, the maximum flow capacity of duct elements, especially bends, becomes of interest. The aerodynamic index to maximum flow capacity is the choking Mach number. Unpublished NACA data and other data from reference 64 are summarized in figure 10. Data are given for 90° bends of both circular and rectangular cross section. For the choking condition, the mean Mach number at the inlet reference station is given as a function of bend radius ratio. For the rectangular bends, curves of constant aspect ratio  $h/w$  are presented. An aspect ratio of 1.0 corresponds to a bend of square cross section. All the rectangular-bend data are for a very thin inlet boundary layer. The curve for the circular bends contains both thick and thin inlet-boundary-layer points.

All the curves indicate that reducing the radius ratio - in other words, increasing the sharpness of the turn - reduces the choking Mach number or flow capacity of the bend. For rectangular bends, the square cross section is optimum with higher or lower aspect ratios producing lower choking Mach numbers. The comparison of the circular and square bends shows the circular bend to be slightly superior. Thickening the boundary layer in the circular bend had no appreciable effect on the choking Mach number. A choking Mach number of 0.7, which is obtainable with the better configurations of figure 10, corresponds to 91 percent of the theoretical maximum weight flow obtainable at a Mach number of 1.0.

#### FLOW IN DUCTED ROTOR BLADE

In the design of pressure-jet-type systems, the aerodynamics of the flow through a ducted helicopter blade becomes important, both from the standpoint of the total-pressure losses involved and from the standpoint of flow conditions produced at the tip burner inlet. Figure 11 illustrates the effect of centrifugal force on the flow in a ducted helicopter blade. The calculations were made by using the one-dimensional expressions and analysis presented in reference 65. The calculations presented in figures 11 to 13 are for a completely insulated duct; therefore, the total temperature rises somewhat due to compression (adiabatic compression) as the flow proceeds from blade hub to tip. The preceding assumption differs from that used in the calculations of reference 65 where an



isothermal compression or constant total temperature was assumed. In the latter case, the heat lost through the duct walls would have to be just sufficient to counteract the tendency for the total temperature to rise due to compression. In the calculations presented herein, the adiabatic assumption was made because it produces more pessimistic answers relative to total-pressure losses and choking Mach number.

Figures 11, 12, and 13 were constructed on the further assumption that the ratio of the ducted-flow total temperature at the rotor hub to the free-stream ambient temperature is 1.0. The value of this ratio affects only the numerical values of rotor-tip Mach numbers identifying the curves of these figures. The curves may be made to correspond to another value of the temperature ratio by multiplying the given values of rotor-tip Mach number by the square root of the desired ratio.

A long straight duct at rest will choke at the exit if sufficient pressure drop is imposed on the flow. This case is illustrated by the dashed lines of figure 11, which, as indicated, correspond to zero rotor-tip Mach number. A single circular duct is illustrated; however, the analysis can be applied also to multiple ducts and to odd cross-sectional shapes. As the flow proceeds down the nonrotating duct, friction losses cause a progressive drop in total pressure accompanied by a dropping density, increasing dynamic pressure, and thus an increasing Mach number. The initial Mach number, 0.57, for the zero-rotation case illustrated, was chosen so as to produce a Mach number of 1.0 or choking at a duct length of 60 diameters. If the duct is rotated at some blade-tip Mach number, such as the 0.95 value in figure 11, the centrifugal forces oppose the friction effects and compress the flow. Since centrifugal force is directly proportional to the radius, the compression effect is not noticeable in a region adjacent to the hub, and the two cases illustrated in figure 11 produce approximately coincident total-pressure curves in this region. At duct lengths exceeding about 15 diameters, the centrifugal forces become predominant and a total-pressure ratio of about 1.35 is eventually attained. Correspondingly, the Mach number for the case with rotation rises initially because of friction effects, and then the curve peaks and starts to drop when the centrifugal effects become stronger. The initial Mach number, 0.77, was chosen so that the duct just choked at the location of the peak. It will be noted that, although the duct is choked, the final Mach number is relatively low, 0.52. The flow capacity of the duct has been appreciably increased by rotation as evidenced by the higher initial Mach number with rotation.

By calculating a number of curves similar to those of figure 11, a map of the net Mach number changes across a given duct length for a range of tip Mach numbers may be constructed. Such a map for a duct length of 60 diameters is presented in figure 12. The plot of figure 12 shows in more detail than figure 11 that increasing the rotor-tip Mach number while maintaining a constant Mach number at the hub decreases the

ducted-flow Mach number at the rotor tip. Also, increasing the rotor-tip Mach number increases the ducted-flow Mach number at the rotor hub corresponding to choking.

Total- and static-pressure ratios across the 60-diameter length of duct are presented in figure 13. The pressure ratios were calculated from the Mach number values of figure 12. The maximum pressure ratio for a given rotor-tip Mach number occurs with no flow (zero hub Mach number). Increasing the flow quantity produces a drop in total-pressure ratio as a result of increased friction losses. The case illustrated indicates that, for a duct length of 60 diameters, total-pressure ratios on the order of 1.8 are obtainable for a rotor-tip Mach number of 1.0.

#### CONCLUDING REMARKS

The following statements summarize the discussion of pertinent items relative to the design of internal-flow systems for helicopter propulsive units:

1. With regard to reciprocating-engine installations in helicopters designed for speeds above 100 mph, a high ram recovery and controllable exit area are required simultaneously in order to avoid excessive cooling-horsepower penalties.
2. The installation in helicopters of turbine engines with axial-flow compressors may be penalized by the sensitivity of some of these engines to velocity and pressure distortions at the compressor face. The use of a plenum chamber upstream from the compressor will aid in overcoming this effect.
3. Relative to the design of turbine-engine installations and pressure-jet systems, high subsonic speeds in duct elements, such as diffusers and bends, produce appreciable depreciation in performance.
4. Choking Mach number data on 90° bends of circular and square cross section indicate that flow capacities equal to 91 percent of the maximum theoretical value are obtainable.
5. Available one-dimensional relations for determining the effects of centrifugal forces on the flow in ducted helicopter rotors are shown to provide an evaluation of flow Mach numbers and pressure ratios.

## REFERENCES

1. Harrington, Robert D.: Reduction of Helicopter Parasite Drag. (Prospective NACA paper.)
2. Bell, E. Barton: Test of a Single-Stage Axial-Flow Fan. NACA Rep. 729, 1942.
3. Rubert, Kennedy F. and Knopf, George S.: A Method for the Design of Cooling Systems for Aircraft Power-Plant Installations. NACA WR L-49, 1942. (Formerly NACA ARR, Mar. 1942.)
4. Becker, John V., and Baals, Donald D.: Analysis of Heat and Compressibility Effects in Internal Flow Systems and High-Speed Tests of a Ram-Jet System. NACA Rep. 773, 1943. (Supersedes NACA WR L-535.)
5. Henry, John R.: Design of Power-Plant Installations. Pressure-Loss Characteristics of Duct Components. NACA WR L-208, 1944. (Formerly NACA ARR L4F26.)
6. Rogallo, F. M.: Internal-Flow Systems for Aircraft. NACA Rep. 713, 1941.
7. Wood, George P., and Brevoort, Maurice J.: Design, Selection, and Installation of Aircraft Heat Exchangers. NACA WR L-341, 1943. (Formerly NACA ARR 3G31.)
8. Katzoff, S.: The Design of Cooling Ducts With Special Reference to the Boundary Layer at the Inlet. NACA WR L-321, 1940. (Formerly NACA ACR, Dec. 1940.)
9. Boelter, L. M. K., Morrin, E. H., Martinelli, R. C., and Poppendiek, H. F.: An Investigation of Aircraft Heaters. XIV - An Air and Heat Flow Analysis of a Ram-Operated Heater and Duct System. NACA WR W-21, 1944. (Formerly NACA ARR 4C01.)
10. Patterson, G. N.: Note on the Design of Corners in Duct Systems. R. & M. No. 1773, British A.R.C., 1937.
11. Patterson, G. N.: Corner Losses in Ducts. Aircraft Engineering, vol. IX, no. 102, Aug. 1937, pp. 205-208.
12. Abramovich, G.: Fluid Motion in Curved Channels. From Collection of Reports on Industrial Aerodynamics and Fan-Construction, Rep. No. 211 (text in Russian), Trans. Central Aero-Hydrodyn. Inst. (Moscow), 1935, pp. 97-151.

- [REDACTED]
13. Patterson, G. N.: The Design of Aeroplane Ducts. Rules To Be Followed for the Reduction of Internal and External Drag. Aircraft Engineering, vol. XI, no. 125, July 1939, pp. 263-268.
  14. Patterson, G. N.: Modern Diffuser Design. Aircraft Engineering, vol. X, no. 115, Sept. 1938, pp. 267-273.
  15. Gibson, A. H.: On the Flow of Water Through Pipes and Passages Having Converging or Diverging Boundaries. Proc. Roy. Soc. (London), ser. A., vol. 83, no. 563, Mar. 2, 1910, pp. 366-378.
  16. Becker, John V.: Wind-Tunnel Investigation of Air Inlet and Outlet Openings on a Streamline Body. NACA Rep. 1038, 1951. (Supersedes NACA WR L-300.)
  17. Becker, John V., and Baals, Donald D.: High-Speed Tests of a Ducted Body With Various Air-Outlet Openings. NACA WR L-486, 1942. (Formerly NACA ACR, May 1942.)
  18. Nelson, W. J., and Czarnecki, K. R.: Wind-Tunnel Investigation of Wing Ducts on a Single-Engine Pursuit Airplane. NACA WR L-407, 1943. (Formerly NACA ARR 3J13.)
  19. Nelson, W. J., Czarnecki, K. R., and Harrington, Robert D.: Full-Scale Wind-Tunnel Investigation of Forward Underslung Cooling-Air Ducts. NACA WR L-115, 1944. (Formerly NACA ARR L-4H15.)
  20. Czarnecki, K. R., and Nelson, W. J.: Wind-Tunnel Investigation of Rear Underslung Fuselage Ducts. NACA WR L-438, 1943. (Formerly NACA ARR 3I21.)
  21. Peters, H.: Conversion of Energy in Cross-Sectional Divergences Under Different Conditions of Inflow. NACA TM 737, 1934.
  22. McLellan, Charles H., and Nichols, Mark R.: An Investigation of Diffuser-Resistance Combinations in Duct Systems. NACA WR L-329, 1942. (Formerly NACA ARR, Feb. 1942.)
  23. Weske, John R.: Pressure Loss in Ducts With Compound Elbows. NACA WR W-39, 1943. (Formerly NACA ARR, Feb. 1943.)
  24. Wirt, Loring: New Data for the Design of Elbows in Duct Systems. Gen. Elec. Rev., vol. 30, no. 6, June 1927, pp. 286-296.
  25. McLellan, Charles H., and Bartlett, Walter A., Jr.: Investigation of Air Flow in Right-Angle Elbows in a Rectangular Duct. NACA WR L-328, 1941. (Formerly NACA ARR, Oct. 1941.)
- [REDACTED]

26. Kröber, G.: Guide Vanes for Deflecting Fluid Currents With Small Loss of Energy. NACA TM 722, 1933.
27. Nichols, Mark R.: Investigation of Flow Through an Intercooler Set at Various Angles to the Supply Duct. NACA WR L-408, 1942. (Formerly NACA ARR, Apr. 1942.)
28. Reid, Elliott G.: Performance Characteristics of Plane-Wall Two-Dimensional Diffusers. NACA TN 2888, 1953.
29. Squire, H. B.: Experiments on Conical Diffusers. Rep. No. Aero 2216, British R.A.E., Aug. 1947.
30. Squire, H. B., and Carter, P.: Further Experiments on Conical Diffusers. Rep. No. 13,499, British A.R.C., Nov. 6, 1950.
31. Biebel, William J.: Low-Pressure Boundary-Layer Control in Diffusers and Bends. NACA WR L-84, 1945. (Formerly NACA ARR L5C24.)
32. Gratzler, L. B., and Smith, R. H.: Boundary Layer Control for Wide Angle Diffusers. Rep. No. 300 (ONR Contract N6ori-217, Task Order I, Project No. NR-061-004), Univ. Washington Aero. Lab., Nov. 22, 1948.
33. Valentine, E. Floyd, and Carroll, Raymond B.: Effects of Some Primary Variables of Rectangular Vortex Generators on the Static-Pressure Rise Through a Short Diffuser. NACA RM L52B13, 1952.
34. Valentine, E. Floyd, and Carroll, Raymond B.: Effects of Several Arrangements of Rectangular Vortex Generators on the Static-Pressure Rise Through a Short 2:1 Diffuser. NACA RM L50L04, 1951.
35. Wood, Charles C.: Preliminary Investigation of the Effects of Rectangular Vortex Generators on the Performance of a Short 1.9:1 Straight-Wall Annular Diffuser. NACA RM L51009, 1951.
36. Wood, Charles C., and Higginbotham, James T.: The Influence of Vortex Generators on the Performance of a Short 1.9:1 Straight-Wall Annular Diffuser With a Whirling Inlet Flow. NACA RM L52L01a, 1953.
37. Wood, Charles C., and Higginbotham, James T.: Flow Diffusion in a Constant-Diameter Duct Downstream of an Abruptly Terminated Center Body. NACA RM L53D23, 1953.
38. Wood, Charles C., and Higginbotham, James T.: Performance Characteristics of a  $24^\circ$  Straight-Outer-Wall Annular-Diffuser—Tailpipe Combination Utilizing Rectangular Vortex Generators for Flow Control. NACA RM L53H17a, 1953.

39. Henry, John R., and Wilbur, Stafford W.: Preliminary Investigation of the Flow in an Annular-Diffuser-Tailpipe Combination With an Abrupt Area Expansion and Suction, Injection, and Vortex-Generator Flow Controls. NACA RM L53K30, 1954.
40. Valentine, E. Floyd, and Copp, Martin R.: Investigation To Determine Effects of Rectangular Vortex Generators on the Static-Pressure Drop Through a 90° Circular Elbow. NACA RM L53G08, 1953.
41. Taylor, H. D.: Application of Vortex Generator Mixing Principle to Diffusers. Concluding Report. Air Force Contract W33-038 ac-21825. U.A.C. Rep. R-15064-5, United Aircraft Corp. Res. Dept., Dec. 31, 1948.
42. Schulze, Wallace M., Erwin, John R., and Ashby, George C., Jr.: NACA 65-Series Compressor Rotor Performance With Varying Annulus-Area Ratio, Solidity, Blade Angle, and Reynolds Number and Comparison With Cascade Results. NACA RM L52L17, 1953.
43. Kahane, A.: Charts of Pressure Rise Obtainable With Airfoil-Type Axial-Flow Cooling Fans. NACA TN 1199, 1947.
44. Mutterperl, William: High-Altitude Cooling. VI - Axial-Flow Fans and Cooling Power. NACA WR L-776, 1944. (Formerly NACA ARR L4111e.)
45. Wallner, Lewis E., Conrad, E. William, and Prince, William R.: Effect of Uneven Air-Flow Distribution to the Twin Inlets of an Axial-Flow Turbojet Engine. NACA RM E52K06, 1953.
46. Conrad, E. William, and Sobolewski, Adam E.: Investigation of Effects of Inlet-Air Velocity Distortion on Performance of a Turbojet Engine. NACA RM E50G11, 1950.
47. Sanders, Newell D., and Palasics, John: Analysis of Effects of Inlet Pressure Losses on Performance of Axial-Flow Type Turbojet Engine. NACA RM E8J25b, 1948.
48. Huppert, Merle C.: Preliminary Investigation of Flow Fluctuations During Surge and Blade Row Stall in Axial-Flow Compressors. NACA RM E52E28, 1952.
49. Bullock, Robert O., Wilcox, Ward W., and Moses, Jason J.: Experimental and Theoretical Studies of Surging in Continuous-Flow Compressors. NACA Rep. 861, 1946.
50. Mark, Herman, and Zettle, Eugene V.: Effect of Air Distribution on Radial Temperature Distribution in One-Sixth Sector of Annular Turbojet Combustor. NACA RM E9I22, 1950.

51. Childs, J. Howard, McCafferty, Richard J., and Surine, Oakley W.: Effect of Combustor-Inlet Conditions on Performance of an Annular Turbojet Combustor. NACA Rep. 881, 1947.
52. Copp, Martin R., and Klevatt, Paul L.: Investigation of High-Subsonic Performance Characteristics of a  $12^\circ$  21-Inch Conical Diffuser, Including the Effects of Change in Inlet-Boundary-Layer Thickness. NACA RM L9H10, 1950.
53. Persh, Jerome: The Effect of the Inlet Mach Number and Inlet-Boundary-Layer Thickness on the Performance of a  $23^\circ$  Conical-Diffuser - Tail-Pipe Combination. NACA RM L9K10, 1950.
54. Little, B. H., Jr., and Wilbur, Stafford W.: High-Subsonic Performance Characteristics and Boundary-Layer Investigations of a  $12^\circ$  10-Inch-Inlet-Diameter Conical Diffuser. NACA RM L50C02a, 1950.
55. Copp, Martin R.: Effects of Inlet Wall Contour on the Pressure Recovery of a  $10^\circ$  10-Inch-Inlet-Diameter Conical Diffuser. NACA RM L51E11a, 1951.
56. Nelson, William J., and Popp, Eileen G.: Performance Characteristics of Two  $6^\circ$  and Two  $12^\circ$  Diffusers at High Flow Rates. NACA RM L9H09, 1949.
57. Young, A. D., and Green, G. L.: Tests of High-Speed Flow in Diffusers of Rectangular Cross-Section. British R. & M. No. 2201, British A.R.C., 1944.
58. Persh, Jerome, and Bailey, Bruce M.: The Effect of Various Arrangements of Triangular Ledges on the Performance of a  $23^\circ$  Conical Diffuser at Subsonic Mach Numbers. NACA TN 3123, 1954.
59. Persh, Jerome, and Bailey, Bruce M.: A Method for Estimating the Effect of Turbulent Velocity Fluctuations in the Boundary Layer on Diffuser Total-Pressure-Loss Measurements. NACA TN 3124, 1954.
60. Persh, Jerome: The Effect of Surface Roughness on the Performance of a  $23^\circ$  Conical Diffuser at Subsonic Mach Numbers. NACA RM L51K09, 1952.
61. Bohm, H., and Koppe, M.: The Influence of Friction on Steady Diffuser Flows at High Speed. Joint Intelligence Objectives Agency (Washington), July 23, 1946. (Also available from CADO, Wright-Patterson Air Force Base, as ATI No. 36689.)
62. Naumann: Wirkungsgrad von Diffusoren bei hohen Unterschallgeschwindigkeiten. FB Nr. 1705, Deutsche Luftfahrtforschung (Berlin-Adlershof), 1942.

- [REDACTED]
63. Froessel, W.: Investigation of Compressible Flow on and Near a Curved Profile. AAF Translation No. F-TS-1517-RE, Air Materiel Command, U.S. Army Air Forces, Aug. 1947.
  64. Young, A. D., Green, G. L., and Owen, P. R.: Tests of High-Speed Flow in Right-Angled Pipe Bends of Rectangular Cross-Section. British R. & M. No. 2066, British A.R.C., 1943.
  65. Henry, John R.: One-Dimensional, Compressible, Viscous Flow Relations Applicable to Flow in a Ducted Helicopter Blade. NACA TN 3089, 1953.
- [REDACTED]



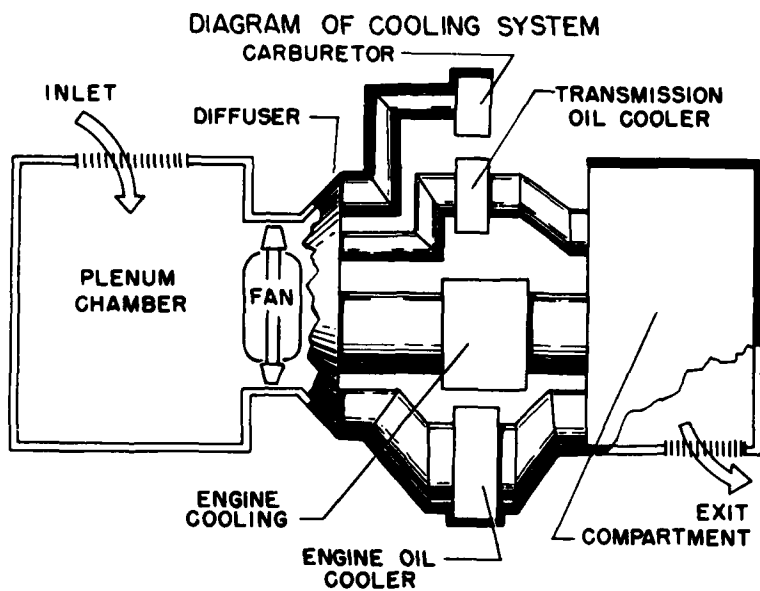


Figure 1

BREAKDOWN OF COOLING HP FOR CASE OF  
 $q_0 = \Delta H_C = \Delta H_F$

CONFIGURATION	FAN SHAFT HP	RESIDUAL PUMPING HP	WAKE HP	TOTAL COOLING HP
(a) EFFICIENT DESIGN FAN COOLER  $\Delta H = 0$	$q_0 Q / 550 \eta$	0	0	$q_0 Q / 550 \eta$
(b) INEFFICIENT DUCT NO FAN OR COOLER  $\Delta H = q_0$	0	$q_0 Q / 550$	$q_0 Q / 550$	$2q_0 Q / 550$
(c) COMBINATION FAN COOLER  $\Delta H = q_0$	$q_0 Q / 550 \eta$	$q_0 Q / 550$	$q_0 Q / 550$	$> 3q_0 Q / 550$

Figure 2

HELICOPTER HORSEPOWER REQUIREMENTS AND ASSUMED FUEL-AIR RATIO

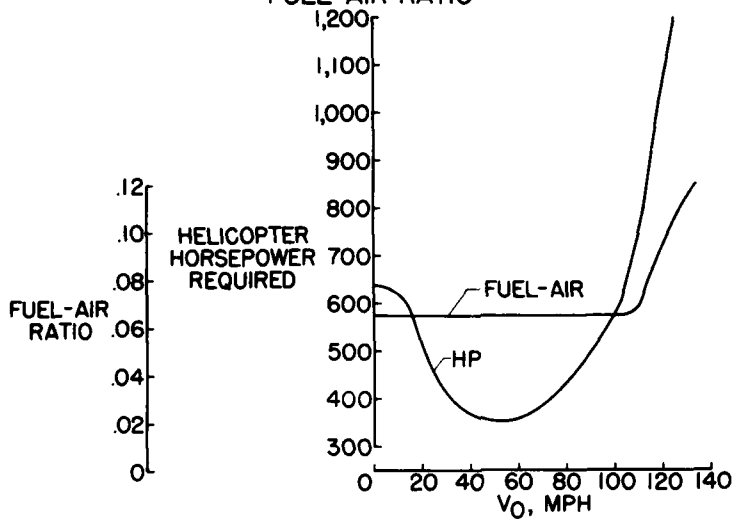


Figure 3

COOLING SYSTEM REQUIREMENTS

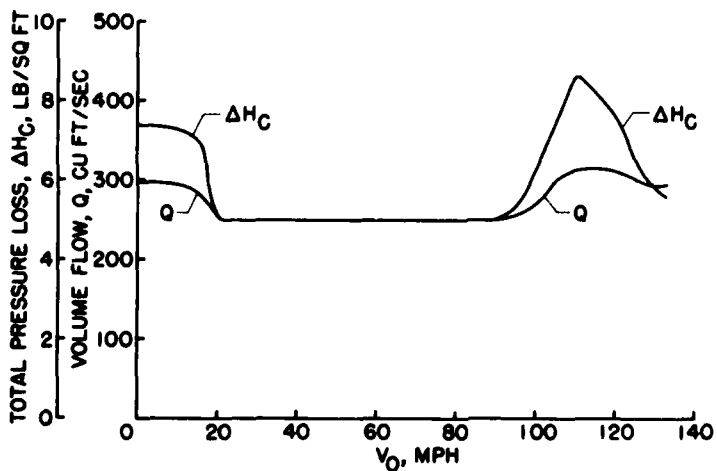


Figure 4

COOLING FAN CHARACTERISTICS

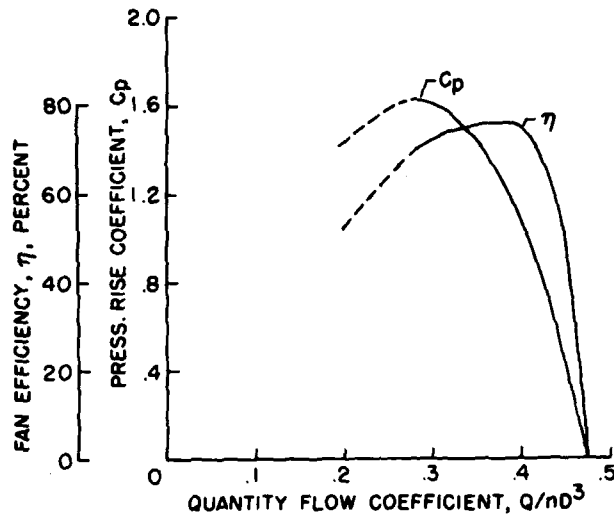


Figure 5

EFFECTS OF VARIABLE FAN GEOMETRY AND RAM RECOVERY FOR CONTROLLED EXIT AREA

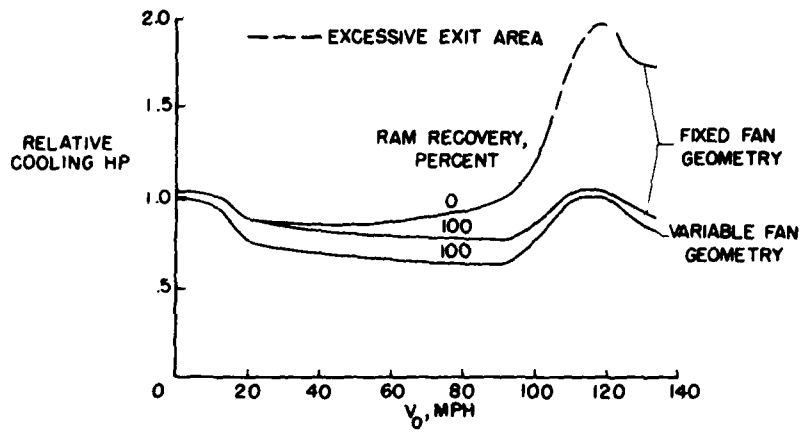


Figure 6

EFFECT OF RAM RECOVERY FOR FIXED EXIT AREA AND FIXED FAN GEOMETRY

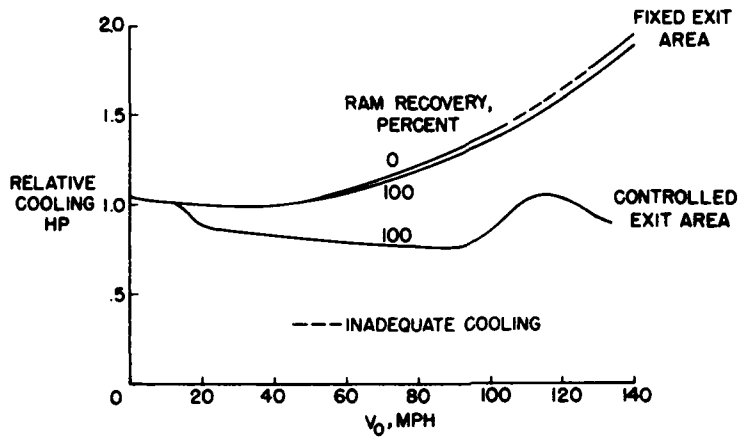


Figure 7

MAXIMUM PERFORMANCE REDUCTIONS DUE TO INLET AIR MALDISTRIBUTION IN TURBINE ENGINE

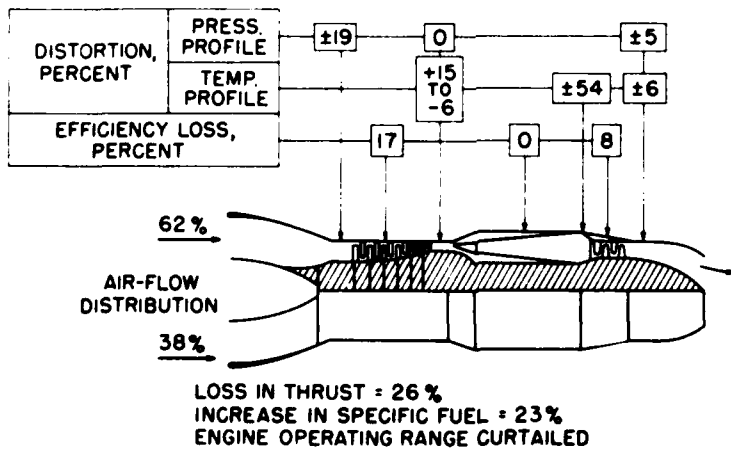


Figure 8

VARIATION OF CONICAL-DIFFUSER LOSS COEFFICIENT WITH MACH NUMBER

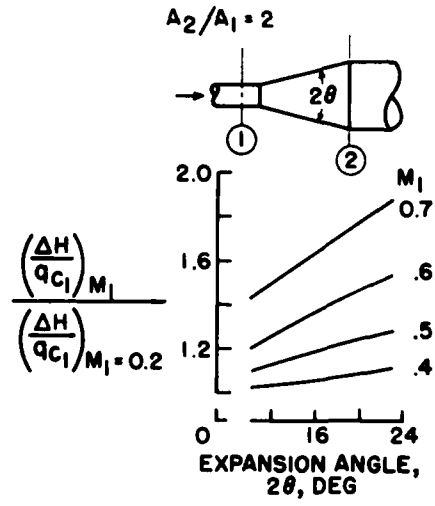


Figure 9

CHOKING MACH NUMBER FOR 90° BENDS

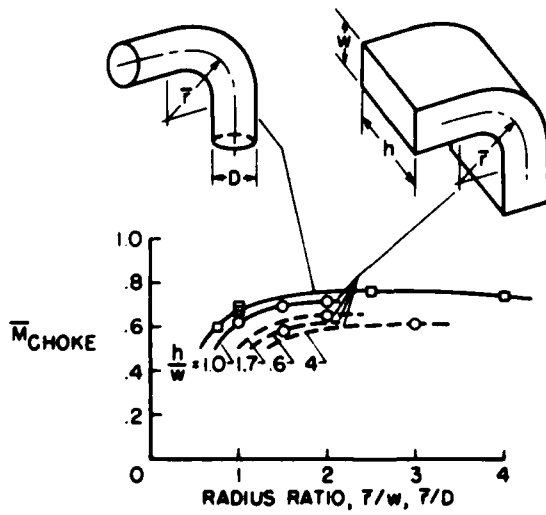


Figure 10

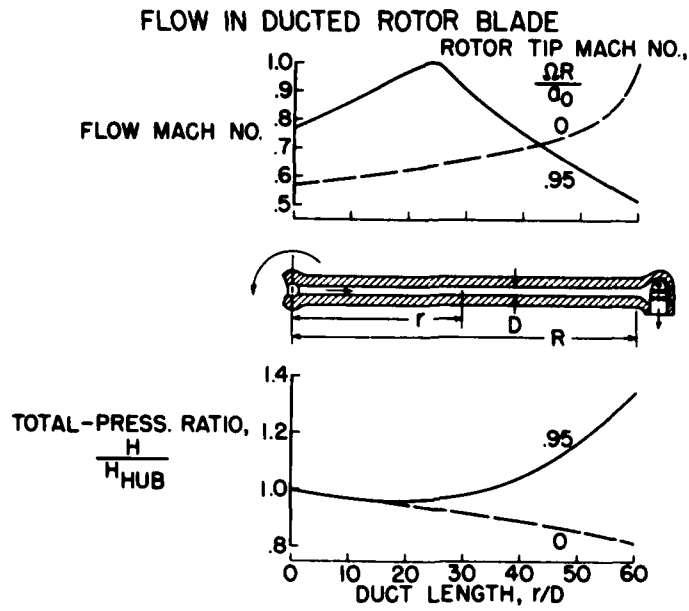


Figure 11

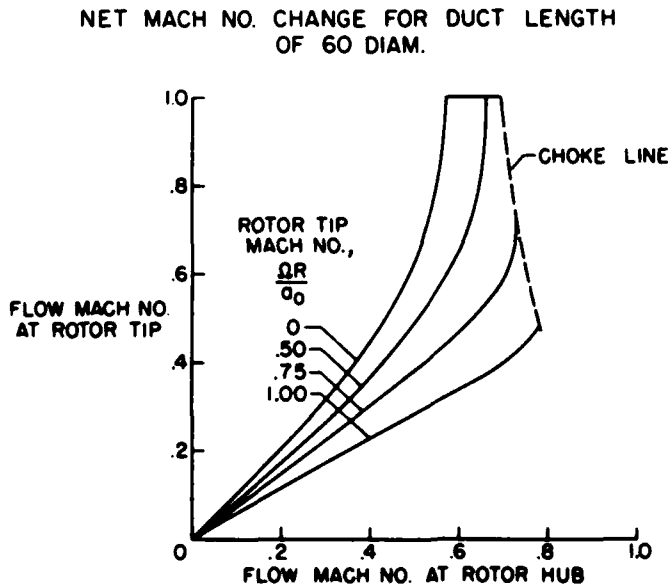


Figure 12

TOTAL- AND STATIC-PRESSURE RATIOS FOR DUCT LENGTH OF 60 DIAM.

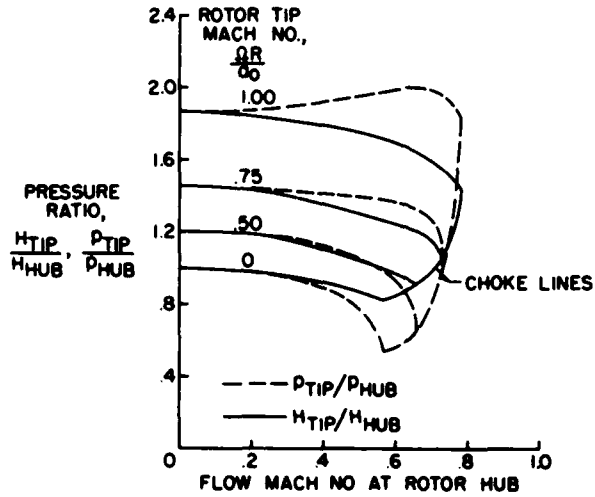


Figure 13

## REDUCTION OF HELICOPTER PARASITE DRAG

By Robert D. Harrington

Langley Aeronautical Laboratory

## SUMMARY

A reduction in helicopter parasite drag is possible but not profitable except in those cases where high speed and long range are primary requirements. For some of the factors causing drag, reduction in parasite-drag area may result in increased weight whereas, in other cases, it does not. The final design, however, must be a compromise between the reduction of drag and the increase in weight.

## INTRODUCTION

In the past, there has been little consideration given to the problem of helicopter parasite drag. Many more serious problems such as vibration, stability, and even adequate hovering performance have required the full attention of the designer. In any event, parasite drag becomes important only in the higher speed range.

Now, however, there are certain uses of the helicopter where high speed and long range are important. Wherever this is the case, it appears that significant benefits can be realized from reductions in parasite drag. The purpose of this paper is to indicate the order of magnitude of these possible benefits and to discuss a few of the ways by which parasite drag can be reduced.

## SYMBOLS

$f$	equivalent parasite-drag area
$\Omega$	rotor angular velocity
$R$	blade radius
$\sigma$	solidity
$\Delta f$	increment of parasite-drag area
$S$	disk area



## EFFECT OF PARASITE DRAG ON PERFORMANCE

In order to illustrate the effect of certain parasite-drag reductions, a theoretical performance analysis has been made for a single-rotor helicopter having a gross weight of 10,000 pounds, a solidity of 0.07, a tip speed of 500 feet per second, and a disk loading of 2.5 pounds per square foot. Figure 1 shows the variation of main-rotor horsepower required with velocity for three assumed values of equivalent parasite-drag area (refs. 1 and 2). A value of 40 square feet was chosen as representative of current practice for helicopters of this size. This value represents a ratio of disk area to parasite-drag area  $S/f$  of 100. The discontinuities in the curves occur at the velocity where tip stall begins on the retreating blade (ref. 3).

The lower curve for  $f = 0$  square feet (fig. 1) represents the minimum power required by the rotor. Obviously, zero parasite drag can never be achieved. However, the area between the top curve and the bottom curve (fig. 1) indicates the total power saving theoretically possible from reduction of parasite drag. In a practical case, it might not be unreasonable to expect that the parasite drag could be reduced 50 percent. The center curve (fig. 1) for a parasite area of 20 square feet indicates the power savings which could be realized from such a 50-percent reduction in parasite drag.

In this particular case, there would be no reason to reduce the drag of the helicopter if it were going to operate below about 40 miles per hour because all the curves practically coincide at and below this velocity. For low-speed operation, higher parasite drag might be acceptable because of simplicity of design and fabrication.

However, for the type of operation where speed and range are of primary importance, a reduction in drag will result in large savings. For instance, if the power available is assumed to be equal to the hovering power, the top speed of this helicopter could be increased 19 miles per hour by a 50-percent reduction in drag. This drag reduction would also result in a 25-percent increase in maximum range and the speed for best range would be increased 11 miles per hour.

## MEANS OF REDUCING PARASITE DRAG

Now, consider a few methods by which the parasite drag may be reduced. There is, of course, extensive literature on this subject, based largely on airplane-drag-cleanup investigations in the Langley full-scale tunnel. Some of these studies, including a couple of fairly complete summaries, are given in references 4 to 10. No effort is made

herein to give a complete review of the subject but only a few basic items are considered. The landing gear, the rotor hub, the engine-exhaust stacks, the cooling losses, and air leakage through joints and gaps in the fuselage are considered. The location and shape of cooling-air exits, fuselage shape, and the location of external protuberances on the surface of the fuselage are also discussed. The savings in parasite drag for these factors are given in the following table:

Item	$\Delta f$ , sq ft
Landing gear . . . . .	20.0
Rotor hub . . . . .	1.2
Exhaust stacks . . . . .	.6
Cooling . . . . .	1.6
Leakage . . . . .	1.6
Cooling-air exits . . . . .	----
Fuselage shape . . . . .	----
Protuberances . . . . .	----
Total	25.0

Landing-gear installation.- Shown in figure 2 are sketches of the landing-gear installations on three different helicopters in the general weight range which is being considered. Past experience with airplanes indicated that the landing gear contributed from one-third to one-half the total drag. Calculations of the parasite drag of helicopter landing gears such as these indicate a parasite-drag area of about 20 square feet. When available drag data for wheels, struts, and tubing are used, a parasite-drag area of 15 square feet is obtained if no interference losses are considered. Experience indicates that the interference drag of the various strut intersections, the strut-fuselage intersection, and the wheel-strut intersection would probably add at least another 5 square feet and thus give a total area of 20 square feet. All this drag increment could be saved by use of a fully retractable landing gear. In some cases it may be impractical or undesirable to retract the gear fully. In that event, significant drag reductions, possibly equal to the sum of all these other items, may still be realized by proper fairing of the wheels and struts. Some data on landing-gear fairings are presented in references 5 and 6. It should be mentioned that there will probably be some weight penalty involved in retracting or fairing the gear. This weight increase would somewhat reduce the estimated power saving.

Rotor hub.- The full extent to which the drag of the rotor hub can be reduced by proper fairing is not known at present. However, some very limited data on the rotor-hub drag of a general research model are

available. The upper sketch of figure 3 shows the original unfaired hub and supporting pylon of the model. The lower sketch of figure 3 shows the fairing which was installed on the hub. Results of the investigation indicate that the parasite-drag area of the helicopter could be reduced 1.2 square feet by the installation of a simple fairing of the type shown. This particular fairing was an ellipsoid of revolution having a fineness ratio of approximately 3.5 to 1.

Engine exhaust stacks.- Two typical radial-engine exhaust-stack installations are shown as figure 4. An increment of 0.93 square foot was measured for the large stovepipe type of installation shown in figure 4. As can be seen, it protrudes from the aircraft nearly normal to the airstream and has excessive form drag in spite of the attempted fairing at the base of the stack. Another installation on an engine of similar power and having the exhaust stacks flush with the surface of the fuselage (fig. 4) produced a drag increment of only 0.31 square foot. In this case, the form drag of the stacks was virtually eliminated, and the measured drag was probably caused by air leakage around the stacks. In this case, a saving of 0.6 square foot was obtained. Examination of several helicopter exhaust-stack installations indicates that even more substantial drag reductions than those obtained herein might be realized by careful detail design.

Cooling-air system.- The discussion on the cooling-air system is based on an analysis for the piston engine installation made by John R. Henry of the Langley laboratory. As shown in that analysis, if the cooling air loses full free-stream dynamic pressure in the inlet, there will be a large parasite drag chargeable to the cooling system. This condition probably exists in most helicopter cooling installations. Calculations assuming complete loss of free-stream dynamic pressure but for an airtight duct system indicate a parasite area of 1.6 square feet for the helicopter flying at 100 miles per hour. This source of drag could be eliminated by designing the cooling system so that the free-stream dynamic pressure is recovered.

At this time, it might also be well to mention that the cooling-air exits should be designed so that the cooling air leaves the body parallel to the external flow. If the cooling air does not exit smoothly, it may disturb the flow over the fuselage and cause premature separation. This separation would result in an additional drag increment over and above that which would be theoretically predicted from the internal losses.

Leakage of air through gaps and joints.- Leakage of air through unsealed gaps and joints, that is, all the gaps and joints, in the fuselage structure may also be a source of much parasite drag. Leakage drag is an item which is dependent to a great extent on the detail design and care in manufacture of the aircraft and is rather difficult to estimate without access to the particular helicopter. However, an estimate based on the average leakage drag of several World War II fighter aircraft indicates that at least 1.6 square feet could be saved

if the helicopter were sealed. Sealing is far from standard practice at the present time.

Fuselage shape and external protuberances.- The effect of fuselage shape and external protuberances on the parasite-drag area is next considered. It is obvious that helicopter fuselages, in general, are not very streamlined; however, the helicopter fuselage may present some special problems. There may be some compromise necessary to insure that the stability and low-speed performance are not unduly penalized in the process of streamlining for high speed. Unfortunately, no explicit data which would indicate the specific areas of high drag on existing shapes are available. Although these data are lacking, it is felt that the general rules of good streamlining should be used as a guide.

One thing specifically, however, might be emphasized; that is the desirability of not locating external fittings and protuberances in regions of local high-velocity flow. Their drag will be increased because of the high local dynamic pressure and it is not unlikely that the air flow will be disturbed sufficiently to cause separation either locally or further downstream on the body.

#### CONCLUDING REMARKS

In conclusion, it might be said that a significant reduction in helicopter parasite drag is possible. However, reduction in drag becomes important only when high speed and long range are primary requirements. An estimate of the possible savings shows a reduction of 25 square feet of parasite-drag area for the factors considered. All these savings may not be possible, however, because there may be some weight penalty involved for such cases as a retractable landing gear or a rotor-hub fairing. The added weight would reduce the estimated power saving somewhat. In this regard, it should be pointed out that the drag of some of the smaller items such as exhaust stacks, cooling, and leakage probably can be eliminated with no sacrifice in weight. Several of these small drag reductions added together can thus produce a sizable saving in drag. In every case, the final design will evolve as a compromise between the reduction in drag and the increase in weight.

## REFERENCES

1. Bailey, F. J., Jr., and Gustafson, F. B.: Charts for Estimation of the Characteristics of a Helicopter Rotor in Forward Flight. I - Profile Drag-Lift Ratio for Untwisted Rectangular Blades. NACA WR L-110, 1944. (Formerly NACA ACR L4HO7.)
2. Gessow, Alfred: Effect of Rotor-Blade Twist and Plan-Form Taper on Helicopter Hovering Performance. NACA TN 1542, 1948.
3. Gustafson, F. B., and Gessow, Alfred: Effect of Blade Stalling on the Efficiency of a Helicopter Rotor as Measured in Flight. NACA TN 1250, 1947.
4. DeFrance, Smith J.: The Aerodynamic Effect of a Retractable Landing Gear. NACA TN 456, 1933.
5. Herrnstein, William H., Jr., and Biermann, David: The Drag of Airplane Wheels, Wheel Fairings, and Landing Gears. - I. NACA Rep. 485, 1934.
6. Biermann, David, and Herrnstein, William H., Jr.: The Drag of Airplane Wheels, Wheel Fairings, and Landing Gears II - Nonretractable and Partly Retractable Landing Gears. NACA Rep. 518, 1935.
7. Dearborn, C. H., and Silverstein, Abe: Drag Analysis of Single-Engine Military Airplanes Tested in the NACA Full-Scale Wind Tunnel. NACA WR L-489, 1940. (Formerly NACA ACR, Oct. 1940.)
8. Lange, Roy H.: A Summary of Drag Results From Recent Langley Full-Scale-Tunnel Tests of Army and Navy Airplanes. NACA WR L-108, 1945. (Formerly NACA ACR L5A30.)
9. Henry, John R.: Design of Power-Plant Installations. Pressure-Loss Characteristics of Duct Components. NACA WR L-208, 1944. (Formerly NACA ARR L4F26.)
10. Hoerner, Sighard F.: Aerodynamic Drag. Publ. by the author (148 Busted, Midland Park, N. J.), 1951.

EFFECT OF PARASITE DRAG ON PERFORMANCE  
GROSS WT. = 10,000 LB;  $\Omega R = 500$  FPS;  $\sigma = 0.07$ ; DISK LOADING = 2.5 LB/SQ FT

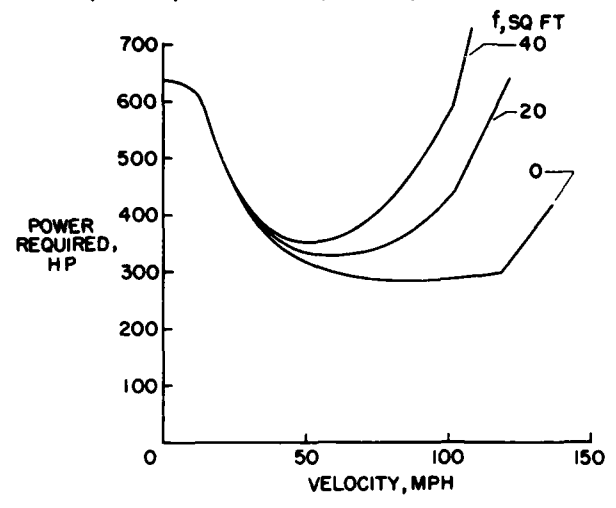


Figure 1

TYPICAL HELICOPTER LANDING GEAR INSTALLATIONS

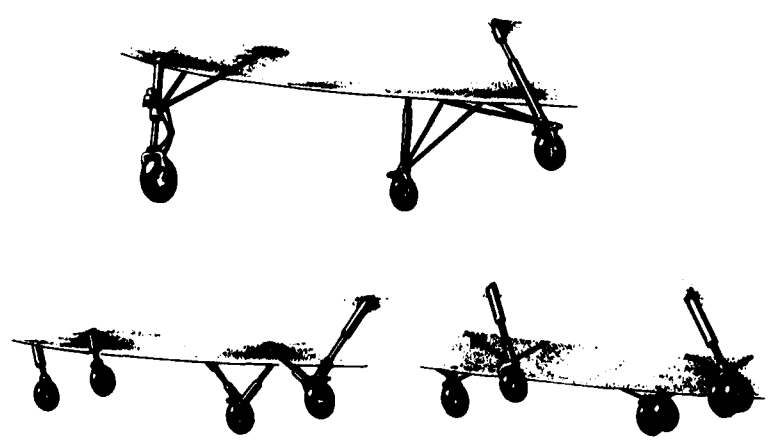
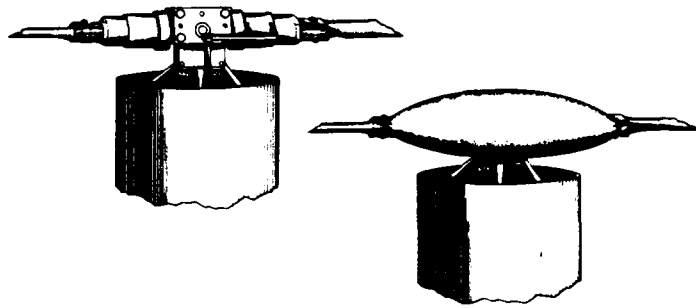


Figure 2

EFFECT OF FAIRING ON HUB PARASITE DRAG



$\Delta f = 1.2$  SQ FT

Figure 3

TYPICAL RADIAL-ENGINE EXHAUST-STACK INSTALLATIONS

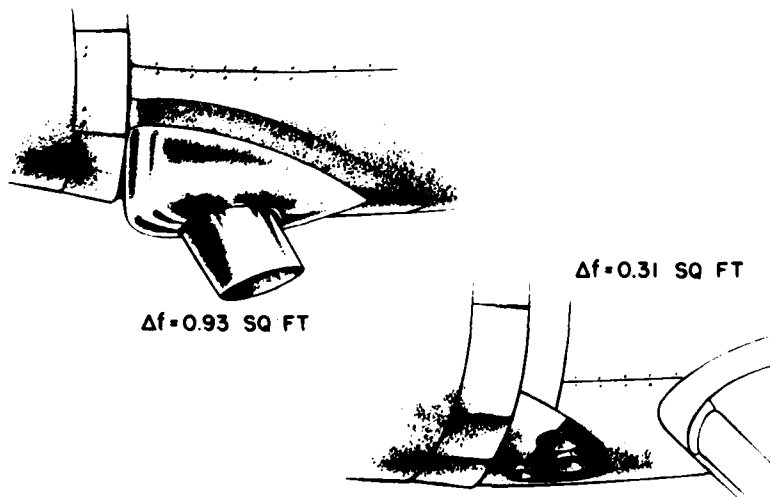


Figure 4

## SOME ASPECTS OF THE HELICOPTER NOISE PROBLEM

By Harvey H. Hubbard and Leslie W. Lassiter

Langley Aeronautical Laboratory

## SUMMARY

Some aspects of the helicopter noise problem are briefly discussed. These discussions deal with the nature of the problem, some tentative criteria for use in evaluating it, and the physical characteristics of noise from helicopters. Overall noise data are presented for a reciprocating-engine helicopter along with discussions of the characteristics of noise from its various components such as the engine, gearing, and rotors. Some consideration is also given to the noise from tip jet rotor systems.

## INTRODUCTION

Until recently noise has not received so much attention as many of the other problems which face the operators of helicopters. Although the difficulties associated with communications in the presence of noise continue to exist, some new noise problems have arisen with the advent of the passenger-carrying helicopter. Some consideration must now be given to the comfort of the passengers as well as the neighbors in the vicinity of heliports and along routes of flight.

Very few studies are available in the literature which deal directly with the noise from helicopters; however, data on noise from propellers, engines, jets, and so forth are available from other noise studies and some of this information can be applied to helicopter noise problems. The purpose of this paper therefore is to indicate the nature of the problem and to present some information that is of general interest in connection with helicopter noise studies.

## INTERNAL NOISE PROBLEM

Figure 1 which was taken from reference 1 shows the envelope of noise spectrums inside several helicopters and compares these with some average levels measured in current airliners. Shown also on this figure is an acoustical comfort index curve from the work of reference 2. Based on airline experience, noise spectrums higher than this curve are definitely uncomfortable for passengers and the optimum conditions of comfort exist only when the noise is well below the values shown here. Thus,



from a comfort standpoint the noise levels in current helicopters tend to be rather high, although it must be recognized that, for flights of a few minutes duration, the passenger may be willing to tolerate a considerably higher noise level than for flights of several hours.

Although it is recognized that some benefits for the passenger may be realized from the use of additional sound treatments, discussions along these lines are beyond the scope of this paper. Emphasis is placed on phenomena related to noise reduction at the source since these are of interest to both the occupant of the aircraft and the ground observer. The phase of the helicopter noise problem which may be the most serious from the commercial operator's point of view involves the ground observer and it is this phase of the problem with which the remainder of the paper will be concerned.

## EXTERNAL NOISE PROBLEM

### Community Noise

The significance of some of the noise data which will be shown later can best be appreciated if the nature of other noises in the communities in which helicopters will operate is known. Some of these are shown in figure 2 (ref. 3). Noise levels are plotted as a function of frequency in octave bands for the noise in residential areas, industrial areas, and for highway traffic. Some variations exist in the levels of various frequency bands; however, it is seen that, in general, these spectrums have a characteristic shape. They peak in approximately the 75 to 150 cps band and fall off rather gradually as the frequency increases. One way of making a noise less objectionable is to place it in an environment which is already noisy and which has a similar noise spectrum. Thus, if the shape of the helicopter noise spectrum resembles these general shapes, it will not be so conspicuous as if, for instance, it had very intense high-frequency components.

### Tolerance Criteria

Another reason why high-frequency noises are undesirable in a community environment is given in figure 3 which illustrates some tolerance criteria that have recently been made available in reference 4. Although criteria are given for sleep and rest, speech interference, and permanent hearing damage, not all of these are considered for the purposes of this paper. Only those pertaining to speech-interference have been made use of and these are given in figure 3. Noise levels in decibels are plotted as a function of frequency for speech-interference levels (S.I.L.) of 45, 55, 65, and 75. The number values represent the average number of decibels

in the 600 to 1200 cps, 1200 to 2400 cps, and 2400 to 4800 cps bands as indicated by the vertical dashed lines and which are considered the most important for speech communication. These curves are based on one's ability to understand conversational speech in the presence of noise and it should be noted that high-frequency noises are more detrimental to speech communication than low-frequency noises. As an example, if the noise spectrum fits in below the curve for S.I.L. = 45, normal speech should be possible in the presence of that noise.

By definition, any noise which exceeds the requirements of the curve S.I.L. = 45 will interfere in some way with normal conversational speech. The following requirements for communication in the presence of noise levels corresponding to various speech-interference-level curves are given briefly, from reference 4, as follows: (a) S.I.L. = 45, normal voice at 10 feet; (b) S.I.L. = 55, normal voice at 3 feet, raised voice at 6 feet; (c) S.I.L. = 65, raised voice at 2 feet, very loud voice at 4 feet; and (d) S.I.L. = 75, very loud voice at 1 foot (minimal efficiency). As a matter of interest it can be noted that the highest levels of community noise of figure 2 approximately correspond to those of the curve for S.I.L. = 55 which is used as a basis for some of the calculations of this paper.

#### Effect of Distance

One way in which any noise problem may be alleviated is to separate the observer by a sufficient distance from the source of the noise. An understanding of the way in which noise is attenuated as a function of distance is thus desirable and this phenomenon is illustrated in figure 4.

A noise spectrum measured for a reciprocating-engine-type helicopter overhead at 100 feet is shown by the solid curve at the top of the figure. These values are adjusted for distance to give the dotted-line spectrums at distances of 300 feet, 1,000 feet, and 3,000 feet. Adjustments for distance are made in accordance with the data of references 5 and 6 and for the assumption of no terrain and wind effects. It can be seen that the high frequencies are attenuated more with distance than the low frequencies are and, as a result of this phenomenon, the spectrum changes shape as it propagates through space.

The curve for S.I.L. = 55 from figure 3 is replotted here and it can be seen that at a distance of 3,000 feet, the noise spectrum of this helicopter meets the requirements of this criterion. Measurements of the type shown here, that is octave-band measurements, are useful in evaluating the seriousness of a problem but give very little information as to the source of the noise. Consequently, the first few bands of the noise have been analyzed by means of a 20-cycle-wide filter arrangement and the results are shown in figure 5.

### Sources of Helicopter Noise

Sound pressures in linear units are shown as a function of frequency also on a linear scale. Relative pressure amplitudes are given for the frequency range of approximately 100 cps to 1400 cps. Since the measuring system for these tests did not record below 100 cps, the estimated levels in that frequency range are indicated by the dashed line. Detailed noise studies for this particular helicopter have made it possible for the bulk of the noise in certain frequency bands of figure 5 to be associated with parts of the helicopter such as engine exhaust, gearing, and so forth, as labeled in figure 5. For instance, noise from the tail rotor appears mainly in the frequency range below 150 cps and has a relatively low level. For the range of approximately 150 cps to 600 cps, within which some of the highest noise levels were recorded, the bulk of the noise is associated with the engine. Noise from the gear box is included in the range of frequencies between 600 cps and 1200 cps, and it is also seen to be a major source of noise. In general, the noise from about 1200 cps to 15,000 cps appeared to be completely random in nature and it is believed that much of this random noise is due to the shedding of vorticity from the main rotor. Random noise from the rotor will also appear in the spectrum below 1200 cps but for the operating conditions of this test the discrete frequencies from the engine exhaust and the gearing are much more pronounced.

Reciprocating engine.- The main source of the noise from the reciprocating engine is the exhaust. The sound pressure levels vary as a function of the type of manifold used and, for a given type of engine, it has been estimated in reference 7 that a 3-decibel increase results from a doubling of the engine power. The noise from the exhaust (fig. 5) is related to a nine-cylinder engine which has only one exhaust exit. The fundamental firing frequency of this engine is approximately 150 cps. The noise consists mainly of discrete frequencies in the range below 600 cps. The present tests as well as the more detailed studies of reference 8 show that the spectrum levels drop off rapidly with increasing frequency above approximately 600 cps. Although it is recognized that there is some noise associated with the high-velocity exhaust-gas streams, this component of noise is thus seen to be much lower in level than the discrete low-frequency components. The other engine noises from valves, gears, carburetor, supercharger, and so forth are believed to be in approximately the same frequency range and are usually 10 to 15 decibels below the level of those from the exhaust (ref. 9).

For any given reciprocating engine, the exhaust muffler can be used as a means of reducing the exhaust noise. Mufflers are usually designed for a particular type of engine since such variables as engine firing frequency, volume of gas flow, and the desired attenuation characteristics are important factors in the design. Although further discussions with regard to exhaust muffling are beyond the scope of this paper, considerable information relating to mufflers and muffling techniques for aircraft engines is included in references 10 and 11.

Gearing.- Gear noise arises from the meshing of gear teeth and may consist of two components as indicated schematically in figure 6. As might be expected, one noise component corresponds to the tooth-contact frequency which is a function of the number of gear teeth and the rotational speed of the gear. Some results of reference 12, relating to the noise from automobile transmissions, indicate that another component of noise may arise from the excitation of natural frequencies of the system. When these natural frequencies of the tooth-gear combinations were at or near some integral multiple of the tooth-contact frequency, a very strong noise component was detected. For the tests of reference 12, these natural frequencies were very important with regard to noise; however, for the measurements of figure 5, it appears that some of the tooth-contact frequencies were clearly predominant.

Rotor systems including tip jets.- The noise from rotors can also be conveniently considered as two separate components, namely, the rotational and vortex components. These are shown qualitatively in figure 7 which gives a noise spectrum for conditions where these two components are of the same order of magnitude. Figure 7, which was taken from reference 13, relates directly to an airplane propeller but these results are believed to apply qualitatively to helicopter rotors as well. The rotational component consists of several discrete tones that are associated with the steady aerodynamic forces on the blades and are most intense in or near the plane of rotation. The vortex component has a continuous-type spectrum that is associated with the unsteady aerodynamic forces on the blades. This component is most intense on the axis of rotation. For the blade geometries and operating conditions currently used, the noise from the tail rotor is mostly rotational noise, whereas vortex noise is the main component from the main rotor.

As in the case of propellers (ref. 13), the rotational noise increases for increased power loading and tip speed and decreases with an increased number of blades. The vortex noise increases with the tip speed of the blades and the blade area and is essentially independent of the power loading and number of blades. This noise can best be kept at a low level by keeping the tip speed low.

In addition to the basic noise from helicopter main rotors, the use of tip jets will superimpose additional sources of noise. The associated noise spectrums will depend on the type of tip jet propulsion used as indicated schematically in figure 8. If pulse jets are used, the noise is mainly associated with the firing frequency of the engine (refs. 14 to 16). The spectrum thus contains a few intense low-frequency discrete components as well as some low-level random components associated with the discharge of the exhaust gases. The fact that much of the noise energy from this type of jet appears in a few discrete frequencies suggests that some noise reduction is obtainable if it were feasible to operate multiple units in proper phase.

The noise from pressure jets consists mainly of random components as indicated schematically in figure 8. During operation at low temperatures, an additional discrete component may appear in the spectrum as indicated by the dashed vertical line. This component is associated with a resonance phenomenon involving the shock-wave formations in the jet stream and, for certain overpressured operating conditions, can be very intense (refs. 17 and 18). Tests have shown, however, that, at high jet temperatures, this noise component is much less pronounced than at low jet temperatures and thus may not be of much concern. There is some indication that the noise from pressure jets is a function of the relative velocity between the jet and the surrounding medium and that the noise from jets in motion is less than in the static case.

In order to compare the noise from various main rotor systems for a 7,000-pound-gross-weight helicopter, the bar chart of figure 9 has been prepared. The abscissa scale is the vertical distance which the particular noise source in question would have to be from an observer in order that its noise would satisfy the speech-interference-level criterion curve labeled 55 which was defined in a discussion of figure 3. Spectrums for these various sources were adjusted for atmospheric losses as in figure 4. In addition to the rotor systems considered, data are included for the helicopter of figure 4 and for a four-engine transport airplane from reference 19 for comparison. When the bar chart is interpreted, it should be noted that the lesser distances are associated with the more desirable noise conditions.

The estimated data for the main rotor of the helicopter for which measurements were made are shown in the second bar from the top. The crosshatched part indicates the estimated increased distance required for an increase in the rotor tip speed from approximately 550 feet per second to 800 feet per second. Thus in the event that rotor tip speeds are increased substantially, the rotor noise levels may then be comparable to the overall noise from current helicopters. The data shown here for the basic rotor are to be interpreted as minimum values because it is believed that, for some operating conditions, the rotor may contribute more substantially to the overall noise than is indicated by figure 9.

When tip jets are used, that is one jet on each blade tip, the rotor system will probably be one of the primary noise sources. For instance, as indicated in the bar chart, the noise from both conventional pulse-jet and pressure-jet rotor systems will probably be much greater than for the bare rotor and will be greater than the overall noise from current helicopters. It should be noted that, for the conditions of figure 9, the observer is assumed to be oriented on the axis of rotation of the rotor. If the observer were in the plane of the rotor, the noise for the bare rotor would be less objectionable and for both tip jet rotors would be more objectionable than indicated in the figure.

## CONCLUDING REMARKS

Some of the sources of the noise from helicopters as well as some general information relating to the ground noise problem of helicopters have been discussed. It has been shown that, for helicopters of current design, the engine and accessories such as the gearing are primary sources of noise. For comparable-sized helicopters utilizing tip jet propulsion, the noise levels will be considerably higher and the rotor system may then be one of the primary sources of noise.

## REFERENCES

1. Douglas, L. L.: The Short Haul Helicopter - An Engineer's View. American Helicopter Society (Presented at meeting of American Helicopter Society, Washington, D. C., Nov. 4, 1953.)
2. Lippert, Stanley, and Miller, Matha M.: A Method for Evaluating Aircraft Acoustical Comfort. Reprinted from Jour. Aviation Medicine, vol. 23, Feb. 1952, pp. 54-66.
3. Anon.: Chicago Noise Survey. The Frontier, vol. 14, no. 4, (Armour Res. Foundation, Ill. Inst. Tech.), Dec. 1951, pp. 9, 15-19.
4. Parrack, Horace O.: Physiological and Psychological Effects of Noise. Proc. Second Annual National Noise Abatement Symposium, vol. 2, Technology Center (Chicago), Oct. 5, 1951, pp. 21-38.
5. Regier, Arthur A.: Effect of Distance on Airplane Noise. NACA TN 1353, 1947.
6. Ingard, Uno: Physics of Outdoor Sound. Proc. Fourth Annual National Noise Abatement Symposium, vol. 4, Oct. 23-24, 1953, pp. 11-25.
7. Rudmose, H. Wayne, and Beranek, Leo L.: Noise Reduction in Aircraft. Jour. Aero. Sci., vol. 14, no. 2, Feb. 1947, pp. 79-96.
8. Stokes, George M., and Davis, Don D., Jr.: The Attenuation Characteristics of Four Specially Designed Mufflers Tested on a Practical Engine Setup. NACA TN 2943, 1953.
9. McFarland, Ross A.: Human Factors in Air Transport Design. McGraw-Hill Book Co., Inc., 1946.
10. Davis, Don D., Jr., Stevens, George L., Jr., Moore, Dewey, and Stokes, George M.: Theoretical and Measured Attenuation of Mufflers at Room Temperature Without Flow, With Comments on Engine-Exhaust Muffler Design. NACA TN 2893, 1953.
11. Davis, Don D., Jr., and Czarnecki, K. R.: Dynamometer-Stand Investigation of a Group of Mufflers. NACA TN 1838, 1949.
12. Glaubitz, H., and Goesele, K.: Experiments on the Origin of Gear Noise. R.T.P. Translation No. 2293, British Ministry of Aircraft Production. (From A.T.Z., No. 7, Apr. 10, 1942, pp. 175-181.)
13. Hubbard, Harvey H.: Propeller-Noise Charts for Transport Airplanes. NACA TN 2968, 1953.

14. Lassiter, Leslie W.: Noise From Intermittent Jet Engines and Steady-Flow Jet Engines With Rough Burning. NACA TN 2750, 1952.
15. Powell, Alan: The Noise of a Pulse Jet. Jour. Helicopter Assoc. of Great Britain, vol. 7, no. 1, July 1953, pp. 32-41.
16. Veneklasen, Paul S.: Noise Characteristics of Pulse Jet Engines. Symposium on Aircraft Noise. (Reprinted from Jour. Acous. Soc. of America, vol. 25, no. 3, May 1953, pp. 378-380.)
17. Lassiter, Leslie W., and Hubbard, Harvey H.: The Near Noise Field of Static Jets and Some Model Studies of Devices for Noise Reduction. NACA TN 3187, 1954. (Prospective NACA paper.)
18. Powell, Alan: A Survey of Experiments on Jet Noise. Aircraft Engineering, vol. XXVI, no. 299, Jan. 1954, pp. 2-9.
19. Hubbard, H. H.: Airplane and Airport Noise. Proc. Fourth Annual National Noise Abatement Symposium, vol. 4, Oct. 23-24, 1953, pp. 81-89.



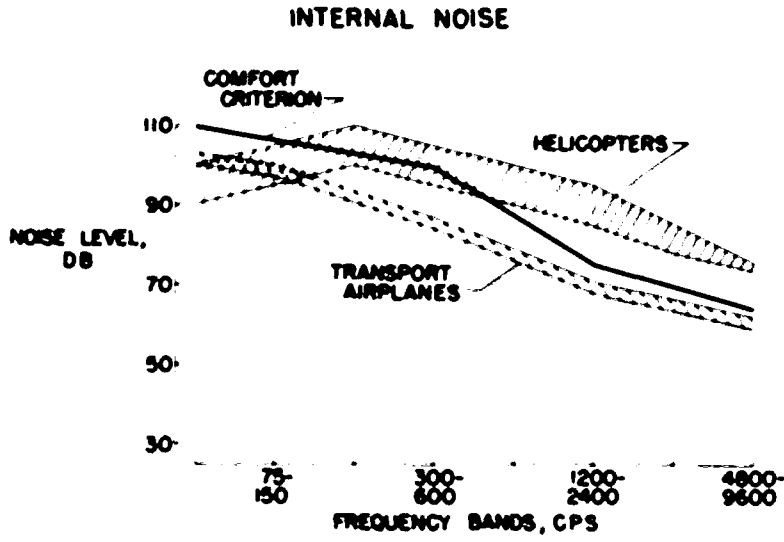


Figure 1

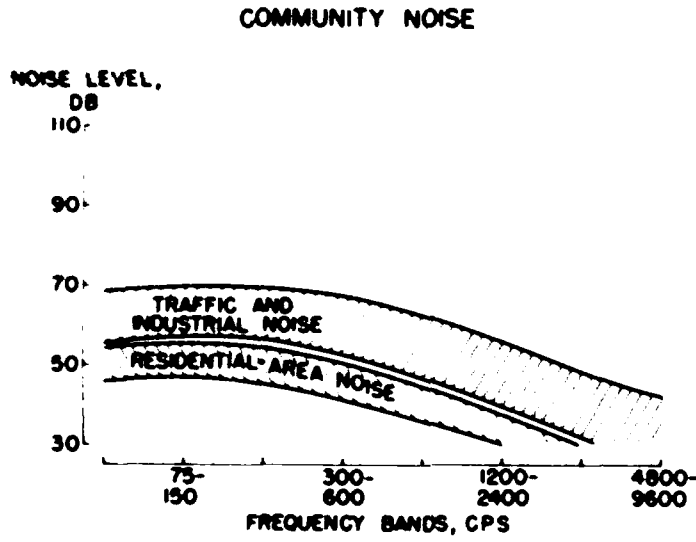


Figure 2

SPEECH-INTERFERENCE LEVELS

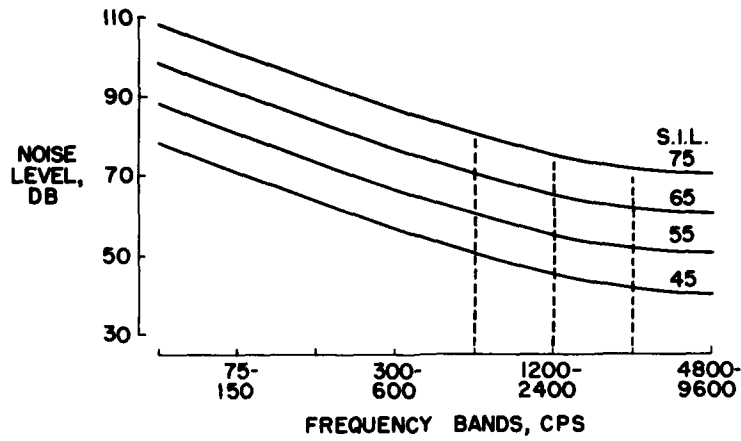


Figure 3

EFFECT OF DISTANCE

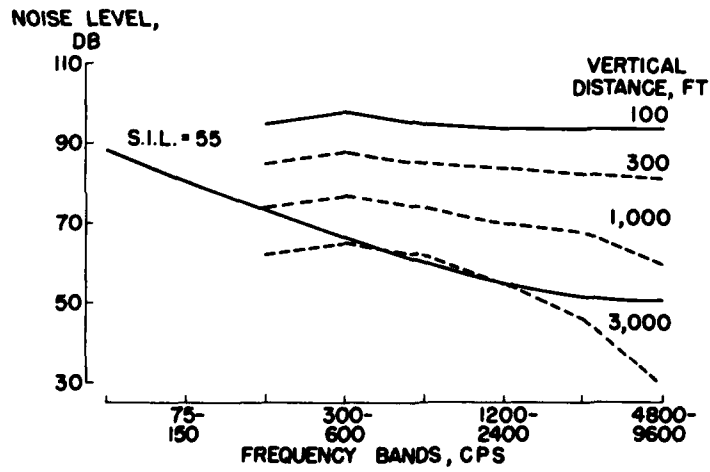


Figure 4

NOISE FROM HELICOPTER IN HOVERING  
 FREQUENCY ANALYSIS WITH 20-CYCLE-WIDE FILTER

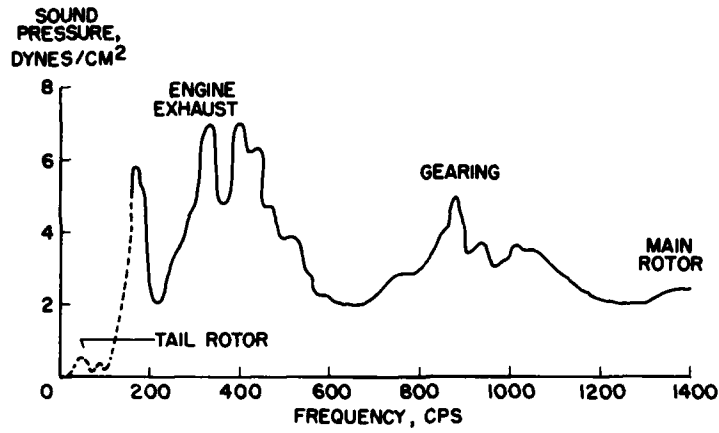


Figure 5

GEAR NOISE

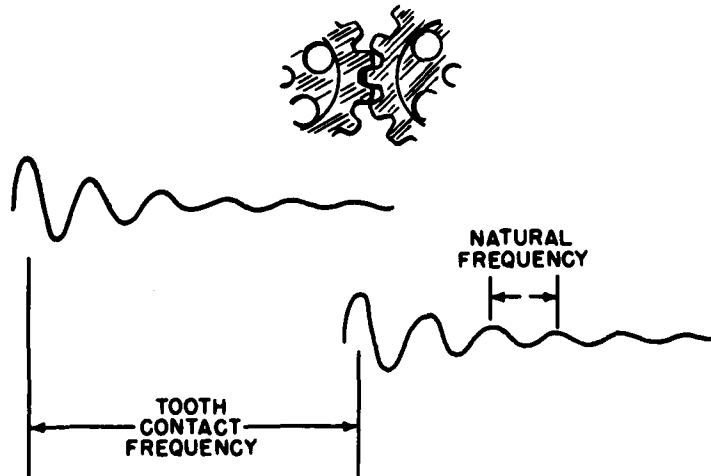


Figure 6

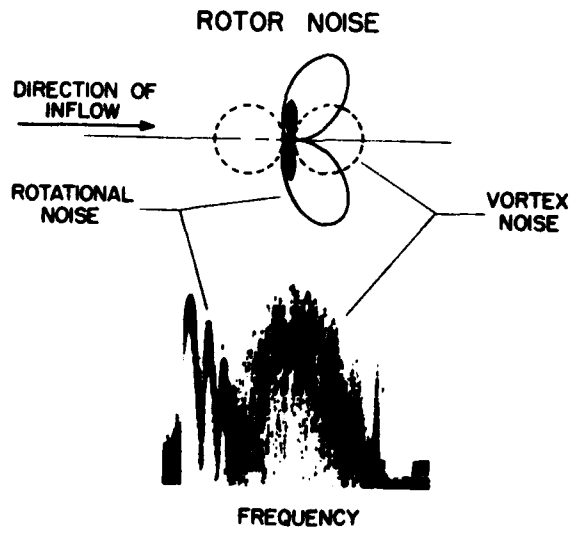


Figure 7

TYPES OF NOISE SPECTRA

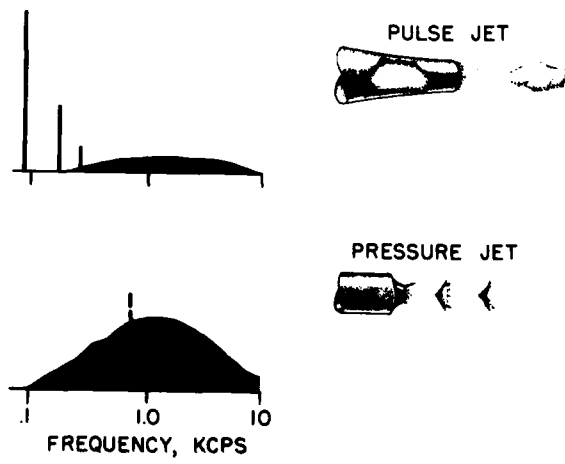


Figure 8

DISTANCE TO SATISFY S.I.L. = 55 CRITERION  
OBSERVER ON AXIS OF ROTATION

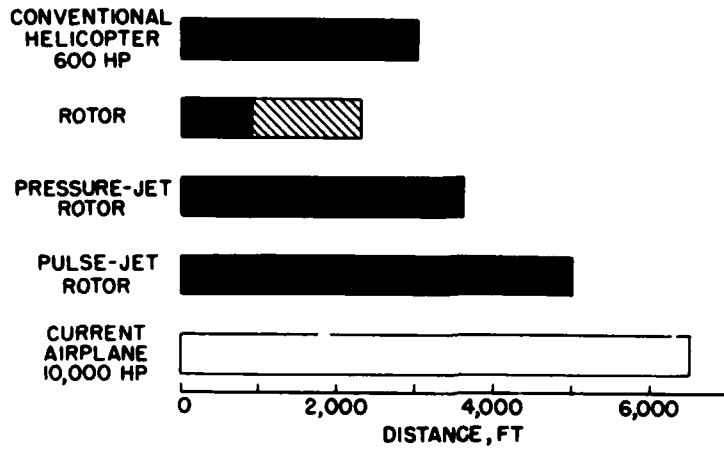


Figure 9

## EXHAUST MUFFLERS AS APPLIED TO THE HELICOPTER

By George M. Stokes and Don D. Davis, Jr.

Langley Aeronautical Laboratory

## INTRODUCTION

In general, when dealing with a conventional helicopter, there are many noise-generating components. Since the integrated effect of these noises are known to produce quite objectionable, if not intolerable, noise levels, it becomes evident that some study should be made to indicate what needs to be done to reduce these noise sources. The objective of this discussion is to show what engine-exhaust-noise reductions may be expected from various size mufflers and what these noise reductions mean when referred to a noise-affected area. In most cases the engine exhaust is found to be the greatest noise-generating component of the helicopter. Consequently, the greatest single gain in reducing the overall helicopter noise can be accomplished by treating this source. This paper will treat the reciprocating-engine noise from the point of view of the ground observer as well as the helicopter passenger. Recently completed muffler research work conducted at the Langley Aeronautical Laboratory indicates a muffler-design method by which mufflers may be designed to provide a given attenuation. The principles set forth in this basic research have been used in the development of the following discussion.

## DISCUSSION

In order to establish a basis by which comparison may be made between various noise conditions, the speech-interference-level (S.I.L.) curves shown in figure 1 (see ref. 1) have been chosen. These curves, as explained in the previous paper by Harvey H. Hubbard and Leslie W. Lassiter, indicate a system by which the speech-interference level may be referred to the frequency spectrum. The S.I.L. curve labeled 55 has been defined as a noise environment which will permit continuous communication, with a normal voice, between two people who are 3 feet apart. For this discussion the S.I.L. curve of 55 will be chosen as a noise criteria condition below which all engine-exhaust noise must fall to fulfill an acceptable noise condition for the ground observer.

Before a muffler having the maximum quieting capabilities for a given engine can be designed, a spectrum of the engine noise is needed. This spectrum is also used to determine the attenuation needed to reduce the noise to the chosen value of S.I.L. Figure 2 shows a band pass

spectrum of typical reciprocating-engine exhaust noise at 200 feet. Such a spectrum is representative of the noise that would be produced by a 180-hp engine. The S.I.L. curve of 55 describes the attenuation envelope which a muffler must have to provide the required quieting. The shaded area in figure 2 shows the part of the spectrum which must be eliminated.

By using the muffler-design method discussed in references 2 and 3 and an exhaust pipe diameter of  $2\frac{1}{4}$  inches, a single-chamber resonator muffler having a diameter of 5 inches and a length of 24 inches would be expected to provide the required S.I.L. of 55 at 200 feet. Since space limitations may require the helicopter designer to use a different size muffler from the one just described, an illustration will be given to show what attenuation can be provided by various muffler sizes. For this illustration, two other mufflers have been selected, one incorporating twice the volume of the original design and one having one-half the volume of the original design. These three mufflers will be referred to as mufflers 1, 2, and 3. The number increase will indicate a muffler-size increase. Figure 3 shows that the exhaust noise should not exceed an S.I.L. of 62 when using the smallest muffler (muffler 1) and should not exceed a value of 49 when using muffler 3. Figure 3 also indicates the relative quieting provided by the three mufflers. If some other exhaust-pipe diameter had been used in the design of these mufflers, the muffler diameter would be changed by an amount proportional to the change in exhaust-pipe diameter.

In order to give physical illustration of what these noise reductions mean, a plot of the noise area reduction provided by each muffler for a specified speech interference level is shown in figure 4. For the unmuffled engine, this specified level of 55 will be reached at 900 feet from the source. Similarly with mufflers 1, 2, and 3, the equivalent noise conditions will be achieved at the distances of 450, 200, and 100 feet, respectively. When comparing the noise reductions resulting from the mufflers in terms of an affected-area coverage, the mufflers reduced the noise-affected area by 75, 95, and 98.8 percent, respectively, of the value it was for the unmuffled engine. This comparison is important in that it shows that the smallest muffler will reduce the noise-affected area by a much greater percentage for the muffler volume used.

When considering the engine noise from the viewpoint of the helicopter passenger, the noise problem is much more severe because of the proximity of the exhaust-noise source to the cabin. For this reason, it will be assumed that the passengers must be subjected to a higher noise condition than was selected at the outset of this discussion. In the conventional Douglas DC-3 airliner, the cabin S.I.L. is approximately 71; consequently, for purposes of this discussion, this S.I.L. value will be chosen as the noise environment which the helicopter passenger will be subjected to. Figure 5 shows the distance the tailpipe exit must be from

the cabin to achieve this passenger S.I.L. of 71. The cabin wall assumed for this case is a 0.025-inch-thick aluminum sheet which provides a 13-decibel noise reduction throughout the noise spectrum. These data are figured on the basis of perfect sound absorption within the cabin; consequently, it should be stated that the S.I.L. within the cabin will be slightly higher than 71 because in practical applications perfect sound absorption is not achieved.

Figure 5 shows that the tailpipe exit must be 32 feet away from the cabin with no muffler, 15 feet away with muffler 1, 7 feet away with muffler 2, and 4 feet away with muffler 3. As a matter of interest, the tailpipe exit would need to be 45 feet away from the cabin in order to achieve a passenger S.I.L. value of 55 with muffler 2.

Some time ago several muffler field tests were conducted at the Langley Laboratory. (See ref. 3.) This investigation was made to determine the effects of certain factors on the acoustical properties of the mufflers. For a test apparatus, a helicopter having a 180-hp engine with two exhaust pipes was used. The mufflers used in the field tests were not designed to provide the greatest attenuation possible but were designed to fulfill specific test criteria. Thus, both the chamber and tailpipe resonant frequencies of these mufflers are different from those of mufflers 1, 2, and 3. The smallest of the mufflers tested on the helicopter provided an overall S.I.L. reduction of 6. This small test muffler was  $1\frac{1}{2}$  times larger than muffler 1. Because of the presence of an unknown amount of helicopter noise, other than engine exhaust, in the measurements, it was not possible to determine the exact exhaust-noise reduction provided by the test muffler. However, since a certain amount of other noise did exist, it can be stated that the exhaust S.I.L. reduction must have been greater than 6. With the use of the muffler theory, an S.I.L. reduction of 9 was predicted for the engine-exhaust noise. Since the test muffler reduced the overall helicopter noise S.I.L. by 6, the same as that of muffler 1, the noise-affected area was reduced by 75 percent. The important point which can be made from these results is that a small muffler should be of considerable aid in reducing the helicopter noise with no treatment of other noise sources. The extent to which the overall noise reduction may be carried with larger mufflers, of course, depends on how much the other noise components are below the exhaust.

This paper has been limited to rather low-powered engines, that is, those having exhaust diameters of the order of  $2\frac{1}{4}$  inches. Large engines, or engines having larger exhaust diameters, introduce the additional problem of higher noise levels, besides the requirement that the muffler volume must increase in proportion to the muffler tailpipe area. Basically, however, the muffler-design method is no different from that used in design of mufflers for low-powered engines.



## CONCLUDING REMARKS

The essence of this discussion indicates the following: (1) There is a muffler theory which will permit an efficient design of an engine-exhaust muffler that can reduce the exhaust noise a predetermined amount and (2) a small muffler is of considerable aid in reducing the noise-affected area.

## REFERENCES

1. Parrack, Horace O.: Physiological and Psychological Effects of Noise. Proc. Second Annual National Noise Abatement Symposium, vol. 2, Technology Center (Chicago), Oct. 5, 1951, pp. 21-38.
2. Davis, Don D., Jr., Stevens, George L., Jr., Moore, Dewey, and Stokes, George M.: Theoretical and Measured Attenuation of Mufflers at Room Temperature Without Flow, With Comments on Engine-Exhaust Muffler Design. NACA TN 2893, 1953.
3. Stokes, George M., and Davis, Don D., Jr.: The Attenuation Characteristics of Four Specially Designed Mufflers Tested on a Practical Engine Setup. NACA TN 2943, 1953.

**SPEECH-INTERFERENCE LEVELS**

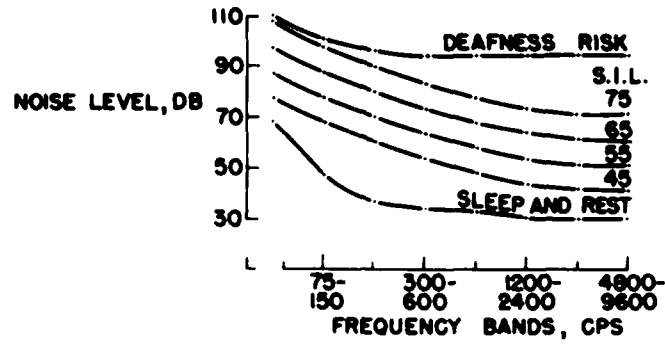


Figure 1

**ATTENUATION REQUIRED FOR GROUND OBSERVER**

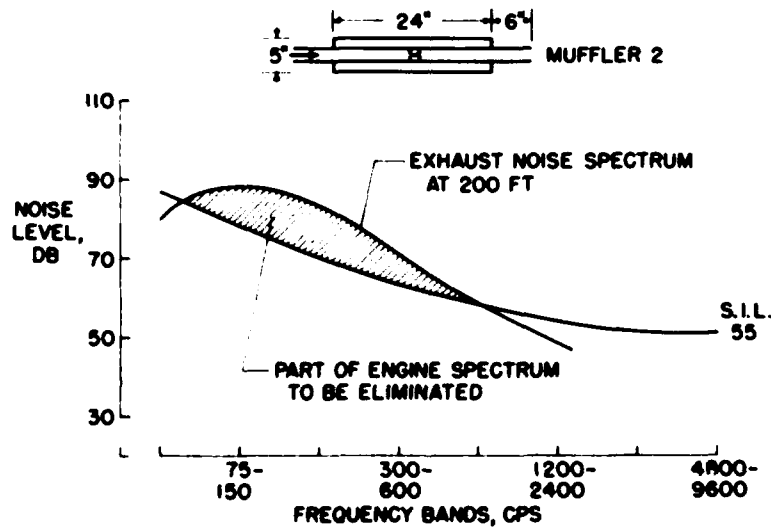


Figure 2

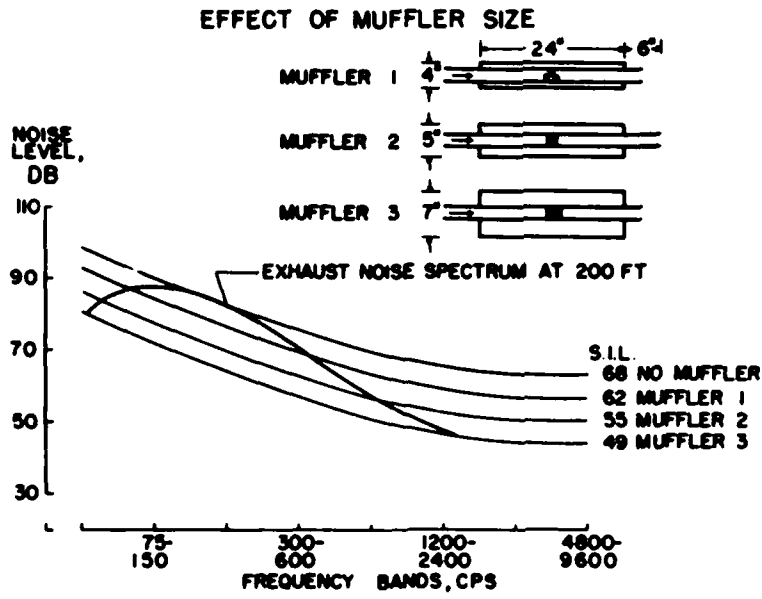


Figure 3

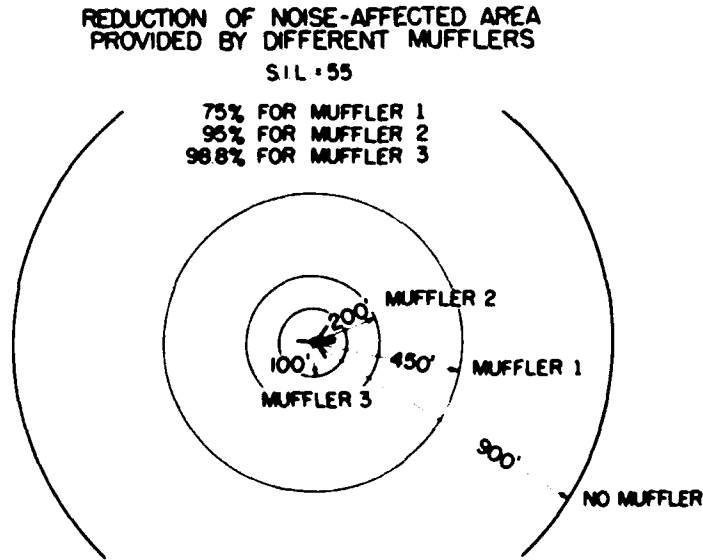


Figure 4

## REQUIRED TAILPIPE DISTANCES FOR A CABIN S.I.L. OF 71

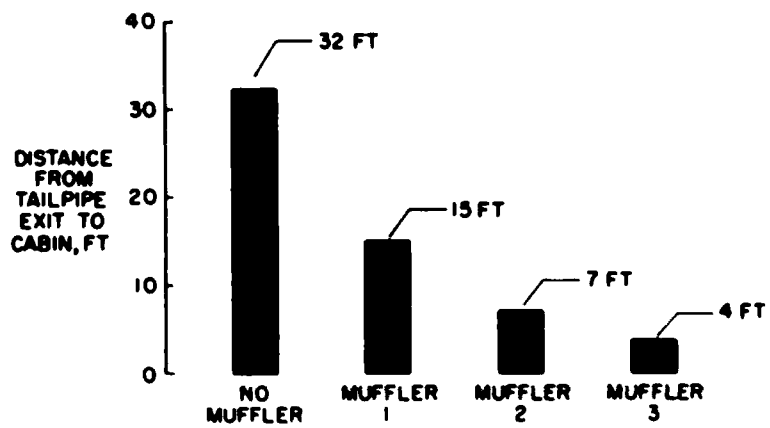


Figure 5

**STABILITY AND  
CONTROL**

## FLYING-QUALITIES CRITERIA FOR GENERAL-PURPOSE HELICOPTERS

By John P. Reeder and F. B. Gustafson

Langley Aeronautical Laboratory

Once the performance capabilities and usefulness of the helicopter had been established, it became increasingly apparent to all concerned that studies of the flying qualities (that is, the stability and control characteristics) of the helicopter were urgently needed. The ultimate purpose of such studies is to establish design criteria which will insure stability and control characteristics that are essential for reasonably easy, safe, and efficient operation. The National Advisory Committee for Aeronautics undertook such an investigation. In this field the NACA had an extensive background in airplane flying-qualities work.

In the study of flying qualities, it is necessary to isolate the important characteristics and define them in terms of the fundamental stability and control characteristics of the aircraft. It is then necessary to obtain a measure of these fundamental characteristics by means of simple repeatable test maneuvers. Correlation of the pilots' opinion of the flying qualities in normal flight with the characteristics measured in the test maneuvers must be established. Quantitative design criteria may be established when a large enough variation in the measureable fundamental characteristics has been experienced to bracket the desirable ranges for satisfactory behavior.

In carrying out the program to date two research pilots experienced in flying-qualities evaluations have been used. Pertinent characteristics of the research helicopters have been varied through a wide range by any means possible for evaluation purposes. In order to supplement pilots' opinion, NACA recording instrumentation has been used to obtain a numerical measure of the evaluation maneuvers and of the accuracy and ease of executing flight problems.

Since these studies form part of the background of references 1 and 2, the requirements are set forth there and no attempt will be made to discuss them in detail. A discussion of the significance of the more important requirements, their development, and our latest thoughts on them seem in order, however.

It is well to point out at this point that with instrumented helicopters and with others in which familiarization flights have been made a range of physical characteristics, which are shown in the following table, have been covered.

Helicopters flown	Ratio of maximum to minimum for -			
	Rotor diameter	Overall length	Gross weight	Pitching inertia
Instrumented	1.5	2.0	3.3	30.0
All types	2.8	3.6	18.0	30.0

The flying qualities of the helicopter which are discussed are:

1. Control and control-force characteristics

- (a) Transient stick forces
- (b) Excessive friction in control systems
- (c) Force-trim provisions
- (d) Control sensitivity
- (e) Control-force gradients

2. Speed stability

3. Longitudinal maneuver stability

- (a) Divergence problem
- (b) Criteria

4. Turn and lateral-oscillation characteristics

Although not included under item 1 of this table for discussion, at least one case of excessive time lag in control is familiar. Improvement in design and the use of power boost systems for larger helicopters have reduced or eliminated items 1(a) and 1(b); however, they may still be problems for some time in small helicopters.

Transient stick forces, item 1(a), occurring with displacement of the controls can be out of phase with the direction of displacement and cause a tendency for the stick to whirl in a circle (ref. 3); thus the pilot's sense of security and his ability to position the control accurately was affected. Even when not out of phase, forces can nevertheless be undesirable in that a force reversal may take place. It does not take large forces to cause the pilot concern. Figure 1 illustrates an unsatisfactory force variation with displacement measured in hovering on the left, while on the right is one that is found acceptable. Note that the satisfactory force is always in a direction to resist the control displacement, whereas in the case on the left, although the forces were very small, the pilot felt uncertain because they did reverse.

[REDACTED]

A large amount of friction in the control system, item 1(b), may hide worse things, but in itself it destroys the ability of the pilot to position accurately the controls and, therefore, the helicopter, particularly in hovering. Cyclic-control systems having 1 to 2 pounds of friction in the static condition have been found to be practically friction free in some small helicopters. Friction permissible in the other controls is greater than this.

It has proved very desirable to have means of trimming control forces to zero, item 1(c), for any flight condition which will be maintained for a period of time. For instrument flying this is not only desirable but necessary if reasonable accuracy and safety is to be achieved.

Excessive control sensitivity, item 1(d), has occurred in some helicopters. The sensitivity referred to is defined as the steady angular velocity per unit control deflection. This definition, however, does not take account of the ability of a control to produce angular acceleration, which varies with inertia, among other things. Our first experience with excessive sensitivity resulting in overcontrol about the roll axis of a small helicopter while hovering where precision of control is desired. Similarly, excessive sensitivity of the directional control has been experienced while hovering and during instrument flight at low speed and high power in some helicopters. These cases are presently recognized in the handling-qualities specifications. Excessive sensitivity in pitch may occur in tandems where high control power is obtainable. Also, the tandem helicopter has the real possibility of having satisfactory sensitivity of directional control, as defined earlier in this paragraph, but having available very low angular acceleration in yaw. Consequently, the requirements of reference 2 attempt to provide a minimum acceptable combination of angular acceleration and yawing velocity.

Some work has been done with control-force gradients, item 1(e), but the subject is far from exhausted. During instrument-flying trials with a boost system having low friction, the pilots liked a gradient of about 2 pounds per inch longitudinally and 1 pound per inch laterally. Higher longitudinal gradients gave excessive trim force changes, particularly with power changes. Longitudinal-maneuver forces, however, even with satisfactory maneuver stability as defined later, were unsatisfactorily low. The pilots liked low lateral forces except for the poor centering which resulted from friction. Consequently, preload was tried, although in itself it is not desirable. Preload somewhat less than that required to center the control exactly was found to be desirable since it permitted some adjustment of the control to compensate for the impossible task of trimming exactly and to correct for small disturbances without fighting the preload.

[REDACTED]



Stability with speed, item 2 in the outline, was one of the earliest requirements to be applied to the helicopter as it was early recognized and best understood. An opportunity was had to vary the speed stability from positive to negative with the test helicopter by means of a horizontal tail while maintaining some maneuver stability. For normal operations it was found that the pilots did not readily recognize a small degree of negative speed stability as it led to only a very slow divergence which was not detected except by holding controls fixed for an abnormal period of time. However, such a small degree of negative stability cannot readily be measured. Of course, the larger amounts of speed instability are unsatisfactory.

During early test flying with the helicopter it was readily apparent that at cruising and high speeds the helicopter continuously tended to diverge, as indicated in item 3(a), despite the fact that it was known to have speed stability. The underlying difficulty proved to be an instability with angle of attack which increases in severity with speed. The type of maneuver this can lead to is illustrated in figure 2 (ref. 3). This is an attempted stick-fixed oscillation at 65 miles per hour, initiated by a slight stick motion and return to trim. After recovery control was applied to check the nose-down motion of the helicopter in this case the stick was moved rapidly to the forward limit which it reached 2 seconds before the acceleration peaked. However, the collective pitch had also been reduced progressively to about  $6^{\circ}$  and a wingover was executed for recovery. In a case such as this, blade stalling very likely occurs as the pitch-up proceeds, causing further nose-up moments.

This instability with rotor angle of attack was the first problem selected for study. The primary test maneuver finally selected for evaluation of this characteristic was the pull and hold from steady, trimmed flight. Since a longitudinal pitching maneuver combines angle-of-attack stability characteristics with damping, the combined characteristics have been labelled maneuver stability. If a helicopter or an airplane has maneuver stability it will trim at some new angle of attack and acceleration if the stick is deflected from trim and held. Consequently, the time-history curve of normal acceleration with time following control displacement will be concave downward from some time soon after the start of the maneuver. If unstable, this curve will be concave upward for an extended time interval. The maneuver stability was varied and made positive for test purposes by the addition of a horizontal tail to the single-rotor test helicopter. In figure 3 are illustrated the time histories of normal acceleration with time for pull-and-hold maneuvers for the original configuration which was unstable and for the tail-on configuration which was stable.

In correlating pilots' opinions of the test maneuvers with a satisfactory degree of stability, considering item 3(b), it was found that

[REDACTED]

when the helicopter was considered satisfactory the curve of normal acceleration became concave downward about 2 seconds after the start of the maneuver (ref. 4). This criterion was later checked with a helicopter in which damping alone was varied through a range of about 2.5 to 1. These tests showed that sufficient damping could also produce satisfactory maneuver characteristics and the 2-second criterion was found to be adequate (ref. 5). Later still, a configuration was tried for which additional factors were revealed. In one flight condition a maneuver was judged marginal although the 2-second criterion was satisfied (ref. 6). (See fig. 4.) The time-to-peak acceleration in this case was increased over previous configurations. This increase could have been a result of the speed instability of this configuration, in which case present requirements for speed stability would prevent its occurrence. However, the pilots' opinions may have been strongly influenced by the pitching velocity which, unlike previous cases, was still increasing at nearly a linear rate with time, even though normal acceleration was approaching a limit. Further studies of the criterion for this configuration may well be indicated.

Next consider item 4 in the outline. Lateral-directional problems found in contact flight with single-rotor helicopters have been minor. However, in the tandem type with long fuselages and high inertia in yaw, oscillatory and maneuvering problems have appeared (ref. 7). For maneuvering it is considered highly desirable that the pilot be able to execute a reasonable turn in either direction from trimmed flight by use of lateral control alone. This insures that gross misuse of the controls will not end in unintentional maneuvers and it reduces the demands on the pilot for accurate and vigorous coordination of controls. In order to satisfy the turn criterion as stated above, it is first necessary that rolling velocity resulting from displacing the lateral control will not reverse. Figure 5 illustrates a case where rolling velocity did reverse and reach as large a value as that in the initial direction. Secondly, it is necessary that heading respond to the bank angle and a turn develop. This means that the sideslip developed must be limited. In the case illustrated no heading change occurred for about 3 seconds. Since sideslip for a helicopter in this maneuver results only from the bank angle and gravity, the maneuver specified for checking compliance with the requirement is of low enough rolling velocity that sideslip has a chance to develop before recovery must be made.

Lateral-directional oscillations of the tandem types are aggravated by the nose-down attitude of the principal axis of inertia with respect to the flight path in forward flight and they tend to be unstable. The period of the oscillations experienced are such that they might become a problem during instrument flight. The oscillation ought at least to be damped in any case as it otherwise adds to the piloting effort involved in all flight conditions. A more specific and stringent degree of damping is probably desirable for instrument flight, as will be indicated in a subsequent paper by Almer D. Crim, James B. Whitten, and John P. Reeder.

[REDACTED]

[REDACTED]

An attempt has been made to establish a basic understanding of the important factors which constitute the handling qualities of the helicopter. This has enabled some of the more important characteristics to be chosen and varied in a systematic manner designed to determine satisfactory ranges for these characteristics. Thus, apparently reasonable goals have been established to serve as a basis for requirements that are universally applicable to helicopters. Since size, configuration, and operational uses of the helicopter are still in a fluid state, more knowledge is undoubtedly needed about characteristics important for specialized demands. Efforts are being continued in the field of all-purpose instrument flight.

## REFERENCES

1. Anon.: Bureau of Aeronautics Specification for the Aerodynamic, Structural, and Power-Plant Requirements for Helicopters. NAVAER SR-189, Bur. Aero., Aug. 1, 1950.
  2. Anon.: Military Specification; Helicopter Flying Qualities, Requirements for. Military Specification, MIL-H-8501, Nov. 5, 1952.
  3. Reeder, John P., and Gustafson, F. B.: On the Flying Qualities of Helicopters. NACA TN 1799, 1949.
  4. Gustafson, F. B., Amer, Kenneth B., Haig, C. R., and Reeder, J. P.: Longitudinal Flying Qualities of Several Single-Rotor Helicopters in Forward Flight. NACA TN 1983, 1949.
  5. Reeder, John P., and Whitten, James B.: Some Effects of Varying the Damping in Pitch and Roll on the Flying Qualities of a Small Single-Rotor Helicopter. NACA TN 2459, 1952.
  6. Amer, Kenneth B.: Some Flying-Qualities Studies of a Tandem Helicopter. NACA RM L51H20a, 1951.
  7. Amer, Kenneth B., and Tapscott, Robert J.: Studies of the Lateral-Directional Flying Qualities of a Tandem Helicopter in Forward Flight. NACA TN 2984, 1953.
- [REDACTED]



### STICK FORCES FOLLOWING ABRUPT STICK DEFLECTION

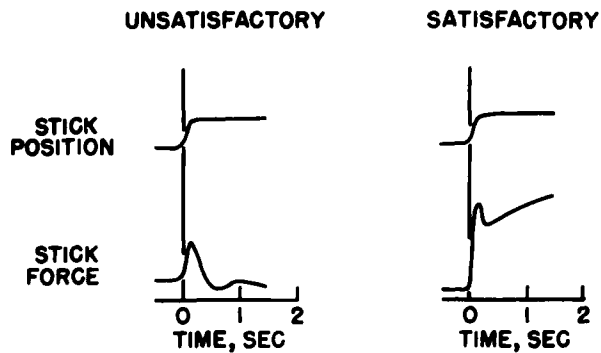


Figure 1

### LONGITUDINAL DIVERGENCE AND RECOVERY AT 65 MPH

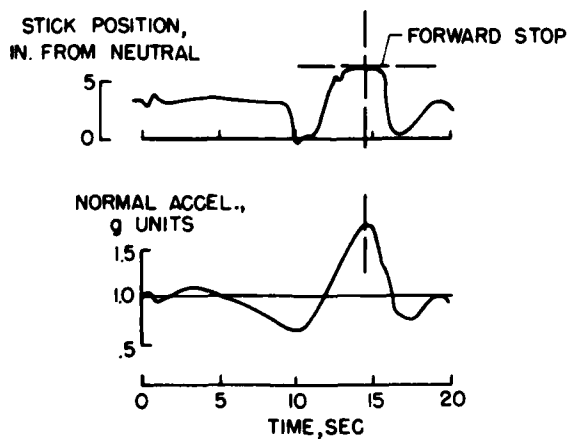


Figure 2





### TYPICAL PULL-AND-HOLD MANEUVERS

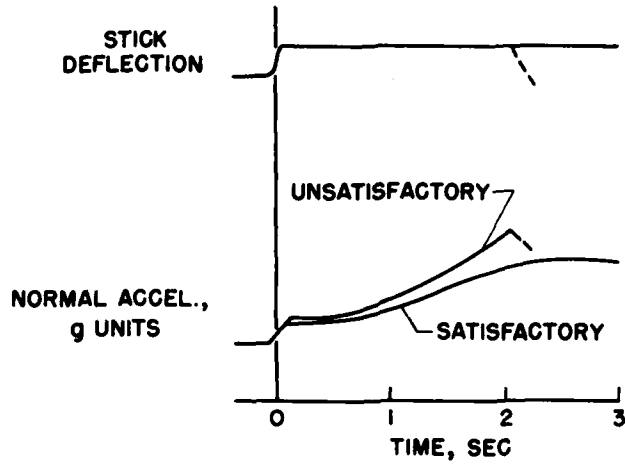


Figure 3

### PULL-AND-HOLD MANEUVER CONSIDERED UNSATISFACTORY BY PILOTS

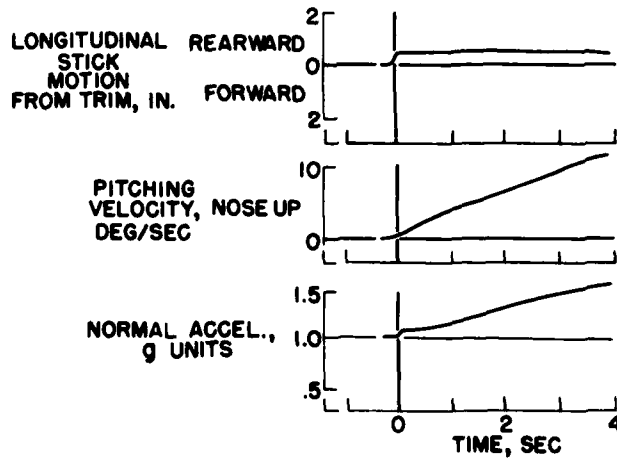


Figure 4



LATERAL CONTROL DISPLACE-AND-HOLD  
MANEUVER AT 70 KNOTS

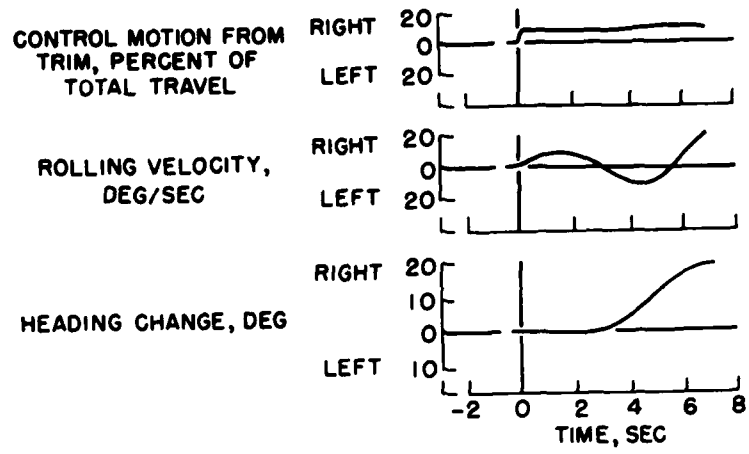


Figure 5

AN INVESTIGATION OF THE EFFECT OF DAMPING ON  
PRECISION MANEUVERS AND INSTRUMENT FLIGHT

By Almer D. Crim, James B. Whitten, and John P. Reeder

Langley Aeronautical Laboratory

Helicopter flight involving precision maneuvers, such as instrument approaches, anti-submarine warfare work, and hoisting operations, may require better flying-qualities characteristics and pilot's instruments than those considered adequate for general-purpose flying. A preliminary study of existing flying-qualities requirements under instrument conditions was reported in reference 1, and some results obtained with improved instrumentation were given in reference 2. On the basis of these studies, it was concluded that both the pilot's instruments and the helicopter flying qualities would require improvement for satisfactory all-weather, all-purpose flight throughout the speed range. Consideration of some of the problems encountered, for example, lateral-directional difficulties at low forward speeds, suggested that additional damping of the helicopter might be at least a partial solution, and the present discussion deals primarily with some effects of varying the damping in roll, yaw, and pitch of a single-rotor helicopter equipped for instrument flight. Figure 1 shows the helicopter used in the program. A set of dual controls, the instrument panel, and a hood were installed in the rear cockpit for the use of the instrument pilot.

In order to provide a convenient and flexible means for simulating various changes in the stability and control characteristics of the test helicopter, components of a modified autopilot were installed and used, in the present tests, to produce a control proportional to rate of roll, pitch, or yaw. The magnitude of this control could be varied in flight, about either or all axes, from zero to a value which produced an effective damping several times greater than that inherent in the basic helicopter. Inasmuch as previous instrument flight tests had indicated the importance to the pilot of desirable control forces, this installation also permitted cyclic stick and rudder controls with very low friction, positive centering, desirable force gradients, and means for trimming steady forces to zero.

The effects of changes in the damping of the helicopter were evaluated by performing a series of maneuvers with different amounts of added damping and comparing the inadvertent deviations in the flight path, the control motions required of the pilot, and the general ease and accuracy with which a given maneuver could be performed. These test maneuvers included visual take-offs, hovering, and landings; instrument ILS approaches at 65 and 25 knots; instrument take-offs; and attempts at instrument hovering. The instrument-landing-system (ILS) approach was

used most extensively in making the comparisons, since it provided a practical, repeatable maneuver that required rather precise flying.

Results thus far obtained have indicated that increased damping can, in general, improve the precision of maneuvers and reduce the effort required of the pilot. Some typical results, obtained during instrument ILS approaches at 25 knots, are shown in figures 2 and 3. Figure 2 shows the variations in rolling and yawing velocity with and without added damping. In each case, the effect of the increased damping is to reduce the random variations in bank angle and heading. Figure 3 illustrates the decreased control motions made by the pilot as a result of added damping. The three top records show the longitudinal cyclic, lateral cyclic, and rudder control applied by the pilot during an ILS approach without added damping, and the lower curves are the corresponding records obtained with increased damping about all three axes.

The relative value of increased damping for precision flying appears to be dependent upon the forward speed and upon the axis about which the damping has been added. For the single-rotor configuration tested, the benefits were greater at low forward speeds and hovering than at cruising speeds, and added damping in roll appeared to be much more effective than corresponding changes in yaw and pitch. At speeds from 65 to 25 knots, the pilots were of the opinion that increased damping in yaw was of some assistance but that added damping in pitch had little effect. There are indications that, for hovering, additional damping in yaw and pitch may be more important, although hovering tests have so far been very limited. It should also be pointed out, in evaluating the changes in damping in pitch, that the longitudinal characteristics of the test helicopter had already been improved at speeds above 25 knots by the addition of the tail surfaces mentioned in reference 1.

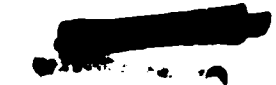
The amounts of increased damping used during these tests were chosen as the maximum values that did not seriously impair maneuverability. The values thus arrived at were found to be, about all three axes, approximately three times greater than the inherent damping of the test helicopter. Larger amounts of damping might, of course, be helpful during random disturbances of the machine but would probably interfere too much with deliberate maneuvers.

In summary, helicopter instrument flight has been shown to be practical if current military flying-qualities specifications are met, although a high degree of concentration and mental effort is required. Additional damping for this helicopter, particularly about the roll axis, increases the accuracy of flight-path control and markedly reduces the effort required of the pilot.



## REFERENCES

1. Crim, Almer D., Reeder, John P., and Whitten, James B.: Initial Results of Instrument-Flying Trials Conducted in a Single-Rotor Helicopter. NACA Rep. 1137, 1953. (Supersedes NACA TN 2721.)
2. Crim, Almer D., Reeder, John P., and Whitten, James B.: Instrument-Flight Results Obtained With a Combined-Signal Flight Indicator Modified for Helicopter Use. NACA TN 2761, 1952.



### TEST HELICOPTER



Figure 1

### EFFECTS OF INCREASED DAMPING ON HELICOPTER MOTION

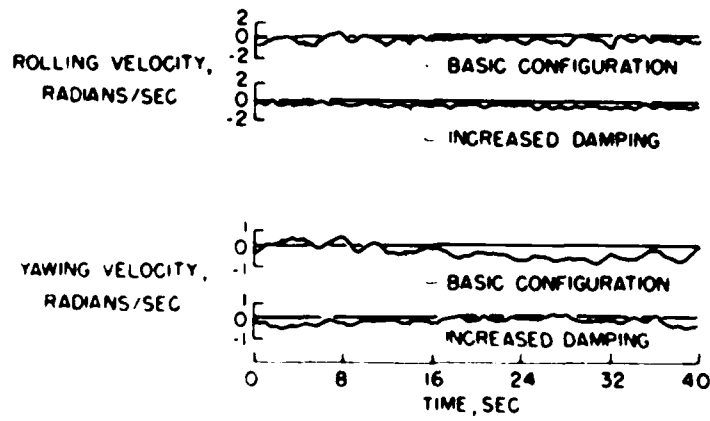
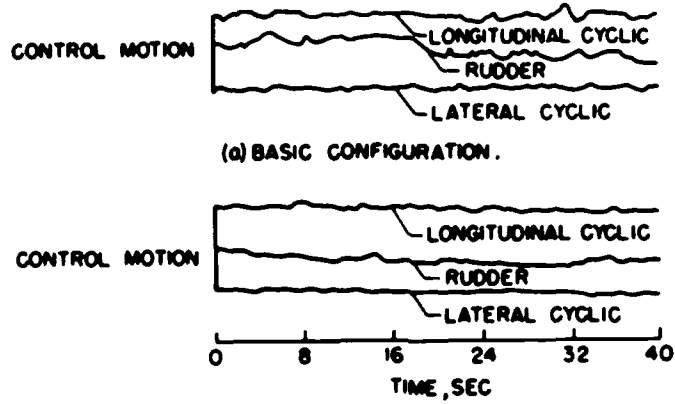


Figure 2





EFFECTS OF INCREASED DAMPING ON PILOTS' CONTROL MOTIONS



(a) BASIC CONFIGURATION.

(b) INCREASED DAMPING IN ROLL, PITCH, AND YAW.

Figure 3



## METHODS OF PREDICTING HELICOPTER STABILITY

By Robert J. Tapscott and F. B. Gustafson

Langley Aeronautical Laboratory

## SUMMARY

Some of the methods of predicting rotor stability derivatives have been reviewed. The methods by which these rotor derivatives are employed to estimate helicopter stability characteristics have been summarized. Although these methods may not always be feasible for predicting absolute values of stability for the complete helicopter, the effects on stability of changes in individual derivatives can be estimated.

## INTRODUCTION

In order to predict helicopter stability - for example, to estimate theoretically whether a prospective helicopter will meet the flying-qualities requirements - both the applicable equations of motion and the necessary stability derivatives must be determined.

The processes for handling equations of motion have been well established in conjunction with airplanes, and the modification of these procedures for helicopter use has been found a secondary problem in comparison with the provision of values of stability derivatives.

The prediction of stability derivatives, in general, requires a knowledge of the contributions of both the rotor and the fuselage. Fuselage characteristics are not open to as specific an analysis as rotor characteristics, and preliminary estimates can be handled on the basis of data from previous designs and from wind-tunnel model tests. The fuselage seems to be subject to greater modification up to the time production starts; consequently, this paper is confined primarily to the rotor contributions to the derivatives. In the past few years, considerable information has been published which permits the most pertinent rotor derivatives to be predicted with fairly good accuracy where no stall is present. A general picture of this work is presented herein.

## SYMBOLS

W	gross weight of helicopter, lb
m	mass of helicopter, slugs-ft <sup>2</sup>
R	blade radius, ft
c	blade-section chord, ft
c <sub>e</sub>	equivalent blade chord (on thrust basis), $\frac{\int_0^R cr^2 dr}{\int_0^R r^2 dr}$ , ft
σ	rotor solidity, bc <sub>e</sub> /πR
θ	blade section pitch angle; angle between line of zero lift of blade section and plane perpendicular to axis of no feathering
ρ	mass density of air, slugs/cu ft
γ	mass constant of rotor blade, expresses ratio of air forces to mass forces, ρcaR <sup>4</sup> /I <sub>1</sub> ; also, climb angle, radians
I <sub>x</sub>	helicopter rolling moment of inertia about center of gravity, slug-ft <sup>2</sup>
I <sub>y</sub>	helicopter pitching moment of inertia about center of gravity, slug-ft <sup>2</sup>
I <sub>z</sub>	helicopter yawing moment of inertia about center of gravity, slug-ft <sup>2</sup>
Δθ	difference in collective-pitch angle of front and rear rotors, positive when rear rotor is greater, radians; also increment of θ
ΔT	difference in thrust of front and rear rotors, positive when thrust of rear rotor is greater, lb
ΔR, Δ(ΩR), Δσ	definitions analogous to that for Δθ

$\Delta\alpha_d$	difference in angle of attack of front and rear rotors due to longitudinal swashplate tilt, positive when rear rotor is greater
$A_1$	lateral projection of angle between rotor shaft and axis of no feathering; therefore, lateral cyclic pitch, radians
$B_1$	longitudinal projection of angle between rotor shaft and axis of no feathering; therefore, longitudinal cyclic pitch, radians
$\delta$	control motion, inches from trim
$V$	true airspeed of helicopter along flight path, ft/sec
$v$	side velocity of helicopter in Y-direction, ft/sec
$\alpha$	rotor angle of attack; angle between flight path and plane perpendicular to axis of no feathering, positive when axis is inclined rearward, radians
$\Omega$	rotor angular velocity, radians/sec
$\mu$	tip-speed ratio, $\frac{V \cos \alpha}{\Omega R}$ assumed equal to $\frac{V}{\Omega R}$
$U_T$	component at blade element of resultant velocity perpendicular to blade-span axis and to axis of no feathering, ft/sec
$u_T = U_T/\Omega R$	
$\psi$	blade azimuth angle measured from downwind position in direction of rotation, radians; also, angle of yaw, radians
$a$	slope of curve of section lift coefficient against section angle of attack, per radian
$L$	rotor lift, lb; also, rolling moment, ft-lb
$T$	rotor thrust, component of rotor resultant force parallel to axis of no feathering, lb
$Q$	rotor-shaft torque, lb-ft
$C_T$	rotor thrust coefficient, $\frac{T}{\pi R^2 \rho (\Omega R)^2}$

$C_Q$	rotor-shaft torque coefficient, $\frac{Q}{\pi R^2 \rho (\Omega R)^2 R}$
$\beta$	blade flapping angle at particular azimuth position, radians; also sideslip angle, radians
$a_0$	constant term in Fourier series that expresses $\beta$ ; therefore, rotor coning angle
$a_1$	coefficient of $-\cos \psi$ in expression for $\beta$ ; therefore, longitudinal tilt of rotor cone
$b_1$	coefficient of $-\sin \psi$ in expression for $\beta$ ; therefore, lateral tilt of rotor cone
$a'$	projection of angle between rotor force vector and axis of no feathering in plane containing flight path and axis of no feathering
$q$	helicopter pitching velocity, radians/sec
$p$	helicopter rolling velocity, radians/sec
$\phi$	angle of roll, radians
$N$	yawing moment, lb-ft
$M$	pitching moment, lb-ft
$h$	height of rotor hub above helicopter center of gravity, ft

Dots over symbols indicate derivatives with respect to time.

#### ROTOR STABILITY DERIVATIVES

In general, calculation of the helicopter stability derivatives needed for a study of helicopter characteristics depends on the knowledge

of the individual rotor derivatives shown in the following table:

$\frac{\partial(C_T/\sigma)}{\partial a}$	$\frac{\partial(C_T/\sigma)}{\partial V}$	$\frac{\partial(C_T/\sigma)}{\partial \Omega}$	$\frac{\partial(C_T/\sigma)}{\partial \theta}$	$\frac{\partial(C_T/\sigma)}{\partial q}$
$\frac{\partial a'}{\partial a}$	$\frac{\partial a'}{\partial V}$	$\frac{\partial a'}{\partial \Omega}$	$\frac{\partial a'}{\partial \theta}$	$\frac{\partial a'}{\partial q} + \frac{\partial b'}{\partial p}$
$\frac{\partial(C_Q/\sigma)}{\partial a}$	$\frac{\partial(C_Q/\sigma)}{\partial V}$	$\frac{\partial(C_Q/\sigma)}{\partial \Omega}$	$\frac{\partial(C_Q/\sigma)}{\partial \theta}$	$\frac{\partial(C_Q/\sigma)}{\partial q}$
$\frac{\partial a_0}{\partial a}$	$\frac{\partial a_0}{\partial V}$	$\frac{\partial a_0}{\partial \Omega}$	$\frac{\partial a_0}{\partial \theta}$	$\frac{\partial a_0}{\partial q}$
$\frac{\partial a_1}{\partial a}$	$\frac{\partial a_1}{\partial V}$	$\frac{\partial a_1}{\partial \Omega}$	$\frac{\partial a_1}{\partial \theta}$	$\frac{\partial a_1}{\partial q}$
$\frac{\partial b_1}{\partial a}$	$\frac{\partial b_1}{\partial V}$	$\frac{\partial b_1}{\partial \Omega}$	$\frac{\partial b_1}{\partial \theta}$	$\frac{\partial b_1}{\partial q}$

As shown the rotor parameters considered are  $C_T/\sigma$  and  $a'$ , the magnitude and tilt of the thrust vector, respectively; rotor torque  $C_Q/\sigma$ ; blade coning angle  $a_0$ ; and  $b_1$  and  $a_1$ , the lateral and longitudinal flapping, respectively. These rotor parameters are functions of five independent variables: rotor angle of attack  $a$ , forward speed  $V$ , rotational speed  $\Omega$ , collective pitch  $\theta$ , and pitching velocity  $q$ . The values of the derivatives are determined by the variations from trim of the rotor parameters with changes in each of the five variables. The total number of derivatives shown here is large; however, it is generally possible to reduce considerably the number needed for most applications. For instance, if the rotor under consideration has no flapping hinge offset, the flapping coefficients are not significant; thus, the number of derivatives to be considered is immediately reduced by about one-half. If necessary, however, these derivatives can be determined from the equations of references 1 and 2.

Of the remaining derivatives, the lift due to pitching and torque due to pitching generally can be neglected. For most cases, then, the derivatives needed have been reduced to those enclosed within the lines in the preceding table. All the  $C_T/\sigma$ ,  $C_Q/\sigma$ , and  $a'$  derivatives can be obtained from figures or equations of references 2 and 3, as will be shown in the following discussion.



The thrust due to angle of attack and collective pitch are presented as functions of tip-speed ratio as shown in figure 1. If the solidity and tip-speed ratio for a given case are known, these quantities can be read directly. The equations on which this figure is based and the processes by which they were derived are discussed in reference 3.

The change in thrust coefficient with tip-speed ratio is presented in reference 3 in the form of an equation from which, when the flight condition is known, the rate of change of thrust coefficient with forward speed and rotational speed can be computed.

The change in inclination of the rotor force vector due to steady pitching or rolling velocity has been derived in reference 2. This derivative is shown in figure 2 as a function of the parameter  $\frac{\dot{\theta}}{C_T/\sigma}$ . As the effect of tip-speed ratio  $\mu$  is small, the equation shown in figure 2 is fairly accurate below a tip-speed ratio of 0.5 for both roll and pitch. The rotor damping moment is determined simply by multiplying the quantity obtained from the figure by  $18/\gamma\Omega$  and by the rotor thrust and rotor height above the helicopter center of gravity; that is,

$$\frac{\partial M}{\partial q} = \frac{\partial a'/\partial q}{18/\gamma\Omega} \times Th \frac{18}{\gamma\Omega}$$

For the rotor-vector angle and rotor torque derivatives, charts such as those shown in figure 3 have been derived and are published in reference 3. These charts are given for a range of collective-pitch angles from 0 to 14° at 2° increments; the sample shown herein is for a collective pitch of 8°. In these charts, the longitudinal rotor-vector angle  $a'$  is plotted against thrust-coefficient—solidity ratio for specified values of tip-speed ratio. Lines of constant power parameter  $C_Q/\mu C_T$  are cross-plotted on the charts. Combinations of these parameters which result in angles of attack of 12° and 16° on the retreating blade are indicated by dashed lines; these lines, in effect, serve as limit lines above which account must be made of stall. By using slopes or differences from these charts in conjunction with other derivatives and some simple equations, the remaining  $a'$  and torque coefficient derivatives can be obtained. As an example, consider the derivative of  $a'$  with respect to angle of attack. From this chart, the rate of change of  $a'$  with thrust coefficient can be obtained at a given tip-speed ratio and thrust coefficient by scaling off the slope of the tip-speed-ratio line at the desired thrust coefficient. When this quantity is multiplied by the change in thrust coefficient with angle of attack, which has already been discussed, the result is the change in  $a'$  with angle of attack. The other  $a'$  and the torque coefficient derivatives can be obtained by similar procedures. These procedures are discussed in reference 3.

██████████

## PREDICTION OF HELICOPTER STABILITY

By using the rotor derivatives that have been discussed, it is believed that the rotor contribution to the essential helicopter derivatives can be predicted. The rotor derivatives discussed are applicable, in most cases, to a study of the stability characteristics of either a single- or tandem-rotor configuration. The difference arises in using the rotor derivatives to determine the helicopter derivatives for use in the equations of motion and in accounting for the effects of flow interference for a specific configuration. For most purposes, the lateral and longitudinal characteristics of the helicopter can be studied separately. Generally, equations of motion derived on the basis of constant forward speed are sufficient and are applicable to both single- and tandem-rotor configurations.

In a study of the longitudinal characteristics of the helicopter (ref. 4), an important criterion is that the time history of the normal acceleration shall be concave downward within 2 seconds after a step input to the longitudinal control. In order to assist in estimating theoretically whether a prospective helicopter will meet this criterion, the following equations of motion were devised:

$$\frac{\partial L}{\partial q} q + \frac{\partial L}{\partial \theta} \Delta \theta + \frac{\partial L}{\partial \alpha} \Delta \alpha - \frac{WV}{g} \dot{\gamma} = 0$$

$$\frac{\partial M}{\partial q} q + \frac{\partial M}{\partial \theta} \Delta \theta + \frac{\partial M}{\partial \alpha} \Delta \alpha + \frac{\partial M}{\partial B_1} \Delta B_1 - I_Y q = 0$$

$$\Delta \alpha = \int_0^t q dt - \gamma - \Delta B_1$$

These equations are based on flight-path axes and derived on the assumptions of constant forward speed, constant rotor speed, and constant stability derivatives. The assumption is also made that the dynamic maneuver can be represented by a series of static conditions; hence, the rotor parameters are always at their equilibrium values as determined by the instantaneous values of angle of attack, pitch angle, tip-speed ratio, and pitching velocity. The first and second equations shown represent, respectively, equilibrium normal to the flight path and equilibrium in pitch. The third equation simply relates the variables of the first two equations to permit a solution.

██████████

The form of the equations as shown applies specifically to the single-rotor configuration; for the tandem, another term must be included to account for the pitching moment due to control motion. For the tandem configuration, this control moment results primarily from differential collective pitch on the two rotors.

In reference 5, these equations of motion have been solved for the climb angle  $\gamma$ , which, in turn, permits an expression to be written for the time history of the normal acceleration. Values of combinations of derivatives have been determined which, when substituted into the expression for the time history of normal acceleration, will result in a time history that is concave downward at 2 seconds. These values have been presented in the form of a chart, as shown in figure 4. The curve in figure 4, therefore, indicates a boundary line separating combinations of significant longitudinal stability derivatives which result in satisfactory characteristics or unsatisfactory characteristics according to the criterion previously mentioned. Shown along with the theoretical curve are data points corresponding to four helicopter configurations. The derivatives for the configurations corresponding to the points shown were measured in flight and the adjacent number is the approximate time for the corresponding normal-acceleration time history to become concave downward. The theoretical curve is indicated to be qualitatively correct for both single- and tandem-rotor helicopters for separating configurations which have satisfactory maneuver stability from those which have unsatisfactory maneuver stability according to the criterion. This indication can be seen by noting that the points for which the normal-acceleration time history becomes concave downward in less than 2 seconds fall in the satisfactory region whereas, for times of more than 2 seconds, the points fall in the unsatisfactory region.

Figure 4 shows an increase in the angle-of-attack stability or damping in pitch (that is, more negative  $M_{\alpha}$  or  $M_q$ ), or increases in the lift-curve slope  $L_{\alpha}$  to be stabilizing. Also, it can be determined from this plot that an increase in pitching moment of inertia  $I_y$  can be destabilizing. Since the change in lift slope can be small only and is not expected to change sign, the primary changes in stability must be brought about by changes in the damping-in-pitch or angle-of-attack stability.

In the discussion of longitudinal stability so far, the forward speed has been assumed constant. For the tandem configuration, however, the downwash effects of the front rotor acting on the rear rotor cause an unstable variation in pitching moment with speed. A study of the speed stability of the tandem was made in reference 6. In that study, on the basis of the available derivatives discussed previously, an expression for the change of stick position with speed was derived. The equation, along with a plot of constants based on the rotor derivatives, is shown in figure 5. The constants for use in the equation are presented

for several values of rotor solidities over a range of tip-speed ratios. After a flight condition is selected and the tip-speed ratio and thrust coefficient are thereby established, the slope of the stick-position variation with speed can be determined. This equation takes into account the effects on speed stability of center-of-gravity position, differential rotor speed, differential rotor radius and solidity, and "longitudinal dihedral." Effects of these parameters can be studied either together or separately.

This analysis of tandem-speed stability is of value especially in the study of the relative effects of changes in the various parameters wherein it is not necessary to know accurately the value of downwash or the fuselage contribution. In order to predict the absolute value of speed stability, the downwash must be estimated for the configuration and flight condition under consideration and the variation of the fuselage moments must be known. The results of flow-field measurements presented in references 7 and 8 should be useful in estimating the magnitude of the downwash applicable to a specific condition.

The next important item in helicopter stability is the lateral-directional characteristics. If roll, yaw, and sideslip are considered as degrees of freedom, the equations of motion are as follows:

$$I_X \ddot{\phi} + \frac{\partial L}{\partial p} \dot{\phi} + \frac{\partial L}{\partial v} v - \frac{\partial L}{\partial \delta} \delta = 0$$

$$I_Z \ddot{\psi} + \frac{\partial N}{\partial r} \dot{\psi} + \frac{\partial N}{\partial v} v - \frac{\partial N}{\partial \delta} \delta = 0$$

$$\left(mV - \frac{\partial Y}{\partial r}\right) \dot{\psi} - \left(mV \sin \eta + \frac{\partial Y}{\partial p}\right) \dot{\phi} - T\phi - T\psi \tan \gamma + m\dot{v} - \frac{\partial Y}{\partial v} v - \frac{\partial Y}{\partial \delta} \delta = 0$$

For convenience in determining the derivatives, these equations are based on principal axes of inertia rather than on the relative wind. In general, the rotor contribution to the derivatives needed in these equations can also be determined from rotor theory. Fuselage contributions can be predicted from wind-tunnel data and previous experience or from flight data where available.

These equations have been found useful particularly in estimating the effects on helicopter characteristics of changes in the individual stability derivatives. As an example, figure 6 shows the theoretically predicted time histories of rolling velocity and sideslip angle of a tandem-rotor helicopter. The curves on the left-hand side of figure 6

represent a case with values of the derivatives estimated for the original helicopter. On the right-hand side of figure 6 are time histories of the same quantities when the effective-dihedral derivative is reduced 50 percent. From this figure, it is indicated that a 50-percent reduction in the effective dihedral would substantially improve the oscillatory characteristics of the helicopter. In an attempt to improve the characteristics, this means was tried experimentally. The results are shown in figure 7 wherein the experimentally measured time histories of rolling velocity and sideslip angle before and after the derivative change are compared. The comparison shows that, as predicted by the theory, a reduction in the effective dihedral improved the oscillation. Thus, in this case, the theory was employed successfully to indicate the course to be followed in making an improvement.

#### CONCLUDING REMARKS

In general, on the basis of the studies discussed herein, it will frequently not be feasible to predict accurately absolute magnitudes for the stability of the complete helicopter particularly because of the difficulty of predetermining final, full-scale fuselage characteristics. However, a first approximation can be made, and by making some comparatively straightforward flight measurements of stability derivatives and re-employing the theory to show what modifications are needed, it appears feasible to handle at least those problems with which direct experience has been had. It appears likely that, in most cases, changes in several derivatives simultaneously would be necessary to achieve most efficiently the desirable stability characteristics, and the equations discussed herein should prove very useful in this type of study.

## REFERENCES

1. Bailey, F. J., Jr.: A Simplified Theoretical Method of Determining the Characteristics of a Lifting Rotor in Forward Flight. NACA Rep. 716, 1941.
2. Amer, Kenneth B.: Theory of Helicopter Damping in Pitch or Roll and a Comparison With Flight Measurements. NACA TN 2136, 1950.
3. Amer, Kenneth B., and Gustafson, F. B.: Charts for Estimation of Longitudinal-Stability Derivatives for a Helicopter Rotor in Forward Flight. NACA TN 2309, 1951.
4. Gustafson, F. B., Amer, Kenneth B., Haig, C. R., and Reeder, J. P.: Longitudinal Flying Qualities of Several Single-Rotor Helicopters in Forward Flight. NACA TN 1983, 1949.
5. Amer, Kenneth B.: Method for Studying Helicopter Longitudinal Maneuver Stability. NACA TN 3022, 1953.
6. Tapscott, Robert J., and Amer, Kenneth B.: Studies of the Speed Stability of a Tandem Helicopter in Forward Flight. NACA RM L53F15a, 1953.
7. Gessow, Alfred: Review of Information on Induced Flow of a Lifting Rotor. (Prospective NACA paper.)
8. Heyson, Harry H.: Flow-Field Measurements Around Single and Tandem Rotors in the Langley Full-Scale Tunnel. (Prospective NACA paper.)

VARIATION OF  $C_T/\sigma$  DERIVATIVES WITH RESPECT TO  $\mu$

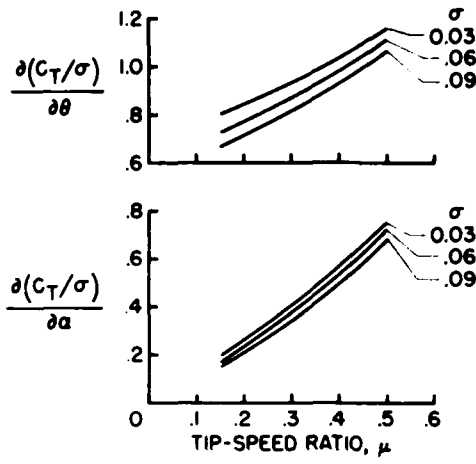


Figure 1

CHART FOR DETERMINING ROTOR DAMPING IN PITCH AND ROLL

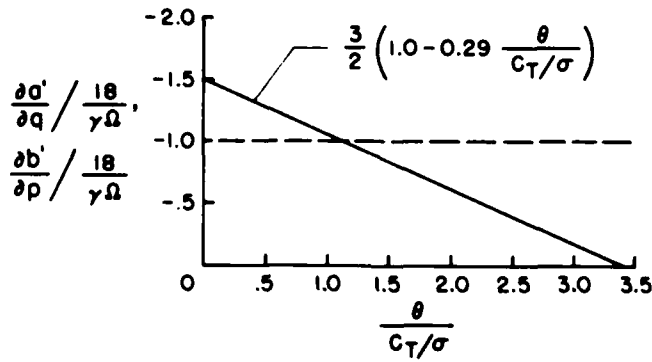


Figure 2

CHART FOR DETERMINING DERIVATIVES OF LONGITUDINAL  
TILT AND TORQUE-COEFF. — SOLIDITY RATIO

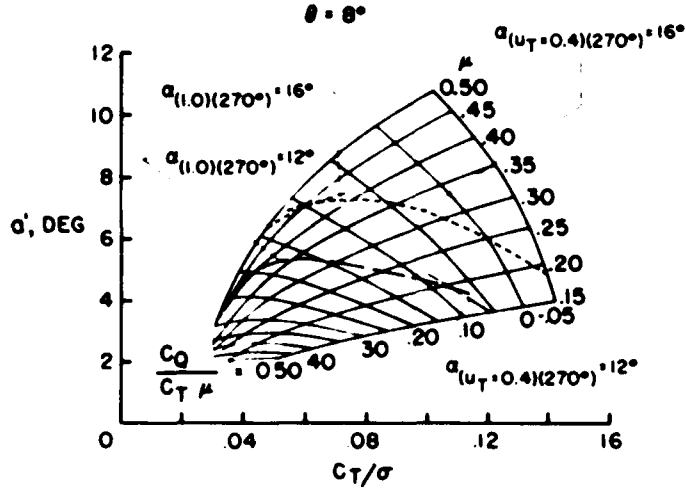


Figure 3

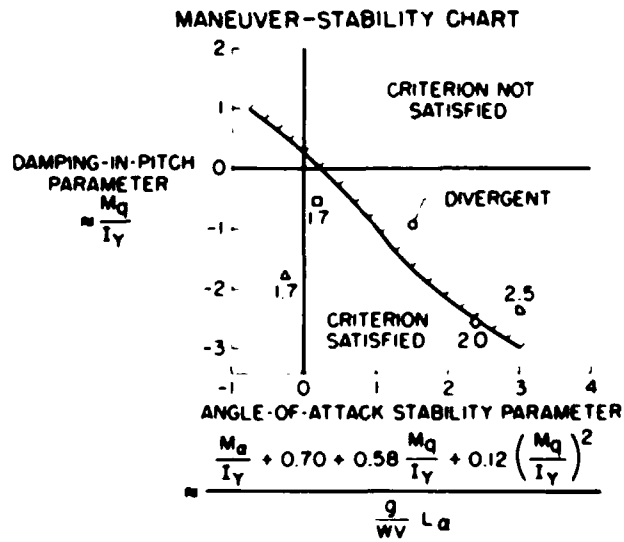


Figure 4



TANDEM SPEED-STABILITY EQUATION

$$\frac{d(\Delta\theta)}{d\mu} + K_1 \left( \frac{C_T}{\sigma} \right)_{AV} \left( \frac{\Delta T}{W} - \frac{\Delta R}{R_{AV}} \right) + K_2 \left( \frac{C_T}{\sigma} \right)_{AV} \left[ \frac{\Delta\sigma}{\sigma_{AV}} + 2 \frac{\Delta(\Omega R)}{(\Omega R)_{AV}} \right] + K_3 \Delta\alpha_d + K_4 C_T$$

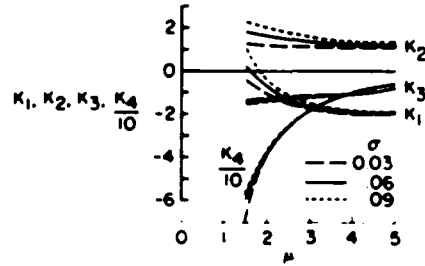


Figure 5

PREDICTED EFFECT OF REDUCTION IN EFFECTIVE DIHEDRAL ON LATERAL OSCILLATION

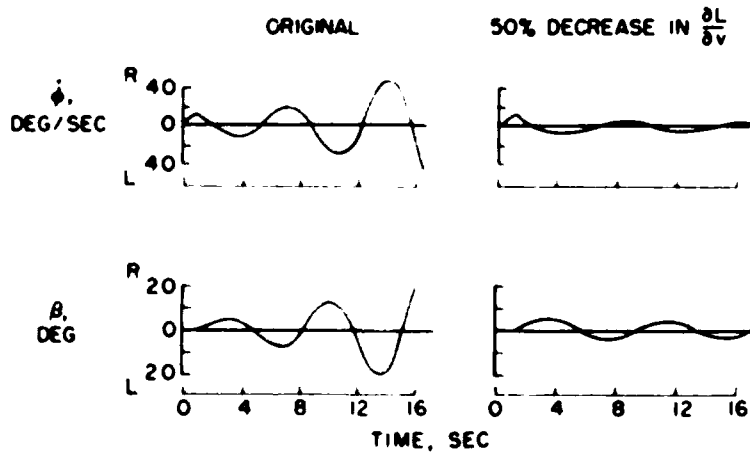


Figure 6



MEASURED EFFECT OF REDUCTION IN EFFECTIVE DIHEDRAL ON LATERAL OSCILLATION

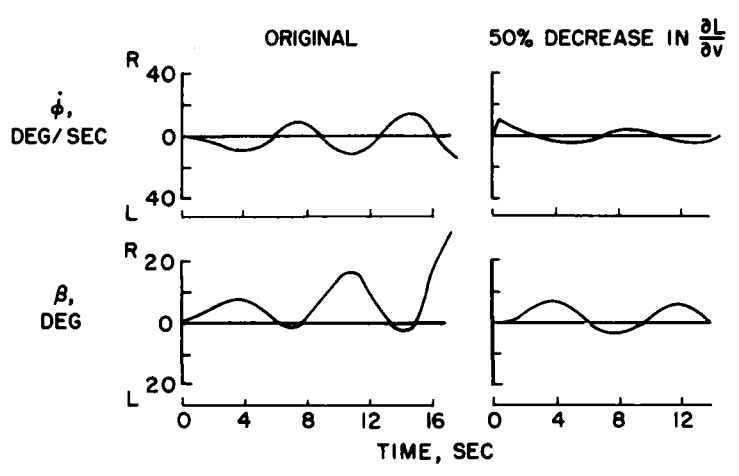


Figure 7



METHODS FOR OBTAINING DESIRED HELICOPTER  
STABILITY CHARACTERISTICS

By F. B. Gustafson and Robert J. Tapscott

Langley Aeronautical Laboratory

SUMMARY

A brief summary is made of methods available to the helicopter designer for obtaining desired stability characteristics by modifications to the airframe design. The discussion is based on modifications made during the establishment of flying-qualities criteria and includes sample indications of theoretical studies of additional methods.

INTRODUCTION

The problems relating to stability of helicopters have been the subject of numerous published works. Requirements established by the military services for satisfactory helicopter stability are specified in reference 1. Some of the pertinent works on this subject by the NACA are listed as references 2 to 13. The purpose of this paper is to summarize some of the physical methods available to the designer for obtaining desired stability values by changing the airframe design. Although the direct application discussed is with a view to meeting flying-qualities criteria, it may be worth pointing out that other reasons often arise for designing a configuration so that specific amounts of stability are provided; for example, in order to obtain the most efficient combination of autopilot and airframe design.

The scope of the present discussion is outlined in the following table:

Characteristic	Rotor type investigated
Sensitivity in roll	Single and tandem
Maneuver stability	Single and tandem
Speed stability	Single and tandem
Lateral oscillation and turn characteristics	Tandem

Available results on directional weathercock stability of tandem helicopters are not included in this discussion because of thorough coverage in reference 2. For helicopter types other than single-rotor or tandem-rotor configurations, no direct information is provided herein but much can be inferred from the more appropriate of the two types covered.

For each of the stability characteristics covered, modifications made to the design in the process of exploring a range of characteristics during the establishing of desired flying-qualities criteria are discussed. The value of the cases illustrated lies in the fact that they are demonstrated cases for which measured stability-parameter values are available. Optimum design generally requires a choice of methods or combinations of methods; therefore, sample indications of theoretical studies of additional methods are included in each case.

#### SYMBOLS

$L_{\delta}$	rolling moment due to control deflection
$L_p$	rolling moment due to rolling angular velocity
$\Delta W_b$	change in weight of blade radius
$R$	blade radius
$I_1$	blade moment of inertia
$\gamma$	blade mass factor
$M_{\alpha}$	pitching moment per unit angle-of-attack change
$M_q$	pitching moment due to unit pitching angular velocity
$L$	rolling moment
$v$	sideslip velocity
$\Omega$	rotor rotational speed
$\sigma$	rotor solidity
$B_1$	longitudinal cyclic pitch
$V$	forward velocity

- $c_m$  section pitching-moment coefficient
- $\Delta\theta$  difference between collective pitch of front and rear rotors

### SENSITIVITY IN ROLL

Sensitivity in roll, which is frequently a major problem in the hovering characteristics of small helicopters, is treated in table I. The test vehicle is a two-place single-rotor helicopter. The parameter discussed is the ratio of control power (that is, the rolling moment per unit stick deflection) to damping, which is the resisting moment per unit angular velocity of the helicopter. Since changes in the value of control power are restricted by trim requirements, this discussion is concerned solely with changes in damping.

The requirement of the current military specification (ref. 1) is that the rate of roll per inch of stick displacement be less than  $20^\circ$  per second. The test helicopter provided the opportunity to explore a fair-sized range of values, always on the satisfactory side, by adjusting a mechanical gyroscopic device. The value of  $L_\delta/L_p$  of 14 is obtained with the device locked out and the value of 5.2 is with the device as far beyond the production setting as feasible. Both from theory and from flight measurements on other helicopters, it is known that, with lighter blades and no special device, the requirement of reference 1 would not have been met. Therefore, examination of a few additional methods for changing the damping and hence the sensitivity is advisable.

Increased blade inertia is one method. If a tip weight is considered, 60 percent of the blade weight is calculated to be needed to duplicate the full change in  $L_\delta/L_p$  from 14 to 5.2. Flapping-hinge offset will increase damping, but bear in mind that the control linkage is assumed here to be changed to prevent increase in control power; else little change in sensitivity would result. With the heavy blades of the test helicopter, an offset of only 2-percent radius should be needed to change  $L_\delta/L_p$  from 14 to 5.2; with light blades, an offset of 5-percent radius would be enough.

A third design approach which makes possible increased damping is the use of aerodynamic servo controls; as viewed from above the rotor in the sketch of table I, one type uses a surface behind the outer part of the blade and another, a surface attached at right angles at the blade root. Such devices apparently can be designed to provide increases in damping sufficient to cover the test range.

Sensitivity in roll for the tandem helicopter requires no separate discussion since, in roll, it is possible simply to consider two single rotors instead of one.

## MANUEVER STABILITY OF SINGLE-ROTOR HELICOPTERS

For the maneuver-stability (or divergence) problems with single-rotor helicopters at cruising speed, two separate cases are treated in table II. With one helicopter, the variations were made by way of angle-of-attack stability, and in the other case, by way of damping in pitch. For the first case, a change to a value of angle-of-attack stability of 300 pound-feet per radian was enough to cause the requirement to be met. The range covered went from the unstable value of +7,000 pound-feet per radian to the stable value of -2,100 pound-feet per radian. (Minus is stable in accepted stability theory.) The test conditions actually extended somewhat farther than the value of -2,100 pound-feet per radian on the stable side but the  $M_{\alpha}$ -values were not recorded.

The tail assembly used has been discussed in published papers, particularly reference 3. It may bear repeating, however, that a total tail area of 0.5 percent of the rotor area could make the difference between the helicopter's diverging excessively in a few seconds and being able to fly through rough air without the longitudinal control being moved. This result was obtained after linking the tail to the cyclic controls, which so reduced the design compromises as to permit use of a somewhat more effective tail.

Tests were made with a different helicopter (labeled (2) in table II), wherein the damping in pitch was varied in such a way as to bracket the condition for which the requirement was met. The value of -1,200 pound-feet per radian needed to cause the specification to be met falls about midway in the range of -700 to -1,900 pound-feet per radian covered. Damping is another quantity where the minus sign is indicative of a stable condition. As to the method used, the investigation was the same as that which provided the damping-in-roll values given in table I.

As to alternate methods, for large changes in angle-of-attack stability  $M_{\alpha}$ , there do not seem to be too many which will cover the range single handed. Increase in rotor speed is listed because the effect of such an increase is calculated to be sufficient to warrant thought of some compromise with design for optimum power. It will be understood that rotational speed is appropriate because in all other respects the design is fixed; more fundamentally, what is implied is lower values of pitch and tip-speed ratio. A 33-percent increase in rotor rotational speed is estimated to give half the range covered and would not have been enough, in itself, to meet the specification. The effects are not linear and much greater increase in stability by this method would cause extreme compromise with performance.

If offset flapping hinges are used, then the aircraft center-of-gravity position affects angle-of-attack stability. An estimate for this helicopter is that, with the hinges at 5-percent blade radius, moving the center of gravity 7 inches (2.5 percent of the rotor radius) forward from the rotor shaft would produce as much change as the 33-percent increase in rotor rotational speed. With the same offset, a center-of-gravity shift of 14 inches, if such is tolerable, would produce the change to the -2,100 value and thus would permit the requirements to be exceeded.

For alternate methods of varying the rotor damping in pitch  $M_q$ , the methods given in the roll-sensitivity discussion again apply.

#### MANUEVER STABILITY OF TANDEM-ROTOR HELICOPTERS

Maneuver stability for the tandem helicopter, again at cruising speed, is treated in table III. The parameter considered is again moment per unit angle-of-attack change, and with the test helicopter the unstable value of 57,000 pound-feet per radian corresponded to a value that would just barely meet the requirements set forth in the specification. The test range shown, from the unstable 72,000 pound-feet per radian to the stable -16,000 pound-feet per radian, went several times farther than just reaching the marginal value. It is desirable to be able to make these larger changes. The test method used was not altogether appropriate for this discussion because so much of the range was obtained by choice of power setting. The available center-of-gravity range produced a useful but subordinate change, forward center of gravity being the more stable.

Calculations, therefore, are again used to illustrate other methods. Changes which affect the relative lift-curve slopes of the front and rear rotors seem especially effective. It is estimated that, if the front-rotor radius is decreased and the rear-rotor radius is increased, with a total difference of 10 percent of the mean radius, the test value of stability increase would be realized. If, instead, the rotor solidities were similarly changed by putting wider blades on the rear rotor and narrower ones on the front rotor, this same stability increase could be obtained with a solidity differential of 45 percent of the mean value.

The size of horizontal-tail surface necessary to contribute the same range was computed, in order to illustrate the conclusion that a horizontal tail is relatively less effective for tandems than for single rotors. A value of 4 percent of rotor area is indicated in distinction to the 0.5 percent used on the single-rotor helicopters. Although the two cases are not strictly comparable, the impression given is considered to be reasonable.

## SPEED STABILITY OF SINGLE-ROTOR HELICOPTERS

Table IV treats the speed stability for the single-rotor case. With fixed pitch and throttle, the stick is required to trim farther forward with increase in speed. The parameter used to measure this change is the longitudinal cyclic pitch  $B_1$  per unit velocity  $V$  (in knots). The range tested ( $B_1/V$  from 0 to 0.06 degrees per knot) was obtained by changes in horizontal-tail setting. When sufficient upload was provided on the tail surface, the stable contribution of the rotor could be cancelled; when download was provided, it could be increased. Incidentally, most of this exploration of near-zero speed stability was obtained with the tail linked to the cyclic stick, the reason being that a high, fixed, nose-up tail setting can be dangerous in event of inadvertent speed increase.

Since the rotor tends to be stable, most concern is felt over destabilizing factors. Fuselage shape can be as destabilizing as a nose-up tail setting, although a range of 30 foot-pounds per knot would be rather large. A large rotor-blade-section diving moment could more than cancel the stable tendency of the rotor. The increment  $\Delta c_m$  of 0.06 actually was suggested by the dangerous characteristics which arose with autogiros having  $c_m = -0.06$ . A rough estimate indicated the value of 0.06 to be the right order of magnitude to produce the change under discussion as well.

## SPEED STABILITY OF TANDEM-ROTOR HELICOPTERS

Table V relates to speed stability of the tandem-rotor type. The longitudinal control of this configuration is obtained primarily by changing the pitch-setting difference between front and rear rotors, and the parameter is written to correspond as  $\Delta\theta/V$ . This quantity was varied from -0.01 to 0.003; thus, the requirement of at least zero is bracketed. This change was accomplished by changing the tilt angle between the front and rear rotor systems. The unstable setting was  $\Delta\theta = 0^\circ$ ; the stable one,  $1.8^\circ$  "toe-in."

Calculations indicate that a center-of-gravity shift from midway between the shafts to 22 percent ahead of the midpoint should produce the equivalent range. The 22-percent value is based on total distance between shafts. Similarly, giving the rear rotor higher solidity and the front less, with a total difference  $\Delta\sigma$  of 34 percent of the mean should achieve this same result. These values are for cruising speed; at low speeds the effect of center of gravity can even reverse, whereas the solidity change becomes more effective. The use of some of each method thus holds special interest. It is also worth noting that these effects act in the same direction for speed stability as they do for maneuver stability.



[REDACTED]

LATERAL-OSCILLATION AND TURN CHARACTERISTICS  
OF TANDEM-ROTOR HELICOPTERS

Tandem-rotor lateral-oscillation and turn characteristics at cruise speed are treated in table VI. One of the most effective parameters for both is roll due to sideslip velocity, or  $L/v$ , measured as foot-pounds of rolling moment per foot per second of sideslip velocity. Fortunately, this quantity, which is the effective dihedral, is not critical in its own right, provided it stays on the stable side. (By convention, stable values are negative.) Most of the required change was obtained by attaching small wings (surface area, 7 sq ft) to the landing gear. The front view and side view are shown. It was most convenient in these flying-qualities trials to further extend the test conditions by change in flight condition; but with so many designs sprouting modest-sized wings (much bigger than the panels used in these tests), making the full change needed may often require only that the right geometric dihedral be determined.

One additional method is to change the vertical location of the center of gravity relative to the side-view area. Only a major change in power-plant location, such as overhead turbines, seems likely to make a change of this magnitude (9 in. shift in center of gravity). Contributing changes, though, including some ventral fin area, may often prove feasible.

Increased damping in roll is another effective parameter that can be considered. This method is discussed, along with still other approaches, in reference 4.

CONCLUDING REMARKS

Examples have been presented to illustrate methods for improving helicopter stability. It will be realized that many of the numerical values which have been given apply only for the case studied. For example, a tandem helicopter might already have lower effective dihedral or might somehow be designed with less nose-down inclination of the principal inertia axis and, in either event, might meet the lateral requirements without reduction in effective dihedral.

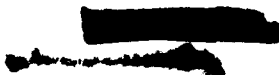
The cases presented are believed to illustrate that it is now feasible to choose one or more important stability parameters from theoretical studies and, in turn, to find a combination of methods whereby parameter values are realized which provide the desired stability characteristics.

[REDACTED]

[REDACTED]



Aside from the degree of fundamental understanding, which involves the usability of theory, a variety of choice of methods is suggested as the key to the obtainance of desired characteristics with a minimum of design compromise. It is hoped that these sample methods may be helpful in suggesting still more approaches to the helicopter designer.



## REFERENCES

1. Anon.: Military Specification; Helicopter Flying Qualities, Requirements For. Military Specification, MIL-H-8501, Nov. 5, 1952.
2. Williams, James L.: Directional Stability Characteristics of Two Types of Helicopter Fuselage Models. NACA TN 3201, 1954.
3. Gustafson, F. B.: Desirable Longitudinal Flying Qualities for Helicopters and Means To Achieve Them. Aero. Eng. Rev., vol. 10, no. 6, June 1951, pp. 27-33.
4. Amer, Kenneth B., and Tapscott, Robert J.: Studies of the Lateral-Directional Flying Qualities of a Tandem Helicopter in Forward Flight. NACA TN 2984, 1953.
5. Amer, Kenneth B.: Method for Studying Helicopter Longitudinal Maneuver Stability. NACA TN 3022, 1953.
6. Tapscott, Robert J., and Amer, Kenneth B.: Studies of the Speed Stability of a Tandem Helicopter in Forward Flight. NACA RM L53F15a, 1953.
7. Reeder, John P., and Whitten, James B.: Some Effects of Varying the Damping in Pitch and Roll on the Flying Qualities of a Small Single-Rotor Helicopter. NACA TN 2459, 1952.
8. Amer, Kenneth B., and Gustafson, F. B.: Charts for Estimation of Longitudinal-Stability Derivatives for a Helicopter Rotor in Forward Flight. NACA TN 2309, 1951.
9. Amer, Kenneth B.: Some Flying-Qualities Studies of a Tandem Helicopter. NACA RM L51H20a, 1951.
10. Amer, Kenneth B.: Theory of Helicopter Damping in Pitch or Roll and a Comparison With Flight Measurements. NACA TN 2136, 1950.
11. Gustafson, F. B., Amer, Kenneth B., Haig, C. R., and Reeder, J. P.: Longitudinal Flying Qualities of Several Single-Rotor Helicopters in Forward Flight. NACA TN 1983, 1949.
12. Reeder, John P., and Gustafson, F. B.: On the Flying Qualities of Helicopters. NACA TN 1799, 1949.
13. Gustafson, F. B., and Reeder, J. P.: Helicopter Stability. NACA RM L7K04, 1948.

[REDACTED]

TABLE I  
SENSITIVITY IN ROLL  
SINGLE ROTOR; 2,200-LB GROSS WT.

PARAMETER	VALUE TO MEET MIL-H-8501	RANGE TESTED	METHOD USED
CONTROL POWER, DAMPING $\frac{L_b}{L_p}$ , DEG/SEC IN.	< 20	14 TO 5.2	AVAILABLE GYRO DEVICE; $L_b$ FIXED



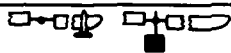
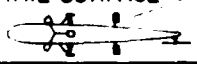
ADDITIONAL METHODS ( $L_b$ FIXED)	AMOUNT FOR RANGE TESTED
INCREASE IN $I_1$ VIA TIP WT. 	$\Delta W_b = 0.6$
HINGE OFFSET WITH $\gamma = 4.7$ 	2% R
AERO SERVOS 	-----

TABLE II  
MANEUVER STABILITY  
SINGLE ROTOR; GROSS WTS.: (1) 5,000 LB AND (2) 2,200 LB;  
CRUISE SPEED

	MAJOR PARAMETER VARIED	VALUE TO MEET MIL-H-8501	RANGE TESTED	METHOD USED
(1)	$M_\alpha$ , LB-FT RADIAN	< 300	7,000 TO -2,100	TAIL SURFACE 
(2)	$M_q$ , LB-FT RADIAN/SEC	< -1,200 (ROTOR)	-710 TO -1,930	AVAILABLE GYRO DEVICE
PARAMETER	ADDITIONAL METHODS		AMOUNT FOR 1/2 RANGE TESTED	
$M_\alpha$	INCREASED RPM		33%	
	FORWARD C.G. WITH OFFSET HINGES		$\Delta$ C.G. = 2.5% R WITH 5% OFFSET	
$M_q$	SIMILAR TO ROLL SENSITIVITY			

[REDACTED]

TABLE III  
MANEUVER STABILITY  
TANDEM ROTOR; 7,000-LB GROSS WT.; CRUISE SPEED

MAJOR PARAMETER	VALUE TO MEET MIL-H-8501	RANGE TESTED	METHOD USED
$M_{\alpha}$ , $\frac{\text{LB-FT}}{\text{RADIAN}}$	< 57,000	72,000 TO -16,000	C.G. AND POWER SETTING

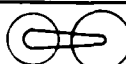


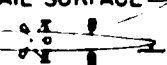
ADDITIONAL METHODS	AMOUNT FOR RANGE TESTED
$\Delta R$ (SAME $\Omega$ ) 	10%
$\Delta \sigma$ 	45%
TAIL SURFACE 	100 SQ FT OR 4% OF TOTAL ROTOR AREA


TABLE IV  
SPEED STABILITY  
SINGLE ROTOR; 5,000-LB GROSS WT.; CRUISE SPEED

PARAMETER	VALUE TO MEET MIL-H-8501	RANGE TESTED	METHOD USED
$\frac{B_1}{V}$ , $\frac{\text{DEG}}{\text{KNOT}}$	> 0	0 TO 0.06	TAIL SURFACE 

ADDITIONAL FACTORS	AMOUNT FOR RANGE TESTED
MOMENTS, FUSELAGE LESS TAIL	$\Delta \frac{\text{FT-LB}}{\text{KNOT}} = 30$
BLADE SECTION PITCHING-MOMENT COEFFICIENT	$\Delta C_m \approx 0.06$

TABLE V

SPEED STABILITY  
TANDEM ROTOR; 7,000-LB GROSS WT.; CRUISE SPEED

PARAMETER	VALUE TO MEET MIL-H-8501	RANGE TESTED	METHOD USED
$\frac{\Delta\theta}{V} \cdot \frac{\text{DEG}}{\text{KNOT}}$	> 0	-0.01 TO 0.003	1.8° $\Delta\alpha_d$ 




ADDITIONAL FACTORS	AMOUNT FOR RANGE TESTED
C.G. SHIFT 	22%
$\Delta\sigma$ 	34%

TABLE VI

LATERAL OSCILLATION AND TURN CHARACTERISTICS  
TANDEM ROTOR; 7,000-LB GROSS WT.; CRUISE SPEED

MAJOR PARAMETER	VALUE TO MEET MIL-H-8501	RANGE TESTED	METHOD USED
ROLL DUE TO SIDESLIP, $\frac{L}{V}$ , $\frac{\text{FT-LB}}{\text{FT/SEC}}$	> -26	-75 TO -37	 TWO WINGS, 7 SQ FT EACH

ADDITIONAL METHOD	AMOUNT FOR RANGE TESTED
VERTICAL CG.-LATERAL C/P RELATIONSHIP	9 IN.

WIND-TUNNEL STUDIES OF THE DIRECTIONAL STABILITY  
CHARACTERISTICS OF TWO TANDEM  
HELICOPTER FUSELAGES

By John D. Bird and James L. Williams  
Langley Aeronautical Laboratory

INTRODUCTION

The results of flight tests of two types of tandem helicopters, one a helicopter with nonoverlapping rotors, which will be referred to as the "nonoverlap helicopter," and the other a helicopter with overlapping rotors, which will be referred to as the "overlap helicopter," showed undesirable directional stability characteristics for certain angles of attack and sideslip. Figure 1 shows the top and side views of the fuselages of these helicopters. The nonoverlap fuselage is characterized by an upward bending of the rearward portion. The overlap fuselage is characterized by a pylon faired to form a thick vertical tail (approximately 35 percent thick) and a thick fuselage rear section. The instability experienced by the nonoverlap helicopter was a directional divergence that occurred predominately in the descent and autorotation conditions of flight and was of sufficient degree to complicate materially the operation of the helicopter. The difficulty experienced by the overlap helicopter was a lack of directional stability at small angles of sideslip which resulted in two stable directional trim points in forward flight, one with about  $7^\circ$  or more of sideslip to the left and the other with about the same amount of sideslip to the right.

Because of the seriousness of these difficulties and the interest in these types of fuselages, an investigation was undertaken in the Langley stability tunnel in order to study their directional stability characteristics and to find solutions, if possible, that would give satisfactory stability. The models employed were not equipped with rotors and hence no measure of rotor effects was obtained. The characteristics of the nonoverlap fuselage will be discussed first in this paper.

## RESULTS AND DISCUSSION

## Nonoverlap-Fuselage Model

The directional stability characteristics of the basic nonoverlap-fuselage model and tail assembly are shown in figure 2. The fuselage-tail configuration is directionally stable over most of the sideslip range for  $\alpha = -10^\circ$  but becomes progressively more unstable as the angle of attack is increased, being unstable for  $\alpha = 10^\circ$  and even more unstable for  $\alpha = 30^\circ$ . This directional instability at positive angles of attack and the large variation of stability with angle of attack is not desirable.

Investigations indicated the instability to result from two main causes, an extreme variation in the stability of the fuselage alone with angle of attack which does not exist for unbent fuselages and a large destabilizing interference caused by an asymmetrical trailing vortex system. The destabilizing interference is shown for  $\alpha = 10^\circ$  in figure 3. It can be seen from a comparison of the result of summing the characteristics of the fuselage and isolated tail with the characteristics of the fuselage and tail tested in combination that a large destabilizing interference increment exists that is presumably attributable to sidewash influences on the vertical tails.

In an investigation of this matter, tuft-grid tests were made and showed an unusual air-flow pattern behind the nonoverlap fuselage at positive angles of attack. This air-flow pattern consisted of an asymmetric trailing-vortex system that emanated from the vicinity of the fuselage nose and center section and resulted in an undesirable sidewash effect over the fuselage and tail surfaces. Figure 4 shows the position of the tuft grid employed in these tests and the arrangement of this asymmetric vortex system in relation to the fuselage and tails at an angle of attack of  $20^\circ$  for  $20^\circ$  of sideslip. The projection of the vertical tails on the grid is also indicated. The movement of these vortices as the angle of sideslip is changed results in an adverse variation of sidewash that materially reduces the effectiveness of the vertical tails in contributing to directional stability. An interesting feature of the tuft-grid tests was the oscillation of the vortices that occurred near zero sideslip. The action of these oscillating vortices on the fuselage and vertical tail surfaces is conducive to erratic directional behavior in this region.

A number of tests were made in an effort to find a simple correction for the directional instability of this fuselage that would be suitable for application to production machines but with little success. However, the results of some exploratory tests in the Langley free-flight tunnel indicated that spoilers located around the nose of a fuselage, though



causing an appreciable increase in drag, would eliminate a large part of the unstable fuselage yawing moment and thereby materially improve the directional stability. Spoilers of this type were employed at Langley to alter the directional stability characteristics of a flight-test vehicle with considerable success. Figure 5 shows the results of wind-tunnel tests made on the nonoverlap fuselage with spoilers installed. The spoilers employed on this model corresponded to full-scale spoilers 4 inches wide and extended almost completely around the nose of the model. The fuselage-tail configuration with spoilers installed was in general directionally stable at the three angles of attack investigated, whereas the same arrangement without spoilers was unstable for  $\alpha = 10^\circ$  and  $30^\circ$ . Addition of the spoilers resulted in an equivalent parasite-area increase of 5 square feet.

#### Overlap-Fuselage Model

Consider now the other phase of the stability-tunnel investigation of tandem-rotor-helicopter fuselages. As mentioned previously, this work was concerned with the directional stability characteristics of an overlap helicopter fuselage. Figure 6 shows the directional stability characteristics of the basic fuselage pylon configuration for three angles of attack. The fuselage-pylon configuration is directionally unstable at these angles of attack for small angles of sideslip but directionally stable for larger angles of sideslip. A study of this situation and results from a few experiments with an extremely thin pylon indicate that this instability at small angles of sideslip is attributable to a considerable degree to the large trailing-edge angle of the pylon-fuselage combination. Previous work has indicated that large trailing-edge angles on wings result in low lift-curve slopes for the low angle-of-attack range. This effect is associated with movement of the point at which the flow separates from the negative pressure side of the airfoil form near the trailing edge as the angle of attack is changed and is similar to the action of a trailing-edge tab with regard to the pressure changes produced on the airfoil. Experiments showed that a thin pylon largely eliminated the instability at small angles of sideslip because of the magnitude and relative linearity of its lift-curve slope throughout the angle-of-sideslip range. Such an arrangement does not offer a practical solution to this directional-stability problem, however, and a suggestion was made that elimination of the large trailing-edge angle of the original pylon-fuselage arrangement by making the sides of the pylon nearly parallel and the trailing edge blunt might offer an acceptable solution. Previous experiments have shown that similar modifications produce material improvements in lift-curve slope for wings with large trailing-edge angles.

Figure 7 shows the result of a series of experiments made to determine the directional stability characteristics of the overlap-fuselage model equipped with pylons of various degrees of bluntness for  $\alpha = 10^\circ$

and  $\alpha = -10^\circ$ . These results show that blunting the rear of the pylon-fuselage combination was extremely effective in making the fuselage model directionally stable and that a blunt trailing edge having a thickness about 33 percent of the maximum pylon thickness was approximately equal in effectiveness to blunt trailing edges having thicknesses either about 66 percent of or equal to (100 percent) the maximum pylon thickness. The addition to the pylon of the 33-percent blunt trailing edge increased the equivalent parasite area 1.5 square feet.

#### CONCLUSIONS

The results of an investigation of the directional stability characteristics of two tandem helicopter models lead to the following conclusions:

1. The bend in the fuselage had an undesirable influence on the directional stability of the nonoverlap fuselage. The use of spoilers on the fuselage nose eliminated the instability of this fuselage at a cost of 5 square feet of equivalent parasite area.
2. The instability of the overlap-fuselage model at small angles of sideslip was attributable to the large trailing-edge angle of the pylon-fuselage combination, and blunting the rear of the pylon eliminated this directional instability.

TOP AND SIDE VIEWS OF FUSELAGES INVESTIGATED

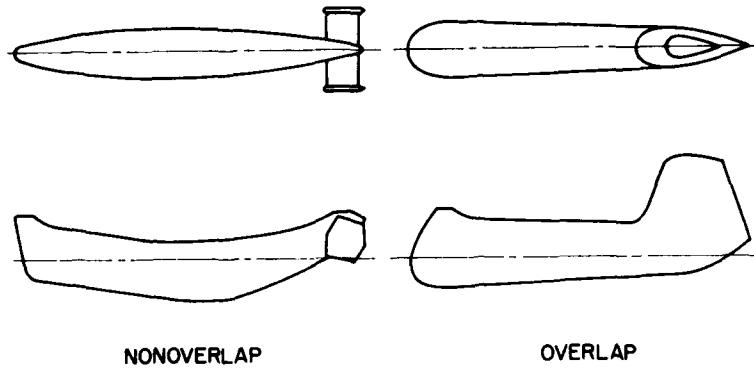


Figure 1

DIRECTIONAL STABILITY CHARACTERISTICS OF NONOVERLAP-FUSELAGE MODEL WITH TAIL

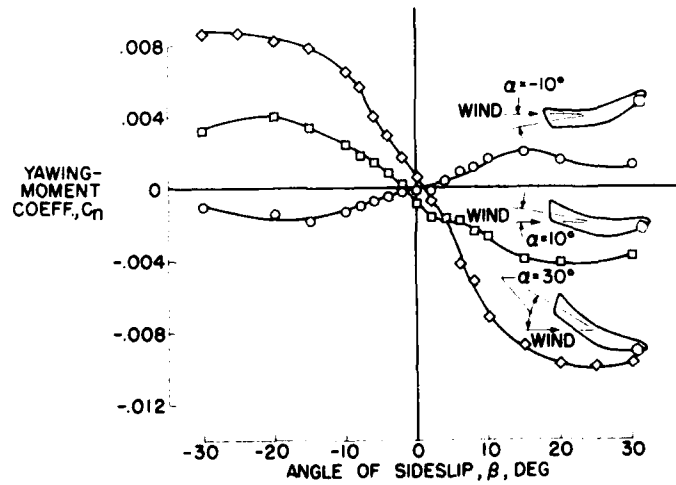


Figure 2

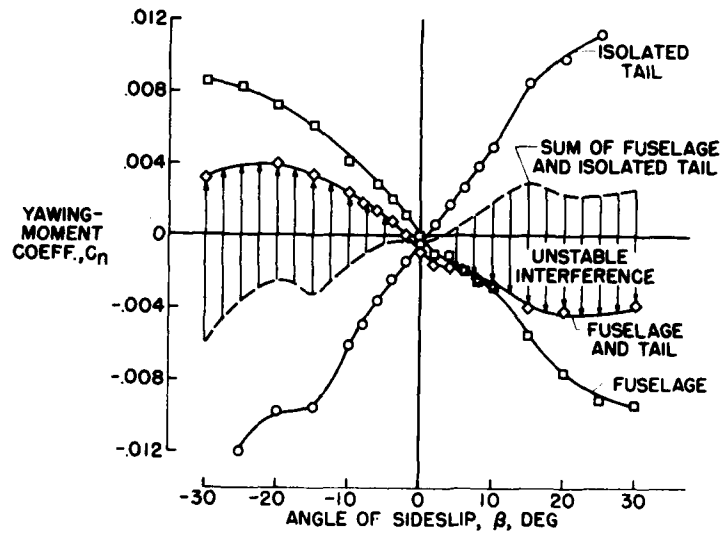
BREAKDOWN OF FUSELAGE AND TAIL CONTRIBUTIONS AT  $\alpha = 10^\circ$ 

Figure 3

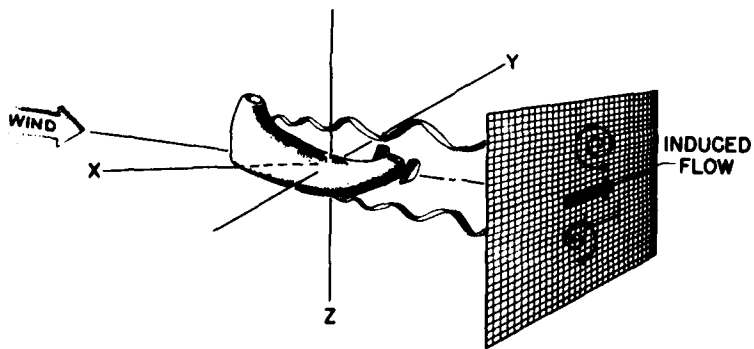
SCHEMATIC OF TUFT-GRID SURVEY  
BEHIND NONOVERLAP FUSELAGE

Figure 4

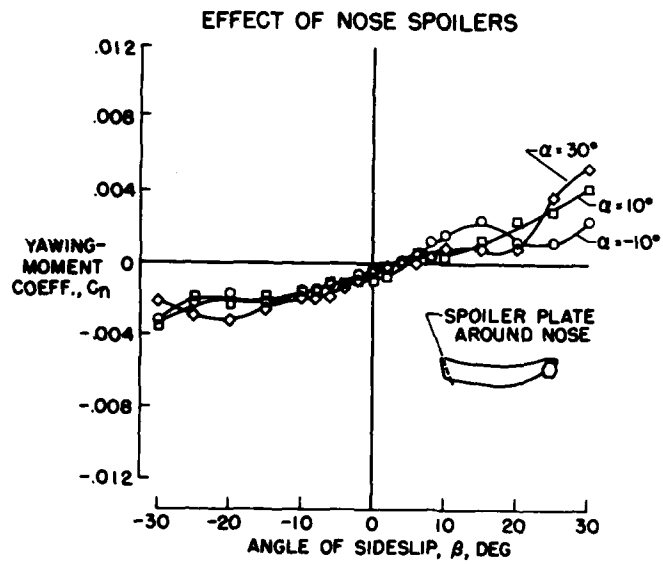


Figure 5

DIRECTIONAL STABILITY OF OVERLAP-FUSELAGE MODEL  
WITH PYLON

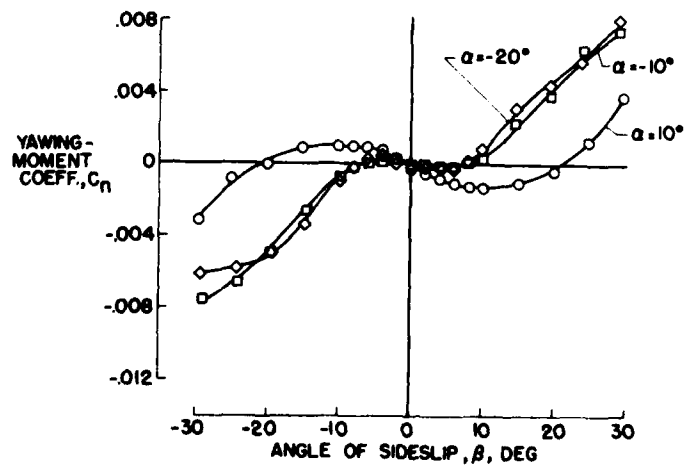


Figure 6

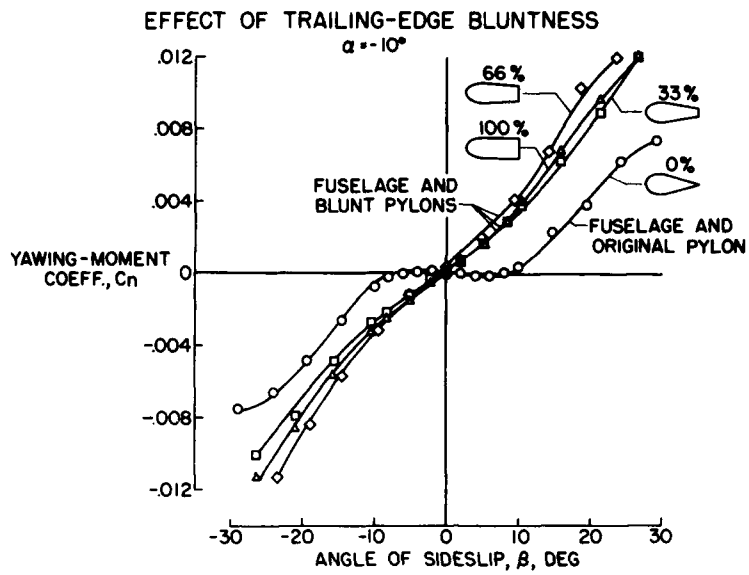


Figure 7(a)

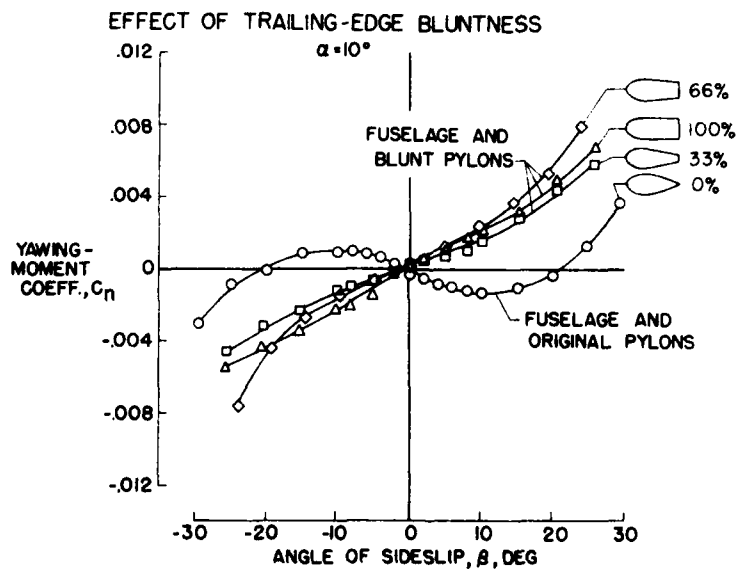


Figure 7(b)

FLIGHT TESTS OF A MAN STANDING ON A  
ROTOR-SUPPORTED PLATFORM

By P. R. Hill

Langley Aeronautical Laboratory

23

The one-man helicopter, which is familiar to all, is usually thought of as an ordinary helicopter with overhead rotor, but reduced in size. An entirely different concept for a one-man helicopter is shown schematically in figure 1 in which the man stands on a platform over the rotor instead of hanging under it. He balances himself on the platform in about the same way that he balances when standing on the ground and uses the same reflex action and balancing mechanism that he used in standing on the ground. Since balance is accomplished by the direct action of the feet, the control column and accompanying linkages are eliminated; this amounts to a basic simplification. This stand-on scheme was proposed by Mr. Charles H. Zimmerman.

The possibilities of such a machine were sufficient to warrant a check of its feasibility. The first step was to test the balance principle involved in the stand-on-type machine. To review briefly the balance principle, the lift is treated as a thrust vector, and attention focused on its direction. If the machine and flyer are in trim, the flyer controls the thrust vector with his feet so that it passes through the combined center of gravity. If out of trim, the flyer puts moments on the machine with his feet to cause the thrust vector to create righting moments about the center of gravity as required. The action is qualitatively the same as that of balancing when standing on the ground. For example, if a man standing on the ground is leaning forward, he presses down with his toes which brings him to an erect attitude. If he is in flight on a platform and is leaning forward, he presses down with his toes. This action has a direct tendency to rotate his body to an erect position. In addition, the platform gives way, producing a rotation of the lift vector which creates an additional moment about the center of gravity in the proper direction.

In order to check the balance principle in as simple a manner as possible, flight tests, reported in reference 1, were made of a man standing on an air-jet-supported platform. Figure 2 is a photograph of a man standing on an air-jet-supported platform. You can see the air nozzle on the bottom of the platform between the four small legs to the platform. Compressed air is supplied through the two fire hoses attached. A slack safety line is attached to an overhead cable not visible in the photograph. Tests like the one shown in figure 2 show that the balance

principle is valid. A man can balance himself on a thrust vector, and with little practice in this case.

In order to obtain a practical scheme with better economy the diameter of the jet must be increased. Although the kinetic energy in the air jet is equivalent to about 400 horsepower, a 7-foot-diameter rotor would require only about 35 horsepower. A teetering rotor was used in order to overcome the gyroscopic couples that would otherwise affect the platform. This rotor was driven by air jets at the tips in order to avoid any appreciable unbalanced torque.

Figure 3 is a photograph of the test vehicle. At the center of the vehicle is a small platform on which the flyer stands. Two foot pads which locate the flyer's feet are visible in the figure. Air comes to the vehicle through two jack-hammer hoses. The air goes through a hollow rotating shaft, out through the teetering pin, through the hollow hub, and out through a 7/8-inch-diameter tube in the blade to the rotor tip where it is directed toward the trailing edge to drive the rotor. The rotor can be seen beneath the pilot's platform. The machine has four legs and also has some superstructure. The pilot has a guard ring to keep him from falling in case of accident. The remainder of the superstructure actually served no useful purpose. A small torque compensation valve, attached to the guard ring, controls the flow of air through two small tubes which run out alongside two opposite legs and direct air in a direction opposite to the direction of rotor rotation to counteract the torque due to friction in the rotor bearing. The weight of the machine is 140 pounds.

The only items of importance on the vehicle which are not visible in figure 3 are the damping springs. A helicopter having a teetering rotor below the center of gravity has a negative damping. This is illustrated in figure 4. In the bottom of the figure in the sketch labeled negative damping component, the circular arrow represents a rate of rotation of the platform. The rate of rotation causes a lag of the rotor plane. The rotor lag relative to the platform causes the thrust vector to pass to one side of the center of gravity, creating a moment tending to increase the rotation rate. This is negative damping. In order to overcome the negative damping, two springs are fastened between the shaft and rotor in such a manner that they tend to restrain any relative motion between the rotor and platform. Then, when the rotor plane lags behind the platform, the action of the springs in restraining the platform amounts to a positive damping component. Flights made without damping springs resulted in some tendency for oscillations to build up. Flights made with the springs installed appeared to be satisfactory.

Figure 5 shows two flyers making typical indoor test flights. The air throttle was controlled by an operator located on a nearby balcony. Safety lines were attached both to a parachute harness worn by the flyer



[REDACTED]

and to the guard rail. Slack in these lines was adjusted to the proper value by controlling an overhead hoist. Numerous flights were made from floor level to 6- or 7-foot elevation above the floor with satisfactory results. The flyer could hover over a spot or move about at will within the confines of the safety lines and air hoses. Motions were accomplished by leaning and tilting the rotor slightly, just as in a conventional helicopter.

Tests were made out of doors in both calm and windy conditions. An overhead cable about 20 feet in the air was used as an attachment point for the safety lines. It was demonstrated that control over the machine could be maintained in rough gusty air with velocities varying rapidly from 10 to 25 miles per hour with one extreme reaching 30 miles per hour. Small changes in elevation above ground level occurred at a given throttle setting as a result of the changes in wind velocity.

Some physical effort is required to fly the machine in very rough air. In order to reduce this effort a refinement was introduced in which the heavy steel frame was isolated from the foot platform by connecting the frame to the platform with sponge rubber. This produced a machine which was physically easier to fly in rough air. A half-hour flight was made with it in rough, gusty air without tiring the flyer. A more complete description of the flights made and of the test results are given in reference 2.

The scope of this investigation did not include the application of a practical power plant. The program was limited to basic research and did not include development. However, the moment of inertia of the present machine is believed to be sufficient to simulate a complete practical machine.

In conclusion, it has been shown, within the obvious limitations of the tests, that the stability and controllability of a spring-restrained teetering rotor-supported platform were satisfactory.

#### REFERENCES

1. Zimmerman, C. H., Hill, Paul R., and Kennedy, T. L.: Preliminary Experimental Investigation of the Flight of a Person Supported by a Jet Thrust Device Attached to His Feet. NACA RM L52D10, 1953.
  2. Hill, Paul R., and Kennedy, T. L.: Flight Tests of a Man Standing on a Platform Supported by a Teetering Rotor. NACA RM L54B12a, 1954.
- [REDACTED]

SCHEMATIC OF ROTOR-SUPPORTED PLATFORM

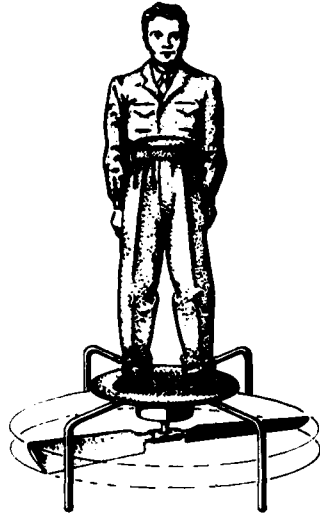


Figure 1

JET-SUPPORTED PLATFORM



Figure 2

TEST VEHICLE

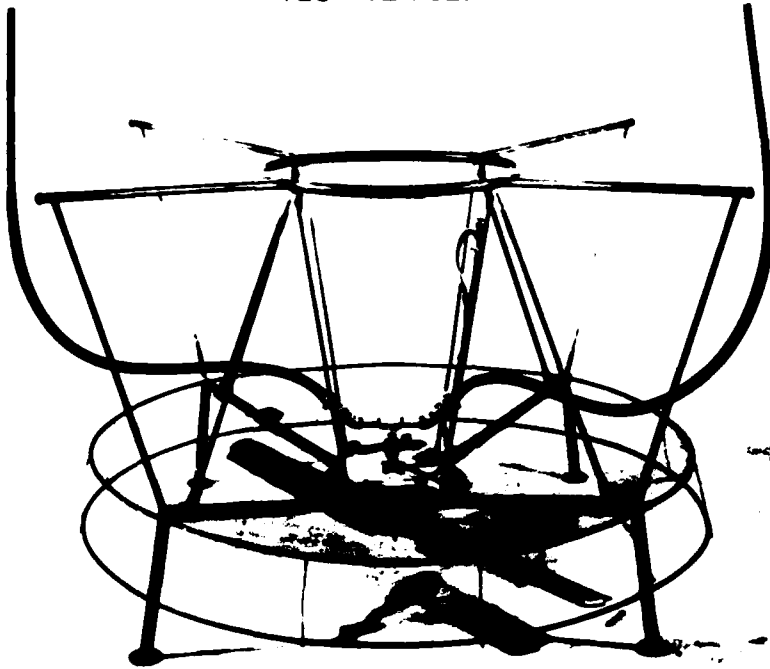


Figure 3

DAMPING COMPONENTS

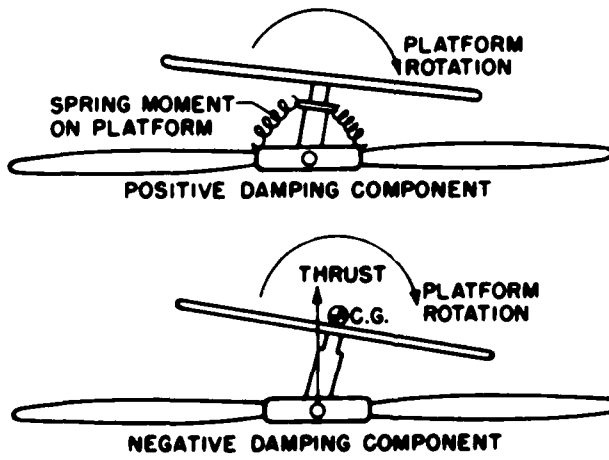


Figure 4



TYPICAL FLIGHT TEST

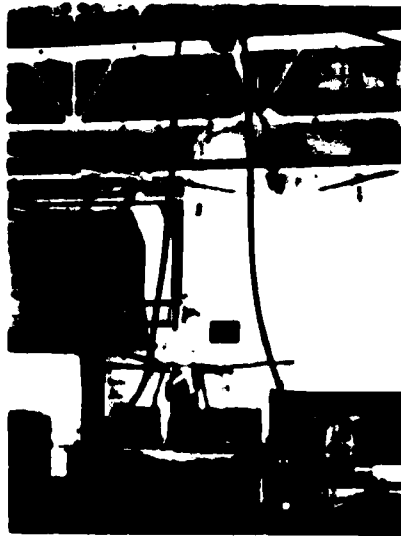


Figure 5(a)

TYPICAL FLIGHT TEST

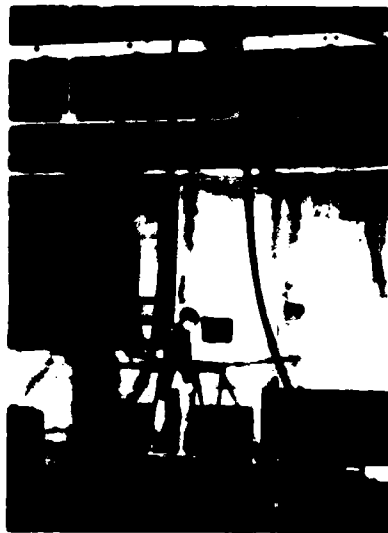


Figure 5(b)

[Redacted]

**LOADS, STRESSES,  
VIBRATION, AND FLUTTER**

A STUDY OF NORMAL ACCELERATIONS AND OPERATING CONDITIONS  
EXPERIENCED BY HELICOPTERS IN SERVICE USAGE

By Marlin E. Hazen and Almer D. Crim

Langley Aeronautical Laboratory

INTRODUCTION

A knowledge of the operating loads and corresponding flight conditions is necessary in establishing a more rational basis for helicopter design. The maximum loads likely to be encountered due to gusts or maneuvers must be determined, and it is desirable to know the percentage of flight time spent in the various operating conditions as an aid in more realistically estimating the service life of certain critical helicopter components.

With this in mind, the National Advisory Committee for Aeronautics has undertaken a program aimed at determining the normal accelerations and associated flight conditions encountered by helicopters undergoing service usage in several different types of operations, both commercial and military.

RESULTS AND DISCUSSION

Data for this investigation are obtained by means of the NACA helicopter VGH recorder. (See fig. 1.) This instrument, which weighs only 15 pounds, records airspeed, normal acceleration, and altitude as a function of time. The total recording time for each film drum is between 15 and 20 hours.

Shown in figure 2 is a typical helicopter VGH record; vertically are the altitude, airspeed, and normal acceleration traces, while horizontally is the time scale in minutes. From records similar to this the percentage flight time spent in the three major flight conditions (take-off and climb, en route, and landing approach) can be determined, as well as the time spent at various speeds. Accelerations resulting from certain specific maneuvers such as the take-off, transition from climb to level flight, transition from level flight to descent, the landing flareout, and landing impact can also readily be determined.

Results of the initial investigation have been reported in reference 1, where the results were analyzed from about 1,700 flights or

253 hours of flying time by a helicopter engaged in airmail operations in the vicinity of Los Angeles and its suburbs.

The present results are based on the data from the Los Angeles installation plus more recent data obtained from an airmail helicopter operating in the vicinity of Chicago, a military pilot-training helicopter used by the Army Ground Forces at Fort Sill, Oklahoma, and a limited number of records from other military operations.

Table I shows the number of flights, flying hours, and average time per flight for each operation analyzed to date. Also included as a matter of interest is the type of helicopter used by each operator. Although there has been no specific survey made to determine whether the type of helicopter used affects the results, it appears that the primary differences in acceleration levels are due to the type of operations for which a helicopter is used.

Among the factors affecting the fatigue life of rotor system components is the percentage time spent at different airspeeds and in different flight conditions or maneuvers. Table II provides a breakdown of the percentage time spent in various speed brackets for the three major operations analyzed to date, that is, the two airmail operations and the military pilot-training operation. Note how the two airmail helicopters spend a major portion of their flight time in the vicinity of about 60 to 85 miles per hour, whereas the speed range of the military pilot-training helicopter is somewhat lower, being primarily in the vicinity of 40 to 60 miles per hour. Similarly, table III shows the percentage time spent in each of the three major flight conditions (take-off and climb, en route, and the landing approach) and as before, there is a notable similarity between the two airmail operations as compared with the military pilot-training operation.

Figure 3 shows a comparison of the normal accelerations experienced by the two airmail operations and the military pilot-training operation. In this figure, as in all subsequent figures, the vertical scale represents the number of flights required to equal or exceed the given value of acceleration increment, whereas the horizontal scale is the acceleration increment  $\Delta a_n$  in g units.

From the similarity of the operating conditions, it was expected that the acceleration levels experienced by the two airmail helicopters would be about the same; however, they are different, with the acceleration level of the Chicago helicopter airmail operation being more severe. A further analysis of the records was therefore made and the results indicated that the air was considerably rougher at Chicago (particularly during the months of November and February) than any encountered in the Los Angeles area. A further breakdown of the data into the three flight conditions (take-off and climb, en route, and landing

approach) shows that the primary difference between the Los Angeles and Chicago helicopter airmail operations occurred during the en-route portion of their flights, where the accelerations appear to be due almost entirely to rough air, with the Chicago helicopter airmail operation having the higher acceleration level. Other interesting points brought out by the analysis of flight conditions were that a large portion of the military pilot-training flight loads were incurred in the landing-approach condition, and that for all three operations the landing-approach condition, which consumed less than 20 percent of the total flight time, contributed at least as many accelerations (particularly the larger ones) as any other flight condition.

The largest gust-load increment recorded to date is 0.90g from the Chicago operation, whereas the largest maneuver-load increments have been 1.4g and -1.25g, both recorded by the military pilot-training installation. No comparably large negative gust-load values have been noted. However, there are indications that gusts may produce stability and control difficulties which may in turn result in fairly large maneuver-load factors.

Figure 4 shows the breakdown of the landing impact accelerations for each of the three operations. The general trend noted for the flight loads is again evident, with the military pilot-training operation experiencing by far the largest loads.

Figure 5 shows the summary plot of all landing and flight load increments (both positive and negative) from all operations analyzed to date. The negative landing loads apparently result from the rebound from initial impact. Note the similarity between the positive and negative flight loads as compared with the lack of similarity in the landing impact accelerations.

The high landing impact accelerations may be a problem when preceded by a loss of rotor lift just prior to landing impact. This may be particularly true for the tandem-type helicopter with the main landing gear midway between rotors where the added inertia effects can give rise to high structural stresses.

Table IV shows the results of an analysis of the cases where the normal acceleration increment just prior to landing impact was noticeably less than 1 g. A careful study of these cases seemed to indicate that they were probably caused by an early landing flareout from an autorotational descent, followed by either a reduction in collective pitch or a loss of rotor rotational speed, and up to a 70-percent loss of lift just prior to impact. Incidentally, another loss of rotor lift may originate from a loss of vertical velocity at the bottom of the impact stroke, when the helicopter's vertical descent goes to zero. Rough calculations were made by assuming constant lift slope and induced flow,



and a vertical descent velocity of 10 feet per second. The resulting answers indicate that up to a 30-percent loss of rotor lift can be expected as the vertical descent velocity becomes zero.

It is hoped that this problem may be investigated in more detail, with the characteristics of both single-rotor and tandem-rotor helicopters being studied.

The scope of the helicopter VGH program is being expanded to include the correlation of blade bending-moment levels with certain specific flight conditions and air turbulence levels.

#### CONCLUSIONS

The following conclusions may be drawn:

1. The military pilot-training operation has produced by far the most consistently high flight and landing impact accelerations of any operation sampled to date.
2. Similar types of operations result in similar operating conditions and when other factors such as rough air are eliminated it is found that similar types of operations apparently produce about the same frequency and magnitude of acceleration.
3. The landing approach has produced as high an acceleration level as any other flight condition encountered in normal operations.

#### REFERENCE

1. Crim, Almer D., and Hazen, Marlin E.: Normal Accelerations and Operating Conditions Encountered by a Helicopter in Air-Mail Operations. NACA TN 2714, 1952.

TABLE I

## FLIGHT-TIME COMPARISON FOR ALL OPERATIONS ANALYZED

OPERATION	TOTAL NO. OF FLIGHTS	TOTAL FLIGHT TIME, HR	AV. TIME PER FLIGHT, MIN	HELICOPTER
MILITARY PILOT TRAINING	1,385	161.9	7.0	BELL H-13 E
LOS ANGELES, AIRMAIL	1,691	253.0	8.0	SIKORSKY S-51
CHICAGO, AIRMAIL	963	140.5	8.7	BELL 47 D
ALL-WEATHER TESTING	152	25.3	10.0	SIKORSKY H-19
NAVY, NORFOLK	134	37.4	16.9	PIASECKI HUP-1
TOTAL	4,325	618.1		

TABLE II

## SPEED COMPARISON

OPERATION	PERCENT TOTAL FLIGHT TIME AT $V_i$				
	0 TO 20 MPH	20 TO 40 MPH	40 TO 60 MPH	60 TO 80 MPH	> 80 MPH
CHICAGO, AIRMAIL	2.0	3.0	8.0	63.0	24.0
MILITARY PILOT TRAINING	15.9	12.5	45.2	26.4	—

OPERATION	PERCENT TOTAL FLIGHT TIME AT $V_i$			
	0 TO 20 MPH	20 TO 65 MPH	65 TO 85 MPH	> 85 MPH
LOS ANGELES, AIRMAIL	5.3	18.7	67.6	8.4

TABLE III  
FLIGHT-CONDITION COMPARISON

OPERATION	PERCENT TOTAL FLIGHT TIME IN—		
	TAKE-OFF AND CLIMB	EN ROUTE	LANDING APPROACH
CHICAGO, AIRMAIL	14.0	77.0	9.0
LOS ANGELES, AIRMAIL	14.5	73.8	11.7
MILITARY PILOT TRAINING	17.9	62.6	19.5

TABLE IV  
NEGATIVE ACCELERATION INCREMENTS  
SURVEY OF 1,000 LANDINGS

NO. OF LANDINGS	ACCEL. INCREMENT, $\Delta a_n$ , g UNITS
14	-0.25
12	-.30
4	-.35
1	-.65
1	-.70

NACA HELICOPTER VGH RECORDER

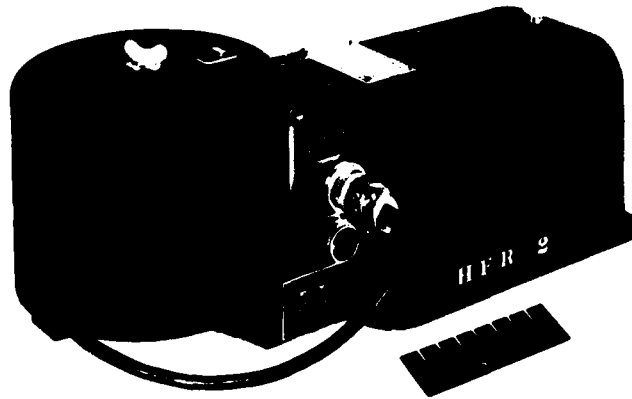


Figure 1

TYPICAL HELICOPTER VGH RECORD

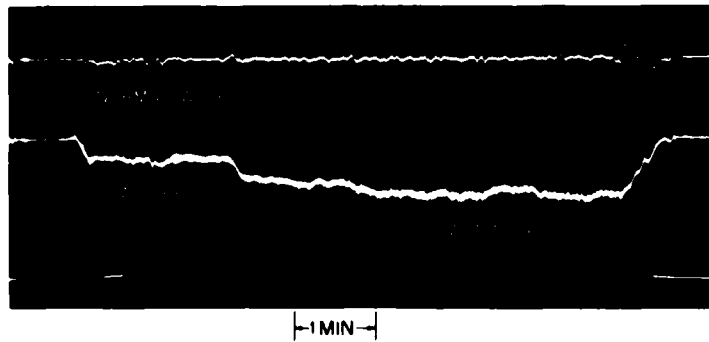


Figure 2

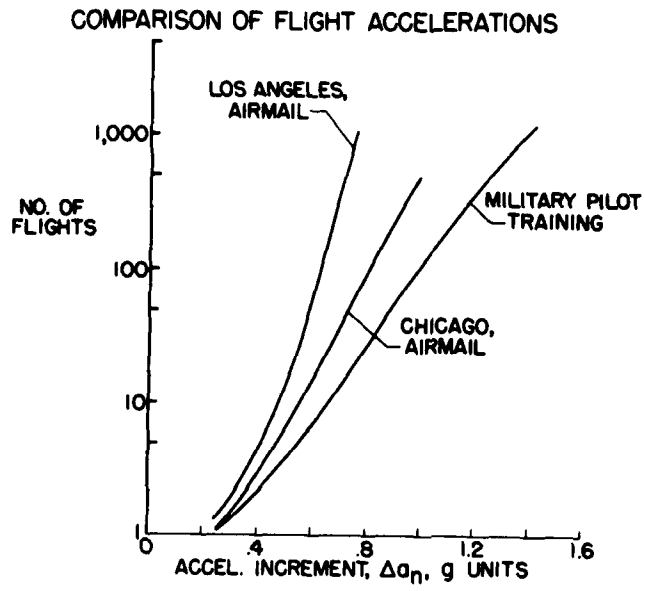


Figure 3

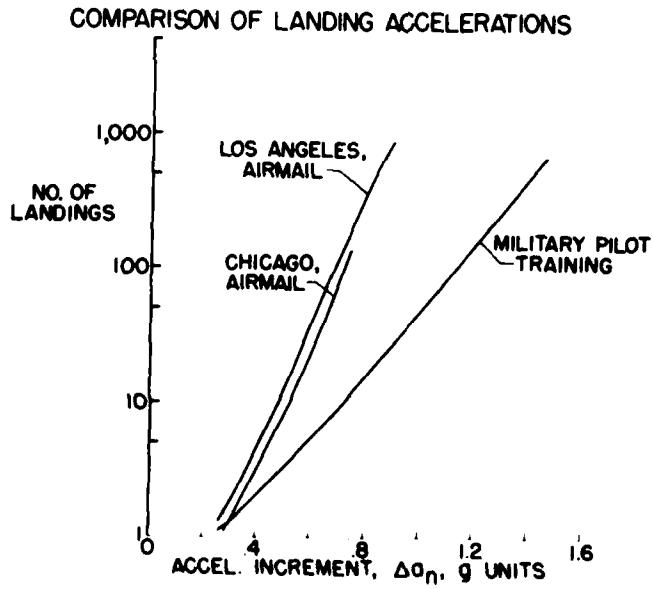


Figure 4

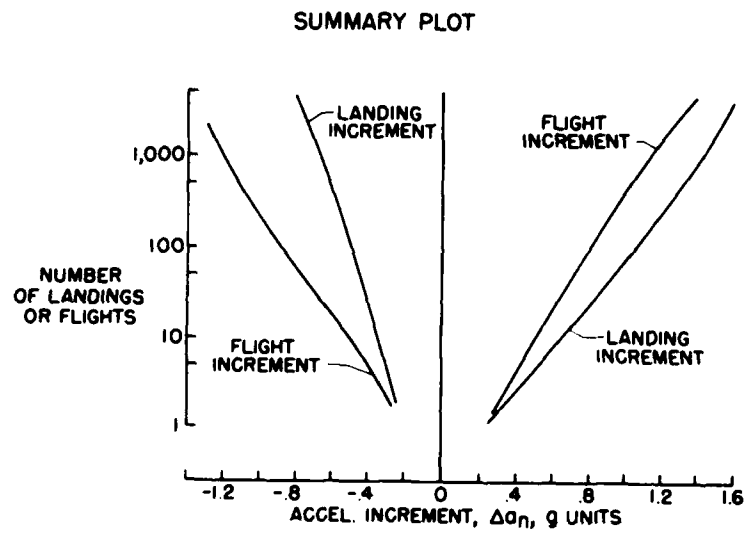


Figure 5

NORMAL ACCELERATIONS DUE TO MANEUVERS AND GUSTS  
AS STUDIED IN FLIGHT

By Almer D. Crim and F. B. Gustafson

Langley Aeronautical Laboratory

INTRODUCTION

The maximum loads attainable in flight are, of course, an important factor to the helicopter designer and to the operator. In addition, there seems to be current problems associated with flight-test demonstration of maximum load factors. Since available evidence indicates that such loads may be higher for new designs and configurations, it is of interest to determine the following: the largest load factors that can be attained by current types, the maneuvers that are most likely to result in such loads, and any correlation of the results that might permit predictions relating to maximum loads for new designs.

With these objectives in mind, a series of flight tests were made in two small, single-rotor helicopters (ref. 1). In each series, the helicopter was put through specific maneuvers wherein the severity of the maneuver was progressively increased by increasing the magnitude of control deflection, the rate of deflection, or the time the deflection was held. The maneuvers included jump take-offs, collective-pitch pull-ups at various airspeeds in both powered and autorotative flight, cyclic-pitch pull-ups at several flight conditions, and combined cyclic and collective pull-ups in which different phasings of the control were used.

DISCUSSION

The response of the helicopter, as measured by the change in normal acceleration, is fundamentally different for the cyclic and collective types of control and is illustrated in figure 1. For cyclic-pitch changes, most of the acceleration develops as a result of angle-of-attack changes of the helicopter, and appreciable time (2 or 3 seconds) is needed to reach the maximum value. For collective-pitch increases, the thrust increases immediately and then begins to drop off because of a reduction in rotor angular velocity and changes in the induced velocity and vertical velocity of the helicopter.

If load factors are defined as the ratio of normal acceleration to the acceleration due to gravity, values around 2.5 were found to be attainable by either cyclic- or collective-pitch maneuvers. It might be inferred that these loads, and perhaps even larger ones, could be obtained more readily by combining the cyclic- and collective-control displacements with suitable phasing. This was found to be the case, and the largest flight loads, as a group, resulted from cyclic pull-ups followed in a few seconds by increased collective pitch. Figure 2 shows a typical response to such a maneuver. The pull-up was initiated by rearward deflection of the cyclic-pitch control and continued by application of the collective-pitch control at about the point where maximum acceleration due to the cyclic-pitch control alone would have occurred. The additive effect of the two accelerations is apparent. When the same maneuver was performed by simultaneous application of the two controls, it was found that the increased thrust due to the collective-pitch control dropped off so rapidly that it contributed little to the maximum acceleration attained.

It is of interest to compare the results of these tests with a relatively simple theoretical method of predicting the maximum loads that can be obtained, from aerodynamic considerations, for a given flight condition. The method, which is described in reference 1, assumes that the maximum thrust of the rotor would be obtained if all blade sections were operating at maximum lift coefficient and that the greatest load factor attainable would be predicted by the ratio between the maximum section lift coefficient and the mean lift coefficient for the particular operating condition. Such a comparison is shown in figure 3. The theoretically predicted relation between mean lift coefficient at trim and the maximum acceleration is shown for one of the test helicopters by the solid line and for the other, by the dashed line. Both were small, single-rotor helicopters, one having a 3-blade flapping rotor, the other, a 2-blade teetering rotor. Based on other flight and wind-tunnel tests, a maximum lift coefficient of 1.2 was assumed in computing both curves, and the largest acceleration values obtained from the flight tests just described are shown for comparison. Of particular interest is the indication that, for designs operating at low mean lift coefficients, there is a possibility of much higher load factors than those shown herein. Conversely, designs operating at high mean lift coefficients, such as load-lifter or cargo types, may not require design values as high as those shown.

Perhaps, it should be emphasized that limitations other than aerodynamic may make it difficult or dangerous to reach the maximum values thus predicted. Feedback of forces into the controls, large amounts of friction, heavy stick forces, and problems of clearance between rotor blades and fuselage are among the reasons why it may be undesirable or impractical to demonstrate the maximum predicted load factors in a particular case.



Another source of helicopter loads is atmospheric turbulence, and some limited flight tests have been made for the purpose of studying the helicopter response to gusts. Since a great deal of information is available on the response of airplanes to gusts, one approach was to fly an airplane and a helicopter in formation in rough air and to compare both the measured and calculated results. If the response of the two machines to a unit gust velocity is calculated by using the simple approach of neglecting alleviation factors and by considering the gust to produce only an angle-of-attack change, the results are as shown in figure 4. The acceleration increment per unit gust velocity is plotted against forward speed and for the airplane shows the familiar sloping straight line. In contrast, the value for the helicopter is almost constant for the higher speeds. The lower end of the helicopter curve is shown as a dashed line to indicate that it is more susceptible to the assumptions used. However, particularly at speeds common to this particular airplane and helicopter, a good starting point is provided for predicting the ratio of helicopter accelerations to airplane accelerations. At 80 miles per hour, for example, the response of the helicopter is predicted to be about 70 percent of that of the airplane, solely because of the difference in lift-curve slopes and physical characteristics of the two machines.

Since there has been much speculation as to the gust alleviation provided by hinged rotor blades, the airplane and helicopter were flown side by side in rough air and the normal accelerations of each measured. The results are shown in figure 5. This figure illustrates the gust experience of the airplane and the helicopter in terms of the average number of miles flown to equal or exceed a given acceleration. At any given distance, the ratio of the two values may be compared with that predicted from the curves of figure 4. The calculated ratio, at 80 miles per hour, was about 0.7 and the flight test ratio, about 0.6; these ratios indicate a slightly greater gust alleviation for the helicopter than for the airplane, at least at this particular speed.

A study of the helicopter flight records obtained in the side-by-side comparison also indicated a substantial variation of acceleration with airspeed. Since the simply calculated curve shown in figure 4 did not indicate such a variation, particularly at higher speeds, additional flight tests were made in which the helicopter was flown in gusty air at different airspeeds over the same ground path. Some results of these flight tests are shown in figure 6 where the number of acceleration increments encountered between 0.1g and 0.2g is shown for various airspeeds. At 15 knots, no values within this range were recorded; at 45 knots, there were 11; and at 75 knots, there were 31. Not enough of these data are available for them to be statistically useful, but they do show a definite trend with airspeed, a trend which indicates that reducing the airspeed should be an effective method of reducing gust effects in rough air. Also, although these studies have indicated gusts to be generally of secondary importance in regard to maximum load factors

for present designs, it appears that, when gust alleviation factors are required, the effect of airspeed should be considered.

#### CONCLUSIONS

Some of the conclusions that may be drawn from this study are as follows:

1. New designs capable of operating at low mean lift coefficients may be subjected to large load factors. Conversely, a possibility of saving weight presents itself where the design permits high mean lift coefficients.
2. It may not always be desirable or practical to demonstrate maximum predicted loads.
3. When gust loads are a design factor, the effect of airspeed may have to be considered in regard to the alleviation factor used.

#### REFERENCE

1. Gustafson, F. B., and Crim, Almer D.: Flight Measurements and Analysis of Helicopter Normal Load Factors in Maneuvers. NACA TN 2990, 1953.

## RESPONSE TO CYCLIC- AND COLLECTIVE-PITCH CONTROL

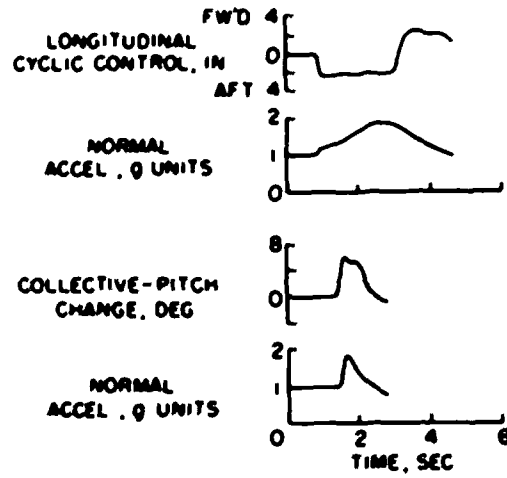


Figure 1

## RESPONSE TO COMBINED CONTROL

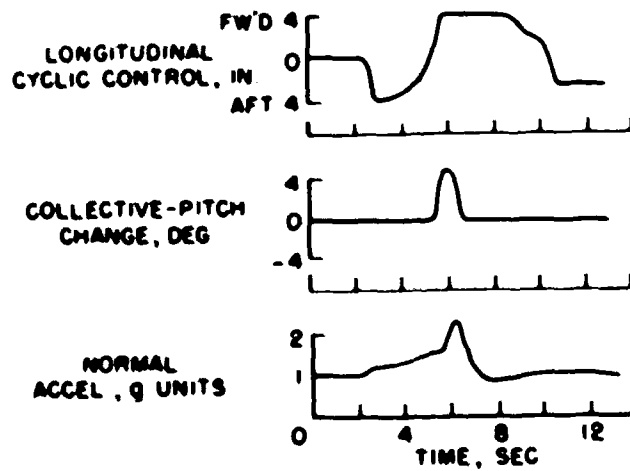


Figure 2

COMPARISON OF THEOR. AND FLIGHT-TEST VALUES OF  
MAX. LOAD FACTOR

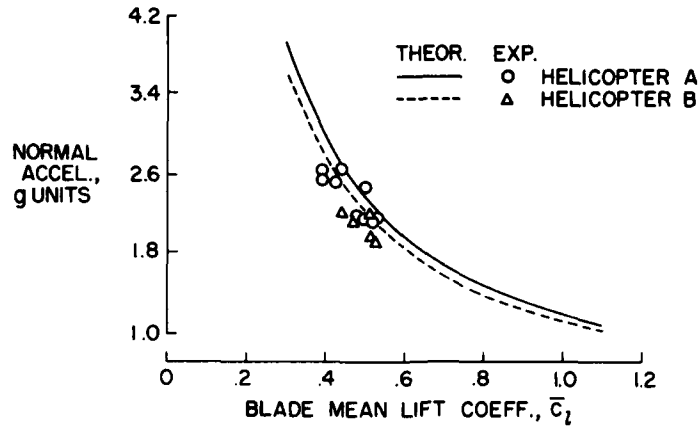


Figure 3

ACCEL. INCREMENT PER UNIT GUST VELOCITY

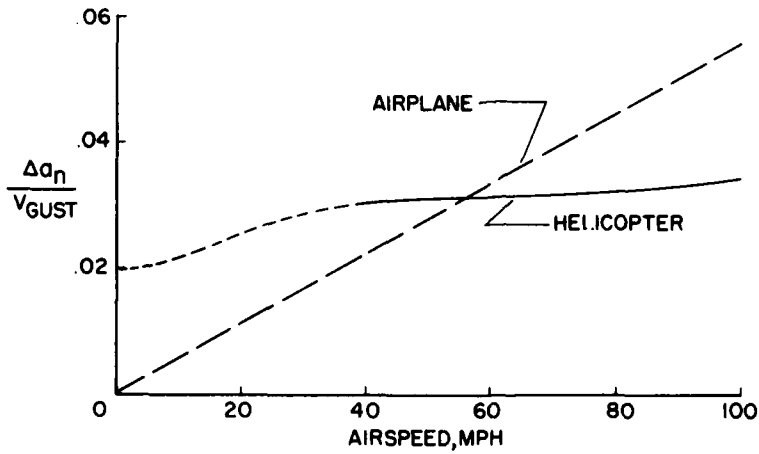


Figure 4

GUST EXPERIENCE OF HELICOPTER AND AIRPLANE IN  
FORMATION FLIGHT AT 80 MPH

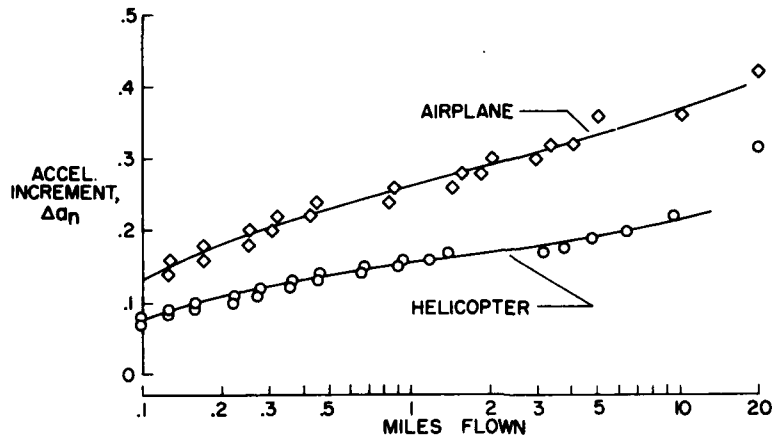


Figure 5

NO. OF ACCEL. INCREMENTS BETWEEN 0.1g AND 0.2g

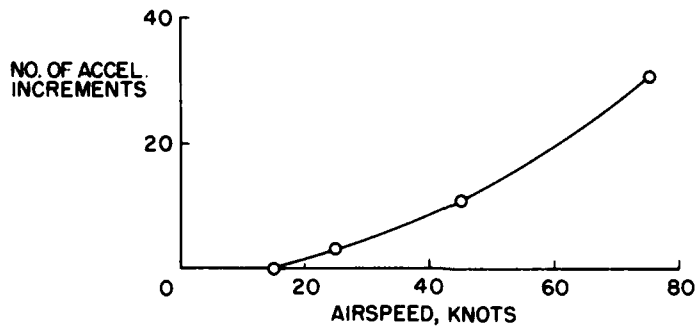


Figure 6

PRELIMINARY EXPERIMENTS ON THE EFFECTS OF GUSTS  
ON HELICOPTER BLADE BENDING MOMENTS

By Domenic J. Maglieri and Joseph W. Jewel

Langley Aeronautical Laboratory

INTRODUCTION

When the effects of gusts on helicopter loads were studied, the flight test results discussed in the previous paper by Almer D. Crim and F. B. Gustafson were supplemented to some extent by tests on the Langley helicopter test tower and by model tests in the Langley gust tunnel. The purpose of these exploratory tests was to obtain a more detailed study of the effects of gusts in producing loads on helicopter blades. In this paper, some of the results obtained from these two facilities are discussed. A more detailed study of the tests conducted on the Langley helicopter test tower is presented in reference 1.

DISCUSSION

A photograph of the full-scale blade used for the outdoor tests on the Langley helicopter test tower is shown as figure 1. This was an actual helicopter blade and was used on a conventional three-bladed rotor with the flapping hinges located at the center of rotation. Strain gages were located at the 25-, 37-, 50-, 62-, 75-, 85-, and 97-percent spanwise radius stations in order to measure bending strains in the flapwise direction. When the tests were conducted, time-history records of bending strain were taken at zero thrust and at 2,100 pounds of thrust in calm air and in gusty winds of about 26 miles per hour. The results obtained are shown in figure 2.

In figure 2 is plotted the total vibratory amplitude of the bending moments against percent of the blade radius for three combinations of rotor thrust and wind condition. The upper curve of figure 2 shows the vibratory bending-moment amplitudes for the loaded rotor operating in gusty winds. The large strain amplitudes shown for this condition are the combined effects of dissymmetry in the rotor downwash under lifting conditions at a simulated flight speed of 26 miles per hour plus the contribution of the gusts. In an attempt to isolate the effects of the gusts, tests were made at zero thrust and in gusty winds. The resultant vibratory bending moments are shown by the middle curve of figure 2. Part of the bending amplitudes shown by this curve may be due to inherent

vibrations in the system, and in order to obtain a measure of these vibrations, tests were made at zero thrust in zero winds. The lower curve of figure 2 for these test conditions shows that there are some vibrations present. The difference in the level of the two lower curves will be considered to be due to gusts, the lower curve being used as a base line. The spread shown is only a small part of the amplitude indicated by the upper curve. On the basis that this gust contribution is independent of rotor thrust, it has been concluded that gusts contribute at most about 20 percent of the total vibratory moments experienced at the rated rotor thrust of 2,100 pounds and in gusty winds averaging 26 miles per hour. Higher wind velocities were not obtainable to determine the effect of the gusts at greater speeds.

Some of the highlights of the tests from the Langley gust tunnel which were made on a teetering or seesaw rotor are considered next. A photograph of the model blade is shown as figure 3. The weight and stiffness characteristics of the blade are within the range of values used in present-day design. Strain-gage stations were located at 8 percent and 66 percent of the blade span as indicated by the cross marks on the blade in order to measure bending strains in the flapwise direction. Only the data for the outboard station are considered herein.

Figure 4 illustrates the test procedure in the gust tunnel and some of the results. In the upper part of figure 4, the gust tunnel is represented by the crosshatched area and is simply an open-throat, low-velocity wind tunnel. It produces a vertical jet of air which has an approximate rectangular velocity profile as shown by the arrows. In order to obtain the data, the rotor was mounted on a rotating arm and moved through the sharp-edge gust at various forward velocities and with a constant rotor angular velocity. Time-history records of bending strain similar to the one shown in figure 4 for the given conditions of rotor-shaft axis tilt  $\alpha$ , blade pitch angle  $\theta$ , rotor angular velocity, gust velocity  $U$ , and advance ratio  $\mu$  were taken.

From this record of bending strain, the various bending frequencies present throughout the run can be noted. The gust velocity of 5 feet per second shown for this run represents a gust of about 15 feet per second when scaled up to full-scale values.

From a series of records similar to the one shown in figure 4 for different advance ratios, the maximum amplitude of the vibratory bending components for the steady-flight condition outside the gust and for the transient condition at the time the rotor entered the gust have been read. The values read are represented by the maximum width of the envelope for the test conditions outside and in the gust. These vibratory bending moments are plotted against the ratio of forward velocity to hovering-induced velocity in the lower part of figure 4.

The curve designated by the circle symbols in figure 4 shows the variation of the maximum vibratory components with the velocity ratio for the steady-flight conditions outside the gust. The induced flow in hovering was small because of the low value of blade pitch angle used in the tests. Accordingly, the peak value in this plot represents a relatively low forward velocity. The curve designated by the square symbols in figure 4 shows the maximum vibratory bending moments which were experienced during the transient condition at the time the rotor entered the gust. The difference between the two curves represents the amplification in the maximum vibratory bending moment due to the gust at various forward velocities. From figure 4, it can be seen that the spread between the two curves is small for the complete range of velocity ratio tested. It appears evident, therefore, that the effect of the gust on the maximum vibratory bending moments is fairly small for the teetering rotor when compared with the vibratory bending moment excited at forward speeds.

#### CONCLUDING REMARKS

In summary, the preliminary tests on helicopter blades on the Langley helicopter test tower and in the Langley gust tunnel indicate that, for the conditions investigated, gusts contribute only about 20 percent to the amplitudes of the vibratory bending moments ordinarily experienced in forward flight for the flapping or teetering rotor blades. Although these amplifications of maximum vibratory bending moment due to gusts appear secondary, they may be important from a fatigue standpoint. The test results are of a limited scope, but further experimental test programs may shed more light on this subject.

#### REFERENCE

1. Jewel, Joseph W., Jr., and Carpenter, Paul J.: A Preliminary Investigation of the Effects of Gusty Air on Helicopter-Blade Bending Moments. NACA TN 3074, 1954.



FULL-SCALE BLADE



Figure 1

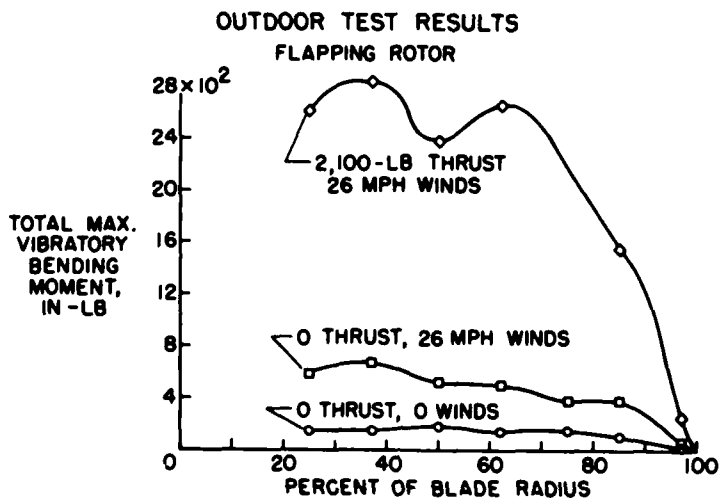


Figure 2

MODEL BLADE

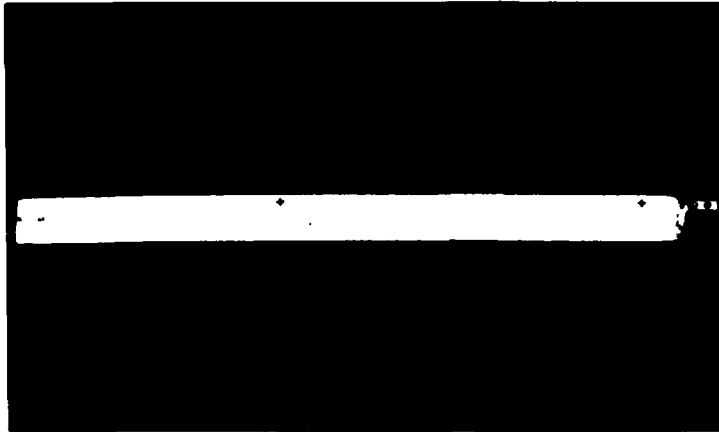


Figure 3

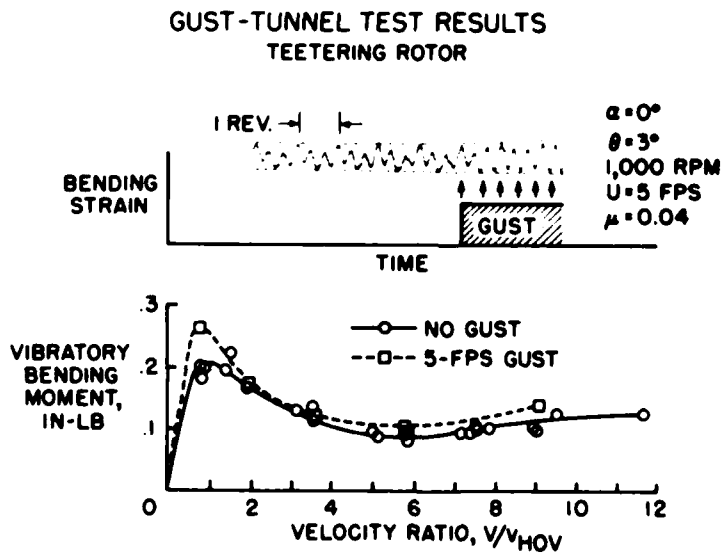


Figure 4

## HELICOPTER ROTOR-BLADE FLUTTER RESEARCH

By Maurice A. Sylvester, A. Gerald Rainey, and George W. Brooks

Langley Aeronautical Laboratory

## I - LOW BLADE ANGLES

As a general rule, helicopter designers are not greatly disturbed by the phenomenon of flutter primarily because rotor blades are generally mass balanced throughout their length in consideration of other more imminent problems such as undesirable control forces. In addition, the relatively low tip speeds of present-day helicopters are beneficial from a flutter standpoint. However, these favorable conditions may not exist indefinitely. For instance, the introduction of irreversible controls may lead the designer to select blades which are not completely mass balanced in order to obtain the desired strength with minimum weight. Or in some cases, the internal structure may make it desirable to achieve mass balance in the form of concentrated weights located at selected spanwise locations. The use of such design features in conjunction with higher tip speeds can cause flutter to become a problem. The purpose of this paper, which is presented in two parts, is to summarize and discuss the results of some studies on rotor-blade flutter. This part of the paper deals with flutter tests of a dynamic model at low blade angles of attack.

A few years ago the NACA constructed a dynamic model of a large unconventional helicopter primarily to investigate the effects of the unusual features on various dynamic problems (ref. 1). The tests showed that the model was only marginally safe from the standpoint of flutter; therefore, these studies were extended somewhat to investigate the flutter characteristics of the model blades in both the hovering and forward flight conditions.

The dynamic model rotor blades and some of their unconventional design features are illustrated by the schematic drawing of the blade in figure 1. The two rotor blades are powered by a pressure-jet system with four exhaust jets at each blade tip. The blade centrifugal forces are transferred to the pylon by means of the two blade retention straps, and two external counterweights are supplied to adjust the blade static moment about the quarter chord. During some of the flutter tests a camera was mounted on the rotor hub and rotated with the blades to obtain motion pictures of the flutter on the model blades. These motion pictures gave a visual record of the character and violence of the classical-type rotor-blade flutter. Although all the unconventional design features of the model would probably affect its classical flutter characteristics to some

extent, the chief interest in this particular model, insofar as flutter was concerned, was in the effect of mass balancing the blades with external counterweights and in the variations in the torsional frequency resulting from changes in control stiffness.

The effect of the counterweights on the blade mass distribution is indicated in figure 2. The upper part of this figure shows the chordwise center-of-gravity location of the blades without the counterweights, in percent chord, as a function of blade span. The figure indicates that the chordwise center-of-gravity position is somewhat rearward of the blade quarter-chord line for all the outboard blade sections. The manner in which the counterweights achieved static mass balance is best shown with the aid of the bottom part of figure 2, where the dead-weight torque about the quarter chord is shown as a function of the blade span for the blades with and without the counterweights. Starting at the blade tip and moving inboard along the solid line, it is noted that, due to the rearward position of the chordwise center of gravity of the blades without counterweights, the dead-weight torque about the quarter chord builds up and results in a considerable amount of static unbalance at the blade root. Now consider the dashed line, which represents the dead-weight torque of the blades with the counterweights. Starting at the tip again, the torque increases until the outboard counterweight position is reached. At this position the added moment of the counterweight reduces the torque about the quarter chord to approximately zero. The torque again builds up and is then reduced to zero at the blade root by the combined effects of the inboard counterweight and pitch-control arm. This result indicates that the blade as a unit is statically mass balanced about the quarter chord even though each blade section is not.

The question now arises as to the effectiveness of this manner of achieving mass balance in eliminating the flutter on the model blades. To answer this question, the model blades were flutter tested in the hovering condition with various counterweight configurations. The results of these tests are shown in figure 3 where five counterweight configurations are listed along with the relative flutter speed for each. Using the blade with no counterweights as reference, the figure shows that addition of the two counterweights resulted in an increase of only 3 percent in the flutter speed. Adding either counterweight alone was likewise ineffective in increasing the flutter speed to any extent. These data show that mass balancing the blades, with concentrated weights ahead of the quarter chord at the spanwise positions indicated, was ineffective in eliminating flutter. However, a small mass (approximately 2.5 percent of blade mass) placed to the rear of the quarter chord near the tip lowered the flutter speed appreciably.

While conducting the flutter tests, it was noted that, in some cases, the blades tended to diverge or go out of track before flutter was encountered; that is, at a certain rotor speed the tip-path planes of the

two individual blades ceased to be coincident and one blade tracked above its normal plane of rotation and the other below. The amount of out of track then increased rapidly with increased rotor speeds. As a matter of interest, it was observed that the counterweights were actually more effective in reducing this tendency of the blades to diverge than they were in eliminating flutter.

The first torsional frequency of rotor-blade systems may vary considerably because of different degrees of control restraint. It therefore seemed desirable to make a series of tests to determine the effect of control stiffness on the flutter speed of the model blades. The results of these tests are presented in figure 4. The rotor speed in revolutions per minute is plotted against the torsional frequency in cycles per minute. The manner in which the torsional frequency was varied is best described by referring to the sketch of the model rotor system shown in figure 4. The torsional frequency of the model rotor system depends on the structural characteristics of the blades, the effective control stiffness represented by the spring connection between the pitch-control arm and the pylon, and the restoring moment due to centrifugal forces acting on the blade retention straps. Variations in the torsional frequency were obtained by varying the control stiffness only. The flutter boundary indicates that flutter was encountered over a wide range of torsional frequencies at rotor speeds above the model normal operating speed. As the torsional frequency was decreased, the flutter speed was reduced appreciably. This result indicates that a reduction in the effective control stiffness can have a detrimental effect on the flutter speed. It should be noted that the centrifugal forces acting on the straps has the effect of increasing the torsional frequency of the model rotor system appreciably. Nevertheless, the results in figure 4 would probably be applicable to a more conventional type of blade without straps and a higher initial control stiffness since the flutter boundary does not depend on the path by which it is reached.

In discussing helicopter rotor-blade flutter, the question often arises as to the effect of forward flight on the classical flutter characteristics of rotor blades, since there are changes in the blade angle of attack and blade velocity as the blades rotate during forward flight. To evaluate the effects of forward speed on flutter, the model was flutter tested in the return passage of the Langley full-scale tunnel where forward speeds could be simulated. The results of these tests are shown in figure 5. The rotor speed in revolutions per minute is plotted as a function of the tip-speed ratio  $\mu$ , which is the ratio of the forward speed to the rotational tip speed. The boundary indicates the rotor speed at which flutter was encountered. For the model blade configuration shown in the figure there is some decrease in the rotor speed at flutter as the model moves from hovering to forward flight. It was also noted that the flutter frequency changed somewhat and the flutter oscillations became very erratic in the region of simulated forward flight.

It appears that, for this model, forward speeds altered the flutter characteristics somewhat but had no appreciably adverse effects.

The magnitude of stresses involved in helicopter vibrations is of considerable interest. Therefore the magnitudes of the strains obtained during flutter and during normal-rotor-speed operations for both the hovering and forward flight conditions are indicated in figure 6. These data were obtained on the blade configuration shown in figure 5. The ordinate of figure 6 is trace deflection which is proportional to blade strain, and the abscissa is again the tip-speed ratio  $\mu$ . The left figure represents torsion strains and the right figure the strains due to bending. The lower solid curves represent the strains due to vibrations at normal operating speed while the upper dashed curves represent the strains due to flutter. The figure shows that both the torsion and bending strains due to flutter are much greater than the corresponding strains due to vibrations at normal operating speeds. This result is true for the model blades throughout the range of tip-speed ratios studied, although the difference between the flutter and normal operating strains is less at the higher tip-speed ratios. Some of the sharp decrease in the flutter strains is probably due to the lower flutter speed at the higher tip-speed ratios which was indicated for this blade configuration in figure 5. On the basis of these limited data it should not be assumed that this decrease in the flutter strains would necessarily continue to higher values of the tip-speed ratio. Flutter strains comparable to those in the figure would probably be destructive to the full-scale helicopter. However, repeated flutter tests on the model resulted in only occasional localized failures. The fact that the model was not destroyed may be attributed, at least in part, to the method of construction which simulated full-scale strains but resulted in lower stresses and good fatigue properties. The high level of strains encountered during flutter and the localized failures on the model serve to reemphasize the violence of the flutter oscillations.

In addition to the experimental results discussed so far, some limited analytical studies have been made to determine the applicability of an unpublished, simplified flutter analysis. The analysis essentially consists of an extension of wing bending-torsion flutter theory to include the effect of spanwise variations in airspeed and the effect of centrifugal forces on the blade uncoupled natural frequencies. The agreement between theory and experiment was fair to good with the theory usually indicating a somewhat higher flutter speed than was obtained experimentally.

## II - HIGH BLADE ANGLES

Previous experience with propeller blades and wing models has indicated that the angle of attack can have important effects on flutter characteristics (see refs. 2 and 3, for example). For this reason then, it was considered desirable to conduct an investigation of these angle-of-attack effects on the flutter characteristics of some typical helicopter rotor-blade configurations. This study was completed recently and has been reported by Brooks and Baker (ref. 4). This paper consists, for the most part, of results of that study.

However, before some of the details of these results are presented, perhaps a brief discussion of a typical variation of flutter velocity with blade pitch angle is in order. Such a typical curve is shown in figure 7. The flutter velocity is shown as a function of the measured geometric blade pitch angle at the 0.8-blade-radius station. This particular angle has been chosen as the parameter of presentation because it is a measured quantity closely related to the actual angle of attack.

As shown in figure 7, the flutter velocity is relatively insensitive to blade angle until the point is reached where separation becomes important. At the higher blade angles the flutter velocity decreases rapidly to values much lower than those at low blade angles. The decrease in velocity is accompanied by changes in the mode of flutter in that at high angles the type of flutter which is normally encountered is almost a pure single-degree-of-freedom flutter occurring in the torsion mode whereas, at the low blade angles, the type of flutter which occurs is usually a coupled bending-torsion type. Since the high-blade-angle flutter is associated with separated flow conditions, it has come to be known as "stall" flutter, whereas the coupled flutter occurring at low blade angles is called "classical" flutter.

Of course, there are many parameters which can affect the flutter characteristics at both low and high blade angles. One of these is the chordwise location of the center of gravity. Some of these effects are illustrated in figure 8 where the flutter velocity is shown as a function of center-of-gravity location for a series of blades having continuous section center-of-gravity locations varying over the range indicated. The upper curve labeled low blade angles applies to the classical-flutter region as discussed in connection with figure 7 whereas the lower curve labeled high blade angles applies to the region of the minimum of the curve shown in figure 7.

The low-blade-angle or classical-flutter velocity is very sensitive to changes in the center-of-gravity location, particularly as the quarter-chord point is approached; whereas the stall-flutter velocity is relatively insensitive to changes in this parameter.

Investigation of another parameter, the structural damping in the torsion mode, indicates an opposite effect in that the flutter velocity at high blade angles was a function of this parameter, but the low-blade-angle flutter velocity was relatively insensitive. Some of the results of this part of the study are indicated in figure 9 where, again, the flutter velocity is shown as a function of the measured pitch angle at the 0.8-blade-radius station for three values of the torsional structural damping coefficient. At the lower blade angles near the transition region there is no consistent variation of flutter velocity for the three values of damping shown; however, at high blade angles the flutter velocity increases significantly with increased damping. Perhaps it should be mentioned that the largest value of damping shown ( $g_a = 0.067$ ) is probably somewhat high with respect to present practical rotor-blade construction and the lowest value of  $g_a = 0.034$  is probably more typical of present construction although it seems that information on this subject is rather limited.

Another question of some importance is the possible effects of the manner of entry into a flutter region. Since in forward flight the helicopter rotor blade operates along a periodically varying velocity—blade-angle curve, it becomes necessary to study the effect of this periodic entry of the flutter region when the velocity—blade-angle operating curve penetrates the flutter boundary. In the first part of this paper some results were presented concerning the effects of forward flight on the flutter velocity for lifting conditions in the region of classical flutter. The periodic-entry problem has not been studied in the stall-flutter region; however, some information has been obtained from tests of a thin cantilever wing model mounted on a mechanism capable of oscillating the wing in pitch at various frequencies. Of course, this type of operation does not completely simulate forward flight since there is no periodic velocity variation; however, it is felt that the information obtained may be of some general interest. The results of this investigation are illustrated in figure 10 where the flutter velocity is shown as a function of pitch angle. The solid curve shown in figure 10 represents the flutter boundary obtained with the wing clamped as a cantilever, that is, not oscillating. The data points indicate the velocity and average pitch angles at which flutter occurred when the wing was pitching sinusoidally over the range indicated by the arrows shown in the figure and at frequencies indicated in the key. The flutter velocities for the oscillating cases are almost the same as those obtained when the wing was not oscillating. In other words, the flutter characteristics seemed to depend more on the average conditions rather than the momentary entry into the "non-oscillating" flutter region. This result agrees in trend, at least, with the results presented in the first part of the paper pertaining to flutter at low blade angles.

Another question of considerable interest is the problem of compressibility effects. Some results of this part of the investigation are



shown in figure 11 where the flutter velocity is shown as a function of the tip Mach number for three blade angles in the stall-flutter region. It can be seen in figure 11 that as the higher Mach numbers are approached the flutter velocity increases rapidly. Presumably this increase is due to the large changes in flow characteristics which must occur at these Mach numbers and, apparently, these flow changes alter the oscillatory aerodynamic derivatives in a stabilizing manner.

With regard to the question of predicting helicopter rotor-blade flutter characteristics it can be said that the available theory based on potential flow seems to be adequate for treating the classical flutter of rotor blades. For the stall-flutter part of the picture, however, none of the presently available theories seem to be completely adequate. For the time being at least, empirical methods must be used. Baker and Brooks (ref. 4) discuss a set of tentative criteria based on information similar to that shown in figure 11 which should provide the designer with some estimate of the probability of a particular configuration encountering stall-flutter difficulties.

#### REFERENCES

1. Brooks, George W., and Sylvester, Maurice A.: Description and Investigation of a Dynamic Model of the XH-17 Two-Blade Jet-Driven Helicopter. NACA RM L50121, 19 1.
2. Baker, John E.: The Effects of Various Parameters Including Mach Number on Propeller-Blade Flutter With Emphasis on Stall Flutter. NACA RM L50112b, 19 1.
3. Rainey, A. Gerald: Preliminary Study of Some Factors Which Affect the Stall-Flutter Characteristics of Thin Wings. NACA RM L52D08, 19 2.
4. Brooks, George W., and Baker, John E.: An Experimental Investigation of the Effect of Various Parameters Including Tip Mach Number on the Flutter of Some Model Helicopter Rotor Blades. NACA RM L53D24, 19 3.



SOME UNCONVENTIONAL DESIGN FEATURES

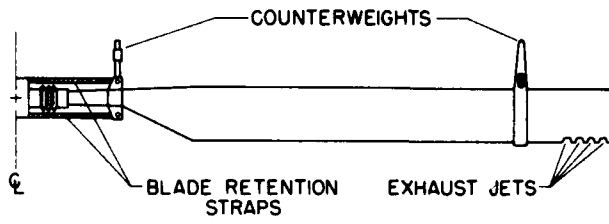


Figure 1

EFFECT OF COUNTERWEIGHTS ON BLADE MASS DISTRIBUTION

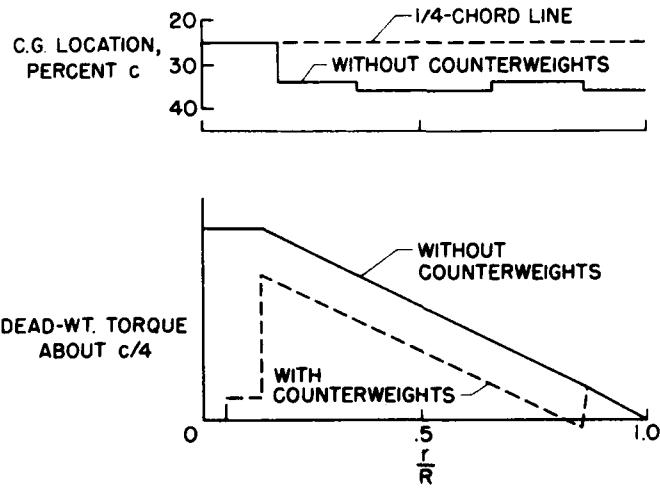


Figure 2



EFFECT OF COUNTERWEIGHTS ON FLUTTER SPEED

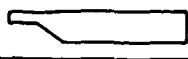
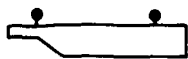
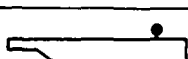
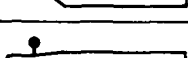
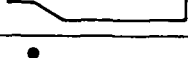
COUNTERWEIGHT CONFIGURATION	RELATIVE FLUTTER SPEED
	1.00
	1.03
	1.03
	1.01
	.78

Figure 3

EFFECT OF CONTROL STIFFNESS ON FLUTTER SPEED

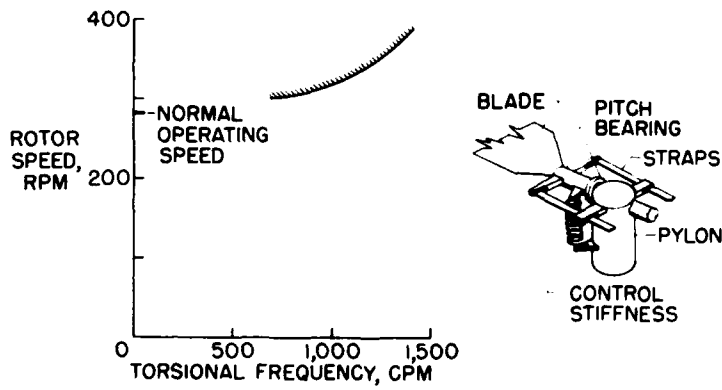


Figure 4

## EFFECT OF FORWARD SPEED ON ROTOR SPEED AT FLUTTER

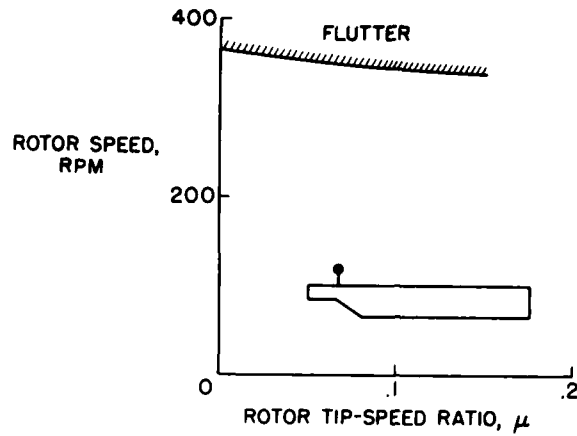


Figure 5

## COMPARISON OF EXPERIMENTAL MODEL BLADE STRAINS

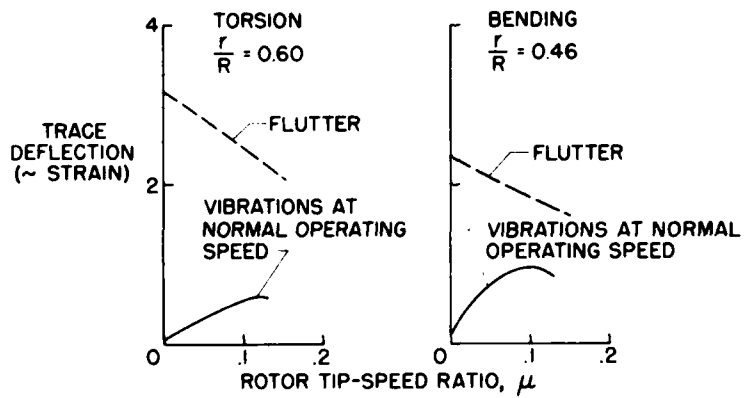
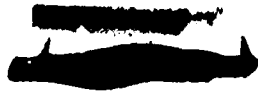


Figure 6



TYPICAL VARIATION OF FLUTTER VELOCITY WITH BLADE ANGLE

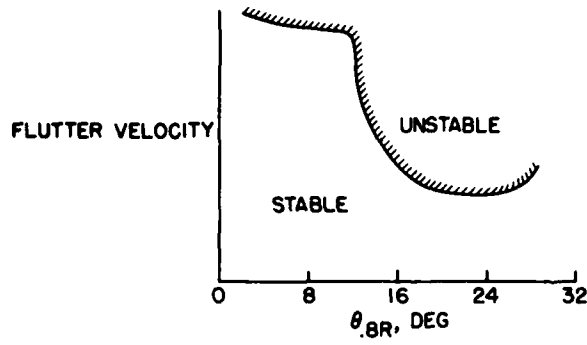


Figure 7

EFFECT OF C.G. LOCATION

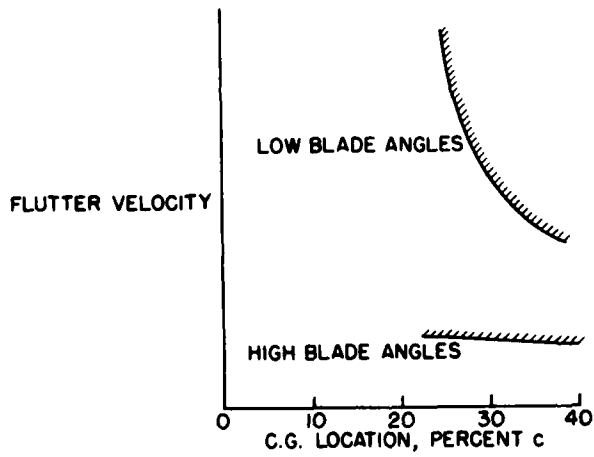


Figure 8



EFFECT OF STRUCTURAL DAMPING ON FLUTTER BOUNDARY

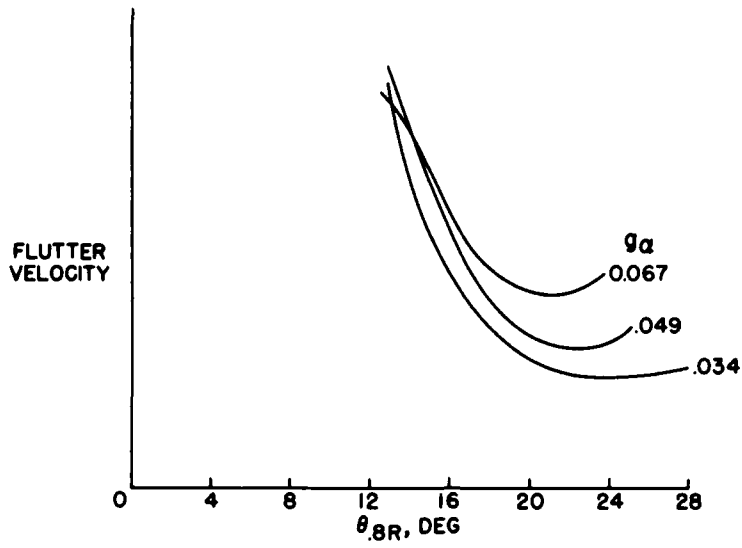


Figure 9

EFFECT OF PERIODIC ENTRY OF FLUTTER REGION

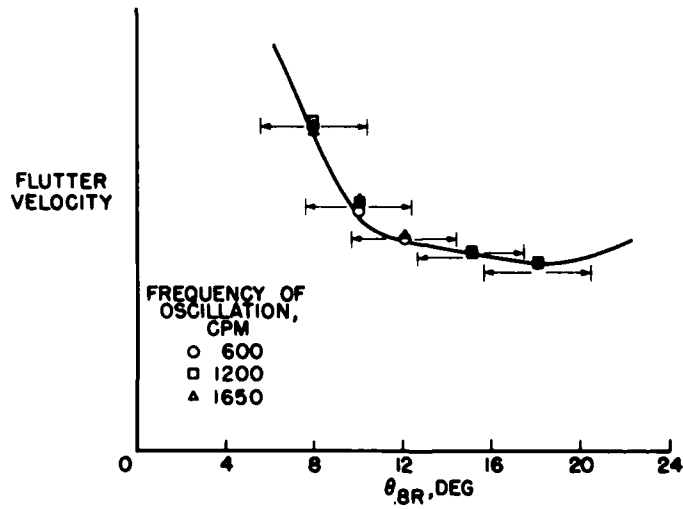


Figure 10

EFFECT OF MACH NUMBER

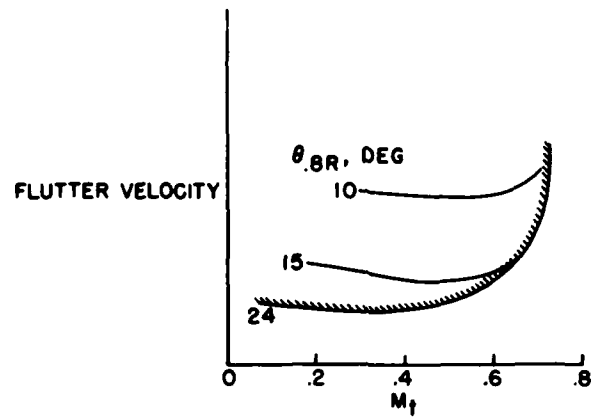


Figure 11

A DYNAMIC-MODEL STUDY OF THE EFFECT OF CONCENTRATED WEIGHTS  
ON THE VIBRATORY STRESSES IN HELICOPTER BLADES

By John Locke McCarty

Langley Aeronautical Laboratory

INTRODUCTION

In the normal operation of helicopters, the helicopter structure is subjected to periodic loads having a wide frequency range. In some cases the response of the structure is such that the frequencies of some of the applied periodic loads may be near resonance with the natural frequencies of different structural modes. This paper presents the results of some experimental studies made on a dynamic model of a helicopter under hovering and forward flight conditions to evaluate the periodic blade stresses encountered when the natural bending frequency of the blades is near resonance with the frequency of the applied third harmonic aerodynamic loading.

DISCUSSION

The model of the helicopter in its entirety is shown in figure 1. It is a two-blade model deriving its power from compressed air which circulates through the flexible hose, up through the pylon, out through the blades, and making its exit through four jet nozzles located at each blade tip. Early tests (ref. 1), made on this dynamic model in the hovering attitude, showed large amplitude periodic blade bending stresses having a frequency of 3 cycles per rotor revolution both at and above the normal operating rotor speed. The prototype of this dynamic model encountered similar periodic stresses while hovering, but when tested under forward flight conditions the stresses were so greatly aggravated that the estimated fatigue life of the blades was reduced to a matter of minutes.

At attempt to rationalize the problem in terms of applied loads and blade response involves the consideration of three possible conditions. The first is the existence of large periodic aerodynamic blade loadings and components of these loadings which have frequencies equal to the lower-order harmonics of the rotor speed. Helicopter flight tests have shown that these loadings are present and that they are magnified as the helicopter enters the region of transition from hovering to forward flight. A second condition is the amplification of the blade response



due to resonance between the frequencies of the aerodynamic inputs and the frequencies of the blade. The third condition for consideration is the possibility of energy absorption by the structure due to the coupling of blade bending and torsion deformations. In an attempt to explain these conditions, figure 2 shows the possibility of blade resonance as well as coupling at the normal operating rotor speed of this helicopter.

This figure shows the frequencies of the first uncoupled elastic bending and torsion modes together with the various harmonics of the rotor frequency as a function of the rotor speed. The significance of the forcing harmonic lines is shown by the following example. At a rotor speed of 200 revolutions per minute, a 2-per-revolution loading, that is, the loading which occurs twice per revolution of the rotor, has a frequency of 400 cycles per minute.

During the preliminary study of the problem, visual inspection of the hovering records showed that large periodic stresses occurred during certain regions of the rotor speed. An analysis showed that these stresses had predominant frequencies equal to the respective harmonics, indicated in the figure by the heavied portions of the harmonic lines. For example, between 210 and the maximum test rotor speed of 360 revolutions per minute, periodic stresses having a frequency of 3 cycles per rotor revolution were measured on the blade. Similarly, 4 cycles of blade vibration per revolution existed between 150 and 198 revolutions per minute.

First consider the problem of stress amplification from the standpoint of resonance. The intersection of the natural frequency curve with a harmonic line would indicate a resonant point. From a consideration of this figure, a resonant condition between the natural bending frequency and the forcing harmonics could be expected to occur in the region of 110, 155, and 350 revolutions per minute. Resonance between the natural torsion frequency and the forcing harmonics at rotor speeds of approximately 210 and 270 revolutions per minute could be expected. At the normal operating rotor speed of 283 revolutions per minute, given in figure 2 by the vertical dashed line, two near-resonance conditions exist: one between the natural-bending-frequency curve and the third harmonic line and the other between the natural-torsional-frequency curve and the fourth harmonic line. Since the predominant periodic stresses measured on the blade during the preliminary tests were primarily of a bending nature, it did not appear that the condition of resonance between the 4-per-revolution line and the torsion curve was very significant.

In minimizing the effects of resonance amplification of the blade stresses, it is desirable, of course, to eliminate completely any resonant conditions in the vicinity of the normal operating range of the helicopter. Since this may not be feasible, it is then desirable to reduce the resonance amplification by separating the input and response frequencies to obtain acceptable stress levels.

Since the third forcing harmonic line is fixed, and since the normal operating speed is determined from the standpoint of performance, the permissible course of action is to change the curve of the natural bending frequency of the blade. One way to achieve this is to attach concentrated weights to the blade at different spanwise locations, and figure 3 will show the results obtained.

This figure shows the effect on the model blade bending frequency of a 1/2-pound weight, which represents about 10 percent of the blade weight, located at two blade spanwise stations. It can be seen from the plot that at the normal operating speed a weight added at the antinode of the blade would put the operating condition of the blades closer to a resonant condition and higher blade stresses might be expected. In the same sense the addition of weight at the nodal point would put the operating condition farther away from resonance with the third harmonic, and yet well clear of the fourth, and would suggest a reduction in the periodic blade stresses.

The rotor system of the dynamic model was then tested under hovering and forward flight conditions in the return passage of the Langley full-scale tunnel to evaluate the predicted effects of added weights on the periodic blade stresses. The results from these three configurations were harmonically analyzed at a particular ratio of forward speed to rotational tip speed of 0.08. This analysis, shown in figure 4, was made to study the individual contribution of each of the first five harmonics to the total periodic stress. The third harmonic is prevalent in the normal configuration and its contribution to the total stress is greatly increased with the addition of 10 percent blade weight on the quarter chord at the antinode of the blade. This further substantiates the fact that this configuration puts the operating condition of the blade closer to resonance with the third harmonic line. On the other hand, when the weight is on the quarter chord at the nodal point, the blade is operating away from resonance to the extent that the third harmonic is no longer the prevalent forcing function.

Whereas the harmonic analysis indicated the results for one value of rotor tip-speed ratio  $\mu$ , figure 5 shows a sample of the results of the tests under forward flight conditions for the range of tip-speed ratios. This figure presents the measured maximum periodic blade strains as a function of this ratio. The data show that the trends of the model periodic blade strains, and consequently the blade stresses, correspond to the results of the prototype flight tests in that the blade stresses are greatly magnified during the transition region. The results of the tests are also in agreement with the previous discussion in that a weight placed at the antinode position resulted in a large increase in blade stresses as compared with the no-weight condition. When the weight was located at the node, the stresses were reduced for all values of the advance ratio. This figure also shows that the stresses are further reduced by moving the weight at the nodal point from the quarter chord

to the leading edge of the blade, which introduces a consideration of the effect of coupling of blade bending and torsion motion. At the normal operating rotor speed, the blade bending frequency is near that of the first torsion frequency. (See fig. 2.) For certain blade-weight configurations, this may lead to coupling of the blade bending and torsion modes. In order to evaluate the extent of coupling, a systematic study of the blade strains was made for variations in the chordwise location of the added weight at two spanwise stations. The results of this study are given in figure 6. To eliminate the possibility of flutter with the added weight at the trailing edge of the blade, a 1/4-pound weight, representing about 5 percent of the blade weight, was used in these tests instead of the previous 1/2-pound weight. The strains recorded are the average of the maximum periodic strains measured on the blade during the transition region. With the concentrated weight at the antinode position, the strains, and, again, consequently the stresses, remain greater than the clean blade with no additional weights regardless of the chordwise location of the concentrated weight. However, there is a decrease in the strains as the weight is shifted toward the trailing edge of the blade. When the concentrated weight is located at the nodal point of the blade during its first elastic bending mode, the strains are appreciably increased as the weight is moved from the leading edge toward the trailing edge of the blade. As the added weight is moved rearward along the chord, it can be seen that there is a chordwise station where the additional weight no longer becomes beneficial in reducing the periodic strains.

These test data were obtained at the 46.2-percent-span station. Stresses were also measured at different spanwise stations on these and other configurations for different rotor speeds and different rotor and pylon attitudes. In general, the trends of the data are similar to those shown.

#### CONCLUDING REMARKS

These data show that the operation of helicopters near conditions of resonance will result in increased blade vibrations which are accompanied by increases in blade stresses. It appears feasible that in some cases the vibrations and stresses may be reduced by the addition of weights to the blades. The results of this experimental investigation indicate that this can be done by moving the resonant condition of the helicopter farther away from the operating condition and by taking advantage of beneficial coupling effects.



REFERENCE

1. Brooks, George W., and Sylvester, Maurice A.: Description and Investigation of a Dynamic Model of the XH-17 Two-Blade Jet-Driven Helicopter. NACA RM L50I21, 1951.



DYNAMIC MODEL



Figure 1

BLADE RESONANT FREQUENCIES

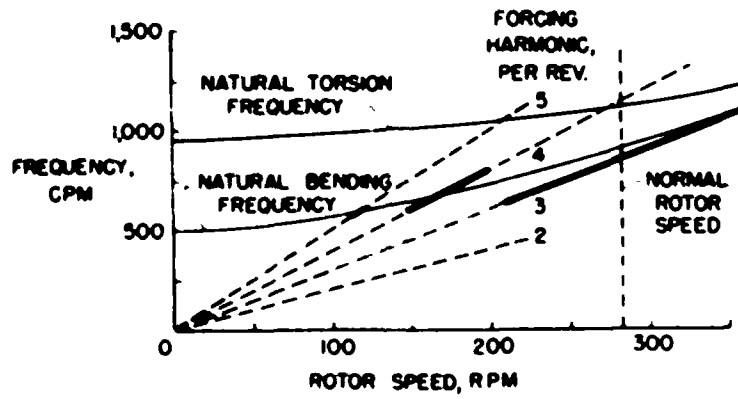


Figure 2

EFFECT OF WEIGHTS ON FUNDAMENTAL BENDING FREQUENCY

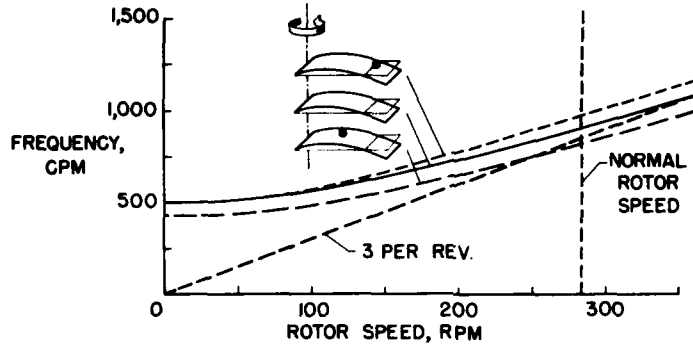


Figure 3

HARMONIC COEFFICIENTS OF BLADE BENDING STRAIN TRANSITION REGION

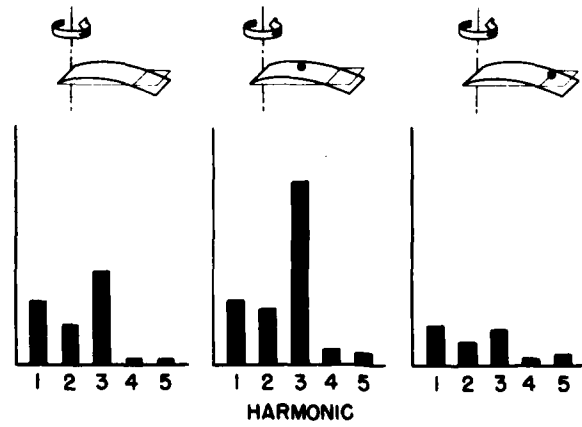


Figure 4

PERIODIC BLADE STRAINS

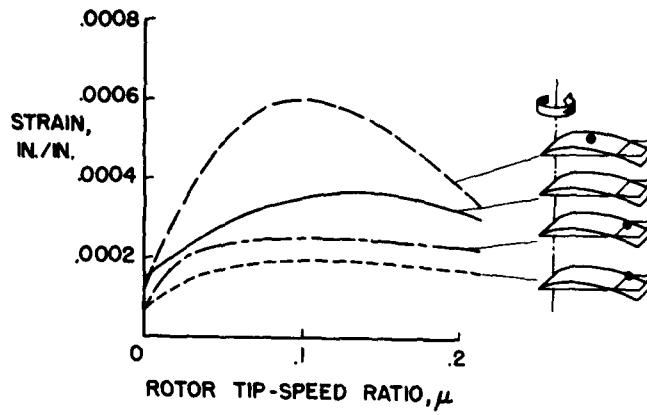


Figure 5

EFFECT OF CHORDWISE LOCATION OF CONCENTRATED WEIGHTS  
 CONCENTRATED WT./BLADE WT.=0.05

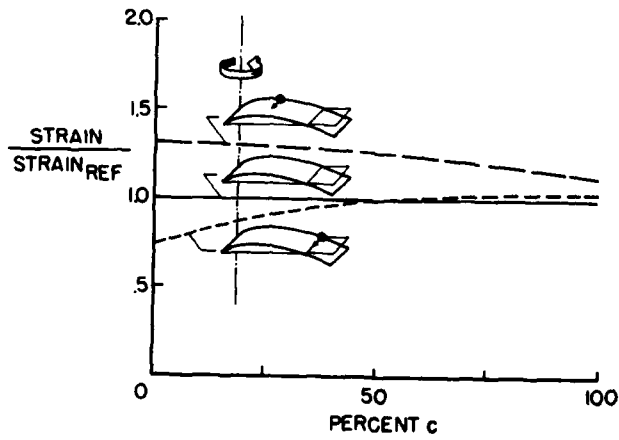


Figure 6

COUPLED BENDING AND TORSIONAL DEFORMATIONS OF ROTATING  
BEAMS UNDER ARBITRARY LOADING

By George W. Brooks and John C. Houbolt

Langley Aeronautical Laboratory

More exact methods of analysis are required for treatment of many of the helicopter dynamic problems such as blade vibrations, divergence, and flutter. In the treatment of these problems, the spanwise and chordwise distributions of the various structural properties such as mass, mass moment of inertia, stiffness, and twist as well as the internal stress distribution of the blade are significant. The various theories available either neglect some of the items or treat them only approximately. A general theory for handling rotor-blade problems which properly treats these various items was developed, therefore, and the purpose of this paper is to present this theory.

A summary of the available theory is afforded by figure 1. The cases given in the figure are separated into two categories, one in which there are no centrifugal forces and one which includes centrifugal forces at least to some extent.

The cases treated without centrifugal forces include bending of an untwisted beam, torsion of an untwisted beam, and coupled bending in two directions and torsion of a twisted beam. The first two cases assume that the elastic axis and center-of-gravity axis are coincident, whereas in the third case coupling is achieved by chordwise separation of these axes.

The cases which have been treated with the inclusion of centrifugal forces are the bending of an untwisted beam, the bending in two directions of a twisted beam, and the torsion of a twisted beam.

The scope of the present theory is shown in figure 2. The theory treats the coupled bending torsion of a twisted rotating beam where the elastic axis, center-of-gravity axis, and tension axis are not necessarily coincident. The tension axis of the beam is defined as the spanwise locus of the point in the cross section where the resultant centrifugal force acts. The generality of the method is such that each of the cases treated previously is a special case of the present method. In its general form the method includes all parameters which are believed to influence the static or dynamic behavior of the structure and is subject only to the limitation that the deformations be sufficiently small that products of the deformations are negligible - an assumption which is accepted in the development of most classical beam theories.



Figure 3 shows the system of coordinate axes used in the derivation of the equations of equilibrium. The position of the undeformed blade, indicated on the figure by the dashed lines, is defined by the  $X, Y, Z$  axes. With reference to this system of coordinates, the blade elastic axis is then deformed, first by an amount  $u$  in the plane of the chord and then by an amount  $w$  normal to the plane of the chord; and last, the sections are rotated through an angle  $\phi$  about the deformed elastic axis.

With respect to the deformed position of the elastic axis, two additional sets of coordinates are employed in the development of the theory: namely, the  $x, y, z$  coordinates and the  $\bar{x}, \bar{y}, \bar{z}$  coordinates. The  $x, y, z$  coordinates remain parallel to the  $X, Y, Z$  coordinates and, as will be shown presently, are natural and convenient for the derivation of the external or applied moments. The  $\bar{x}, \bar{y}, \bar{z}$  coordinates remain parallel and normal to the cross section during the deformation of the blade and are natural and convenient for the derivation of the elastic resisting moments.

The nature of the external applied forces is shown in figure 4. The coordinate axes which were shown in figure 3 are repeated. The elevation shows the blade in the flapping plane and indicates the nature of the forces acting on a blade element which produce moments about the  $x$ -axis which is normal to the flapping plane. The plan view (underside view) shows the blade in the plane of the chord as well as the forces acting on the element which produce moments about the  $z$ -axis. In this case, the centrifugal force is resolved into two components, one in the spanwise direction and one in the chordwise direction. The forces shown also include the transverse inertia forces and the aerodynamic lift and drag forces.

In addition to producing bending moments about the  $x$ - and  $z$ -axes, the applied forces shown also produce torsion moments about the elastic axis.

An analysis of the directions of the applied forces with respect to the  $x, y, z$  coordinates indicates that this system of coordinates is convenient for the evaluation of the applied moments due to these forces. And since the  $\bar{x}, \bar{y}, \bar{z}$  coordinates define the physical cross section of the blade normal to the elastic axis, as shown in the plan view, this set of coordinates is appropriate for the derivation and discussion of the internal or elastic resisting moments.

Reference has been made to the moments about the various axes because, in the present method, the derivation of these moments constitute the first step in the derivation of the differential equations of equilibrium which are desired. The nature of these moments and the procedure followed in the determination of the equations of equilibrium are indicated as follows:

Applied moments  $M_x$ ,  $M_y$ , and  $M_z$  involve:

Centrifugal forces Transverse inertia forces of bending and torsion Applied loads (aerodynamic)	}	Functions of $w$ , $\phi$ , and $u$
--	---	-------------------------------------

Elastic resisting moments  $M_{\bar{x}}$ ,  $M_{\bar{y}}$ , and  $M_{\bar{z}}$  involve:

Elastic bending forces Elastic torsion forces Tensile stress distribution over the cross section	}	Functions of $\bar{w}''$ , $\bar{\phi}'$ , and $\bar{u}''$
---	---	--

$$\begin{bmatrix} M_x \\ M_y \\ M_z \end{bmatrix} = \left[ \text{Transformation} \right] \begin{bmatrix} M_{\bar{x}} \\ M_{\bar{y}} \\ M_{\bar{z}} \end{bmatrix} \qquad \begin{bmatrix} w'' \\ \phi' \\ u'' \end{bmatrix} = \left[ \text{Transformation} \right] \begin{bmatrix} \bar{w}'' \\ \bar{\phi}' \\ \bar{u}'' \end{bmatrix}$$

The applied moments  $M_x$ ,  $M_y$ , and  $M_z$  all involve centrifugal forces, transverse inertia forces of bending and torsion, and applied aerodynamic loads, all of which are functions of the blade deflections  $w$ ,  $\phi$ , and  $u$ .

The elastic resisting moments involve the cross-sectional stress distribution which results from bending, torsion, and tension. These bending and torsional stresses can be expressed conveniently in terms of  $w''$ ,  $\phi'$ , and  $u''$  where  $w$ ,  $\phi$ , and  $u$  are the deformations relative to the  $x$ -,  $y$ -, and  $z$ -axes and a prime denotes a derivative with respect to blade span.

These two sets of moments must be related and the relationship is given by the moment transformation shown, which is a function of initial blade twist and certain angles associated with the blade deflections. However, when the moments are equated in this fashion, a function of  $w$ ,  $\phi$ , and  $u$  is obtained on the left and  $\bar{w}$ ,  $\bar{\phi}$ , and  $\bar{u}$  on the right. The next step is the elimination of the unknown  $\bar{w}$ ,  $\bar{\phi}$ , and  $\bar{u}$ , and this is achieved by use of the curvature transformation on the right, which, by the way, is identical to the moment transformation.

By following the procedure indicated, the differential equations of equilibrium result. The form of these equations as well as the nature of the terms involved is indicated as follows:

$$\frac{d^2}{dy^2} \left( EI \frac{d^2 w}{dy^2} \right) = \frac{d}{dy} \left( T \frac{dw}{dy} \right) + m\omega^2 w + me\omega^2 \phi + P_{\text{lift}} -$$

$$\left[ \frac{d}{dy} \left( e\phi \frac{dT}{dy} \right) + \frac{d^2}{dy^2} (\phi T e_A) \right]$$

$$- \frac{d}{dy} \left( GJ \frac{d\phi}{dy} + T k_A^2 \frac{d\phi}{dy} \right) = me\omega^2 w + I_{\alpha} (\omega^2 - \Omega^2) \phi + Q_{\text{moment}} +$$

$$\left[ \Omega^2 \frac{dw}{dy} \int_y^R m(u_{0\eta} - e_{\eta}) d\eta + \Omega^2 me u_0 \phi + \frac{d}{dy} (T e_A \frac{dw}{dy}) \right]$$

$$\frac{d^2}{dy^2} \left( EI_c \frac{d^2 u}{dy^2} \right) = \frac{d}{dy} \left( T \frac{du}{dy} \right) + m(\omega^2 + \Omega^2) u + P_{\text{drag}} +$$

$$\left[ \frac{d}{dy} \left( e \frac{dT}{dy} \right) - \frac{d^2}{dy^2} (T e_A) + m\Omega^2 (u_0 - e) \right]$$

In order to reduce the complexity of the expressions for purpose of discussion, however, the case of a harmonically oscillating untwisted blade at zero pitch angle has been chosen.

The three simultaneous equations are, in the order in which they appear, the equation for bending in the flapping plane, the equation for torsion about the elastic axis, and the equation for bending in the plane of the chord. The terms which appear outside the dashed lines are those which have appeared in one form or another in previous work. The terms which appear inside the dashed lines are new to all previous treatments of the problem and appear to be due to the inclusion of coupling by centrifugal force.

In order to point out the nature of some of these terms, the elements of the first equation will be considered. Each of these terms is in the form of a loading per unit length of the blade, that is, the loading on a blade element at some spanwise station. The first term is the conventional resisting or stiffness loading. The second term is the loading due to centrifugal forces where  $T$  is the centrifugal force. The third and fourth terms are the well-known inertia loading terms due to bending and coupling with torsion, where  $e$  is the chordwise distance between the center of gravity of the cross section and the elastic axis. The fifth term is the applied lift or aerodynamic loading. The first term inside the dashed lines is a coupling term which arises from the centrifugal force  $T$  and is again due to the fact that the center-of-gravity axis is not coincident with the elastic axis. The last term is also a coupling term which is a function of the chordwise distribution of the internal stresses and arises when the center of tension or effective center of centrifugal force is displaced chordwise from the elastic axis by an amount  $e_A$ .

The theory has been applied to calculate effects of coupling on blade frequencies and to evaluate the qualitative effect of concentrated weights on blade bending moments in response to an arbitrary forcing function.

Figure 5 shows a comparison of the uncoupled and coupled frequencies for the flapping and first bending mode, and the first two torsion modes of a helicopter blade with a concentrated mass of approximately 10 percent of the blade mass located near the node of the first mode at the leading edge of the blade. The ordinate is the natural frequency and the abscissa is the rotor speed. The rotor speed at which this blade might normally be operated for aerodynamic reasons is also shown in figure 5. The uncoupled frequencies are shown by means of dashed lines in contrast to the coupled frequencies which are shown by the solid line.

As might be expected, the effect of bending-torsion coupling on the natural frequencies is more pronounced in the region where the natural frequencies for the uncoupled modes become identical. This effect is shown in figure 5 in the region of intersection of the uncoupled frequency curves for first bending and first torsion.

The ratio of the first torsional frequency to the first bending frequency at zero rotor speed is perhaps less for the case shown than for the general case; however, the calculations show that the natural frequencies of the coupled modes may be appreciably different from those of the uncoupled modes. This difference in natural frequencies may be of considerable importance in the determination of rotor speeds where resonance conditions exist between certain harmonic-forcing functions and blade natural frequencies. Even for conditions where the differences in coupled and uncoupled natural frequencies are small, there still may be a large effect of coupling on blade loading because of changes in the amplitudes and phase angles of the aerodynamic forces.

The experimental investigation discussed by John Locke McCarty in a previous paper showed considerable effect of concentrated weights attached to the blade at selected location on the blade bending moments, the major components of which had a frequency of 3 cycles per rotor revolution. It was of interest to see, qualitatively, whether the measured trends could be predicted by the method presented. Consequently, the blade flapwise bending moment at the blade midspan was calculated as a function of rotor speed in response to an assumed blade-tip forcing function having a frequency of 3 cycles per rotor revolution and an amplitude proportional to the square of the rotor speed. Both aerodynamic and structural damping were included in the analysis.

Figure 6 shows a comparison of the measured and calculated bending moments for the basic blade and three concentrated-weight configurations. The concentrated-weight configurations consisted of a weight at the quarter chord at the antinode point, a weight at the quarter chord at the node point, and a weight at the leading edge at the node point. In each case, the added weight represented approximately 10 percent of the blade weight. The experimental results are shown by the solid bars and the calculated results are shown by the crosshatched bars.

Since the purpose of the calculations was to determine the applicability of the method to the prediction of experimental trends, the amplitude of the forcing function was chosen so that the magnitude of the experimental and calculated bending moments were in agreement for the basic blade configuration shown by the heavy black line under the bare-blade configuration in figure 6.

The results show that, despite expected differences in magnitudes (which are probably due to the very approximate nature of the loading assumed in the calculations), the trend predicted by the calculations concerning the effect of changes in counterweight configurations on blade bending moments is verified by the experimental results.

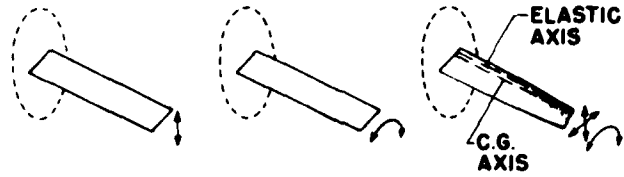
In consideration of the configurations listed in figure 6, the differences between the bending moments for the first three configurations are attributed to different proximities of the applied exciting forcing frequency and the natural resonant frequency of the first elastic bending mode - the first configuration being the nearest to resonance and the third configuration being farthest from resonance. The additional reduction in bending moments, when the weight, located at the node point, is moved to the leading edge, is attributed to beneficial bending, torsion, coupling effect of inertia, and centrifugal-force loadings.

In summary, a general theory has been developed for the coupled bending and torsional deformations of rotating beams under arbitrary loading in which structural properties of the blades such as mass, mass

moment of inertia, stiffness, and twist as well as the internal stress distribution of the blade are included. New and significant coupling terms between bending and torsion which arise as a result of centrifugal forces have been found. The method has been applied to determine the effect of coupling on natural frequencies and the effect of concentrated weights on blade bending moment due to an arbitrary loading. The use of the more exact equations of the present method should permit designers to make a better evaluation of the coupled vibrations of rotor blades, particularly in the analysis of blade stresses and instabilities such as divergence and flutter.

STATUS OF PREVIOUS THEORY

NONROTATING BEAMS



ROTATING BEAMS (CENTRIFUGAL FORCES INCLUDED)

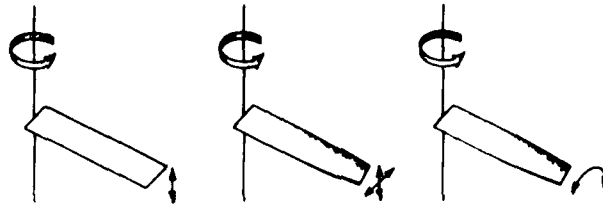


Figure 1

PRESENT THEORY

CASE OF COUPLED BENDING-TORSION OF TWISTED ROTATING BEAM

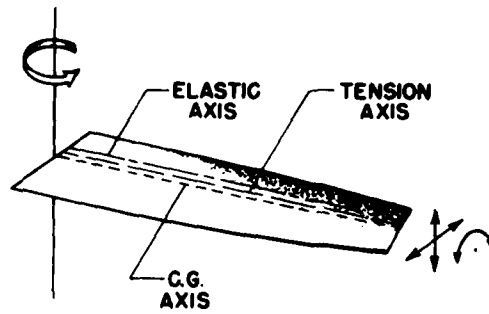


Figure 2

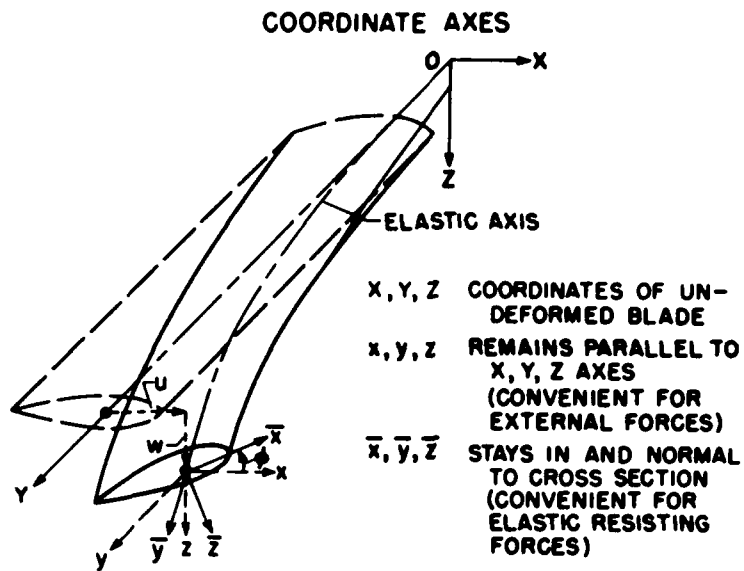


Figure 3

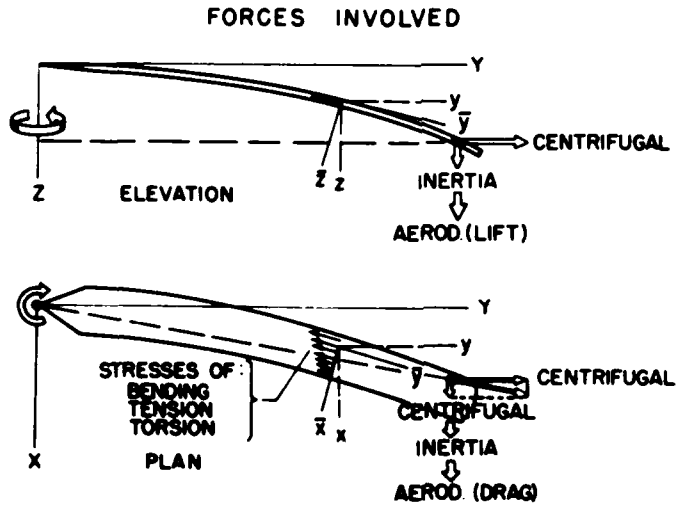


Figure 4



EFFECT OF COUPLING

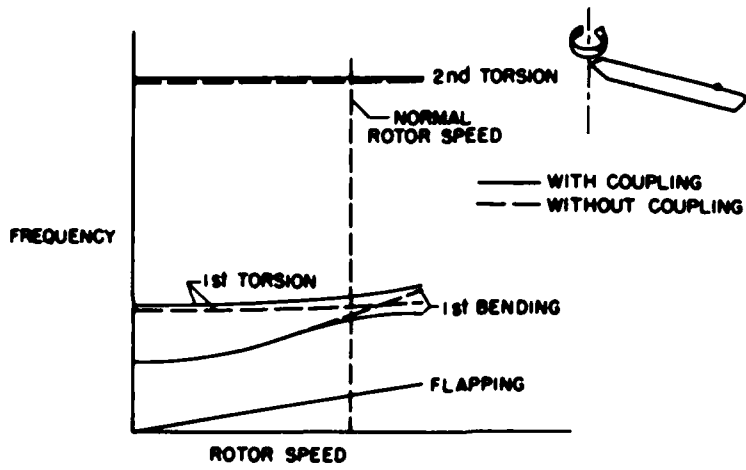


Figure 5

MEASURED AND CALCULATED MOMENTS

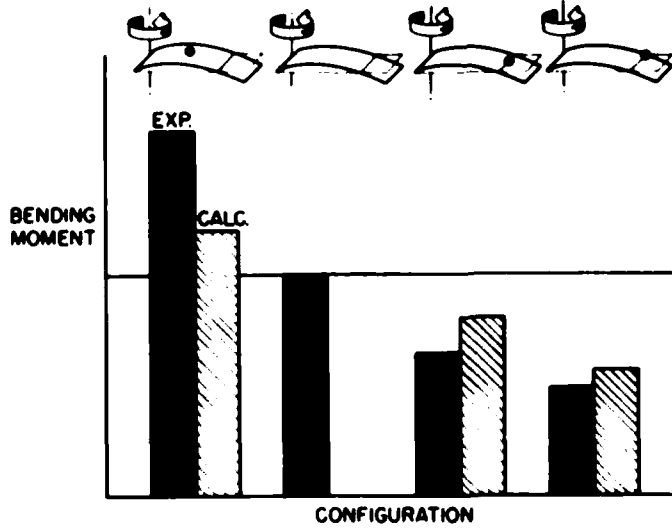


Figure 6

## RAPID ESTIMATION OF BENDING FREQUENCIES OF ROTATING BEAMS

By Robert T. Yntema

Langley Aeronautical Laboratory

## SUMMARY


A procedure is presented in the form of charts which permits the rapid estimation of the natural bending frequencies of helicopter rotor blades, both rotating and nonrotating. Since the approach is based on Southwell's equation, an evaluation of the method with regard to such things as higher modes, blade offset, and variable mass and stiffness distributions is also given. The evaluation shows that when nonrotating beam bending modes are used, Southwell's equation yields reasonably accurate bending frequencies for rotating helicopter blades. Example comparisons of frequencies estimated using the charts with values given by the manufacturer for several actual blades show that the simplified procedure yields good practical results.

## INTRODUCTION

The purpose of this paper is to present results in chart form which permit the rapid estimation of bending frequencies of rotor blades. The proposed method of frequency determination makes use of the familiar Southwell form; thus, it is also the purpose of this paper to show that this approach works quite well when such things as higher modes, blade offset, and variable mass and stiffness distributions are considered. The paper is divided into three parts as follows: In the first part a review and an evaluation of the Southwell approach is given, in the second part frequency charts are presented, and in the third part the results of applying these charts to some actual helicopter blades are given to indicate the order of accuracy obtainable in practical cases with this procedure.

## REVIEW AND EVALUATION OF SOUTHWELL APPROACH

The basic form of the Southwell equation which defines the bending frequencies of a rotating beam is given as



$$\omega_R^2 = \left[ \frac{\int_0^L EI(y'')^2 dx}{\int_0^L my^2 dx} \right] + \left[ \frac{\int_0^L T_1(y')^2 dx}{\int_0^L my^2 dx} \right] \Omega^2 \quad (1)$$

where

$\omega_R$  bending frequency of rotating beam

$\Omega$  rotational speed of beam

$m$  mass distribution for beam

$EI$  stiffness distribution for beam

$T_1 \Omega^2$  tension force in beam

$L$  length of beam

$x$  spanwise coordinate along beam

$y, y', y''$  beam mode shape and derivatives with respect to  $x$

Equation (1) yields exact values for the bending frequencies of a rotating beam if the mode shapes of the rotating beam are known. Since these exact shapes are usually not known, however, it is necessary to assume mode shapes from which approximate frequencies can then be estimated. If the nonrotating mode shape is substituted into the first term of equation (1) and the coefficient of  $\Omega^2$  is replaced by  $K$ , the Southwell constant, the Southwell equation takes the following form:

$$\omega_R^2 = \omega_{NR}^2 + K\Omega^2 \quad (2)$$

where

$\omega_{NR}$  nonrotating bending frequency of beam

$K$  Southwell constant

If the hinge or point of fixity of the rotating beam is offset from the axis of rotation, it may easily be shown that the Southwell constant can be written in the form:

$$K = K_0 + K_1 \epsilon \quad (3)$$

where

- $K_0$  zero-offset Southwell constant  
 $K_1$  offset correction coefficient for Southwell constant  
 $\epsilon$  distance hinge is offset from axis of rotation

If equation (3) is substituted into equation (2),

$$\omega_R^2 = \omega_{NR}^2 + (K_0 + K_1 \epsilon) \Omega^2 \quad (4)$$

If certain constants for the beam are introduced into equation (4), it can be written as

$$\omega_R^2 = a_n^2 \frac{EI_0}{m_0 L^4} + (K_0 + K_1 \epsilon) \Omega^2 \quad (5)$$

where  $I_0$  and  $m_0$  are measured at the root of the beam and

- $L$  length of beam outboard of hinge or point of fixity  
 $a_n$  nonrotating frequency coefficient for beam vibrating in  
 nth mode

In order to provide a basis for estimating the accuracy, usefulness, and possible limitations of the Southwell approach, a systematic series of blades was selected and frequencies were calculated by the Southwell approach and a more exact process. Figure 1 shows the cases studied using both methods. These cases include the uniform cantilever offset 0, 5, and 10 percent and the uniform hinged beam with the same offsets. The "linear" type beams are beams in which the mass and stiffness both vary linearly from the root value to zero at the tip. Zero- and 10-percent offset were treated for this type of beam with both the cantilever and hinged root.

The Southwell frequencies were obtained with the use of the mode shapes for the nonrotating beam whereas the true or reference frequencies were obtained by a Rayleigh-Ritz energy procedure involving expansion of the rotating beam modes in terms of the nonrotating modes of a uniform beam. For the cantilever beams, five nonrotating uniform

modes were used in the expansion. For the hinged beams, a pendulum mode was used in addition to the five nonrotating modes. Some of the results of this investigation are shown in figures 2 to 4.

The variation of bending frequency with rotational speed for a uniform hinged beam is shown in figure 2. The range of  $\left[ \frac{\Omega}{(\omega_{NR})_{1st}} \right]^2$  in this figure is roughly 25 percent above that encountered in current helicopters. From the results shown it is evident that the Southwell results are quite accurate, the maximum error being about 3 percent in frequency squared or only about  $1\frac{1}{2}$  percent in frequency. This maximum error is about the same for all three modes.

In order to avoid confusion, results for the 5-percent-offset case are not shown in this figure. They fall roughly midway between the 0- and 10-percent-offset curves and show the same type of agreement between exact and Southwell results.

Frequency results for the "linear" type hinged beam are shown in figure 3. From this figure it is apparent that the Southwell results are extremely accurate, even for the highest rotational speeds shown.

A comparison of frequency results for the uniform and the "linear" type hinged beam is given in figure 4. The most important thing to be noted from this comparison is the difference in slope between the dashed and solid line for each mode. The slope of each of these lines is directly proportional to the Southwell constant. The large difference in slope, particularly evident for the first mode, indicates that a single value of the Southwell constant for each mode could not adequately predict the variations of frequency with rotational speed which are shown in the figure.

Results obtained for the cantilever beams show roughly the same type of agreement between exact and Southwell results.

From the foregoing evaluation of the Southwell approach it was concluded that Southwell constants based on the nonrotating beam mode shapes lead to reasonably accurate bending frequencies of rotating helicopter blades. The evaluation also showed that the Southwell constants vary appreciably with beam mass and stiffness distribution.

#### CHARTS FOR FREQUENCY DETERMINATION

In order to provide a means for rapidly estimating rotor-blade bending frequencies, the nonrotating frequency coefficients, zero-offset

Southwell constants, and offset correction coefficients for Southwell constants have been computed for a series of beams with linear mass and stiffness distributions. The range of mass and stiffness distributions was selected to encompass variations found in currently manufactured blades with some latitude for new design. All the constants are based on the mode shapes of the nonrotating beam.

The variation of the nonrotating frequency coefficient  $a_n$ , with beam mass and stiffness distribution is shown in figure 5. The abscissa is the ratio of tip mass to root mass, 1.0 represents a constant mass beam, and 0 the case where the mass varies linearly to zero at the tip.

The solid curves are for beams with constant stiffness along the length, the short-dashed curves for beams where EI drops to half the root value at the tip, and the long- and short-dashed curve for beams where EI is zero at the tip.

Figure 6 permits selecting an accompanying value for the Southwell constant for beams with zero hinge offset. The variation with stiffness distribution appears quite small, particularly for the first mode. Actually, however, there is a maximum difference of about 5 percent. The variation with mass distribution is obviously somewhat more pronounced for all the modes shown.

In order to account for cases where the hinge is offset from the axis of rotation, offset correction coefficients  $K_1$  have also been computed for this family of beams. These coefficients, when multiplied by the offset given as a fraction of the free beam length, yield the correction to be added to the zero-offset Southwell constant.

The variation of this offset coefficient is shown in figure 7. It is evident that this variation is quite similar to that shown in figure 6.

Results similar to those shown in figures 5 to 7 have also been obtained for cantilever beams and are shown in figures 8 to 10.

#### EXAMPLE RESULTS

In order to illustrate the type of accuracy which can be expected in using the frequency charts of figures 5 to 7, bending frequencies have been estimated for the first three modes of four existing helicopter blades. The following procedure was used in this estimation:

(1) Straight lines were faired through the  $m$  and EI distributions for the blade, large values near the root being ignored.

(2) From these fairings, the root values of  $m$  and  $EI$  and the necessary tip-to-root ratios were obtained.

(3) By using these ratios, values of  $a_n$ ,  $K_0$ , and  $K_1$  were obtained from the charts.

(4) Substitution of these constants into the Southwell equation yielded the bending frequencies at zero and at rated rotor speed.

The results are shown in table I. The  $m$  and  $EI$  distributions for the blades are shown on the left-hand side of the table. The actual distribution is given by the solid lines. The dashed line is the linear approximation selected to represent this variation. It should be emphasized that these linear approximations used in estimating the frequencies were the initial ones selected and were not juggled to obtain the best agreement. The frequencies shown as exact in this figure are values furnished by the manufacturer.

If the exact and estimated results for the blades are compared, it is evident that the results are quite accurate when the crudeness of the linear approximations used is considered. It is interesting to note that in all cases the estimated frequency of the rotating beam is more accurate than that for the nonrotating beam; this indicates that the linear approximations yield more accurate values for the Southwell constant than for the nonrotating frequency coefficients.


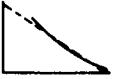

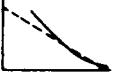
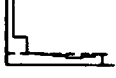



Although no comparisons have been made for fixed end blades, it is believed that even more accurate results should be obtainable for this end condition since large values of root stiffness can be more accurately accounted for by using the offset correction factors.

#### CONCLUDING REMARKS

To summarize, it has been shown that the Southwell approach, based on nonrotating mode shapes, provides a reasonably accurate means of predicting frequency changes due to rotational speed for most current helicopter blades. It has been found, however, that a single Southwell constant for each mode cannot yield accurate results for all cases, particularly if the mass distribution of the blades is quite different. In order to aid the designer, charts have been presented which permit the rapid estimation of nonrotating frequencies, of Southwell constants, and of the offset correction coefficients for Southwell constants, from which reasonably accurate frequencies can be readily obtained for rotating blades. In example applications, the method gave good estimations of the bending frequencies of actual rotor blades.

TABLE I

EXACT AND ESTIMATED FREQUENCIES FOR SEVERAL  
MANUFACTURED BLADES

m	EI	MODE	$\omega_{NR}$ , RADIANS/SEC		$\omega_R$ , RADIANS/SEC	
			EXACT	EST.	EXACT	EST.
		1st	17.3	17.4	49.2	47.7
		2nd	48.5	50.0	86.8	85.7
		3rd	95.5	101.0	137.0	137.8
		1st	21.6	21.1	50.6	49.2
		2nd	58.9	60.5	92.4	92.2
		3rd	112.1	122.0	148.0	154.0
		1st	21.9	21.1	74.0	78.3
		2nd	63.7	59.5	132.0	134.4
		3rd	126.0	125.5	200.0	207.5
		1st	13.4	14.6	37.9	37.8
		2nd	43.7	41.6	71.0	70.3
		3rd	94.9	94.5	125.0	124.0

ROOT TIP ROOT TIP



BEAMS TREATED BY "EXACT" AND SOUTHWELL METHODS

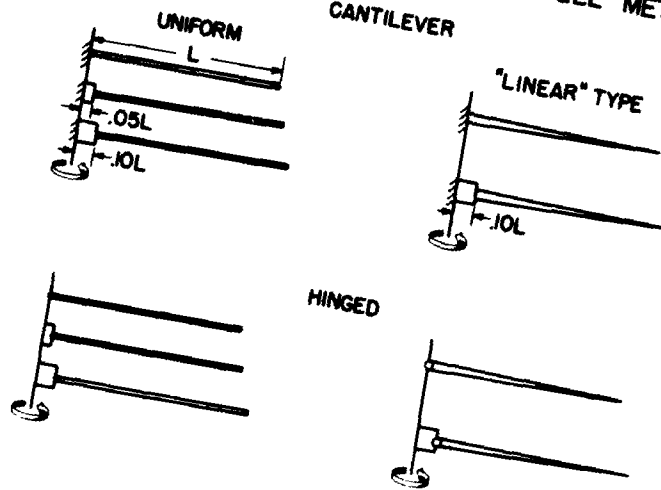


Figure 1

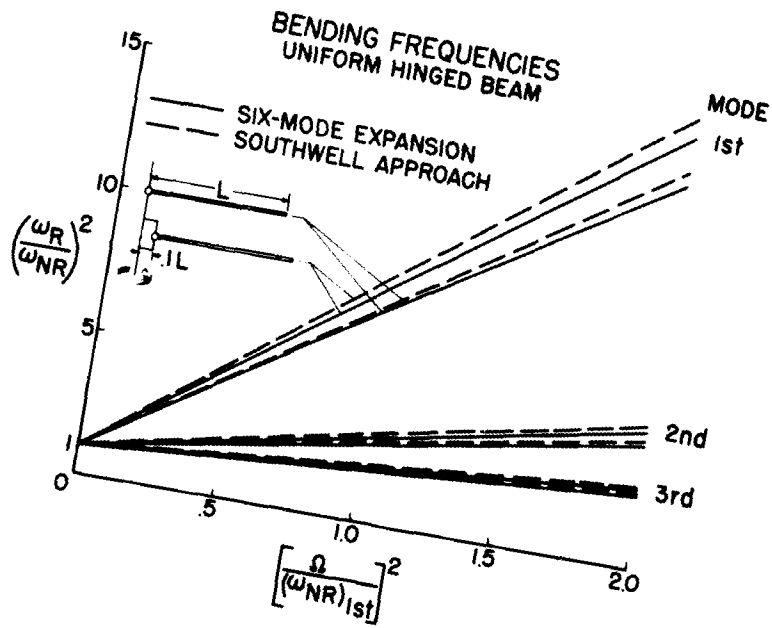


Figure 2

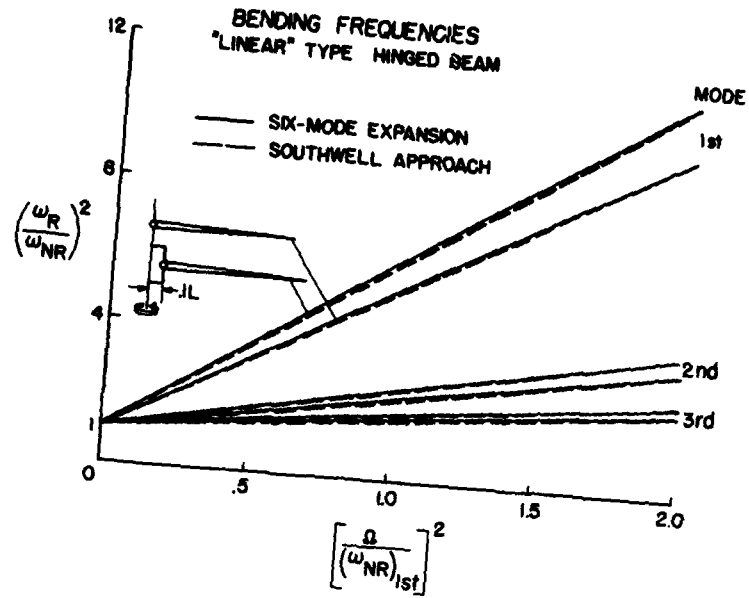


Figure 3

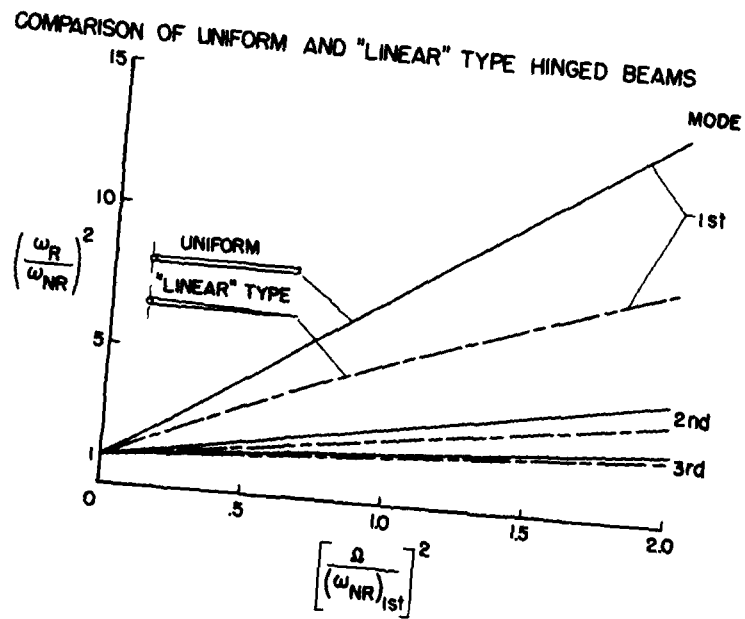


Figure 4

BENDING FREQUENCY COEFFICIENTS  
"LINEAR" HINGED BEAMS

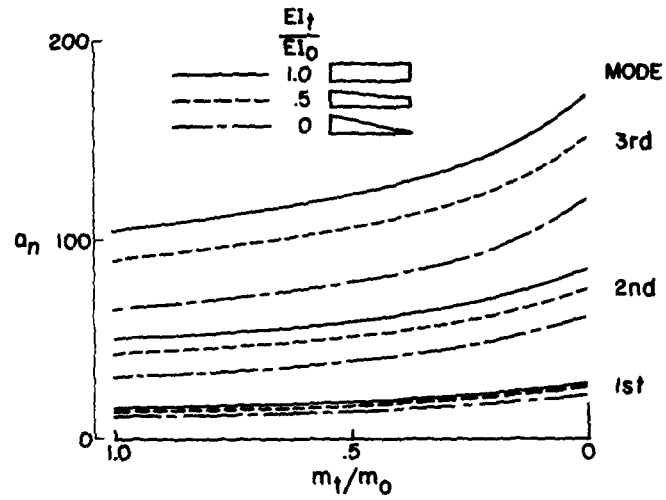


Figure 5

SOUTHWELL'S CONSTANT  
ZERO-OFFSET "LINEAR" HINGED BEAMS

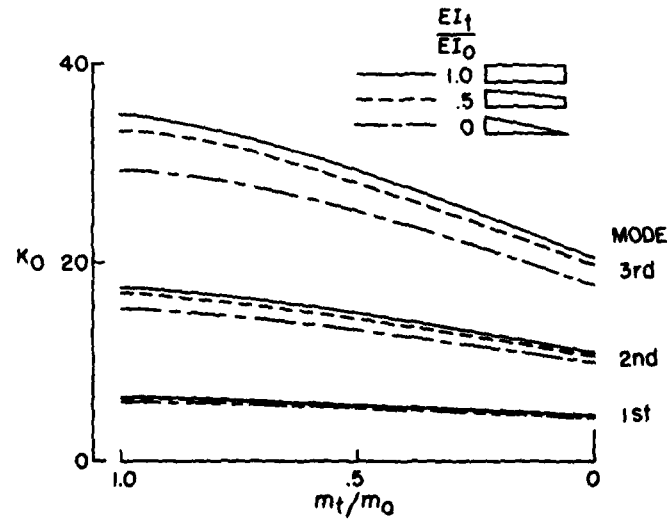


Figure 6

OFFSET CORRECTION COEFF. FOR SOUTHWELL'S CONSTANT  
"LINEAR" HINGED BEAMS

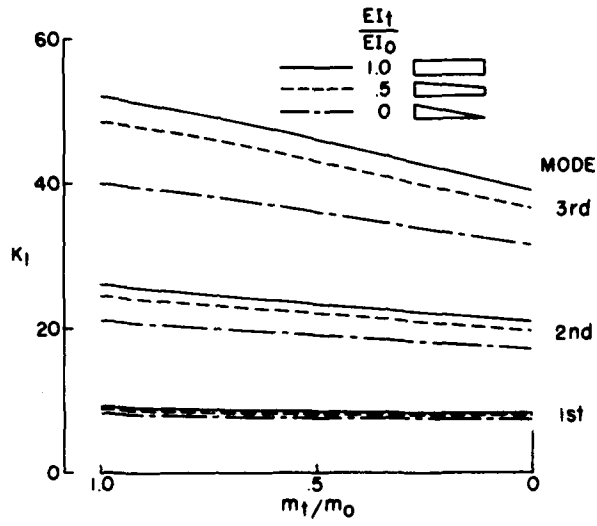


Figure 7

BENDING FREQUENCY COEFFICIENTS  
"LINEAR" CANTILEVER BEAMS

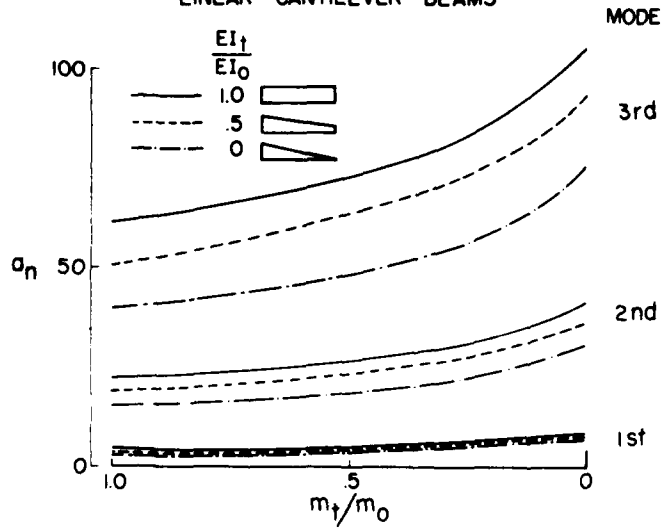


Figure 8

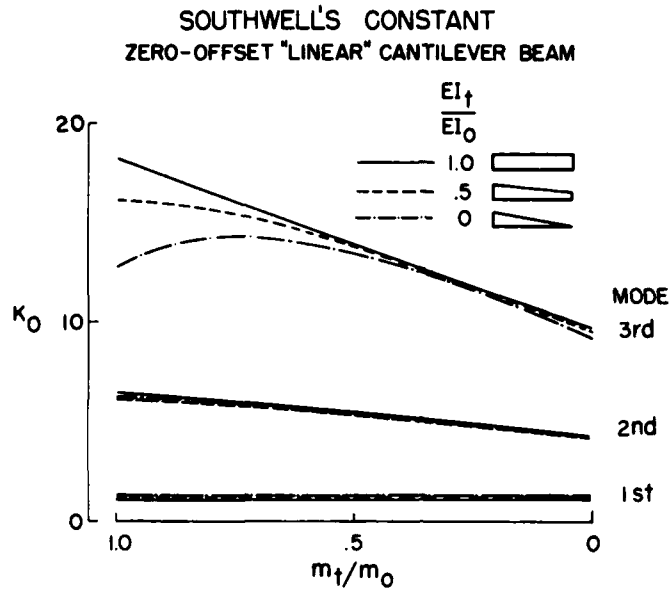


Figure 9

OFFSET CORRECTION COEFF. FOR SOUTHWELL'S CONSTANT  
"LINEAR" CANTILEVER BEAMS

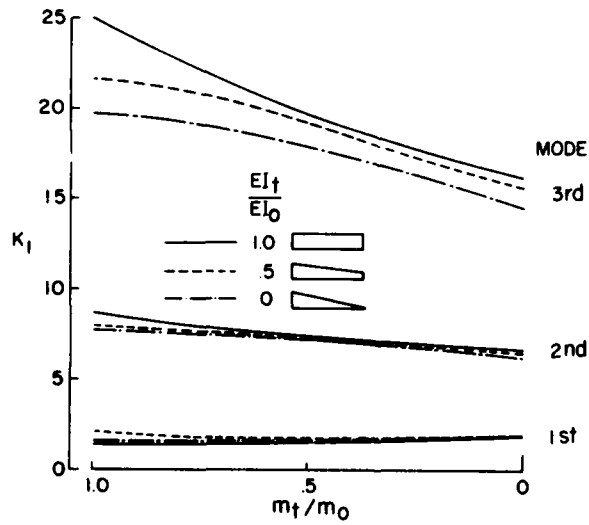


Figure 10

## DYNAMIC-MODEL DESIGN TECHNIQUES

By George W. Brooks

Langley Aeronautical Laboratory

### INTRODUCTION

The interest in dynamic models as a means for solving complicated engineering problems is steadily increasing, and such models have proven to be valuable aids both in the development of aircraft and as essential tools in aeronautical research. In the broad sense, a dynamic model is one used to simulate motions and, in the general case, these motions include the motions of structural deformation. When considering the use of a dynamic model in a given investigation, the prospective user must find satisfactory answers to many questions before he is in a position to begin the model construction. Perhaps the most important questions which arise are:

- (1) What are the problems of primary interest?
- (2) What are the characteristics of these problems with regard to forces involved and structural response?
- (3) What are the essential requirements for simulation of these forces in a dynamic model?
- (4) How should the model be designed to meet the specifications and facilitate construction and testing within the allowable limits for time and cost?

The purpose of this paper is to present information intended to assist prospective designers of dynamic models of helicopters to obtain workable answers to the questions posed and, in so doing, to outline the steps involved in the evaluation and design of dynamic models.

### GENERAL DISCUSSION OF HELICOPTER PROBLEMS

With respect to the first and second questions, it is well-known that there are many types of helicopter problems, and the phenomena which distinguish them vary from the mild vibrations due to engine unbalance to the violent instabilities of ground resonance. All these problems arise, however, as a result of different combinations of three basic types of forces.

These three types of forces, in abbreviated notation, are shown in figure 1 as vertices of a "triangle of forces." The forces are due to aerodynamics, elasticity, and inertia, and there is a damping force associated with each of these.

This method of presentation was first used by Collar of Great Britain in a discussion of aeroelastic problems of fixed-wing aircraft; however, it appears to be equally applicable to the discussion of helicopter problems.

Also listed on the diagram are a number of helicopter problems which are grouped in two categories according to the number of forces involved. The problems listed in the center of the triangle are dependent on all three types of forces; whereas those problems listed on the sides of the triangle are primarily dependent only on the two types of forces at either end of the side of the triangle.

A point worth noting is the fact that the problems which are dependent on the coupled aerodynamic and elastic forces are few in number and minor in character. This is due to the fact that the centrifugal accelerations couple the inertia forces with the other two types of forces and, thereby, bring the problems, which are ordinarily of this type, within the triangle. The twist and divergence of rotor blades are examples of this.

With regard to figure 1, the primary objective insofar as the problems are concerned is the classification of the problems into different groups. The types of forces involved in a given problem must be known before the problem can be placed in a particular category. Most of the helicopter problems, however, are fairly well defined and, therefore, figure 1 serves as a convenient index of helicopter problems and the forces which couple to create them.

If a study of one or more of these problems by means of dynamic-model tests is desired, the triangle of forces may be referred to in order to obtain a general idea of the necessary complexity of the model. For example, when the characteristics of problems listed in the center of the triangle are studied, the conditions for similarity of all the primary forces must be satisfied; whereas for the problems on the outside of the triangle, one type of force becomes secondary.

#### REQUIREMENTS FOR SIMILARITY

After satisfactory answers are obtained to the first two questions in regard to the problems of primary interest and the forces involved, it is then necessary to determine the requirements for the simulation of

these forces in the dynamic models used to study the problems. Accumulated experience gained by dynamic-model studies indicates that the cost and time involved in a dynamic-model test program goes up rapidly as the scope of the investigation and the complexity of the model are increased. In the interest of obtaining practical solutions, therefore, a knowledge of the essential requirements for similarity of dynamic models designed for use in the study of various helicopter problems is highly desirable. A convenient method for visualizing these requirements is presented in figure 2 which essentially assigns the forces of the triangle to the components of the aircraft structure.

The first column consists of a list of several typical helicopter problems ranging from performance to weaving. In the other columns are listed significant variables which are separated into aerodynamic and structural characteristics. The structural characteristics are further subdivided into those pertaining to the blades, the hub, and the fuselage. The aerodynamic characteristics listed are the lift coefficient or slope of the lift curve, Reynolds number, Mach number, and fuselage or airfoil shape. Under structural characteristics, the following are listed: mass, stiffness, and damping of the blades; the natural frequency and damping of the hub; and the mass, stiffness, and damping of the fuselage with the undercarriage included.

In an effort to point out the apparently essential requirements for similarity, three notations have been chosen: black squares, crosshatched squares, and blank spaces. With respect to a particular problem, the black squares mean that the variables are of primary importance and must be simulated in a distributed manner. The crosshatched squares signify that the variables may be simulated by choosing average or lump values. Blank spaces indicate that the variables are believed to be of secondary importance and that simulation of these variables may be neglected for the sake of model simplicity.

In order to illustrate the use of the chart, consider a specific example such as flight vibrations. For the model to simulate properly the full-scale helicopter, the mass and stiffness of the blades and fuselage must be scaled in a distributed manner; whereas the damping of the blades, hub, and fuselage, as well as the natural frequency of the hub, can probably be duplicated satisfactorily by choosing average values of the proper magnitude for each component. Selection of a similar mean lift coefficient and airfoil shape is desired, but the simulation of Mach number and Reynolds number would appear to be in the nature of a refinement rather than a requirement.

With respect to the chart as a whole, there are two general considerations to be noted. First, the existence of black squares in almost every column shows a wide variation of helicopter problems and indicates that a dynamic model designed to simulate the essential components for



each individual problem would have to be closely scaled in its entirety to simulate satisfactorily the full-scale helicopter with respect to all the problems simultaneously. Second, the emphasis given to different variables is subject to variation for different configurations and may change as a result of further knowledge of the problems. For example, the scaling of the mass distribution of the fuselage of a single-rotor helicopter does not appear to be as critical as it is for a tandem configuration, and the damping of the higher fuselage bending modes may have some influence on stall flutter if encountered.

The selection of the actual scale factors for the design of a dynamic model was discussed in considerable detail in reference 1. Other available references and textbooks appear to cover adequately the subject and no further discussion on the selection of model scale factors appears to be required at the present time.

### DESIGN TECHNIQUES AND METHODS OF CONSTRUCTION

After the requirements for similarity, including the determination of the scale factors, have been established, the final problem which confronts the designer is the selection of methods of model construction which will permit fabrication of the different components to the specifications dictated by the scale factors. A number of techniques have been employed successfully, and the remainder of the paper is devoted to a discussion of some of these.

In the same sense that it is possible to design a good helicopter or good automobile in different ways, it is also possible to vary the design of dynamic models and yet achieve the desired results. The selection of the actual method of construction is perhaps a matter of association or experience rather than of design evaluation, particularly when time and money are limiting factors, as is usually the case. Several different methods of construction which the NACA has used for different models are discussed and the choice of a suitable method is left to the reader.

#### Blades, Wings, and Fuselages

Among the many possible methods of model construction, those which receive the widest usage are segmented construction, stressed-skin construction, and spar-insert construction. All these methods are adaptable to either the lifting surface or the fuselage, and the selection of the method used is to some extent arbitrary. There are, however, some considerations which make one type preferable to another such as the speed of the model tests, the urgency for model test results, the need for the

reproduction in the model of higher modal characteristics of the prototype, and the investigation of such complicated phenomena as skin buckling.

Segmented construction.- Segmented construction has received perhaps the widest usage of any method of model fabrication to date. As shown in figure 3, this type of model construction consists of selecting a spar structure which is designed to have the required bending and torsional stiffness and strength. The spar is placed in the wing or fuselage structure in the proper geometrical position with respect to the cross section to obtain the required location of the elastic axis of the lifting surface or the required shear center of the fuselage. The blade or fuselage segments are then designed so that each section, together with the contributions of the spar, provides the proper values of mass, moment of inertia, and so forth. These quantities, as shown by figure 3, can be varied readily by varying the amount and chordwise location of the masses added to each blade segment. The segments are then attached to the spar and the gaps between segments are sealed with thin strips of rubber.

This type of construction is often preferred because of its simplicity and relative ease of fabrication. Among its limitations is the fact that the design does not provide duplication of skin effects and, for low-aspect-ratio structures, it does not provide good similitude of prototype structures involving higher structural modes.

Stressed-skin construction.- The stressed-skin type of model construction is also used to a considerable extent and has many advantages as well as some disadvantages. The extent to which the model is made to simulate the prototype is mostly a function of effort on the part of the designer in that the model can be made to simulate roughly the prototype or it can be made a replica model. Inasmuch as this design is probably the nearest thing to the prototype for current configurations at least, it can be used for complicated structures such as low-aspect-ratio, highly tapered, and highly swept structures. It can also be used to study skin phenomena such as buckling or skin flutter.

If the familiar type of rivet construction is used, the stressed-skin construction can be time consuming and expensive. However, with the use of modern adhesives and forming techniques, this type of construction merits greater consideration and, as the construction techniques are improved and the number of types and gage sizes of various materials are increased, stressed-skin construction may well become the preferred type of construction for most dynamic models. Figure 4 shows a few details of the stressed-skin rotor blade used on a dynamic helicopter model which was designed, constructed, and tested at the Langley Laboratory.

Spar-insert construction.- An example of spar-insert construction is shown in figure 5 and consists of a spar imbedded in a structure which may vary from weak, lightweight plastic to a strong and heavy wood. The structural properties of the model may be provided by the spar, the surrounding structure being used primarily to obtain the desired shape, or they may be provided by the surrounding structure. This type of construction is often used for studying the overall effects of different parameters on dynamic-model response, for example, the effect of mass distribution on natural frequency. Generally, in models constructed in this manner, the model parameters vary as a continuous function of the span.

This type of structure is highly versatile in that the cross section of the spar can be selected to give a wide range of bending and torsional stiffnesses. The mass, center of gravity, and moment of inertia can be conveniently varied by placing inserts in holes such as shown on the sketch.

Other types of model construction.- A few types of construction have been mentioned which may be used in dynamic-model fabrication. There are many others such as those shown in figure 6. Occasions arise where each of these methods has merit. The solid section is, of course, desirable from the standpoint of simplicity. If the proper material is available, it may give close approximations to full-scale parameters. Surface inserts provide convenient means for varying model stiffness. In other cases, the desired torsional stiffness may be obtained by slotting the model trailing edge and covering the slots to maintain aerodynamic integrity. The wrapped construction, which consists of wrapping a material such as fiber glass around a core, is convenient either for fabricating a model from the beginning or for changing the structural characteristics of an existing model. The torsional stiffness is conveniently varied by changing the amount of bias of the warp. The multispar design may be used for models which must be strong but must also accommodate a lot of internal apparatus such as wires and tanks. A light-weight, high-strength construction can be obtained by use of a porous filler and an external cover. This method is essentially a variation of the stressed-skin design previously mentioned.

#### Dampers, Springs, and Landing Gear

So far, the discussion of structural design techniques has been limited to a consideration of the fuselage and lifting-surface structures. Of equal importance is the design of dampers, springs, and other model components.

The design of dampers and springs to provide a given model with the required dynamic characteristics depends, of course, on the type of model,

the space available, and the nature of the damper and spring constants desired, that is, whether the damping is independent of velocity or proportional to velocity or velocity squared and whether the spring constants are linear or nonlinear.

A sketch of a simple damper design which the NACA has used quite successfully is shown in figure 7. This damper has only one moving part and can be used to dampen either rotary or linear motions. The damping coefficient is constant throughout the range of motion for a given clearance, viscosity, and wetted area and is easily changed by variation of any of these factors. It was used on a dynamic helicopter model to damp both the pylon and landing-strut motions.

The spring and damping constants of tires change with air pressure and it is desirable, if possible, to achieve the scaled prototype values of these parameters by use of small tires. Figure 8 illustrates the use of a model airplane tire in connection with a loop spring and damper to achieve the scaled prototype values for the spring and damping constants for the landing strut of a model helicopter. In figure 8, the details of the damper are obscured by a rubber boot which covers the damper and acts as a dust shield. The spring constant can be changed by varying the air pressure in the tires or by adding detachable stiffening clamps to the loop springs. The damping constant is easily varied by changing the viscosity of the oil in the dampers.

#### Instrumentation

Another important factor in dynamic-model design is that of model instrumentation. Instrumentation becomes a problem chiefly because of the limitations on model weight and space. When reasonable requirements for model instrumentation are being determined, the fact that an accelerometer, or for that matter any other instrument, is about the same size whether it is used on the model or the prototype must be considered. Add to this the fact that the data obtained on the model must be at least as reliable as that obtained on the prototype, particularly if the model is being used to study the effect of minor changes in prototype configuration and the result is a somewhat complicated problem which must be solved by designing simple gadgets which are both small and reliable. For instance, relative motion can be measured by means of small, flexible, strain-gage—beam arrangements such as the one shown in figure 9. It may not be feasible to install enough instruments to get all the desired data simultaneously; therefore, tests may have to be repeated to obtain additional data to meet the requirements.

## CONCLUDING REMARKS

In conclusion, an attempt has been made in this paper to present basic requirements for similarity of dynamic models suitable for study of various helicopter problems, together with some of the techniques and methods which the NACA has used in the construction and testing of dynamic models of various types. It is questionable whether any group can present an optimum design or method of construction for dynamic models because of the endless scope of the subject. Each contribution to the science or art, as the case may be, is valuable if it reveals some techniques which are applicable to other related studies or if it provides the desired data for a particular investigation. The extent to which a dynamic-model test program will be successful is a function of many things but chiefly a function of the ability of the personnel involved to design simple mechanisms which can solve complex problems at reasonable cost.

## REFERENCE

1. Brooks, George W.: The Application of Models to Helicopter Vibration and Flutter Research. American Helicopter Society, Inc. (Proc. Ninth Annual Forum, Washington, D.C., May 14-17, 1953.)

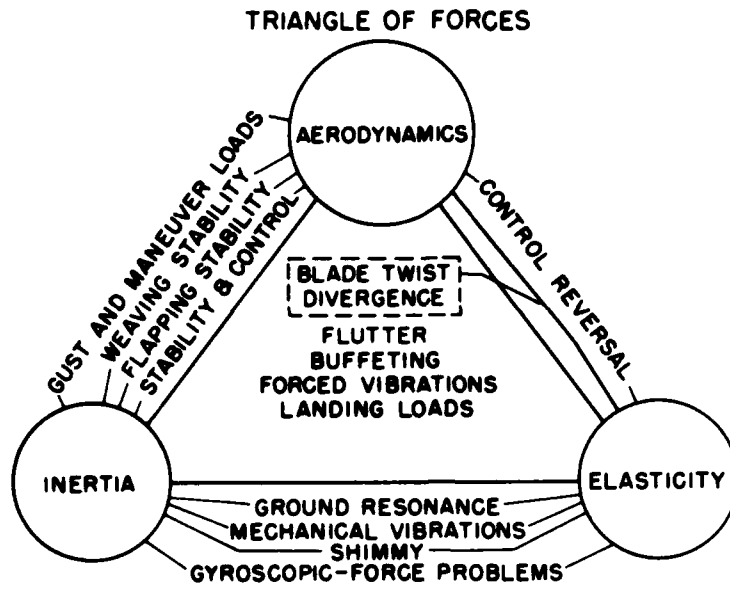


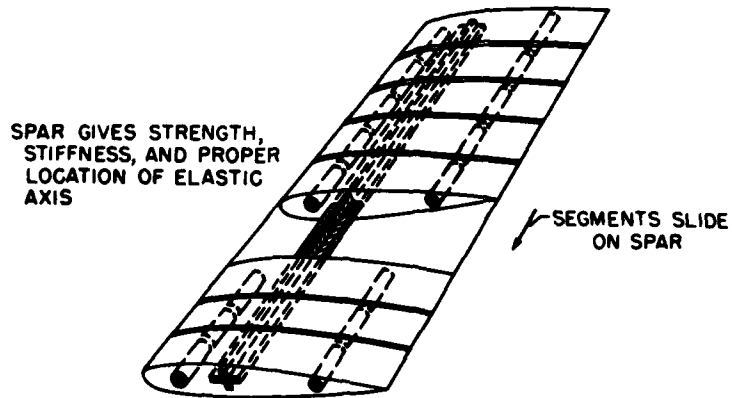
Figure 1

**REQUIREMENTS FOR SIMILARITY**

	AERODYNAMICS				STRUCTURAL CHARACTERISTICS							
	$c_l$ OR $\frac{dc_l}{d\alpha}$	RN	M	SHAPE	BLADES			HUB		FUSELAGE		
					MASS	EI AND GJ	$\lambda_B$	$\omega_n$	$\lambda_H$	MASS	EI AND GJ	$\lambda_F$
PERFORMANCE	■	■	■	■	■					■		
STABILITY		■		■	■		■			■		
CONTROL FORCES	■			■	■			■		■		
FLIGHT LOADS	■			■	■					■		
FLIGHT VIBRATIONS	■			■	■	■	■	■	■	■	■	■
GROUND RESONANCE					■	■	■	■	■	■	■	■
CLASSICAL FLUTTER		■		■	■	■	■	■	■	■	■	■
STALL FLUTTER	■	■	■	■	■	■	■	■	■			
WEAVING	■			■	■							

Figure 2

### SEGMENTED CONSTRUCTION



BALANCE WEIGHTS GIVE MASS AND MOMENT OF INERTIA

Figure 3

### STRESSED-SKIN CONSTRUCTION



Figure 4

## SPAR-INSERT CONSTRUCTION

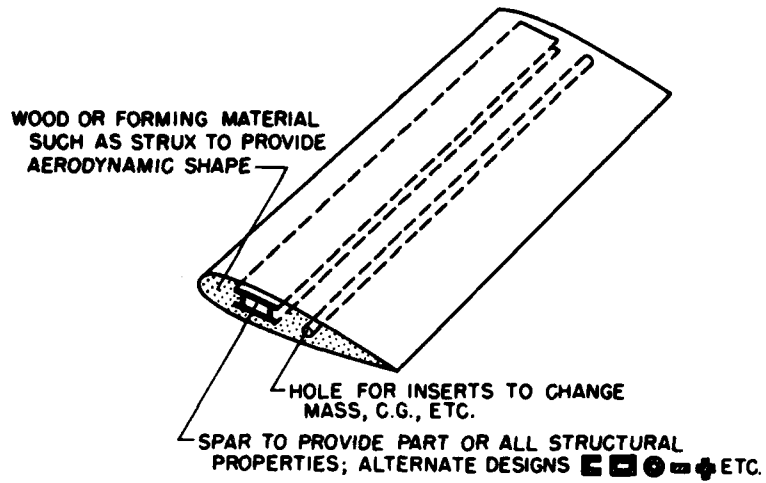


Figure 5

## ADDITIONAL CONSTRUCTION TECHNIQUES

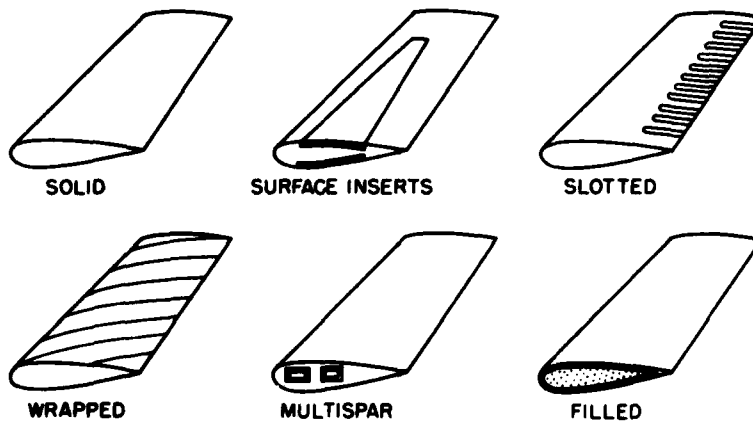
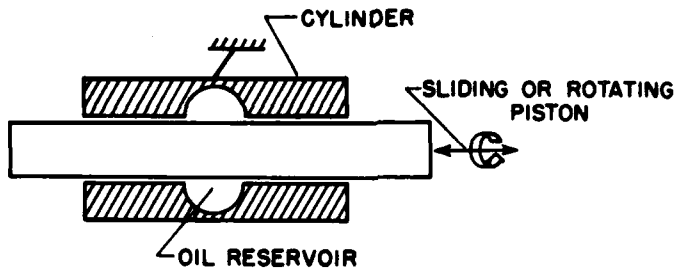


Figure 6



DAMPER DESIGN



DAMPING PROPORTIONAL TO FIT, VISCOSITY, AND VELOCITY

Figure 7

LANDING-GEAR DESIGN

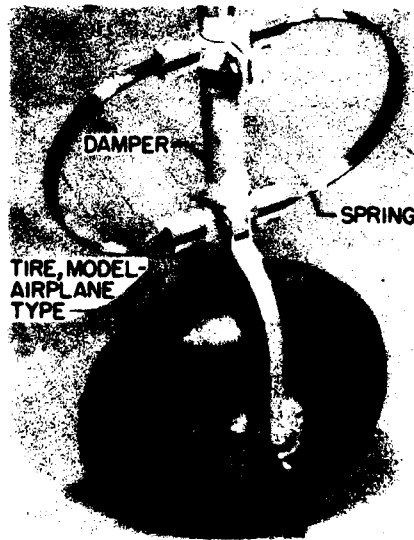


Figure 8

STRAIN-GAGE-BEAM ARRANGEMENT  
FOR MEASURING RELATIVE MOTION

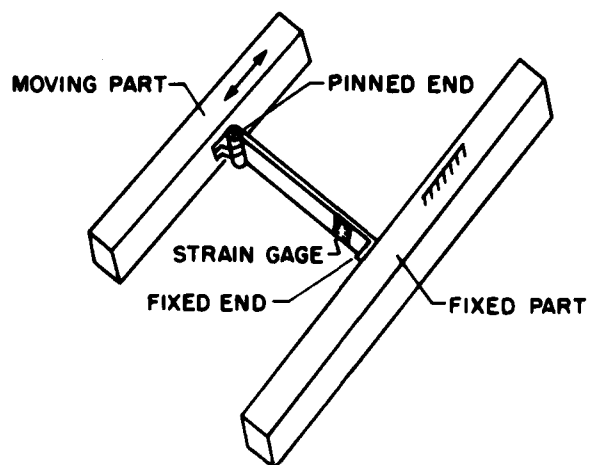


Figure 9

METHODS OF PREDICTING THE FATIGUE CHARACTERISTICS  
OF STRUCTURAL PARTS CONTAINING STRESS CONCENTRATIONS

By Herbert F. Hardrath

Langley Aeronautical Laboratory

In the design of helicopters, as in the design of any other structure subjected to repeated loading, one must consider the possibility of failure by fatigue, but design for fatigue involves consideration of many parameters for which no quantitative rules have been available. The result is that millions of dollars have been spent on fatigue tests of many kinds. References on the subject are numbered in the thousands and current bibliographies (ref. 1) indicate that approximately 200 more are being published each year.

In the work at the Langley Laboratory, some simple design rules are sought out of this profusion of information to help minimize the amount of testing required in the future. This paper summarizes the results of this approach on the study of effects of stress concentrations in fatigue. This is probably one of the more important aspects of the overall fatigue problem since practically every part of any machine or structure has some change in cross section which affects the stress distribution and makes the part especially vulnerable to fatigue failure.

The first step in any fatigue consideration is the determination of the appropriate S-N curve for the case at hand. Consider, for example, the case of a part containing a circular hole and subjected to completely reversed axial loads. The maximum average stress on the net section is plotted in figure 1 for test conditions producing static failure and fatigue failures in 2 to 10<sup>8</sup> cycles.

The discussion deals with methods of predicting this curve in three regions: first, the endurance limit indicated by the test point; second, the intermediate stress range shown as a solid line; and last, the high-stress region shown by the dashed curve. The prediction of a similar curve for loading conditions other than completely reversed is discussed next, and then a brief discussion of the cumulative effect of repeated stresses that vary in amplitude is given. In all that follows it is assumed, first, that the expected loading conditions are known, second, that the static stress-strain properties and the fatigue behavior of unnotched parts made of the same material as that of the part have been determined in tests at constant amplitude for a variety of combinations of mean and alternating stresses, and, third, that the theoretical stress-concentration factor for the configuration involved is known.

In order to establish the endurance limit for the curve in figure 1, compare this S-N curve with a similar one for unnotched specimens made of the same material and tested under completely reversed loads (see fig. 2) and with the stress-strain curve for the material (see fig. 3). For both of these curves the endurance limit is a stress well below the yield strength of the material. It is known, of course, that the maximum local stress in a specimen with a small hole is about three times the average stress plotted in figure 2. This local stress is also below the yield strength of the material. Since all stresses are elastic (at least in the engineering sense), one might expect that the ratio between the endurance limits would be equal to the elastic stress-concentration factor. This turns out to be an overly conservative assumption. If the endurance limit for unnotched specimens is divided by the net-section stress corresponding to the endurance limit in notched parts, an effective stress-concentration factor is obtained. This factor is called the fatigue factor for brevity.

In figure 4 the points illustrate how this fatigue factor varies with the radius of a hole in 2-inch-wide aluminum-alloy specimens tested under completely reversed axial loads. Each point represents the fatigue factor at the extreme right end of the S-N curve for a specimen with a different hole size. The solid curve shows that the theoretical factor (ref. 2) in such specimens decreases from a maximum value of 3 for a specimen with a very small hole and becomes asymptotic to 2 for a specimen with a large hole. Note that the difference between the fatigue and theoretical factors is small for large radii and becomes greater for smaller radii. This effect, called the geometric-size effect, has been recognized by many investigators for the last 20 years and several relationships have been proposed to predict its magnitude. The most promising of these appears to be a relationship originally developed by Neuber (ref. 3). Predictions by his hypothesis are indicated by the dashed curve in this figure.

Figure 5 presents the Neuber formula which involves  $K_T$ , the theoretical factor,  $\omega$ , the flank angle in an arbitrary notch (and for the case under consideration this value is zero),  $r$ , the radius at the base of the notch, and a constant  $A$  which is a property of the material. The development of this formula can probably best be rationalized on the consideration that practical materials are granular and therefore not homogeneous and isotropic over volumes of the order of the size of grain. The theory of elasticity, which is used to establish the theoretical stress-concentration factor, assumes perfect homogeneity and therefore does not give accurate predictions when small volumes are considered. This formula, in effect, assumes a small volume which may be assumed to be statistically homogeneous but across which no stress gradient exists. The size of this volume cannot be measured physically, so it is adjusted to suit the data. A value of  $A$  of 0.02 inch has been found for 24S-T and 75S-T aluminum alloys to give predictions which agree best with fatigue test results.

A similar analysis of results of tests on steel specimens (ref. 4) shows that  $A$  varies with ultimate tensile strength (see fig. 6). Comparisons between predictions by the Neuber formula using values of  $A$  from figure 6 and test results for several hundred sets of data indicate that satisfactory predictions are possible. The previously mentioned value of 0.02 inch for the aluminum alloys is indicated by the points.

It should be pointed out that the predictions by the Neuber formula and other methods which are discussed cannot be expected to be perfect. There is always a certain amount of scatter associated with fatigue test data, and when large volumes of data from several laboratories are being correlated, there are many secondary factors which are not consistently controlled. In most cases, however, the predictions are within the limits of scatter in the data. The immediate and most obvious application of this work on size effect is to point out the danger in the indiscriminate use of results from laboratory tests on small specimens in the design of larger parts. On the other hand, the method also shows how such data can be used in the design of parts of practical size if the proper corrections for size are made.

It has been shown how the size-effect considerations just described permit prediction of the extreme right-hand end of the S-N curve in figure 2 for a notched part made of steel or aluminum alloy and subjected to completely reversed loads. For certain parts which are loaded rather heavily but less frequently and for occasional overloading of other parts, it is necessary to know the fatigue strength at somewhat higher stresses. Therefore, consider the problem of prediction at higher stresses where failure takes place in  $10^4$  to  $10^7$  cycles. Again, the discussion is limited to cases where the applied load is completely reversed. In many of these cases the maximum local stress exceeds the elastic limit for the material and some plastic redistribution of stress takes place. It appears, then, that the desired prediction method will involve the effects of plasticity on notch stresses. If the fatigue factor is computed at various lifetimes along these curves, it is found that it decreases with increasing stress as indicated in figure 7.

In figure 7 the solid curve illustrates this decrease in fatigue factor with increasing net-section stress. The dashed curve presents the results of an investigation of plastic stresses at notches under static conditions. This formula, developed at the Langley Laboratory (ref. 5), has been found to predict satisfactorily the plastic stress adjacent to the notch in a variety of combinations of configurations and materials. The relation involves the theoretical stress-concentration factor  $K_T$ , the secant modulus of the material at the notch  $E_{SEC}$ , and the secant modulus  $E$  appropriate for points far from the notch. Note that the stress-concentration factor remains at its elastic value until local stresses exceed the yield strength and then it decreases sharply to approach a value of 1 at the tensile strength. There is fair agreement

between the fatigue and plastic factors at the higher stresses, but a discrepancy exists in the elastic region. However, it was shown previously that the Neuber formula predicts the endurance limit as indicated by the tick and the upper end of the curve for the fatigue factor. If the theoretical factor in this formula is replaced with the Neuber factor to correct for size, the elastic portion is lowered but the sloping portion is essentially unchanged. Very good agreement is thus obtained at all stress levels by a combination of size-effect and plasticity-effect considerations.

Figure 8 gives a similar comparison for steels. The curve for the plastic stress-concentration factor is defined as before but is, of course, computed for the appropriate stress-strain curve. Here, however, the curves for the fatigue factors for various steels and configurations are likely to lie anywhere in the rather wide scatter band defined by the two solid curves. In each case the curve of the fatigue factor has roughly the same shape as the curve for plastic stress concentrations and the Neuber factor is a good approximation of its maximum value. However, the stress at which plastic action begins to reduce the stress-concentration factor must be adjusted. Note that in some cases the adjustment must be to a lower stress and in some cases to a higher stress. Inspection of the data reveals that this action begins when the local stress equals the endurance limit for unnotched specimens.

It develops that a simple hyperbola of the type in figure 9 gives a good approximation to the fatigue factor for approximately 150 cases found in the literature. The constants  $M$  and  $C$  are adjusted to produce a value of 1 for the stress-concentration factor at the ultimate tensile strength and to pass the hyperbola through the Neuber factor at the endurance limit for unnotched materials. This is admittedly a strictly empirical formula, but it appears to have some physical significance on the basis of the following discussion.

In figure 10 the original stress-strain curve for the material is plotted as a solid line. The dashed curves are the curves obtained when the formula for the plastic stress-concentration factor is solved backwards to find the stress-strain curve which would have resulted in the variation in fatigue factor predicted by the empirical hyperbola. The lower curve is for a case where the fatigue factor fell near the lower limit of the scatter band in figure 8 and the endurance limit for unnotched specimens was significantly lower than the yield stress of the material. According to physicists, the fatigue mechanism requires some form of local plastic action in order to initiate a crack which ultimately causes failure. If this is true, there must be plastic action at stresses just above the endurance limit in steels even when this stress is well below the engineering yield stress. The dashed curve represents the case of a very mild steel where the endurance limit is higher than the yield strength. Such materials will not fail in fatigue even when stressed

well into the plastic range but just below the endurance limit. The material undoubtedly hardens during the first few loading cycles to produce a new yield stress much higher than the first. The dashed curves shown in this figure are probably not physically measurable stress-strain curves. They are merely conceptual models that may aid in understanding the predictions of the fatigue factors previously described.

Usable relationships have been developed for predicting the fatigue factor for notched steel and aluminum alloys tested under completely reversed loads. The predicted factor together with the S-N curve for unnotched specimens (see fig. 2) provide a means for computing the S-N curve for the part in question at stresses producing failure in  $10^4$  cycles or more. The approach just outlined breaks down at the higher stresses because the S-N curve for unnotched specimens ceases to exist for life-times less than  $10^5$  or  $10^4$  cycles. Since unnotched specimens can withstand a stress practically equal to their ultimate strength for this number of cycles, and since the fatigue-factor predictions just described approach a value of 1 at this stress, the predicted S-N curve for notched specimens would rise sharply at lives just below  $10^4$  cycles to intersect the S-N curve for unnotched specimens at this point. Actually, recent tests at the Langley Laboratory (ref. 6) have shown that notched specimens can and do fail in much smaller numbers of cycles as indicated by the dashed curve. This is a phenomenon not clearly understood at this point, but failures in this region have been encountered in service. This particular curve, for instance, indicates that approximately 100 cycles of a load equal to two-thirds of the ultimate strength will cause failure of the part. Parts with higher stress concentrations will fail in correspondingly fewer cycles.

Predictions in this range will undoubtedly involve consideration of progressive strain hardening in specimens subjected to repeated loading. This effect is probably small at the lower stresses and has, therefore, been neglected in the procedures described. Data in this range are extremely scarce, and experimental research is being conducted to fill this gap in knowledge (ref. 6). Data from auxiliary tests in which local stresses in notched specimens subjected to repeated loading are measured would aid in verifying or modifying the assumptions made in the proposed methods and would aid in extending the work to higher stresses.

So much for failure under completely reversed loading. Most parts of aircraft and helicopters are subjected to a steady load with an oscillating load superimposed. Steady stresses in rotor blades, for instance, are likely to be in the neighborhood of three or more times the amplitude of the dynamic stresses.

Figure 11 illustrates the S-N curve for the same type of specimen previously discussed, except that in this case the loading is zero to

tension or  $R = 0$  instead of completely reversed. This type of loading is assumed for simplicity, but the method to be developed is generally applicable to other cases as well. Several previous investigators (ref. 7) have attempted to predict this curve by applying the theoretical stress-concentration factor to the alternating stress and not the mean stress, or to both, or to the maximum stress with various assumptions regarding mean stresses. Most methods break down sooner or later when large numbers of tests are analyzed. The following is a method which is believed to have considerable merit: If the endurance limit of this curve is multiplied by the Neuber factor to determine the maximum local stress, it is found, in many cases, to be higher than the yield strength. A plastic correction must therefore be applied at the endurance limit. Figures 12 and 13 show how this correction should be made.

Figure 13 shows the stress-strain curve in tension and compression for the material under consideration. Figure 12 portrays the variations of stress with time for a part with a Neuber factor equal to 3.5 and a maximum nominal stress of 20 ksi. The nominal curve shows the variation in net-section stress with time and the dashed curve is the prediction of maximum local stress if everything were elastic. Actually the local stress exceeds the elastic limit and is therefore subject to reduction by the plastic considerations previously described to a value indicated by the solid curve. Upon unloading, however, it appears reasonable to assume that all stresses again become elastic, that future cycles will reproduce the maximum value, and that the range of stress becomes the Neuber factor times the nominal stress range. The net result of the plastic action appears to be an effective reduction in mean stress near the notch. Previous tests at the Langley Laboratory (ref. 8) showed that the maximum local stress is repeated, at least during the first 100 cycles of load. The assumption that the local stress range is the Neuber factor times the range of stress on the net section has not been verified experimentally, but it appears to be a reasonable first assumption. In fact, if the life of an unnotched specimen subjected to this loading history (solid curve) is determined, it serves as a reasonable prediction of the life of the notched part under consideration. Note that the required data on unnotched specimens must be for a mean stress and alternating stress which are not related in a simple manner to the net-section stresses in the notched specimen under consideration. What is needed is a Goodman or similar diagram which facilitates interpolation between various S-N curves.

If this line of reasoning is continued to higher stresses, the case where the unloading portion of the cycle produced local stresses which exceed the compressive yield strength of the material is eventually approached. In the limiting case the local stress probably oscillates between equal values of tension and compression stress, and the mean stress is reduced to zero. The life of an unnotched specimen tested under completely reversed stress equal to the maximum local stress determined in this manner will then provide a reasonable prediction of the



life of the specimen under consideration. The same limitations on minimum life apply here as noted in the case of completely reversed stresses. Extension to shorter lives and higher stresses will again be possible only after additional experimental work.

Up to this point it has been seen, first, how considerations of the absolute size of a notch have resulted in the method of predicting the endurance limit of notched steel and aluminum-alloy specimens tested under completely reversed loading and, second, how elementary plasticity considerations have helped provide a means for predicting fatigue behavior of similar specimens tested at higher stresses and under loading conditions other than completely reversed. The methods described have been checked against large numbers of test results from NACA and other laboratories and have been found to produce predictions which are generally within the limits of scatter of the data.

The cumulative effects of stresses varying in amplitude are discussed next. Most of the experimental data available on this effect are from two-step tests in which the specimen is stressed at one stress level for some fraction of its expected life and then tested to failure at some other stress level. Results are generally analyzed by what is frequently called the Miner hypothesis (ref. 9) which adds up the fraction of expected life which was endured at each stress level. The answer is usually something very different from the value of 1 predicted by the Miner hypothesis. However, very few practical parts are subjected to such a simple load history. Where two discrete stress levels are actually encountered, they will probably occur alternately at random intervals. More generally, however, some sort of spectrum of stresses is involved. The tests that have been performed with spectrum loading tend to produce results which are somewhat more consistent when analyzed by the Miner method, but the summation may still be very different from 1. Other prediction methods have been proposed (refs. 10 to 12) but have not been shown to be consistently superior to the Miner method. It appears that many more tests of this type are required before predictions of cumulative damage under variable amplitudes can be made realistically. The development of more reliable prediction methods may become possible when these tests and others performed in other laboratories provide a larger volume of data with which to work.

## REFERENCES

1. Anon.: References on Fatigue.
  - I. STP No. 9-C, A.S.T.M., 1952.
  - II. STP No. 9-D, A.S.T.M., 1953.
2. Howland, R. C. J.: On the Stresses in the Neighbourhood of a Circular Hole in a Strip Under Torsion. Phil. Trans. Roy. Soc. (London), ser. A., vol. 229, Jan. 6, 1930, pp. 49-86.
3. Neuber, Heinz: Theory of Notch Stresses: Principles for Exact Stress Calculation. J. W. Edwards (Ann Arbor, Mich.), 1946.
4. Kuhn, Paul, and Hardrath, Herbert F.: An Engineering Method for Estimating Notch-Size Effect in Fatigue Tests on Steel. NACA TN 2805, 1952.
5. Hardrath, Herbert F., and Ohman, Lachlan: A Study of Elastic and Plastic Stress Concentration Factors Due to Notches and Fillets in Flat Plates. NACA Rep. 1117, 1953. (Supersedes NACA TN 2566.)
6. Hardrath, Herbert F., and Illg, Walter: Fatigue Tests at Stresses Producing Failure in 2 to 10,000 Cycles - 24S-T3 and 75S-T6 Aluminum-Alloy Sheet Specimens With a Theoretical Stress-Concentration Factor of 4.0 Subjected to Completely Reversed Axial Load. NACA TN 3132, 1954.
7. Grover, H. J., Bishop, S. M., and Jackson, L. R.: Fatigue Strengths of Aircraft Materials. Axial-Load Fatigue Tests on Notched Sheet Specimens of 24S-T3 and 75S-T6 Aluminum Alloys and of SAE 4130 Steel With Stress-Concentration Factors of 2.0 and 4.0. NACA TN 2389, 1951.
8. Griffith, George E.: Experimental Investigation of the Effects of Plastic Flow in a Tension Panel With a Circular Hole. NACA TN 1705, 1948.
9. Miner, Milton A.: Cumulative Damage in Fatigue. Jour. Appl. Mech., vol. 12, no. 3, Sept. 1945, pp. A-159 - A-164.
10. Bland, Reginald B., and Sandorff, Paul E.: The Control of Life Expectancy in Airplane Structures. Aero. Rev., vol. 2, no. 8, Aug. 1943, pp. 7-21.
11. Richart, F. E., Jr., and Newmark, N. M.: An Hypothesis for the Determination of Cumulative Damage in Fatigue. Proc. A.S.T.M., vol. 48, 1948, pp. 767-798.

12. Shanley, F. R.: A Theory of Fatigue Based on Umbonding During Reversed Slip. Rep. P-350-1, The RAND Corp., Nov. 11, 1952 (rev. May 1, 1953).

TYPICAL S-N CURVE FOR ALUMINUM ALLOY

R = -1

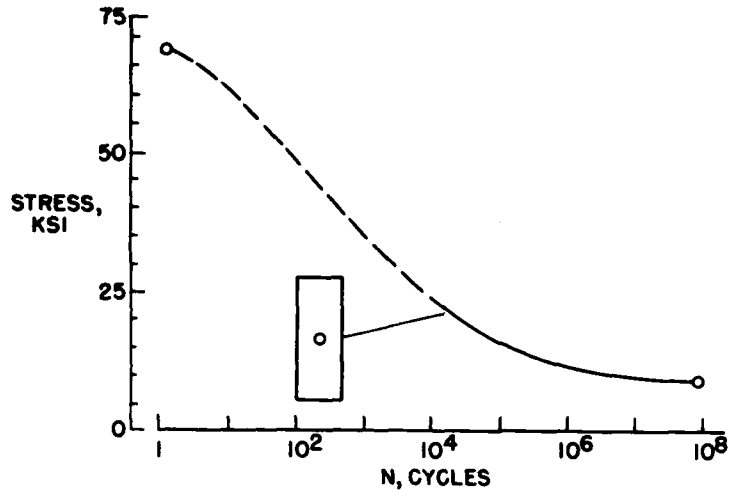


Figure 1

TYPICAL S-N CURVES FOR ALUMINUM ALLOY

R = -1

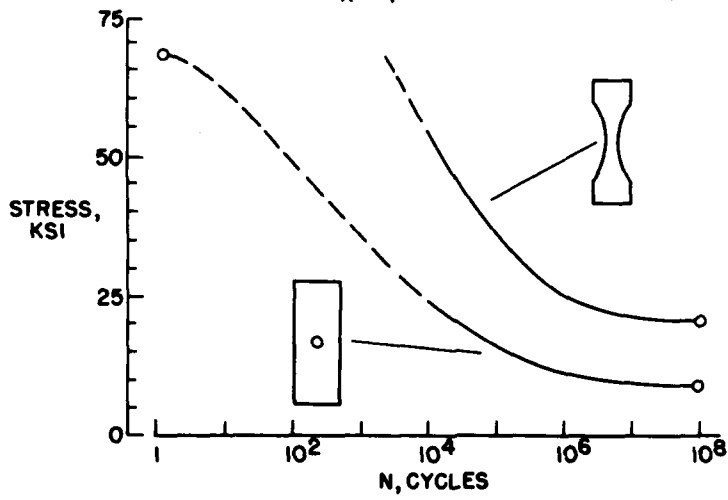


Figure 2

STRESS-STRAIN CURVE FOR 24S-T3 IN TENSION

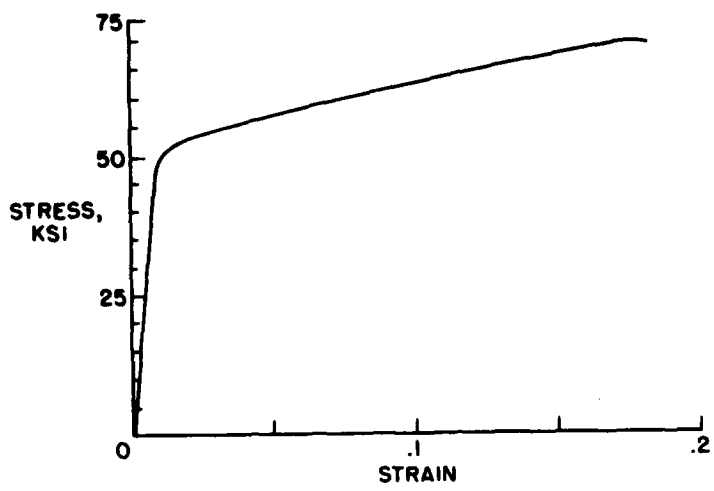


Figure 3

STRESS CONCENTRATIONS IN FATIGUE TESTS OF SPECIMENS WITH HOLES  
24S-T3 SHEET; R=-1

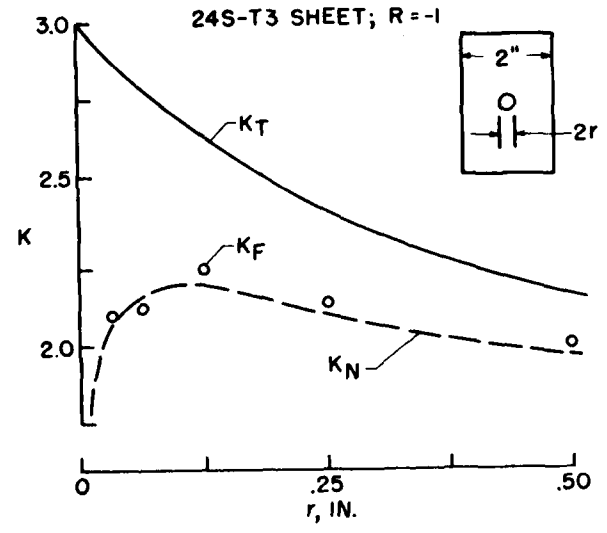
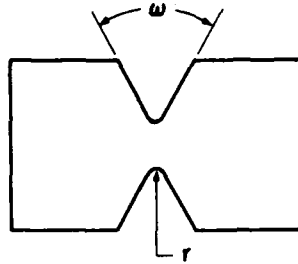


Figure 4

## NEUBER FACTOR



$$K_N = 1 + \frac{K_T - 1}{1 + \frac{\pi}{\pi - \omega} \sqrt{\frac{A}{r}}}$$

Figure 5

## NEUBER CONSTANT, A

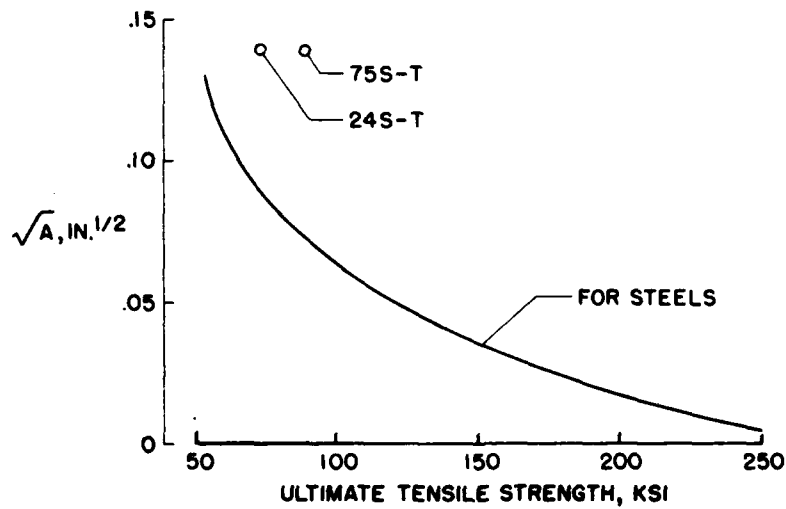


Figure 6

EFFECTS OF PLASTICITY ON STRESS-  
CONCENTRATION FACTORS  
ALUMINUM ALLOYS

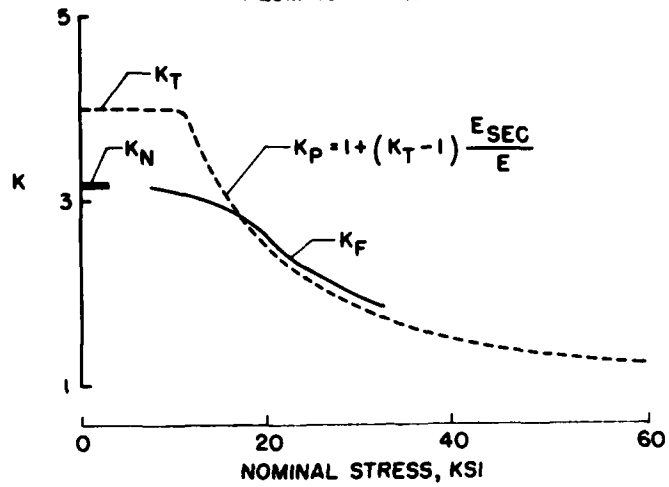


Figure 7

EFFECTS OF PLASTICITY ON STRESS-  
CONCENTRATION FACTORS  
STEELS

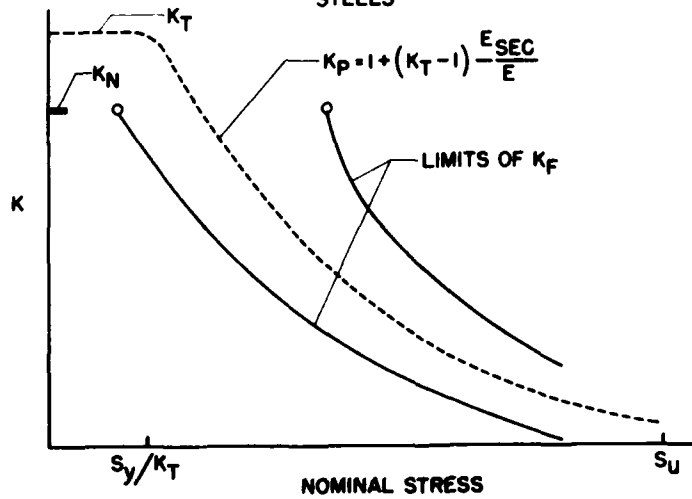


Figure 8

UNCLASSIFIED

PREDICTION OF FATIGUE FACTOR FOR STEELS

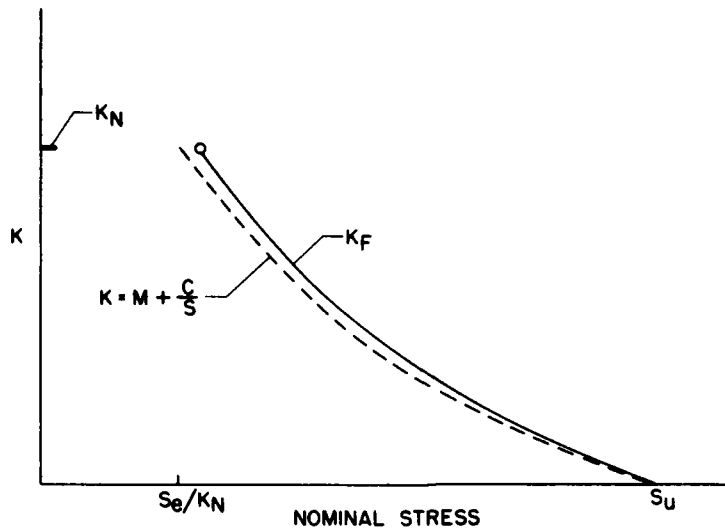


Figure 9

EFFECTIVE STRESS-STRAIN CURVES FOR FATIGUE OF NOTCHED STEEL SPECIMENS

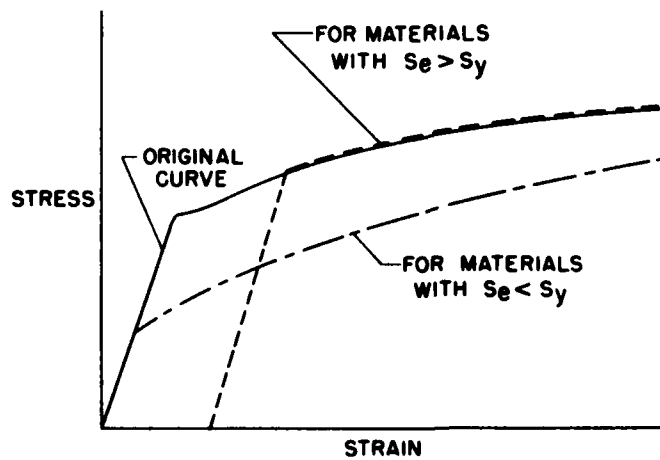


Figure 10

UNCLASSIFIED



TYPICAL S-N CURVE FOR ALUMINUM ALLOY  
R=0

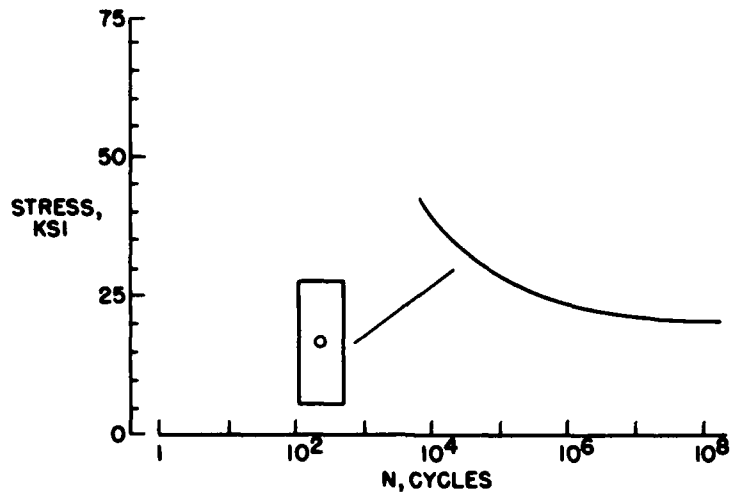


Figure 11

STRESSES AT NOTCHES IN SPECIMENS LOADED REPEATEDLY  
K<sub>N</sub> = 3.5; S<sub>MAX</sub> = 20 KSI

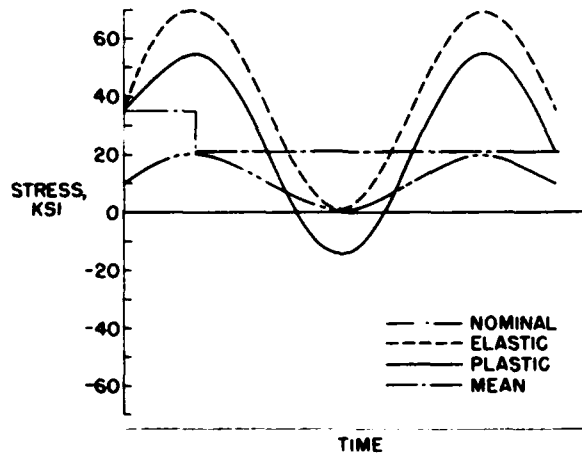


Figure 12

UNCLASSIFIED

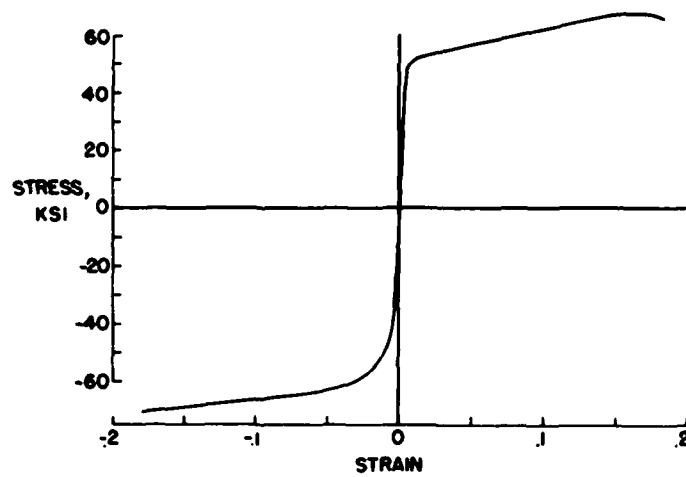
STRESS-STRAIN CURVE FOR 24S-T3  
TENSION AND COMPRESSION

Figure 13

UNCLASSIFIED